A THEORETICAL AND EXPERIMENTAL INVESTIGATION OF MULTI-PHASE INTERACTIONS IN PURE AND MULTICOMPONENT DROPLET EVAPORATION

By

COURTNEY LEIGH HERRING BONUCCELLI

A thesis submitted in partial fulfillment of
the requirements for the degree of

MASTER OF SCIENCE IN CHEMICAL ENGINEERING

WASHINGTON STATE UNIVERSITY
Department of Chemical Engineering

December, 2006

To the Faculty of Washington State University,

The members of the Committee appointed to examine the thesis of COURTNEY LEIGH HERRING BONUCCELLI find it satisfactory and recommend that it be accepted.

_____

Chair

_____

_____

ACKNOWLEDGEMENTS

This research was funded by Isothermal System Research Inc. (ISR) and Washington State University Chemical Engineering Department. I would like to thank the whole ISR team for their help and encouragement. Special thanks to Mr. Chuck Tilton, Vice President of Research and Development at ISR for bringing me on as a working graduate student. It was Chuck Tilton's interest in understanding and modeling multi-phase interactions in multicomponent droplet evaporation which started this research effort. Much appreciation also goes to Mr. Tom Weir, Mr. George Wos, and Mr. John Schwarzkopf at ISR for their input and guidance throughout this project.

I am very grateful to Dr. Richard Zollars, Professor and Department Chair at WSU for his continuous guidance, input, and suggestions and support in pursuing scholastic activities. Also big thanks to the rest of my committee, Dr. Bernie Van Wie and Dr. KNona Liddell for their support in pursuing scholastic activities.

Last, sincere thanks to my husband, Tony, for his unwavering emotional support and to my family who has always supported my wildest dreams and aspirations.

A THEORETICAL AND EXPERIMENTAL INVESTIGATION OF MULTI-PHASE INTERACTIONS IN PURE AND MULTICOMPONENT DROPLET EVAPORATION

ABSTRACT

by Courtney Leigh Herring Bonuccelli, M.S.
Washington State University
December 2006

Chair: Richard Zollars

This study addresses the separation between the theoretical and experimental aspect of multicomponent droplet evaporation. This research provides a numerical model and experimental data of the vapor concentration and temperature trends while a series of non-interacting droplets are dispensed through a closed chamber where they evaporate and condense depending on vapor-liquid equilibrium. Droplets composed of pure ethanol, pure water, and various compositions of ethanol and water were tested and modeled in an initial nitrogen or air environment. Such work is important in providing a basic link between the theoretical and experimental understanding of binary droplet evaporation. Research will provide a backbone to future studies involving multicomponent droplet evaporation in sprays.

Two one-dimensional models were developed to understand the interactions between mass and heat transfer in multicomponent droplet evaporation; one for an open (or constant

pressure) system and the second for a closed system. Numerical data of the vapor concentration profile and vapor temperature profile were compared to experimental data. The models were developed to incorporate the use of a mass transfer matrix composed of binary mass transfer coefficient pairs. This matrix was assumed spatially constant but varied with time depending on temperature and composition of the liquid and vapor phase.

The results show that in the case of water evaporation the closed system model over predicts the experimental vapor composition by 2.6%, and over predicts the published psychrometric data by 3.9%. In the case of ethanol evaporation the open system model over predicts the experimental vapor composition by 3.4%. The open system model was also used to model evaporating ethanol-water droplets, under predicting the ethanol vapor composition by 3.7% and over predicting the water vapor composition by 4.4%. Overall, the concept that multicomponent evaporation can be modeled by using a matrix of mass transfer coefficients instead of the simplifying case of an effective diffusion coefficient was shown to be valid in comparison to experimental and published data.

TABLE OF CONTENTS

LIST OF FIGURES

LIST OF TABLES

DEDICATION

This thesis is dedicated to all parents and educators who tirelessly work to instill courage, patience, dedication, and perseverance to our youth. Without you, none of us would succeed in realizing our full potential.

CHAPTER 1: INTRODUCTION

Droplet evaporation is attracting significant interest due to the crucial role it plays in a variety of applications which use sprays and atomization including spray cooling, spray combustion, spray drying, fire suppression, and air-fuel premixing. These applications each rely on a dispersed liquid phase, in the form of a large number of discrete droplets, convecting and vaporizing (or evaporating) in a continuous gas phase. The most interesting multi-phase applications are those which use the mechanism for enhancing heat transfer for the electronics industry. In each case, current cooling schemes utilize pure fluids. But as the heat removal requirement of technology steadily increases there is an ever-pressing need for new cooling options. One option is looking into the performance of binary fluids. By minimizing the system to two liquid components we are able to fine-tune thermal properties without creating such a complex fluid that it becomes too tedious to model.

However, studying and modeling multi-phase systems is not easy and managing the additional complexities when more than one component is interacting, can create scientific and computational chaos. As a result of the mathematical complexity of the momentum, energy, and mass transfer mechanisms, previous work can be classified as either involving pure fluids (*Mashayek*, 2001; *Yuen and Chow*, 1978; *Hubbard et al.*, 1975; *Frössling*, 1938; *Newbold and Amundson.*, 1973; *Masliyah and Epstein*, 1972; *Hoffman and Ross*, 1972), complex fluids involving more than two components (*Lehtinen et al.*, 1998; *Tamim and Hallett*, 1995; *Torres et al.*, 2003; *Zhu and Reitz*, 2002; *Abdel-Qader and Hallett*, 2005; *Kotake and Okuzaki*, 1969), or binary fluids (*Krishna and Standart*, 1976; *Aggarwal and Chen*, 1991; *Chen et al.*, 1997). Previously studied mechanisms of mass transfer can be described by the inclusion of either a

binary mass diffusion coefficient (*Aggarwal and Chen*, 1991; *Chen et al.*, 1997), an effective mass diffusion coefficient (*Landis and Mills*, 1974; *Landis and Mills*, 1974; *Newbold and Amundson*, 1973; *Lehtinen et al.*, 1998; *Sezen*, 2000; *Chen et al.*, 1997; *Aggarwal* ., 1991), or a mass diffusion matrix (*Krishna and Standart*, 1976; *Alopaeus and Norden*, 1999; *Alopaeus et al.*, 1999; *Krishna*, 1981; *Taylor and Krishna*, 1993). Separating research even further, studies have either focused on vaporization of fuels or other fluids at increased temperatures and pressures (*Landis and Mills*, 1974; *Crespo and Linan*, 1975; *Chen et al.*, 1997; *Tamim and Hallett*, 1995; *Torres et al.*, 2003; *Zhu and Reitz*, 2002; *Aggarwal and Chen*, 1991; *Kotake and Okuzaki*, 1969; *Law et al.*, 1987; *Marchese and Dryer*, 1996), spray drying of fluids containing solid particles (*Elerin and Krasovitov*, 1995; *Negiz et al.*, 1995; *Charlesworth and Marshall*, 1960; *Chen and Lin*, 2005; *Papadakis and King*, 1988), or the evaporation of droplets (*Frössling*, 1938; *Hubbard et al.*, 1975; *Yuen and Chow*, 1978).

The driving application in technology is spray or flame combustion due to the wide use of combustion in the fuel and chemical industry. Under this application the use of a constant mass diffusion coefficient is both practical and effective. Following with this trend, the majority of models consider the vaporization of complex fuels at increased temperatures and pressures by using an effective mass diffusion coefficient. For example, a constant mass diffusion coefficient is obtained by treating a complex fluid as a continuum of its own, with bulk properties, and therefore does not provide information of vapor composition changes due to unequal mass flux from the liquid-phase.

Recently research has improved the calculation processes used in previous studies by either speed or accuracy. This has been accomplished by eliminating droplet temperature from the model (*Lehtinen et al.*, 1998), creating new calculation algorithms (*Alopaeus and Norden*,

1999; *Alopaeus et al.*, 1999; *Krishna and Standart*, 1976), and considering previously neglected effects like internal liquid circulation (*Landis and Mills*, 1974; *Abdel-Qader and Hallett*, 2005; *Kerstein*, 1984), variable properties (*Hubbard et al.*, 1975), a non-constant diffusion matrix (*Krishna and Standart*, 1976), and droplet interactions (*Labowsky*, 1978) to name a few. Conversely, this research effort is interested in both the theoretical and experimental investigation of the interactions in a single binary liquid droplet evaporating into a ternary vapor phase which also contains an inert vapor component. This research is focusing on evaporation effects under ambient pressure and moderate temperatures of 270K-320K. This study will specifically focus on the use of a spatially constant unsteady mass diffusion matrix in the calculation of mass transfer.

Given that minimal experimental work has been done to validate a binary droplet - ternary vapor evaporation model in terms of vapor concentrations, and vapor temperature, the objective is to develop an evaporation model, and to then perform experiments to validate or disprove the theoretical results. As a result this research effort is made as a first step in fully understanding the mechanisms behind multicomponent system evaporation.

The five chapters in this thesis describe the use, experiments, and modeling of multicomponent system evaporation. The second chapter of this thesis starts with a brief description of applications for this research, focusing on the advantages of spray cooling, which uses two-phase cooling, as an enhancement over typical thermal management schemes. A literature review of previous research in related topics concludes the chapter.

A complex mathematical model was developed in order to understand the behavior of the defined system and to provide predictive capabilities for future multicomponent evaporation systems. The third chapter of the thesis describes a mathematical model, for the fluids tested in

the fourth chapter. The model, a 1-dimensional analysis, assumes Stefan diffusion based on a diffusivity matrix, as opposed to an effective diffusivity, using a non-ideal solution and an ideal gas, and surface renewal theory. Chapter four describes the design and operation of experiments conducted in testing the time-dependent mass and energy transfer in multicomponent evaporation systems. The defined binary fluid was composed of various concentrations of ethanol and water, which was tested at designated initial vapor/liquid temperatures, and vapor composition. Liquid solutions ranged in composition from pure ethanol to pure water, in order to validate the model for both binary and pure fluids.

The validity of the model, described in chapter three is then assessed by comparing its predictions to the experimental liquid and vapor final compositions and temperatures discussed in the fourth chapter. In predicting measured equilibrium concentrations and temperatures of ethanol droplets the model showed an average over prediction from experimental data of 3.4%. For water droplets the model showed an average over prediction of 4.0% from published psychrometric data and 2.6% from experimental data. Finally, for droplets composed of various compositions of ethanol and water, the model showed an average under prediction of the ethanol vapor content of 1.3% and an average over prediction of the water vapor content of 7.0%.

Results were obtained by monitoring a constant spatial location within an evaporation chamber with a Fourier Transform Infrared (FTIR) Spectrometer. The chamber was assumed to be well-mixed; however, no mechanical means were used. Furthermore, the model did not account for size, velocity, or composition distributions among droplets, or internal droplet composition and temperature gradients. Deviations between the model and the data suggest that the effects of vapor mixing and the presence of a vapor concentration gradient amongst species may contribute to the predicted total mass flux.

Chapter 5 summarizes the results and analysis from chapters 3 and 4, and chapter 6 recaps with final conclusions and suggestions for further avenues of research. The thesis closes with an appendix which contains a listing of nomenclature in section A.1, and an example of a closed system mathematical model using air as the non-condensing gas is section A.2. Raw data from all calibrations and experiments has been included for completeness in section A.3. Finally, important fluid properties and relations are located in section A.4, and experiment design data in section A.5.

CHAPTER 2: BACKGROUND

In the analysis of engineering problems involving liquid spray, knowledge of the behavior of an evaporating liquid droplet is essential for the understanding and prediction of the performance of the spray as part of an engineering system (*Yuen and Chow*, 1978). Increases in the utilization of synthetic and derived fuels have spurred interest in studying multicomponent liquid droplets. However, there is a more complex theory involved for multicomponent systems than previously seen in single component modeling. By combining existing mass transfer theory, novel time dependent mathematical modeling, and droplet evaporation behavior, it is possible to track vapor phase composition changes with continuous binary droplet evaporation. This effort will lead to a better understanding of multicomponent system evaporation.

2.1 Applications for Research

A large diversity of multi-phase gas-liquid flows of both scientific and practical interest involve the evaporation (or condensation) of near spherical liquid droplets in high (and low) temperature, turbulent (and laminar) environments. Such flows cover a wide range of applications including spray cooling, spray combustion, spray drying or spray humidification, fire suppression, and air-fuel premixing in combustors (*Miller et al.*, 1998). Among these are a number of thermal management schemes that have been used over the years to achieve necessary cooling requirements for industrial and government applications. Breakthroughs in many of today's cutting edge technologies are becoming increasingly dependent upon the ability to safely

dissipate enormous amounts of heat from very small areas (i.e. >1000W/cm^2). This leads to the necessity of discovering a novel approach to cooling advanced technologies which are becoming denser with far greater heat fluxes. To remove heat from electronic devices, air convection is traditionally used, while other thermal management schemes include liquid convection and pool boiling, and the use of jet or spray impingement cooling. The demand for high-heat-flux dissipation from surfaces in a large number of applications has stimulated much research in the area of jet impingement cooling, spanning over fifty years.

Early research focused mainly on single-phase cooling. Recently, however, researchers have turned their focus more toward two-phase cooling because of new technological advances in many industries (*Estes and Mudawar*, 1995). Figure 1, below, shows the advantage in terms of the achievable heat transfer coefficient for two-phase cooling; especially spray cooling, when compared to the more practiced natural and forced convection (*ISR*, 2005). From the figure there is an eight order of magnitude difference (from 0.0001 W/cm^2 to 1000W/cm^2), achieved in the heat transfer coefficients between natural air convection and spray cooling with water. Focusing research on alternative fluids can potentially push the limit up past that of water spray cooling.

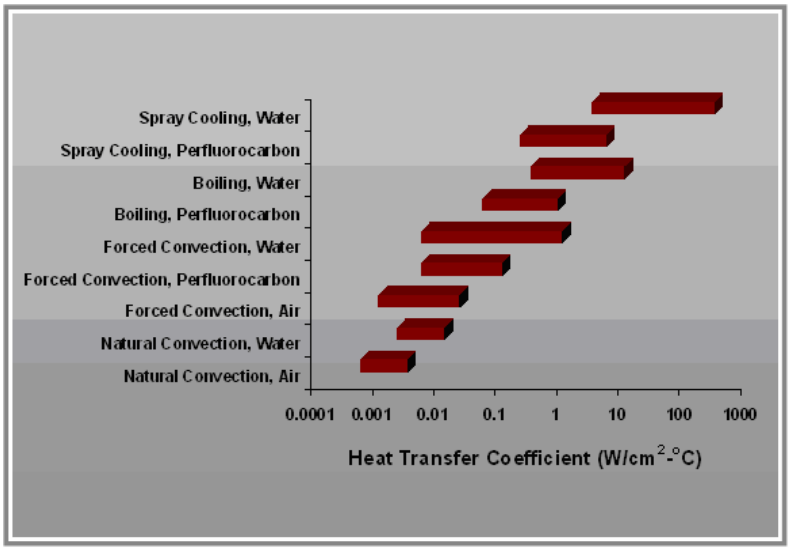

Figure 1: Comparison of Heat Transfer Coefficients for Thermal Management Schemes

Preliminary research into the heat transfer capabilities of alternative fluids has shown a distinct improvement from traditional dielectric fluids. The long-term goal of this research is to aid in the modeling capability of alternative fluids for spray cooling applications.

2.1.1 Spray Cooling

Both jets and sprays are produced by forcing a liquid through a small diameter orifice. In the case of sprays, however, the liquid is purposely shattered into a dispersion of fine droplets prior to impact with a heated surface. Once a spray droplet strikes the heated surface, it flattens into a thin disk whose thickness is much smaller than the diameter of the droplet. High heat fluxes can be obtained due to the formation and evaporation of a thin liquid film on the heated surface. The maximum heat flux, known as critical heat flux (CHF), is the point at which the surface no longer remains wetted and is seen by a dramatic increase in surface temperature. Spray cooling atomization is dominated by two categories depending on the mode of spray generation: pressure atomization, where the high pressure liquid is atomized by the pressure differential across a nozzle (also known as plane orifice spray), and air atomization, where a stream of high velocity secondary gas helps in atomizing the liquid into very fine spray. While atomized sprays are widely used in many industries because of their superior cooling, the presence of air greatly complicates condensation of the coolant in electrical applications due to the need for deaeration.

Spray cooling is used to cool high heat density electronic devices and systems (ranging from 10^2-10^3 W/cm^2) through the direct impact of a dielectric fluid with the heated surface

(*Mudawar*, 2000). This results in the formation of a thin film on the heated surface, wherein the majority of the heat is released through the latent heat of vaporization. Despite its advantages, superior dielectric fluids are still necessary to keep up with heat removal requirements of advancing technology.

The greatest potential lies in using multicomponent systems to strategically optimize key properties like viscosity, thermal conductivity, and surface tension, to name a few. Two-phase heat transfer is dependent on liquid temperature and composition, internal pressure, and the surrounding vapor temperature and composition. Therefore, a time-dependent spray evaporation model is crucial to the quantitative analysis of heat removal in a multicomponent system. The prospect of replacing the usual fluid of choice, perfluorocarbons, which have relatively poor heat transfer properties (*Mudawar*, 2000), high global warming potential, and are exceedingly costly, with a binary fluid, which mitigates these detrimental characteristics, led to the work in this thesis.

In this thesis, by approaching the high heat flux problem in a novel way, spray cooling performance can be enhanced. Traditionally, research in spray cooling and other thermal management schemes have focused on pure fluids. I propose that multicomponent systems having a normal boiling point and optimized thermal properties could out perform currently used fluids. However, to accomplish this, droplet evaporation would first have to be modeled and understood before proceeding to a full spray analysis, and then finally a fluid's thermal performance could be quantified through CHF.

2.2 Previous Related Research

Multicomponent evaporation is governed by species volatility, rate of diffusion, and the nature of fluid movement in the droplet, unlike pure fluid systems where evaporation is eventually driven to the wet bulb temperature. In multicomponent systems the transport of one species can be augmented by the transport of another (*Newbold and Amundson*, 1973). For example, it is possible to observe various interaction phenomena occurring; osmotic diffusion is noted by a diffusion of a component in the absence of a composition gradient for that species, while a diffusion barrier is noted by a lack of component transfer even though a composition gradient exists for it, and reverse diffusion is seen by a diffusion of a species against its composition gradient.

A critical difference between the studies of a single drop and a spray, whether the drops are evaporating, combusting, or contain solid particles, is that in a non-dilute spray we can not assume a non-interacting model. This was shown by Sacks (1951) when he found by using gravimetric analysis that the experimentally observed droplet evaporation rate was 100 times smaller than that predicted by Prober (1946) with his non-interacting model.

The first attempt at theoretically and experimentally investigating the evaporation of a single evaporating liquid drop was done by Frössling in 1938. In his work he photographed the changing size of a stationary drop subjected to a constant air current. After examining nitrobenzene, aniline and water he formulated an equation calculating the evaporation rate:

$$\frac{dM}{dt} = 4\pi D \frac{MW}{R} \frac{\Delta P}{T} \frac{d_p}{2} \left(1 + \mathrm{K}\sqrt{\mathrm{Re}}\right) \tag{2.1}$$

where $\frac{dM}{dt}$ is the evaporation rate in $\frac{g}{\text{second}}$, D is the diffusion coefficient in $\frac{cm^2}{\text{second}}$, MW is the molecular weight, R is the universal gas constant, T is the absolute temperature; ΔP is the difference between the pressures of vapor at the surface (approximately the saturation temperature) and in the streaming air, d_p is the droplet diameter, Re is Reynolds number defined below as:

$$\text{Re} = \frac{d_p \cdot \rho_a \cdot u}{\eta_a} \tag{2.2}$$

where ρ_a is the air density, u is the relative velocity, η_a is the air dynamic viscosity and defined as:

$$\eta = \rho \nu \tag{2.3}$$

where ν is the kinematic viscosity of the fluid.

In Equation 2.1 K is the characteristic constant for the evaporating substance and is approximately defined as:

$$\text{K} = \frac{0.276}{\sqrt[3]{\frac{D}{\nu}}} \tag{2.4}$$

Basic single droplet combustion models were formulated in the 1950's by Godsave (1950), Spalding (1950), and Goldsmith and Penner (*Goldsmith and Penner*, 1954) for an isolated pure-component droplet steadily burning in stagnant, oxidizing environments. These lead to what has been termed the d^2-law, predicting that the square of the droplet diameter decreased linearly with time. At the same time Ranz and Marshall (*Ranz and Marshall*, 1952), (*Ranz and Marshall*, 1953) formulated the analogy between heat and mass transfer at low Reynolds numbers, and verified a simple expression for the Nusselt number at zero Reynolds

number, known as the Ranz-Marshall Correlation, by studying suspended water drops evaporating in air. More recently, studies by Deng et al. (*Deng et al.*, 1992) and Mashayek (2001) have begun to look into the evaporation rates of surface deforming drops. Since then, more sophisticated studies that relax restrictions of the original pure-component single droplet model by including internal circulation, non-uniform temperature, and concentration gradients have been studied both experimentally and theoretically.

Significant research has studied the composition and temperature changes within a droplet with spray combustion (Santangelo *et al.,* 1998) along with an abundance of theoretical and experimental studies covering the evaporation and combustion of sprays. Major reviews of spray combustion and evaporation models and their comparison with measured values can be found by Faeth (1977) and Harrje and Reardon (*Harrje and Reardon*, 1972). A model known as particle-source-in-cell (PSI-CELL) was designed for gas-droplet flows (Crowe *et al.*, 1977). This model was then adapted for specific use with spray drying (Negiz *et al.*, 1995). The PSI-CELL model assumes a dry air stream flowing co-currently. In the case of a spray cooled system the surrounding vapor is essentially at rest, however, the PSI-CELL model allows for a good simplifying case from which to start.

In 1973 Newbold and Amundson (*Newbold and Amundson*, 1973) derived a mathematical model for the evaporation of a multicomponent droplet in stagnant gas. In their study they found that Stefan flow played an essential role in modeling a multicomponent fluid. Using the ordinary mass, volume, and energy differential equations for evaporation they were able to use a concentration-temperature phase diagram for the analysis of droplet behavior. Results were presented for both two- and three-component droplets; however, in the derivation they used an effective mass diffusion coefficient for the liquid mixture instead of progressing

with a mass diffusion matrix and respective matrix equation model to account for changes in mass diffusivity over time.

Lehtinen et al. (*Lehtinen et al.*, 1998) studied the condensation and/or evaporation of a multicomponent droplet. Their models were based on the elimination of the droplet surface temperature from the quasi-steady-state multicomponent mass and heat transfer equations of Newbold and Amundson (*Newbold and Amundson*, 1973). Under conditions in which Stefan diffusion was negligible the results were practically identical. However, in cases where the vapor pressure and mass transfer rates were high and the temperature difference between the gas and droplet large, there was a significant error associated with attempts to linearize the Clausius-Clapeyron equation, showing that a closed-form analytical solution to the multicomponent mass fluxes is possible. Once again in this work they continued to use the effective mass diffusion coefficient instead of a mass diffusion matrix approach to account for multicomponent mass transfer.

In 1976 Krishna and Standart (*Krishna and Standart*, 1976) first incorporated an expression for calculating multicomponent gas phase mass transfer coefficients by using an exact matrix method of solution to the Maxwell-Stefan equations. They compared their exact matrix method with linearized theory approach of Stewart and Prober (1964) and Toor (1964) which basically assumes that the matrix of diffusion coefficients [D] stays constant across the film. The comparison highlighted the inadequacies of the linearized theory approach for an example of an acetone and benzene droplet through a stagnant helium gas. In 1979 Krishna (1981) developed an alternate linearized theory of a non-iterative procedure for the calculation of the component molar fluxes for use in the prediction of multicomponent mass transfer. This procedure consists in assuming that the product of the bootstrap matrix known as [β] and the matrix of Fickian

diffusion coefficients [D] is constant along the diffusion path. However, in his discussion he emphasizes that there is no theoretical or experimental reason to suppose that the product of [β] and [D] is any less constant than the matrix [D].

In 1991 (*Aggarwal and Chen*, 1991) and again in 1997 (*Chen et al.*, 1997) investigations considered the dynamics and vaporization of both a pure and multicomponent fuel droplet in a laminar flow field. They considered the cases of evaporating droplets in a relatively low-temperature environment. Under these conditions the time scale associated with the rate of change of droplet size was not small compared with that of the transient liquid-phase process, unlike cases under high-temperature conditions. The theoretical and experimental study of the gasification behavior of a liquid droplet was done by using three different mathematical models: thin-skin, diffusion-limited, and infinite-diffusion. Again however, these models were all based on an effective mass diffusion constant. Nonetheless, results were obtained for hexane, decane, and a mixture of hexane and decane. For each case the predictions of the three vaporization models are compared with the experimental measurements. Their findings were that the vaporization behavior of a multicomponent fuel droplet is better simulated by the infinite-diffusion model. However, deviation between the infinite-diffusion and diffusion-limited models was not very significant, compared to the deviation seen by the thin-skin model.

In 1993 Taylor and Krishna published their in-depth coverage of multicomponent mass transfer. From this work the methodology of using a mass transfer matrix [D] instead of previously used binary mass transfer coefficient scalar to describe the transport phenomena in a two-phase multicomponent system was developed.

Despite the abundance of research focused on spray drying, evaporation of drops containing solids, spray combustion, and droplet vaporization, very few studies have analyzed

the evaporation of a binary droplet in a multicomponent system (*Krishna and Standart*, 1976). There is an absolute need to understand the unique transport phenomena seen in multicomponent liquid-phase mass transfer. In addition, both theoretical and experimental analysis is needed to fully characterize and understand the phenomena. With such work more progress can be made in improving heat and mass transfer capabilities in spray cooling and other applications.

CHAPTER 3: MODELING MULTICOMPONENT EVAPORATION

3.1 General Equations

The objective of this study is to model the changing vapor composition of a pure and binary evaporating droplet in a well-mixed gas environment. The model will be capable of predictions for systems of one or two liquid (and vapor) species and a single non-condensable gas species. The goal is to provide an accurate prediction of both pure and binary liquid evaporation under ambient pressure and temperatures ranging from $20^{o}C$ - $40^{o}C$. However, with validation the model will be capable of predictions beyond the tested temperatures and pressures.

3.1.1 Assumptions

The model assumes up to a three-component system in which one of the components is non-condensable and insoluble in the liquid phase. In this case the non-condensable was either air or nitrogen, depending on the experiment. The gas phase is assumed to be well-mixed with isolated, spherical liquid droplets falling vertically through the gas. It is assumed for both the liquid and vapor phase that there is no temperature or composition gradient within the phase. According to Landis and Mills (1974) the assumption of a well-mixed liquid phase is acceptable at lower temperatures (< 600K). Two independent system models are developed, one assumed an isobaric (or open system), while the second assumed a closed system. Both models can be

run with nitrogen or air as the non-condensable vapor species. The use of both of these models is necessary to capture the full range of test conditions.

The vapor phase is assumed to be ideal since >99% volume was air or nitrogen and the operating temperature and pressure remained near ambient. In addition, non-ideal gas behavior is characterized by system temperatures >100psi and reduced temperatures <0.8. In this research system pressures never exceeded 14 psi and reduced temperatures were >1.5. However, the liquid phase solution is considered non-ideal since distinctly different components (ethanol and water) made up the liquid droplet. This non-ideal solution behavior is taken into account in the modified Raoult's Law by the inclusion of activity coefficients for each component. Tabulated properties, such as liquid density, vapor density, liquid viscosity, vapor viscosity, liquid heat capacity, vapor heat capacity, and thermal conductivity, are used to generate temperature dependent curve-fits over temperature ranges which included $20^{o}C$ - $40^{o}C$. Both liquid and vapor property calculations use a composition weighted-average in determining the mixture properties. In the case where experimental values are not available, such as ethanol-water gas diffusivity, ethanol-nitrogen gas diffusivity, and water-nitrogen gas diffusivity, the Chapman-Enskog correlation (*Bird et al.*, 2002) was used to approximate the binary diffusivity coefficients.

By assuming all droplets are spherically symmetric with uniform initial temperature and composition it is determined that droplets had an average diameter of approximately 60 μm regardless of composition and droplet frequency. Were droplet frequency was adjusted between 25 drops/second and 1000 drops/second. The average droplet diameter is determined by an experiment where a known number of droplets were dispensed into a pre-weighed container, and then the liquid mass and density of the fluid is used to determine an average droplet size.

$$d_p = \left(6 \frac{\rho_l \cdot Freq}{\pi \cdot W^{total}} \right)^{-\frac{1}{3}} \tag{3.0}$$

where d_p is the average droplet diameter, ρ_l is the liquid density, $Freq$ is the total number of droplets dispensed, and W^{total} is the total measured fluid mass.

If the assumption of uniform initial temperature and composition from droplet to droplet is not made, it would be necessary to determine a method of measuring each individual droplet's initial temperature and composition. By assuming spherically symmetric droplets, and that droplets remained spherical throughout flight, we are able to proceed with a 1-dimensional mass and heat transfer model. Due to the relatively large average droplet size, increased pressure effects inside the drop (theory of corrected pressure) due to droplet curvature can be neglected. Droplet sizes that are significantly affected by internal pressure are typically on the order of droplet diameters $d_p \leq 1 \times 10^{-10} m$.

The MATLAB numerical program developed uses a numerical ordinary differential equation (ODE) solver for the initial value problem (IVP). The stiff integrator, ode15s, is chosen as an implicit, multi-step numerical differentiation solver of varying order (1^{st}-to 5^{th}-order), for its ability to solve stiff problems that require moderate accuracy. The infinite-diffusion unsteady-state theory is chosen as the mass transfer model, so that an arbitrary film thickness did not have to be calculated. The Ranz-Marshall correlation is used to relate the Nusselt number and the heat transfer coefficient. Since the gas phase was assumed ideal the Maxwell-Stefan diffusion coefficients are equal to the Fickian diffusion coefficients. The diffusion matrix is assumed spatially constant but changed temporally due to liquid-phase temperature and composition changes. In order to relate molar diffusion flux to molar flux the Stefan diffusion bootstrap method is used since the method assumed a non-condensing component.

3.1.2 Diffusion Theory

In an infinite-diffusion (surface renewal or penetration) model, the inherent assumption is that the internal fluid circulation is so fast that the droplet temperature and composition are maintained spatially uniform, though still temporally varying. In the surface renewal model, fluid elements (or eddies) arrive at the interface from the bulk fluid phase and reside at the interface for a period of time, t_{ep}, the exposure time. During the exposure time mass exchange takes place with the adjoining vapor phase by a process of unsteady-state diffusion, where the diffusion process is purely molecular. After exposure the fluid element returns to the bulk fluid phase and is replaced by fresh eddies. The vaporization process is expected to resemble that of batch distillation. The temporal variations of droplet composition and temperature are determined from the overall mass and energy conservation equations.

In diffusion-limited (or effective diffusivity) models, both temperature and composition gradients occur inside the droplet. The transient heat and mass transport in the liquid are assumed to be governed by the unsteady heat and mass diffusion equations. Since the droplet is evaporating, the diffusion field has a moving boundary. In this liquid heating model there is a spatially transient liquid phase process which is not present in the infinite-diffusion model.

The thin-skin model is based on the assumption of a high liquid Lewis number and a high droplet evaporation rate. Under these conditions, we may assume that the droplet surface temperature and concentration distributions remain constant. The thin-skin model is an extension of the single-component d^2 law to the multicomponent case.

In a film model, all the resistance to mass transfer is assumed to be concentrated in a thin film adjacent to the phase boundary. Mass transfer occurs within this film by steady-state molecular diffusion. In the bulk fluid, the level of mixing is so high that all composition gradients are eliminated. The thickness of this hypothetical film is in the range of 10-100μm for liquid phase transport (*Taylor and Krishna*, 1993). The diffusion process is fully determined by the one-dimensional steady-state form of the continuity equation in terms of molar flux.

3.1.3 Property Calculations

Pure fluid properties and constants for ethanol, water, air, and nitrogen are determined by curve fitting published data over a general temperature range of 250K-420K. In some cases the temperature ranges varied but all ranges included the key operating temperatures of 290K-320K. Pure fluid property equations, their temperature range, and reference are located in section A.4.

Average properties are used when a multicomponent liquid or vapor phase property is needed. In most cases these average properties, denoted by $\overline{Q}$, were simple weighted averages. For example, $\overline{Q} = Q_1 q_1 + Q_2 q_2 + Q_3 q_3$, where Q_i is the calculated pure property of component i and q_i is the mass or mole fraction of component i in the mixture.

3.1.4 Chapman-Enskog Theory

Chapman-Enskog Theory for low density gases is used to approximate the binary diffusivity coefficient for ethanol-water, ethanol-nitrogen, and water-nitrogen. (*Bird et al.*, 2002)

$$D_{ij} = \frac{0.0018583\sqrt{T^3\left(\frac{1}{MW_i}+\frac{1}{MW_j}\right)}}{P\sigma_{ij}^2\Omega_{ij}} \tag{3.1}$$

where $\kappa = 1.38066\times10^{-23}\ {}^{J}\!/_{K}$ is Boltzmann's constant, MW_i is the molecular mass of component i, Ω_{ij} is the Lennard-Jones collision integral for diffusion which is a function of dimensionless temperature:

$$\frac{\kappa T}{\varepsilon_{ij}} \tag{3.2}$$

T is temperature in K, and ε_{ij} is the Lennard-Jones parameter.

$$\varepsilon_{ij} = \sqrt{\varepsilon_i \varepsilon_j} \tag{3.3}$$

σ_{ij} is the Lennard-Jones molecular diameter, defined:

$$\sigma_{ij} = \frac{1}{2}\left(\sigma_i + \sigma_j\right) \tag{3.4}$$

Values for ethanol, water, air, and nitrogen are located in the appendix section A.4.1

3.2 Vapor Liquid Equilibrium (VLE)

An important assumption is that VLE exists between the droplet-vapor interfaces, thereby assuming minimal resistance to mass transfer via a thin film. The equilibrium mole fraction of the gas-phase at the liquid-vapor interface is calculated by knowing the liquid phase mole fraction and using Raoult's law:

$$y_i P = x_i P_i^{sat} \tag{3.5}$$

where P is the total pressure, y_i is the vapor phase mole fraction of component i, x_i is the liquid phase mole fraction of component i, and P_i^{sat} is the vapor pressure of the pure species i at the temperature of the system. Since P is defined as:

$$P = \sum_i x_i P_i^{sat} \tag{3.6}$$

We can re-write Raoult's law for a binary system as:

$$y_i = \frac{x_i P_i^{sat}}{x_i P_i^{sat} + x_j P_j^{sat}} \tag{3.7}$$

However, the above form of Raoult's law makes two assumptions: the vapor phase is an ideal gas, and the liquid phase is an ideal solution. The first assumption means that Raoult's law can apply only for low to moderate pressures. In the case of this study, an ideal gas is an appropriate assumption since pressures will not exceed ambient pressure. The second assumption implies that it can have approximate validity only when the species that comprise the system are chemically similar.

When at low to moderate pressures and when the liquid phase can no longer be assumed ideal a more realistic equation for VLE results when the second major Raoult's law assumption is abandoned, and the liquid phase non-ideality is accounted for by a factor, γ_i, inserted into Raoult's law.

$$y_i P = x_i \gamma_i P_i^{sat} \tag{3.8}$$

γ_i is known as the activity coefficient, and is a function of temperature and liquid-phase composition, but ultimately based on experiments. In the case of a non-ideal solution P can be defined as:

$$P = \sum_i x_i \gamma_i P_i^{sat} \tag{3.9}$$

Therefore, the modified Raoult's law can be written for a binary system as:

$$y_i = \frac{x_i \gamma_i P_i^{sat}}{x_i \gamma_i P_i^{sat} + x_j \gamma_j P_j^{sat}} \tag{3.10}$$

The vapor pressure of the pure species i at the temperature of the system, P_i^{sat}, is determined by the Antoine equation where Ψ', Ψ'', and Ψ''' are the Antoine coefficients and are specific for each component.

$$P_i^{sat} = 10^{\left(\Psi' - \frac{\Psi''}{\Psi''' + T}\right)} \tag{3.11}$$

The Antoine equation is a relatively simple empirical equation that correlates vapor pressure – temperature data extremely well.

The Van Laar equation is used in determining γ_i for calculating the non-ideal liquid vapor equilibrium at the droplet gas interface. In the binary case the Van Laar equation requires two binary interaction parameters E_{12} and E_{21}. Interaction parameters are specific for each binary component pair. The Van Laar equation is as follows:

$$\ln \gamma_i = E_{ij}\left[1 + \frac{E_{ij} x_i}{E_{ji} x_j}\right]^{-2} \tag{3.12}$$

values for ethanol and water are located in the appendix section A.4.2.

3.3 Conservation Equations

The current model is based on an unsteady-state, one-dimensional analysis of mass and energy change in an isolated falling liquid droplet in a well-mixed gas.

3.3.1 Conservation of Mass

The mass change of component i over time in one droplet is:

$$\frac{dm_i}{dt} = -\pi \cdot d_p{}^2 \cdot N_i \tag{3.13}$$

where m_i is the number of moles of component i, t is the model time, and N_i is the molar flux of component i with respect to a stationary reference.

3.3.2 Conservation of Energy

The average temperature change of one droplet over time is the summation of latent and sensible heat.

$$\frac{dT_l}{dt} = \alpha \cdot (T_v - T_l) - (\lambda_1 - \lambda_2) \cdot \frac{\pi \cdot d_p{}^2}{(M_1 + M_2) \cdot c_{p_l}} \tag{3.14}$$

Where T_l is the liquid droplet temperature, T_v is the vapor temperature, M_i is the mass of component i in a droplet, c_{p_l} is the liquid heat capacity of the droplet, λ_i is the latent heat of component i, and α is the heat transfer coefficient calculated from the Ranz-Marshall correlation for convective heat transfer between a droplet and the vapor.

$$\alpha = \frac{Nu \cdot \mu}{d_p} \tag{3.15}$$

where μ is the liquid mixture thermal conductivity, and Nu is the Nusselt number, defined by the Ranz-Marshall correlation as:

$$Nu = 2 + 0.6\,\mathrm{Re}^{1/2} \cdot \mathrm{Pr}^{1/3} \tag{3.16}$$

where Re is the Reynolds number,

$$\mathrm{Re} = \frac{\rho_v \cdot d_p \cdot u_p}{\eta_v} \tag{3.17}$$

and Pr is the Prandtl number,

$$\mathrm{Pr} = \frac{c_{p_v} \cdot \eta_v}{\mu_v} \tag{3.18}$$

u_p is the velocity of the droplet, η_v is the dynamic vapor viscosity, μ_v is the vapor thermal conductivity. To calculate the energy equation, the latent heat for each component was needed. However, since latent heat is defined from a temperature difference and an arbitrary reference temperature, T^{ref}, was chosen as the initial temperature. The numeric value of T^{ref} is insignificant since the value merely acts as a constant found for all evaporating components. The component latent heat is calculated from the following equation:

$$\lambda_i = \left(\Delta H^{ref} + c_{p_{i,v}}\left(T_v - T^{ref}\right)\right)N_{i,mass} \tag{3.19}$$

where $N_{i,mass}$ is the mass flux of component i with respect to a stationary reference, T^{ref} is the reference temperature, and ΔH is the change in enthalpy. Similar to the calculation of latent heat, ΔH requires a difference between the enthalpy at two different temperatures. Below are the corresponding equations to calculate the change in enthalpy for each evaporating component.

$$\Delta H_i^{ref} = \Delta H_i^{vap} + H_i\left(T^{vap}\right) - H_i\left(T^{ref}\right) \tag{3.20}$$

$$H_i\left(T^{vap}\right) = \int_0^{T^{vap}} c_{p_{i,v}}\, dT \text{ is the enthalpy at } T^{vap} \tag{3.21}$$

$$H_i\left(T^{ref}\right) = \int_0^{T^{ref}} c_{p_{i,v}}\, dT \text{ is the enthalpy at } T^{ref} \tag{3.22}$$

The energy conservation equation on the vapor side is more simplistic, where the average temperature change of the vapor space over time is directly calculated from the energy change in one droplet over time as follows:

$$\frac{dT_v}{dt} = -\frac{dT_l}{dt}\frac{(M_1 - M_2)\cdot c_{p_l}}{M_v^{total}\cdot c_{p_v}} \tag{3.23}$$

where M_v^{total} is the total mass of vapor in the evaporation chamber.

$$M_v^{total} = M_{1,v} + M_{2,v} + M_{3,v} \tag{3.24}$$

3.4 Surface Renewal Models

Surface renewal theory models fluid elements (or eddies) as arriving at the interface from the bulk fluid phase and residing at the interface for a period of time. During this exposure time mass exchange takes place between the liquid and vapor phase by unsteady-state diffusion. After exposure time the fluid element returns to the bulk liquid phase and is replaced by another fluid element from the bulk liquid.

The governing differential equations for unsteady-state diffusion process by the fluid element during its exposure time at the interface can be written as:

$$c^{total}\frac{\partial y_i}{\partial t} + \frac{\partial N_i}{\partial z} = 0 \tag{3.25}$$

where z represents the direction coordinate for diffusion and c^{total} is the total vapor concentration and y_i is the mole fraction. Summing the above equation for all species in the mixture gives:

$$\frac{\partial N^{total}}{\partial z} = 0 \tag{3.26}$$

from which we can conclude that the total mixture flux N^{total}, is not a function of position z and only dependent on time. Before the start of the diffusion process in each liquid droplet we have a uniform bulk composition, leading to the initial condition:

$$z \geq 0 \qquad t = 0 \qquad y_i = y_{i,b} \tag{3.27}$$

The boundary condition, at the liquid vapor interface, is assumed to be the equilibrium vapor composition based on the well-mixed bulk liquid composition after each fluid elements diffusion process, providing the boundary condition:

$$z = 0 \qquad t \geq 0 \qquad y_i = y_{i,e} \tag{3.28}$$

The classic penetration model of Higbie (1935) is based on the assumption that all the fluid elements reside at the interface for the same length of time. The surface age distribution for this model leads to the average mass transfer coefficient:

$$[k] = 2\frac{[D]^{1/2}}{\sqrt{\pi\, t_{ep}}} \tag{3.29}$$

where $[k]$ is the matrix of binary mass transfer coefficients. $[D]$ is the matrix of binary diffusion coefficients and will be discussed further in section 3.6 and is defined in Equation 3.60.

3.5 Mass Transfer Coefficients

The development for multicomponent mixtures is best carried out in the book by Taylor and Krishna (*Taylor and Krishna*, 1993). The following equations are heavily based from their work in which case $(n-1)$ dimensional matrix notation is used, where n is referred to as the total

number of components. We, therefore, define a matrix of finite flux mass transfer coefficients $[k^{\bullet}]$ by

$$(J) = (N) - (y)N^{total} = c^{total}[k^{\bullet}](y - y_e) = c^{total}[k^{\bullet}](\Delta y) \tag{3.30}$$

The finite flux coefficients are related to the zero-flux or low-flux coefficients by a matrix equation of the form

$$[k^{\bullet}] = [k][\Xi] \tag{3.31}$$

where $[\Xi]$ is a matrix of correction factors and (J) is the vector matrix of molar diffusion flux relative to molar average velocity. The calculation of the mass transfer coefficient matrices and the correction factor matrices for a multicomponent system can be sensitive to the mass transfer model chosen. In Equation 3.30 we define $(n-1)$ by $(n-1)$ elements of the mass transfer coefficients with the help of $(n-1)$ linear equations. It follows that the elements $k_{ij}^{\bullet}$ are not unique; that is, another set of these coefficients can also lead to the same value of the fluxes N_i. Put another way, making mass transfer measurements in a multicomponent system for the fluxes N_i and Δy_i does not uniquely determine the values of the mass transfer coefficients. A large set of measurements of N_i and Δy_i will be necessary to obtain a set of coefficients. In practice, a slightly different method is used, in which values of the multicomponent mass transfer coefficients are predicted from binary mass transfer correlations, using as a basis, the generalized Maxwell-Stefan equations.

3.5.1 Interaction Effects

Taking a look at the diffusion interaction effects with the help of Equation 3.30 and Equation 3.31, rewritten for a ternary system.

$$(J) = c^{total}\left[k^{\bullet}\right](\Delta y) = c^{total}\begin{bmatrix} k_{11}^{\bullet} & k_{12}^{\bullet} \\ k_{21}^{\bullet} & k_{22}^{\bullet} \end{bmatrix}\begin{bmatrix} \Delta y_1 \\ \Delta y_2 \end{bmatrix} \tag{3.32}$$

where

$$\begin{aligned}\left[k^{\bullet}\right] = [k][\Xi] &= \begin{bmatrix} k_{11} & k_{12} \\ k_{21} & k_{22} \end{bmatrix}\begin{bmatrix} \Xi_{11} & \Xi_{12} \\ \Xi_{21} & \Xi_{22} \end{bmatrix} \\ &= \begin{bmatrix} k_{11}\Xi_{11}+k_{12}\Xi_{21} & k_{11}\Xi_{12}+k_{12}\Xi_{22} \\ k_{21}\Xi_{11}+k_{22}\Xi_{21} & k_{21}\Xi_{12}+k_{22}\Xi_{22} \end{bmatrix}\end{aligned} \tag{3.33}$$

Therefore,

$$\begin{aligned} J_1 &= c^{total}k_{11}^{\bullet}\Delta y_1 + c^{total}k_{12}^{\bullet}\Delta y_2 \\ J_2 &= c^{total}k_{21}^{\bullet}\Delta y_1 + c^{total}k_{22}^{\bullet}\Delta y_2 \end{aligned} \tag{3.34}$$

Since, in general, $k_{12}^{\bullet}$, $k_{21}^{\bullet}$, $k_{11}^{\bullet}$, $k_{22}^{\bullet}$, and mole fractions Δy_1 and Δy_2 can take on any sign, depending on the physical constraint imposed on the system, we could encounter any one of the following situations.

1. Osmotic diffusion (*Toor*, 1957) is when even though the constituent driving force Δy_1 is zero, there could be a non-vanishing J_1. Or in other words there could be a diffusion flux of component 1 even in the absence of a composition gradient for component 1.

$$J_1 \neq 0 \qquad \Delta y_1 = 0 \tag{3.35}$$

2. A diffusion barrier is considered to exist for component 1 (*Toor*, 1957) if under a certain set of operating conditions and system properties the term $k_{12}^{\bullet}\Delta y_2$ may be of the same magnitude and

of opposite sign to $k_{11}^{\bullet}\Delta y_1$ leading to species 1 not diffusing at all despite a composition gradient for species 1.

$$J_1 = 0 \qquad \Delta y_1 \neq 0 \tag{3.36}$$

3. Species 1 experiences reverse diffusion (*Toor*, 1957) in the case that the term $k_{12}^{\bullet}\Delta y_2$ is larger and of opposite sign than $k_{11}^{\bullet}\Delta y_1$ giving rise to the possibility of species 1 diffusing in a direction opposite to that indicated by its own concentration gradient.

$$\frac{J_1}{\Delta y_1} < 0 \tag{3.37}$$

The ratio of the driving forces $\frac{\Delta y_1}{\Delta y_2}$ plays an important role in enhancing diffusion interaction effects in multicomponent mass transfer. Thus, a small cross-coefficient $k_{12}^{\bullet}$ may be linked to a large Δy_2, resulting in large interaction effects.

3.6 Boot-Strap Problem

Methods for estimating the low flux mass transfer coefficients $[k]$ and calculating the high flux coefficients $[k^{\bullet}]$ in order to calculate the diffusion fluxes J_i and the all important molar fluxes N_i are needed. N_i is needed because it is these fluxes that appear in the material balance equations. Therefore, even if J_i is known the molar fluxes N_i can not immediately be calculated because all n of these fluxes are independent, whereas only $(n-1)$ of the J_i are independent. One other piece of information is needed to calculate N_i; this additional relationship is dictated by the context of the particular mass transfer process. The problem of

determining the N_i knowing the J_i is referred to as the bootstrap problem. There are several special cases of the bootstrap problem.

Equimolar counter diffusion (or mass transfer) is when the total molar flux vanishes and the component molar fluxes N_i equal the corresponding molar diffusion fluxes J_i for all species of the mixture.

$$N_i = J_i \qquad \left(N^{total} = 0\right) \tag{3.38}$$

In multicomponent distillation the total flux N^{total} vanishes if the molar latent heats are assumed equal, then the total flux can be written as:

$$\sum_{i=1}^{n} N_i \Delta\lambda_i = 0 \tag{3.39}$$

In the cases of condensation mixtures the ratio of the component molar flux N_i to the total flux N^{total} are specified as the flux ratio, $\varsigma_i = \dfrac{N_i}{N^{total}}$, or when reaction stoichiometry dictates the flux ratios, the flux simplifies to:

$$N_i = \varsigma_i N^{total} \tag{3.40}$$

Then the following relationship between N_i and J_i can be established.

$$N_i = \frac{J_i}{\left(1 - \dfrac{y_i}{\varsigma_i}\right)} \tag{3.41}$$

Stefan diffusion is known as the case of mass transfer in a mixture where one component has a zero flux. This situation is very common for condensation in the presence of a noncondensing gas, evaporation in the presence of a noncondensing gas, or in absorption where one of the components of the gas stream is insoluble in the absorbing liquid and therefore has a

zero flux. In our case we have both the condensation and the evaporation in the presence of a noncondensing gas (air or nitrogen).

The component with zero flux is denoted as species n. Thus,

$$N_n = J_n + y_n N^{total} = 0 \tag{3.42}$$

The total molar flux N^{total} is, therefore, given by

$$N^{total} = \frac{-J_n}{y_n} \tag{3.43}$$

Thus, the relation that allows the calculation of the nonzero N_i from J_i is

$$\begin{aligned} N_i &= J_i + y_i N^{total} = J_i - \frac{y_i J_n}{y_n} \\ &= \left(1 - \frac{y_i}{y_n}\right) J_i - \frac{y_i}{y_n} \sum_{\substack{k=1 \\ k \neq i}}^{n-1} J_k \end{aligned} \tag{3.44}$$

The general bootstrap expression is derived as follows, where the generalized determinacy condition is written in the form

$$\sum_{i=1}^{n} \varpi_i N_i = 0 \tag{3.45}$$

where the ϖ_i can be considered to be the determinacy coefficients. To relate N_i to J_i we multiply Equation 3.44 by ϖ_i and then sum over all species to obtain,

$$\sum_{i=1}^{n} \varpi_i J_i + N^{total} \sum_{i=1}^{n} \varpi_i y_i = 0 \tag{3.46}$$

At this point the total flux N^{total} can be expressed in terms of the diffusion fluxes as

$$N^{total} = -\left(\sum_{i=1}^{n} \varpi_i J_i \Big/ \sum_{i=1}^{n} \varpi_i y_i \right) = -\sum_{k=1}^{n-1} \Lambda_k J_k \tag{3.47}$$

where the coefficients Λ_k are the determinacy coefficient parameters defined by

$$\Lambda_k = \frac{(\varpi_k - \varpi_n)}{\sum_{j=1}^{n} \varpi_j y_j} \tag{3.48}$$

Finally, N^{total} can be substituted to obtain

$$N_i = \sum_{k=1}^{n-1} \beta_{ik} J_k \tag{3.49}$$

where β_{ik} , the bootstrap coefficients are defined as

$$\beta_{ik} \equiv \delta_{ik} - y_i \Lambda_k \tag{3.50}$$

where δ_{ik} is the Kronecker delta.

For Stefan diffusion we make all the ϖ_i zero except for one which has to have a value of one. In which case Equation 3.50 simplifies to

$$\beta_{ik} \equiv \delta_{ik} + \frac{y_i}{y_n} \tag{3.51}$$

Where the bootstrap matrix $[\beta]$ can be written for the ternary case as

$$[\beta] = \begin{bmatrix} 1 + \frac{y_1}{y_3} & \frac{y_1}{y_3} \\ \frac{y_2}{y_3} & 1 + \frac{y_2}{y_3} \end{bmatrix} \tag{3.52}$$

Therefore, the required molar flux expression is as follows

$$(N) = [\beta](J) \tag{3.53}$$

3.7 Binary Diffusion Coefficient Matrix

For ideal gases $[D]=[B]^{-1}$, where (3.54)

$$[D]=\begin{bmatrix} D_{11} & D_{12} & \Lambda & D_{1,n-1} \\ D_{21} & D_{22} & \Lambda & D_{2,n-1} \\ \mathrm{M} & & & \mathrm{M} \\ D_{n-1,1} & D_{n-1,2} & \Lambda & D_{n-1,n-1} \end{bmatrix} \tag{3.55}$$

is the matrix of binary diffusion coefficients for each binary component pair. The matrix [D] is a $(n\times 1)$ dimensional square matrix. [B] is the matrix function of inverted binary diffusion coefficients and is also a $(n\times 1)$ dimensional square matrix.

$$B_{ii}=\frac{y_i}{D_{in}}+\sum_{\substack{k=1\\ i\neq k}}^{n}\frac{y_k}{D_{ik}} \tag{3.56}$$

$$B_{ij}=-y_i\left(\frac{1}{D_{ij}}-\frac{1}{D_{in}}\right) \tag{3.57}$$

$$[B]=\begin{bmatrix} B_{11} & B_{12} & \Lambda & B_{1,n-1} \\ B_{21} & B_{22} & \Lambda & B_{2,n-1} \\ \mathrm{M} & & & \mathrm{M} \\ B_{n-1,1} & B_{n-1,2} & \Lambda & B_{n-1,n-1} \end{bmatrix} \tag{3.58}$$

In the case of this research $n=3$ (ethanol =1, water =2, and air =3), therefore, [D] and [B] are both $(2x2)$ dimensional matrices of the form

$$[B]=\begin{bmatrix} \frac{y_1}{D_{13}}+\frac{y_2}{D_{12}}+\frac{y_3}{D_{13}} & -y_1\left(\frac{1}{D_{12}}-\frac{1}{D_{13}}\right) \\ -y_2\left(\frac{1}{D_{12}}-\frac{1}{D_{23}}\right) & \frac{y_1}{D_{12}}+\frac{y_2}{D_{23}}+\frac{y_3}{D_{33}} \end{bmatrix} \tag{3.59}$$

$$[D]=\begin{bmatrix} \frac{1}{\|B\|}B_{22} & -\frac{1}{\|B\|}B_{12} \\ -\frac{1}{\|B\|}B_{21} & \frac{1}{\|B\|}B_{11} \end{bmatrix} \tag{3.60}$$

where exact values for the binary diffusion coefficient pairs are located in the appendix A.4.1.

For the case of a non-ideal system the relation between the matrix of Fick diffusion coefficients and Maxwell-Stefan diffusion coefficients is

$$[D]=[B]^{-1}[\Gamma] \tag{3.61}$$

where $[\Gamma]$is the thermodynamic factor matrix. $[\Gamma]$ is calculated using the Van Laar activity coefficient model for a binary system

$$\Gamma_{ij}=\delta_{ij}+x_i\frac{\partial \ln \gamma_i}{\partial x_i} \tag{3.62}$$

Solving for $\frac{\partial \ln \gamma_i}{\partial x_j}$ from the Van Laar model yields a thermodynamic factor matrix, for a ternary system of the form

$$[\Gamma]=\begin{bmatrix} 1+x_1\frac{\partial \ln \gamma_1}{\partial x_2} & x_1\frac{\partial \ln \gamma_1}{\partial x_2} \\ x_2\frac{\partial \ln \gamma_2}{\partial x_1} & 1+x_2\frac{\partial \ln \gamma_2}{\partial x_1} \end{bmatrix} \tag{3.63}$$

where the $\frac{\partial \ln \gamma_i}{\partial x_j}$ are defined as follows:

$$\frac{\partial \ln \gamma_1}{\partial x_2}=\frac{2B_{12}}{\left(1+\frac{B_{12}x_1}{B_{21}x_2}\right)^3}\left(\frac{B_{12}}{B_{21}x_2}+\frac{B_{12}x_1}{B_{21}{x_2}^2}\right) \tag{3.64}$$

$$\frac{\partial \ln \gamma_2}{\partial x_1} = \frac{2B_{21}}{\left(1+\frac{B_{21}x_2}{B_{12}x_1}\right)^3}\left(\frac{B_{21}}{B_{12}x_1}+\frac{B_{21}x_2}{B_{12}x_1^{\,2}}\right) \tag{3.65}$$

3.8 Toor-Stewart-Prober Formulation

The solution to the linearized equations is a special case of an exact solution of the Maxwell-Stefan equations. The non-linear continuity equation for multicomponent diffusion can be written as

$$\frac{\partial(c)}{\partial t} + \nabla \cdot \left(N^{total} \cdot (x)\right) = \nabla \cdot \left(c^{total}\,[D] \cdot (\nabla x)\right) \tag{3.66}$$

where (c) is the matrix vector of component concentrations. The non-linear equation above represents a set of $(n-1)$ coupled partial differential equations. The basis of the method put forward by Toor (1964) and by Stewart and Prober (1964) is the assumption that c^{total} and $[D]$ can be considered constant. With these assumptions Equation 3.66 can be reduced to

$$c^{total}\,\frac{\partial(x)}{\partial t} + \nabla \cdot \left(N^{total} \cdot (x)\right) = c^{total}\,[D] \cdot \left(\nabla^2 x\right) \tag{3.67}$$

For the multicomponent penetration model, the following expression for the matrix of mass transfer coefficients is obtained:

$$\left[k^{\bullet}\right] = [\mathcal{P}]\ \left[\hat{k}^{\bullet}\right]\ [\mathcal{P}]^{-1} \tag{3.68}$$

where $[\mathcal{P}]$ is the modal invertible matrix whose columns are the eigenvectors of $[D]$, $[\mathcal{P}]^{-1}$ is the inverse of the modal invertible matrix, and $\left[\hat{k}^{\bullet}\right]$ is a diagonal matrix whose nonzero elements are the eigenvalues of $\left[k^{\bullet}\right]$

$$\hat{k}_i^{\bullet} = \hat{k}_i \hat{\Xi}_i \tag{3.69}$$

and where

$$\hat{k}_i = 2\sqrt{\frac{\hat{D}_i}{\pi\, t_{ep}}} \tag{3.70}$$

$$\hat{\Phi}_i = \frac{N^{total}}{c^{total} \hat{k}_i} \tag{3.71}$$

$$\hat{\Xi}_i = \frac{\exp\left(\frac{\hat{\Phi}_i^2}{\pi}\right)}{1 + erf\left(\frac{\hat{\Phi}_i}{\sqrt{\pi}}\right)} \tag{3.72}$$

These are the eigenvalues of $[k^{\bullet}]$ the matrix of mass transfer coefficients, $[\Phi]$ the mass transfer rate factor, and $[\Xi]$ the high flux correction factor matrix, respectively.

The matrix of mass transfer coefficients can be determined by:

$$[k^{\bullet}] = \frac{\hat{k}_1^{\bullet}[[D] - \hat{D}_2[I]]}{\hat{D}_1 - \hat{D}_2} + \frac{\hat{k}_2^{\bullet}[[D] - \hat{D}_1[I]]}{\hat{D}_2 - \hat{D}_1} \tag{3.73}$$

where $[I]$is the identity matrix. Equation 3.73 may be expanded as follows:

$$k_{11}^{\bullet} = \frac{\hat{k}_1^{\bullet}(D_{11} - \hat{D}_2)}{\hat{D}_1 - \hat{D}_2} + \frac{\hat{k}_2^{\bullet}(D_{11} - \hat{D}_1)}{\hat{D}_2 - \hat{D}_1} \tag{3.73(a))}$$

$$k_{12}^{\bullet} = \frac{(\hat{k}_1^{\bullet} - \hat{k}_2^{\bullet})}{\hat{D}_1 - \hat{D}_2} D_{12} \tag{3.73(b))}$$

$$k_{21}^{\bullet} = \frac{(\hat{k}_1^{\bullet} - \hat{k}_2^{\bullet})}{\hat{D}_1 - \hat{D}_2} D_{21} \tag{3.73(c))}$$

$$k_{22}^{\bullet} = \frac{\hat{k}_1^{\bullet}(D_{22} - \hat{D}_2)}{\hat{D}_1 - \hat{D}_2} + \frac{\hat{k}_2^{\bullet}(D_{22} - \hat{D}_1)}{\hat{D}_2 - \hat{D}_1} \tag{3.73(d))}$$

Equation 3.68 serves as a starting point for computing the mass transfer coefficients and, hence, the molar fluxes.

3.9 Solution Algorithm

Using Equation 3.59 calculate the matrix of Fick diffusion coefficients $[B]$ and then from Equation 3.60 calculate the Maxwell-Stefan diffusion coefficient matrix $[D]$ while assuming an ideal gas. Once the diffusion coefficient matrix is known the eigenvalues $\hat{D}_i$ can be determined.

Using Equation 3.70, and first assuming $[\Xi]=[I]$, calculate eigenvalues $\hat{k}_i$ of the mass transfer matrix $[k]$. At this point, from knowing the mass transfer matrix eigenvalues the mass transfer matrix $[k]$ can be determined from substitution of Equation 3.31 into Equation 3.73. Next, calculate $[\beta]$ from Equation 3.52 while using the equilibrium vapor mole fractions corresponding to the liquid droplet mole fractions.

The molar diffusion flux matrix (J) is then calculated from Equation 3.32, with the initial guess that $[\Xi]=[I]$. The molar flux matrix (N) can then be calculated with the use of Equation 3.53, and the total molar flux, N^{total}, is calculated from the Stefan diffusion bootstrap relation found in Equation 3.44. However, the equation needs to be solved in terms of the liquid mole fractions, $N_i = J_i + x_i N^{total}$. Once all the molar fluxes are known N^{total} can be determined by summing all the component molar fluxes noting that N_3 (corresponding to the non-condensable component) is zero.

Now that an initial estimate of molar flux has been made, the next step is to calculate $\hat{\Phi}_i$ for each diffusing component from Equation 3.71. Then new values of $\hat{\Xi}_i$ can be calculated for each diffusing component using Equation 3.72. With a new high flux correction it is necessary to calculate a corresponding value of $\hat{k}_i^{\bullet}$ for each diffusing component using Equation 3.69. From the eigenvalues, use Equation 3.73 to determine the new matrix $\lfloor k^{\bullet} \rfloor$. Finally, repeat the above process from the calculation of (J) with Equation 3.32 through the calculation of $\lfloor k^{\bullet} \rfloor$ until convergence of the molar flux matrix is met. In our case the convergence was set at $\left| N_1^{old} - N_1^{new} \right| = 10^{-16}$ and $\left| N_2^{old} - N_2^{new} \right| = 10^{-16}$.

CHAPTER 4: MATERIALS AND METHODS

The difficulty in validating a multicomponent fluid evaporation model, is obtaining the necessary measurements. A Particle Image Velocimetry/Planar Laser-Induced Fluorescence (PIV/PLIF, from TSI) can be used to measure in-flight liquid droplet and vapor composition, however, this equipment would still only provide a volume average analysis, and was not available for use while research was in progress. As research progressed it was determined that there really is no such analysis tool available for in-flight monitoring of multicomponent concentrations, while this did not prove to be a stopping point in the present research, it did pinpoint the need for development of capable equipment. It was possible, however, to use a Fourier Transform Infrared (FTIR) Spectrometer to analyze a stationary vapor composition along the path of the Infrared beam, and thermocouples to monitor system temperatures.

Knowing the rate of increase or decrease of ethanol and water in the vapor space, and the temperature trend, it is possible to estimate the average rate of evaporation or condensation of each component per droplet. More precisely, the evaporation process will progress as a changing rate of evaporation; as the vapor composition approaches the equilibrium state (defined by the vapor temperature, vapor initial composition, and inlet liquid composition) the rate of evaporation will decrease.

Since the liquid inlet temperature and liquid inlet composition will remain constant throughout each experiment and the vapor composition and vapor temperature will only be affected by the successive evaporation of individual droplets and ambient heat transfer, it is reasonable to assume that the final steady state should be the vapor-liquid equilibrium (VLE) associated with the final vapor temperature, pressure, and initial liquid composition. Due to the

small size of the droplets in comparison to the total vapor space volume, this transition to equilibrium will be very slow; this is why an experimental system has been designed to allow for drop-on-demand droplet frequencies upwards of 1000 drops/second. It is the goal that by increasing the droplet frequency we minimize the experiment duration while still capturing the concentration trend. Figure 2 is a block diagram of the experimental design; the dashed blue lines represent the flow of data or signals, and solid red lines represent the flow of power.

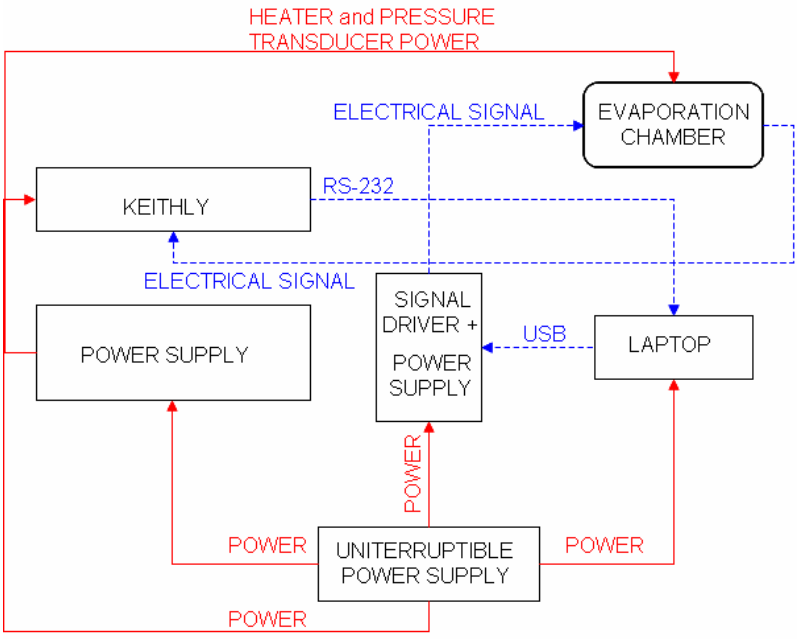

Figure 2: Block Diagram of Experiment Design

4.1 Experimental Apparatus Design

Several detailed drawings of the experimental apparatus can be found below in Figure 3, Figure 4, and Figure 5. The experimental apparatus structure consists of an evaporation chamber and a liquid recovery chamber, both manufactured out of 6061 Aluminum Alloy. Additional critical equipment/parts associated with the design include: an ActivePipette (pico-pipette), a

fluid delivery system and signal driver, inlet/outlet vapor ports, ZnSe (Zinc-Selenide) view windows, T-type thermocouples and data acquisition system, and thin film heaters and power supply.

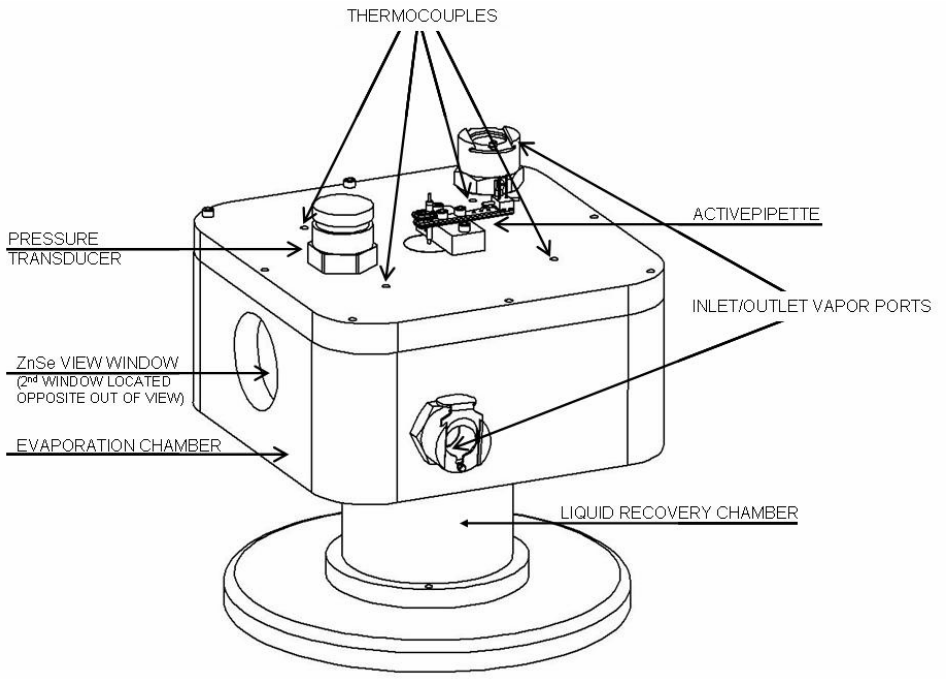

Figure 3: External Sketch of Experimental Apparatus

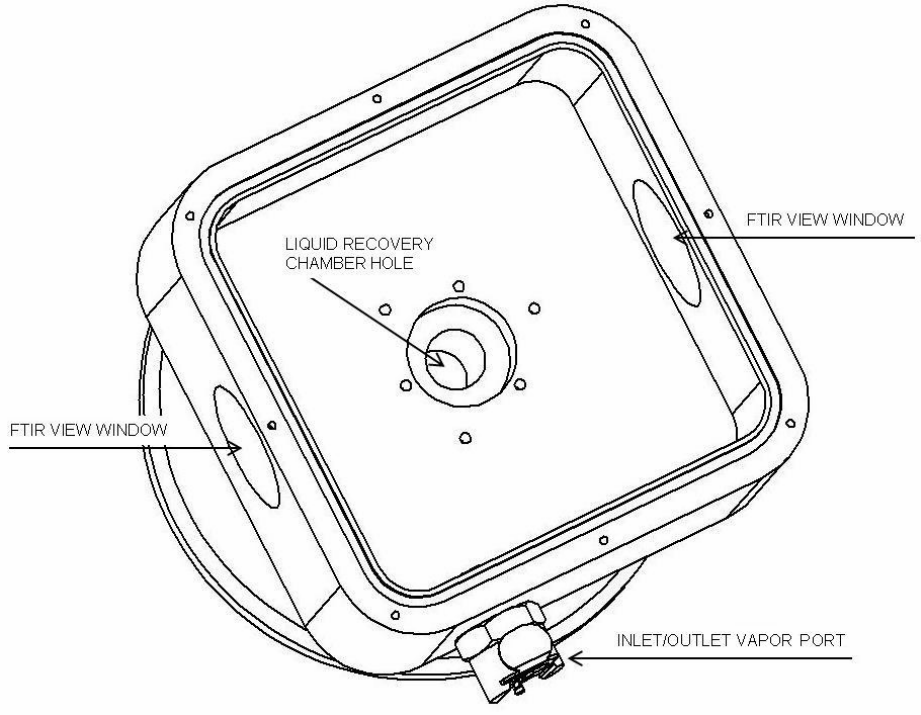

Figure 4: Internal Sketch of Experimental Apparatus

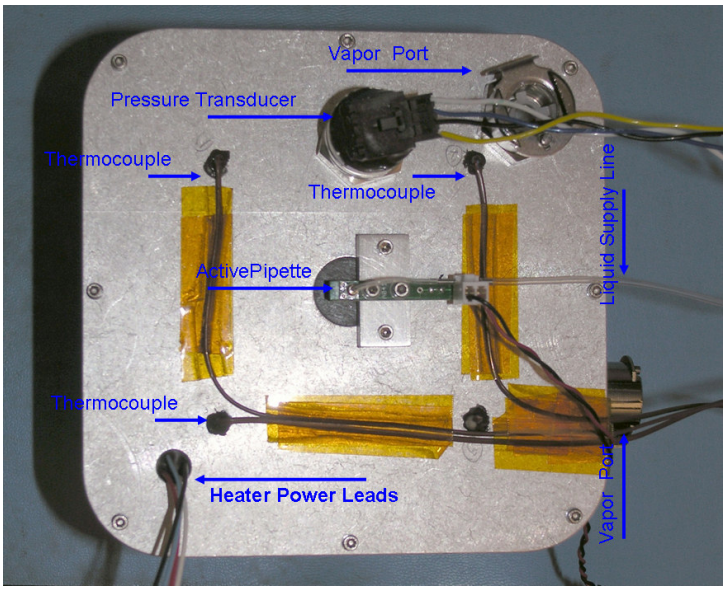

Figure 5: Top-Side View of Experimental Apparatus

The ActivePipette is mounted into the top of a curved-cubical evaporation chamber with the nozzle tip located inside the evaporation chamber (seen in Figure 3 through Figure 5). The pipette injects droplets into the center of the evaporation chamber, the droplets the free-fall vertically while evaporating before passing between the evaporation chamber and liquid reservoir chamber and settling in the liquid reservoir chamber. Tests were conducted to verify that the evaporating droplet path was consistently straight, thus eliminating the chances of liquid accumulation at the bottom of the evaporation chamber.

Figure 6 shows a sketch of the ActivePipette. Attached to the ActivePipette is the fluid-delivery-system (Figure 7). The fluid-delivery-system consists of a reservoir bottle, 2 µm solvent filter, priming syringe, air tube, 3-way valve, fluid supply tube, and electrical signal connection.

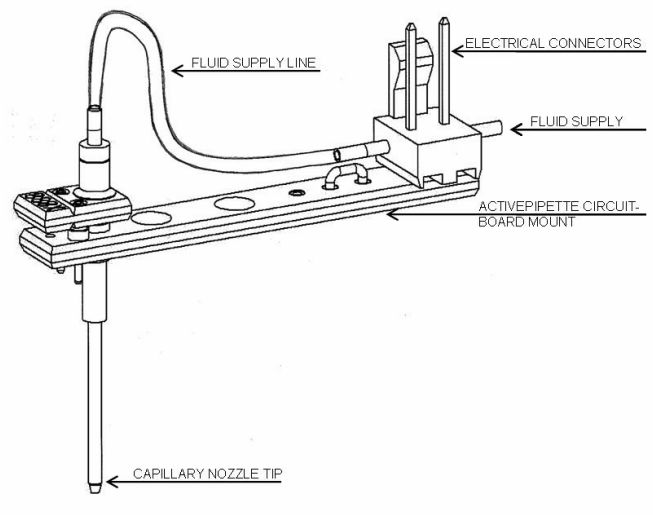

Figure 6: Sketch of ActivePipette

The evaporation chamber is built with two inlet/outlet vapor ports for purging purposes (nitrogen or dry air, as needed). One vapor port is located on the evaporation chamber lid while the other is located along the bottom 1/3rd of the evaporation chamber. This arrangement is to allow for better circulation of the purging gas than if both ports were located on the chamber lid. Thus vapor can be pumped into the side vapor port while simultaneously a vacuum is being pulled on the top vapor port. Purging is used to evacuate the evaporation and liquid recovery chambers of any trace of water or ethanol vapor. In other words, purging is only used when both the initial water vapor and the initial ethanol vapor concentrations in the chamber vapor space need to be zero.

A 0-30pisa pressure transducer is threaded into the lid of the evaporation chamber so that internal pressure can be monitored. The fitting was built in such a way that the pressure transducer can be removed and replaced with a pressure relief valve (PRV). While the PRV was never used in this research it is possible that future work may require its use.

Glued into place, on opposite sides of the evaporation chamber, are two ZnSe crystal FTIR view windows (perpendicular to droplet flight). These windows allowed for an air-tight seal while enabling the FTIR to measure concentrations within the chamber.

Three T-type thermocouples are used to monitor vapor temperature within the evaporation chamber vapor space, and one T-type thermocouple is used to monitor the ambient lab temperature.

Located around the full inner circumference of the evaporation chamber are three thin film Kapton heaters. The heaters varied in length and resistance to accommodate their placement between the ZnSe windows and vapor port. Heaters are arranged in parallel to minimize the quantity of wires protruding through the chamber.

The liquid recovery chamber is attached directly to the bottom of the evaporation chamber and opposite from the pico-pipette inlet. With the exception of a single vertical trough (0.55 inch diameter and 0.646 inch depth) located at the center of the chamber, the liquid recovery chamber is a solid piece of 6061 Aluminum Alloy. The design of the trough was two-fold, to minimize any secondary liquid evaporation which may have occurred due to un-evaporated droplets, while still recovering 100% of un-evaporated droplets. Visual verification of 100% non-evaporated liquid accumulation was satisfied in each experiment with the presence, if any, of liquid at the bottom of the liquid reservoir but no liquid accumulation along the bottom of the evaporation chamber.

4.1.1 FTIR and OMNIC Interface

The FTIR (Nicolete 4700 from Thermo Electron Corporation) will enable single point analysis of the vapor space composition. Changes will be seen as a result of each successive droplet's total mass loss/gain to due to evaporation/condensation while in the chamber. This single point is actually more like a constant line segment through the vapor volume. Since the FTIR measures the absorbance of light through the entirety of its beam length, the concentration is actually an average concentration measurement within the chamber along the beam path. This point of analysis will always remain constant throughout an experiment run, and the ambient vapor concentration will not factor into the measured concentration since a background scan is always taken at the beginning of each experiment and its result is subtracted from the absorbance measurement. The evaporation chamber and assembly will be located within the FTIR so that the IR beam can be passed through the evaporation chamber via the two ZnSe windows. Since the FTIR measures the absorbance at specific wavelengths it is necessary to calibrate with known concentrations of water and ethanol so that a correlation between absorbance and concentration for the desired wavelengths can be determined. See section 5.2.3 for more information on Beer's Law and correlating absorbance to concentration. Section A.5.4 contains data and figures regarding the absorbance - concentration calibration in Figures 74 through Figure 70.

ZnSe windows (Zinc Selenide windows from Thermo Electron Corporation) are chosen because they are not affected by moisture vapor or liquid water and have IR range between 10,000 – 550 cm^{-1}. All other potential windows, including ZnSe, and BaF_2, are slightly water soluble and in the event of a highly humid chamber environment could become fogged, preventing accurate measurements of the vapor composition.

Once each succession of droplets has been dispensed into the evaporation chamber, OMNIC, a software program connected to the FTIR along with a programmable interface (MacrosBasic) was used to direct the FTIR to take a data point reading of the concentrations in the chamber. Section A.5.6 contains an image of the MacrosBasic programmable interface and the program used to designate a time interval between FTIR scans (Figure 72). The OMNIC program is used in the collection of FTIR images for the droplet evaporation experiments. From these concentration readings we are able to calculate the respective mass fraction, mole fraction, or total mass of each component. Therefore, over the duration of the experiment these single point readings are combined to generate a pure and multicomponent evaporation curve, and combined with the monitored vapor temperature we can obtain a complete picture of the evaporation trend in a pure or multicomponent environment. Section A.5.6 contains images from the OMNIC analysis system where the peaks for both ethanol and water are isolated during the testing of a multicomponent mixture droplet (Figure 73 through Figure 76).

4.1.2 Power Supply and Heater

The heaters served one of two purposes depending on the experiment. For the majority of experiments the heaters were used to "pre-heat" the vapor space so that experiments could all begin at the same initial vapor temperature regardless of any day to day differences in ambient lab temperature. Once the desired "pre-heat" temperature was reached and the experiment started, the heaters were turned off. In the case of Test #30, however, the heaters were used to manually control the internal chamber temperature to something greater than the ambient

temperature. This type of experiment is important so experimental and various temperatures can be verified against the mathematical system model.

Power is provided to the three Kapton (insulated) heaters (from Minco) by a, 6603A - 3 Amp/60 Volt DC power supply (from SpenceTek). The Kapton heaters have the following dimensions and specifications: 1.5 in x 1.5 in and 11.0 Ohms, 1.5 in x 3.0 in and 6.6 Ohms, and 1.5 in x 6.0 in and 4.2 Ohms. The heaters were connected in parallel, to minimize the number of wires exiting the evaporation chamber lid, and then connected to the power supply.

4.1.3 Thermocouples and Data Acquisition System

A 2700 Multimeter Keithly Data Acquisition System (from Keithly) is used to record thermal resistances measured by three T-type thermocouples located within the upper vapor space of the evaporation chamber, and one located outside the chamber monitoring ambient temperature. T-type thermocouples have a published temperature range of -200^{o}C to 400^{o}C with a resolution of 0.0001^{o}C (Model 2700 User's Manual 3-33). The thermocouples are calibrated by comparison with a calibrated thermocouple (J-type) and thermometer (Fluke 54 II). Calibration data can be found in section A.5.3 in Table 6 and Table 7. The Keithly acquisition system is connected via RJ232 cord to a computer where the user interface ExceLINX is used to record values from the four thermocouples. Images of the ExceLINX input pages are found in section A.5.2 in Figure 64 and Figure 65.

The three internally located thermocouples are inserted through the evaporation chamber lid until they hang approximately 1 inch into the vapor space below the chamber lid. The

thermocouple monitoring the ambient temperature is suspended in the air approximately 5 cm-10 cm from the experiment.

To cancel the effects of unwanted thermal voltage, the thermocouple circuit requires a reference junction that is at a known temperature. A reference junction is the cold junction in a thermocouple circuit which is held at a stable, known temperature. It is at the cold junction where dissimilar wire connections must be made. The standard reference temperature is the ice point ($0^{o}C$). The ice point can be precisely controlled, and the National Bureau of Standards uses it as the functional reference for its voltage-to-temperature conversion tables. However, other known temperatures can be used. There are two ways for Model 2700 to acquire the cold junction temperature. It can measure the cold junction using a thermistor or 4-wire RTD, or the known temperature value can be entered by the user. There are three reference junction types supported by Model 2700: simulated reference junction, internal reference junction, and external reference junction. The internal reference junction was used in the research; this implied that a temperature transducer was used to measure the cold junction. In this case the cold junction is the screw terminal, with voltage temperature sensors strategically placed to measure the temperature of the cold junction. A table summarizing the Type T polynomial associated with temperature as a function of voltage is located in section A.5.3 in Table 8.

4.1.4 ActivePipette System and Signal Driver Interface

A long-tip ActivePipette (pico-pipette from Engineering Arts) is used for the consistent generation of individual liquid droplets (see Figure 7). The ActivePipette works on an electric signal where every second a user defined frequency of liquid drops are formed and dispensed.

The Signal Driver Interface allows the user to define a drop-on-demand signal pulse-shape (Figure 8) which allows a droplet frequency between 1 Hz – 1,000 Hz (1 Hz = 1 droplet/second). The ActivePipette is mounted on the center top of the evaporation chamber so that drops can vertically fall through the evaporation chamber and evaporate, before accumulating in the reservoir chamber. Section A.5.1 contains a listing of the ActivePipette System Operating Specifications (Table 5).

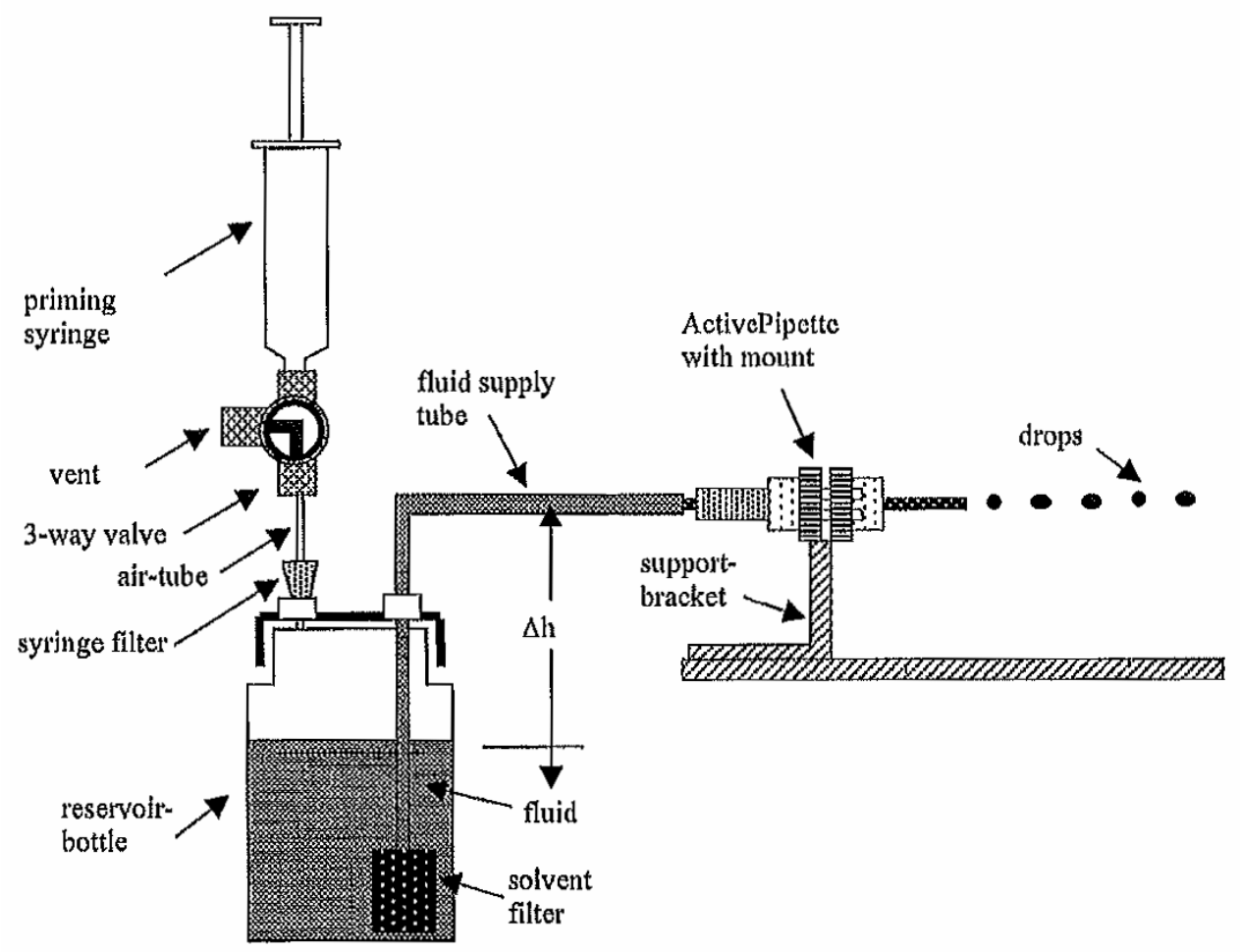

Figure 7: Sketch of ActivePipette System

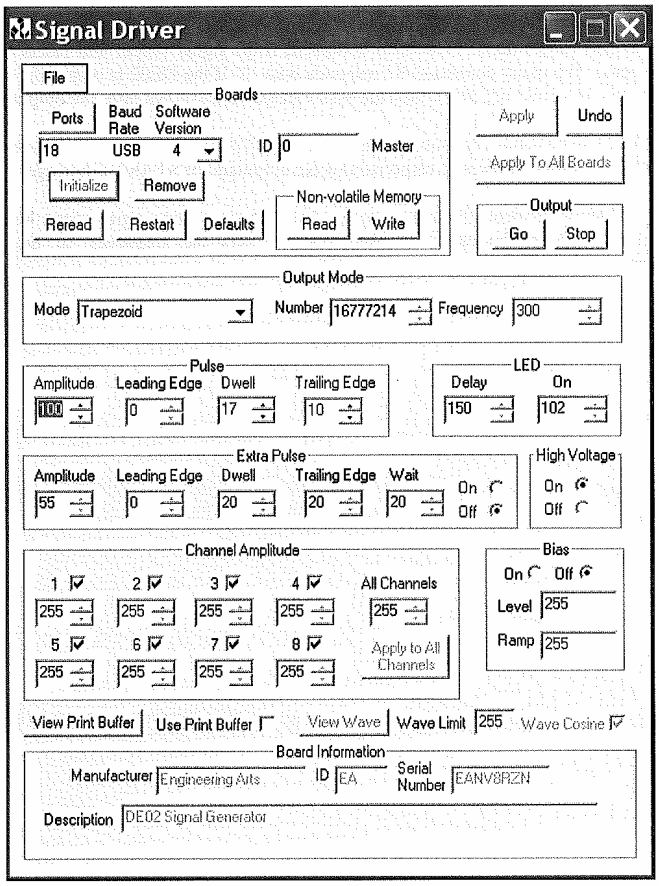

Figure 8: Signal Driver Interface Input Parameter Page

The ActivePipette (pico-pipette) consists of a glass capillary inside a piezoelectric element potted in a metal housing. A circuit-board with two gold-plated pins provides the electrical interface to the piezoelectric element. Applying an electrical pulse to the two pins causes a drop of fluid to be ejected from the glass capillary nozzle. A 20 gauge stainless steel tube provides the fluid interconnection and a 2-pin header provides the electrical connection.

The Reservoir System supplies the system fluid to the pipette. The fluid is filtered by a 2 μm filter. A Teflon supply tube connects directly to the 20 gauge tube. Relative pressure, defined as the pressure head between the fluid supply reservoir-bottle and the nozzle, plays an important role in the Active Pipette operation. Adjusting the height of the reservoir-bottle relative to the nozzle regulates the relative pressure. The height of the fluid in the reservoir-

bottle should be equal to or lower than the nozzle height. In the case of fluids with higher surface tension, like water for example, the fluid leveling the reservoir-bottle can be ±5.0 inches above or below the pipette nozzle.

The Signal Driver provides the electrical drive signal to dispense drops from the ActivePipette. The Signal Driver and user interface allows the drive signal pulse-shape to be tuned for optimal dispensing performance (Figure 8). Actuating the piezoelectric element of the pipette induces momentary regions of negative pressure in the fluid. This can drive dissolved gasses in the fluid out of solution. The resulting air bubbles can interfere with the proper functioning of the pipettes. Therefore, all fluids must be degassed prior to supplying them to the pipettes. Further information of the degassing of the liquid sample can be found below in section 4.1.5.

An important feature of the ActivePipette is that the system is not rated for use under pressure. The reasoning is that if enough pressure builds in the evaporation chamber it could counteract the siphoning action and cause fluid to be pushed back into the reservoir. It is plausible to suggest that with enough pressure head on the reservoir side that the tolerable pressure could be increased by increasing the elevation of the reservoir bottle above the nozzle tip. However, the height to internal pressure relationship was not investigated.

4.1.5 Fluids

Absolute 200 proof, non-denatured, ethyl alcohol (AAPER Alcohol and Chemical Company), and reagent grade (ASTM, CAP and NCCLS Type I) filtered Water with a resistance of 18.1 m-Ohms (NANOpure Infinity Model D8991) were used as my stock solutions for

evaporation experiments. For pure ethanol experiments compressed nitrogen (Oxarc) was used to purge the system prior to the FTIR background scan. This eliminates the possibility of the initial ambient humidity playing a role in the equilibrium concentration of ethanol. However, in all experiments using water or a water mixture the system was not purged with nitrogen, in which case the initial water humidity must be figured into the final concentration values. The compressed nitrogen was also used to purge the internal reservoir of the FTIR. This was done to eliminate the possibility of erroneous water contamination measurements sometimes observed when the FTIR is not purged.

Due to requirements surrounding the operation of the Active Pipette all fluids are degassed at approximately -29 inHg until bubble generation stops. In the case of fluid mixtures, degassing becomes more difficult because the fluids have to be degassed separately and then mixed together to maintain a bulk component concentration. The 2 μm filter had to be submerged in fluid during the degas process; therefore the liquid component which would make up the greatest concentration of the total mixture was the fluid the filter was submerged in. Once both fluids were degassed and mixed, the fluid line was flushed to remove approximately 10 mL from the filter. Since the filter only holds 3 mL, flushing 10 mL out of each bottle allowed for several mL of bulk fluid to be circulated through the filter before experiments begin. These additional steps were done so that the filter would not be overly concentrated with either fluid but would be a mix of the bulk fluid composition. This is important because the flow rate out of the reservoir-bottle through the fluid-deliver-lines is very small, therefore a significantly different concentration in the filter from the bulk fluid could cause dramatic errors in experiments simply because the initial fluid concentration may not be constant or known.

4.2 Procedures

To prepare the chamber for testing, seal the evaporation chamber lid. Make sure that ZnSe view windows are not being obstructed from the inside or outside. In all cases this obstruction has been wires from the heaters. Before all tests the FTIR internal chamber must be purged. This is done by connecting the compressed nitrogen line to the FTIR intake regulator, and allowing system to flow for a minimum of 5 minutes.

If a pure ethanol experiment is being run, then a nitrogen purge is necessary. To prepare for a nitrogen purge, connect a compressed nitrogen tank line to one vapor port on the evaporation chamber and connect a vacuum line to the unused vapor port. Begin the flow of nitrogen into evaporation chamber and turn on the vacuum. This process will simultaneously pull any gas/vapor out of the chamber and fill the chamber with nitrogen gas. Therefore, experimental conditions can assume no initial water vapor despite the lab humidity.

Once the chamber is sealed and purged (when necessary), place the chamber assembly on the FTIR base plate; connect the power supply to the heater connection, and turn on the Keithly, Power Supply, and Laptop. Next, begin heating the chamber. An initial vapor temperature of $30^{o}C$ is used in order to accelerate evaporation at the beginning of each experiment. While the chamber is being heated the FTIR analysis program and interface can be initialized. To ensure that the FTIR is operating properly run through a manual diagnostic check by using the sight measurement to adjust chamber assembly into the best location on FTIR base-plate. The best location will be denoted by a red wave peak as opposed to a blue wave peak.

To make the desired fluid mixture, fill the reservoir-bottle approximately 3/4 full with fluid and then seal the cap. Then degas the fluid, reservoir-bottle, and submerged 2 μm filter by

applying a -29 mmHg vacuum for approximately 1/2 hour or until bubbles are no longer generated. After removing the reservoir bottle from the vacuum chamber, purge no less than 10 mL of fluid through the delivery line to ensure a well-mixed fluid is contained in the filter. If this purge is not followed it is possible that an overly concentrated mixture can be in the filter. This will cause the first 5 mL - 10 mL of dispensed fluid during the experiment to have a different composition that the bulk fluid. Since fluid delivery can be as slow as 18 μL/min, the initial 10 mL could last the entire experiment and cause dramatic errors when comparing the theoretical results, which are based on the bulk fluid mixture, and the experimental results.

In the case of a pure fluid experiment, the same procedure for filling and degassing the reservoir bottle apply. However, since there will be no concentration gradient between the inside of the filter and the bulk fluid outside the filter, the 10 mL purge is not necessary. However, it is still good practice to clear the fluid-delivery-lines to prevent any contaminants from clogging the pipette nozzle.

The next step is to prime the pipette, attach the fluid-supply-line to the 20 gauge stainless tube; turn the 3-way valve to pressurize the reservoir-bottle. Push down on the syringe plunger to force fluid towards the pipette nozzle. After the fluid has reached the nozzle, turn the 3-way valve to vent the reservoir-bottle. Gently wick excess fluid away from the nozzle with a lint-free tissue (Kimwipe). Once purging/priming of the lines is complete make all electrical connections between the Active Pipette and Signal Driver, and connect all fluid lines.

At this point the FTIR, chamber assembly, and Active Pipette are ready and it is time to begin the experiment. Begin the FTIR Macro. First a background scan will be taken, after which the program will begin taking sample scans at specified time intervals. These parameters are all entered prior to the start of the experiment through Macros Basic, the actual code behind

Macros. Once the background scan is complete (approximately 30 seconds) insert and secure the ActivePipette into the chamber lid and begin the Signal Driver program. As with the Macro interface, all parameters for the Signal Driver are to be entered prior to the start of the experiment.

An experiment is complete when there is no or only minimal change in the absorbance (concentration) and temperature in the vapor space. It is important to remember that changes in the concentration can have as much as a 60 minute delay behind a deviation in the temperature in the typical 8 hour experiment . To terminate the experiment, switch the 3-way valve to pressurize and pull the syringe plunger to retract fluid out of the Active Pipette. Power-down and disconnect all electric connections.

4.3 Experiment Conditions

A table of all the experimental conditions is given below in Table 1. All experiments will be referred to by *Test #*, in further reading this number will be used to designate which experiments are being discussed. The numbering of experiments includes all tests run during the experiment process; a few earlier experiments were excluded from the final results due to errors associated with experimental setup. Otherwise, all experimental results were included. When N/A appears as the purging fluid this means that no purging was done, and therefore the non-condensable vapor was ambient air. In these cases it was necessary to measure the relative humidity and calculate the initial concentration of water in the vapor phase. The relative humidity was monitored by a household quality temperature and humidity meter located on the lab bench. When the ambient temperature is given by N/A this was because initial experiments

were run without the ambient temperature being recorded, however, this procedure was changed for the remaining experiments. The lack of information about the ambient temperature does not affect the experimental results; however, it did provide insight into the fluctuations (or drifts) in the ambient lab temperature. Mixture mole fractions were determined by two methods: IR spectroscopy and a density meter. The ambient pressure in the lab was not measured for earlier tests however, when the pressure was measured the variation was less than 0.01 psi, therefore pressure data was not recorded for each test. In the case of Test #11 two unique equilibria were achieved due to a prolonged increase in laboratory temperature, before the standard temperature was achieved.

Test #	Ethanol (mole fraction)	Droplet Frequency (drops/second)	Water (mole fraction)	Final Vapor Temperature (^oC / K)	Ambient Temperature (^oC / K)	Purging Fluid	Ambient Relative Humidity (%)
5	1.000	100	0.000	24.88 / 298.03	N/A	N_2	N/A
7	1.000	50	0.000	24.88 / 298.03	N/A	N_2	N/A
8	1.000	25	0.000	23.42 / 296.57	N/A	N_2	N/A
10	1.000	100	0.000	24.70 / 297.85	N/A	N_2	N/A
11 11b	1.000	50	0.000	24.91 / 298.06 26.78 / 299.93	N/A	N_2	N/A
12	1.000	100	0.000	24.36 / 297.51	N/A	N_2	N/A
13	0.000	100	1.000	23.55 / 296.70	22.20 / 295.35	N/A	12.0
14	0.000	100	1.000	23.63 / 296.78	24.00 / 297.15	N/A	36.0
15	0.000	50	1.000	24.05 / 297.20	22.80 / 295.95	N/A	26.0
16	0.000	50	1.000	23.38 / 296.53	23.88 / 297.03	N/A	15.0
18	0.000	100	1.000	24.29 / 297.44	25.00 / 298.15	N/A	41.0
19	0.000	100	1.000	25.15 / 298.30	23.30 / 296.45	N/A	9.0
21	0.396	100	0.604	24.81 / 297.96	25.00 / 298.15	N/A	33.0
22	0.500	100	0.500	26.05 / 299.20	25.00 / 298.15	N/A	30.0
23	0.500	300	0.500	24.85 / 298.00	25.00 / 298.15	N/A	30.0
24	.0698	500	0.930	24.94 / 298.09	25.00 / 298.15	N/A	30.0
25	0.210	500	0.790	25.19 / 298.34	23.62 / 296.77	N/A	30.0
26	0.000	1000	1.000	25.21 / 298.36	23.50 / 296.65	N/A	33.0
27	0.000	300	1.000	25.73 / 298.88	24.00 / 297.15	N/A	41.0
28	0.000	300	1.000	25.82 / 298.97	25.00 / 298.15	N/A	40.0
29	0.000	100	1.000	26.00 / 299.15	22.50 / 295.65	N/A	37.0
30	0.000	300	1.000	27.65 / 300.80	27.65 / 300.80	N/A	29.0
31	0.703	300	0.297	24.24 / 297.39	23.00 / 296.15	N/A	42.0
34	0.909	300	0.091	25.71 / 298.86	23.00 / 296.15	N/A	34.0
35	0.831	300	0.169	24.87 / 298.02	23.00 / 296.15	N/A	36.0
37	1.000	200	0.000	25.06 / 298.21	23.80 / 296.95	N_2	N/A

Table 1: Table of Experimental Conditions

CHAPTER 5: RESULTS AND DISCUSSION

The control during this research was pure water experiments since psychrometric charts are easily available for any altitude and could be used to validate the experiment. The equilibrium concentration of pure water experiments at any temperature and pressure should be equal to 100% humidity on a psychrometric chart for the same temperature and pressure. The theoretical results of a closed system model with pure water droplets were compared against both psychrometric data and experimental results. In the case of pure ethanol droplets and ethanol-water droplets theoretical results from an open system model were compared directly to experimental data. The closed system model assumed an ideal gas for the vapor mixture. The open system model operated with the embedded assumption that the non-condensable gas is the only vapor lost in the open system. The effect of this assumption is that there may be an over prediction of the final ethanol and water vapor concentrations since in the true experiment it is possible that a small amount of ethanol and water vapor was lost. A comparison between the two theoretical models was done in an effort to visually highlight the differences between them since each represents an extreme case.

In order to accurately test the multicomponent system evaporation model, experimental data was collected for the evaporation of liquid droplets of pure ethanol, pure water, and various mixtures of ethanol and water in an air or nitrogen environment. All data collected along with temperature and concentration profiles are supplied in section A.3 (Figure 37 through Figure 63). Ambient air was used for tests with pure water and ethanol-water mixtures, while nitrogen was used for all the pure ethanol tests. The ambient air contained anywhere from 6–10 ppm (mg of water vapor per liter dry air) of water vapor. Ambient air was not used in the pure ethanol tests due to the interaction the pre-existing water vapor (humidity) would have on the evaporating

ethanol. If ethanol tests were conducted using ambient air the results would have shown a corresponding equilibrium of an ethanol-water system instead of a pure ethanol system. The same interaction would occur if a water test were conducted in the presence of ethanol vapor.

5.1 Humidity Effects

To account for all initial water vapor present in the evaporation chamber, the lab contained a thermometer / relative humidity gauge, which was used for recording of relative humidity throughout the experiments. Knowing the laboratory humidity was necessary in cases when a nitrogen purge of the evaporation chamber was not used, such as in water and ethanol-water mixture tests. Through the use of a web-based calculator (*PsycFunc*, 2006), the density of air at a specific temperature and pressure was determined. Then an Excel add-in called PsycFunc Psychrometric Functions for Excel (Linric Company, www.linric.com) was used to determine the humidity ratio $\frac{\text{grams Water Vapor}}{\text{kilograms Dry Air}}$ (or specific humidity, SH) from temperature, relative humidity, and elevation, at which point the ambient parts per million (PPM) of water vapor in the ambient air could be determined.

$$\text{PPM}\left(\frac{mg \text{ water vapor}}{L \text{ dry air}}\right) = \rho_a\left(T, \text{Elevation}\right) \cdot \text{SH}$$

It was critical to know the ambient water content since the FTIR works off the same principle as gauge pressure; where the ambient spectrum is used as a base-line and any changes in the vapor content are measured with respect to the base-line. Therefore, the initial vapor content must be known to convert the gauge (or relative) concentrations to absolute

concentrations. This conversion was necessary when the chamber was not purged (ethanol tests), and only when liquid mixtures contained water (water and ethanol-water mixture tests). It was assumed that the ambient air did not contain ethanol vapor in any measurable concentration.

5.2 Measurement Calibration, Repeatability and Uncertainty

As this experiment was designed there were three main origins of uncertainty: FTIR absorbance calibration and repeatability, thermocouple calibration and repeatability, and pressure transducer calibration.

In all cases the equipment was calibrated against a known measurement or setting. In the case of the FTIR, Beer's Law acts as the quantitative relation between the absorbance at a particular wavenumber and the corresponding concentration. In the case of the pressure, the pressure transducer was calibrated by the manufacturer at a specific input voltage. Each thermocouple was calibrated against a pre-calibrated thermocouple.

5.2.1 Calibration of Thermocouples

Each of the four non-calibrated (T-type) thermocouples was calibrated by comparison against a calibrated thermocouple (J-type) used in conjunction with a thermometer (Fluke 54 II). The calibrated thermocouple is accurate to 0.001^{o}C, and the thermometer has a resolution of 0.001^{o}C. Certificate information is provided in section A.5.3. The T-type thermocouples used have a resolution of 0.001^{o}C over a temperature range of -200^{o}C to 400^{o}C.

The thermocouples were all exposed to three different temperature baths of 35.90°C, 29.80°C, and 21.60°C. These temperatures were chosen so that the best resolution surrounding the temperature range of the experiments could be. Bath temperatures were known by measurements from the calibrated thermocouple. A 50 mL Pyrex beaker of water was used as the temperature bath, thin film heaters were used to maintain fluid temperatures. Data for the four non-calibrated thermocouples was recorded by a Keithly data acquisition system, while measurements from the calibrated thermocouple were recorded to the hand-held thermometer.

Calibration data was taken at each temperature for two minutes. Data accumulation began when the calibrated thermocouple measured a constant and uniform fluid temperature independent of spatial location in the beaker. Care was taken to ensure that the thermocouples ends were fully immersed in the liquid bath but were not in contact with the walls of the container.

At each bath temperature the average temperature measurements were determined for each non-calibrated thermocouple and for the calibrated thermocouple. These average measurements were used to generate a linear relationship between the calibrated temperature and each of the four non-calibrated temperatures.

From the calibration data the following linear relations were determined.

$$\text{Thermocouple\_1: } T^{calibrated}\left(^{o}C\right) = 0.921 \cdot T^{non-calibrated}\left(^{o}C\right) + 1.841$$

$$\text{Thermocouple \_2: } T^{calibrated}\left(^{o}C\right) = 0.959 \cdot T^{non-calibrated}\left(^{o}C\right) + 0.996$$

$$\text{Thermocouple \_3: } T^{calibrated}\left(^{o}C\right) = 0.963 \cdot T^{non-calibrated}\left(^{o}C\right) + 0.900$$

$$\text{Thermocouple \_4: } T^{calibrated}\left(^{o}C\right) = 0.948 \cdot T^{non-calibrated}\left(^{o}C\right) + 1.209$$

where $T^{non-calibrated}$ is the actual temperature measured by the T-type thermocouples and $T^{calibrated}$ is the adjusted temperature based on data from the calibrated thermocouple. Section A.5.3

contains more information on the tabular data obtained from the thermocouple calibration tests (Table 6 and Table 7).

Based on the resolution of the calibrated thermocouple, the thermometer, and the T-type thermocouples these linear relationships are subject to a maximum deviation of ±0.458^{o}C. In addition, calculations were done to determine the repeatability of each thermocouple's measurement. It was determined that at any temperature each thermocouple can repeat its previously measured value within a tolerance of ±0.041^{o}C. Therefore, the maximum error associated with any temperature measurement was ±0.458^{o}C. This error in temperature measurements did not affect the experimental results but did give rise to uncertainty in the predicted results since one of the critical inputs is system temperature. The ±0.458^{o}C error in thermocouples propagated into a ±4.943 ppm error in the pure ethanol model, a ±0.593 ppm error in the pure water model, and a ±3.04 ppm and ±0.490 ppm error in the ethanol-water model for ethanol and water concentrations, respectively.

5.2.2 Calibration of Pressure Transducer

The pressure transducer used was a Honeywell product capable of measuring from 0-30 psia, and came calibrated for operation at 10 Volts. Therefore, the power supply is tuned and set to 10 V using a hand-held voltmeter, at which point the pressure transducer has been calibrated. At the calibrated 10 V the pressure transducer measured an average ambient laboratory pressure of 13.3 psia (or 0.91 atm). This will be the pressure used for numerical modeling and data validation.

5.2.3 Correlating Absorbance to Concentration: Beer's Law

The FTIR output is a spectrum with absorbance (or transmittance) as the y-axis and wavenumber (cm^{-1}) as the x-axis. According to Beer's Law absorbance and concentration are linearly related by the following:

$$A_i = a_i \cdot b_i \cdot c_i$$

where A is absorbance, a is absorptivity, b is path length, and c is concentration. Since absorptivity and path length are held constant throughout the experimental process we can further simplify the relation to

$$A_i = L_i \cdot c_i$$

where $L_i \equiv a_i \cdot b_i$ is a constant specific for each vapor species at each wavenumber. By measuring two known vapor concentrations of each pure component (ethanol and water) a slope relating the two points is the constant L_i.

The infrared spectra for water vapor and ethanol vapor are below as Figure 9 and Figure 10. For each component two wavenumbers were chosen as characteristic only for that species. These peaks are marked on the respective figures. For water the characteristic wavenumbers were 1558 $cm^{-1}$and 1652 cm^{-1}, for ethanol the characteristic wavenumbers were 2900 $cm^{-1}$and 2987 cm^{-1}. Since each wavenumber predicted a slightly different concentration; the average of the two concentrations was used in determining the resultant vapor composition in data analysis.

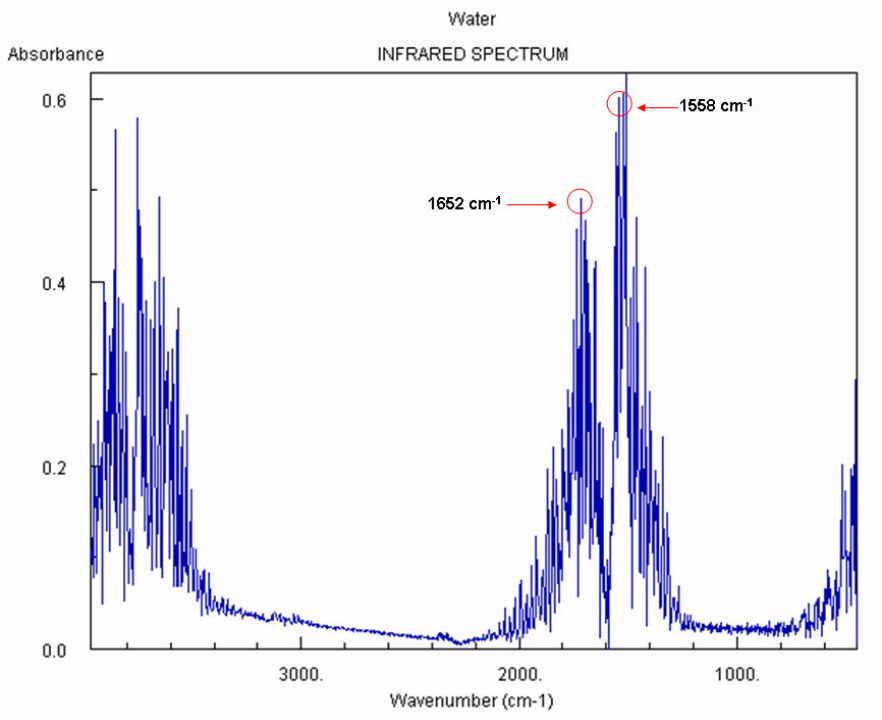

Figure 9: Water IR Spectrum

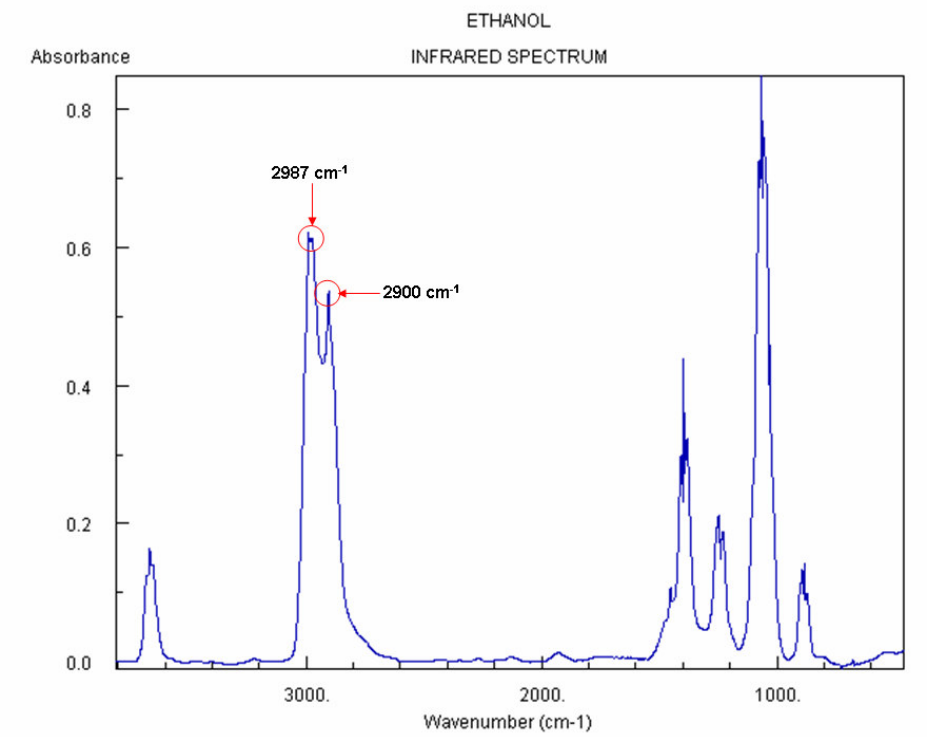

Figure 10: Ethanol IR Spectrum

Concentration data points were taken by one of two methods. For ethanol calibration, the evaporation chamber was heated to approximately 32°C (a temperature known to vaporize ethanol liquid). Next a calibrated plunger syringe was used to incrementally inject known volumes of liquid ethanol. The FTIR was used to continuously monitor concentration, a corresponding absorbance was noted as the point in which the absorbance peaks stopped increasing and remained constant. This procedure was followed several times using different total liquid volumes each time. The method used for water calibration was more exact. The evaporation chamber was again heated, but set to different temperatures for each calibration point. The ActivePipette was used to dispense water droplets. Again, the absorbance was monitored continuously until the peaks were observed to remain constant. The corresponding concentration was then determined from psychrometric data at (0.91 psia and the chamber temperature).

When calculating the constant L_i from the concentration-absorbance data it was assumed that the y-intercept was zero, since at zero concentration the absorbance should also be zero. Zero absorbance at zero concentration was also confirmed by purging the chamber with dry air, and taking a scan of the vapor space. Beer's Law corresponding to each of the above mentioned wavenumbers is as follows:

Wavenumber, 1558-cm^{-1}: $c_2(ppm) = 113.886 \cdot A$; $R^2 = 0.999$

Wavenumber, 1652-cm^{-1}: $c_2(ppm) = 146.293 \cdot A$; $R^2 = 0.996$

Wavenumber, 2900-cm^{-1}: $c_1(ppm) = 126.800 \cdot A$; $R^2 = 0.965$

Wavenumber, 2987-cm^{-1}: $c_1(ppm) = 106.535 \cdot A$; $R^2 = 0.965$

The linear trend lines for water showed better R^2 values since the concentrations were based on psychrometric data, where the ethanol concentrations were calculated from a known liquid volume and assuming that all the mass was evaporated. Since there was no way to guarantee all the mass evaporated, this is cause for a smaller R^2 value in the ethanol correlations. Graphical data regarding the absorbance calibration can be found in section A.5.4 (Figure 67 through Figure 71).

5.2.4 Repeatability of Absorbance Measurements

In order to determine the accuracy in the FTIR measurement of the same concentration at the same temperature, multiple measurements of absorbance (translated to concentration) were taken at the same temperature. A known concentration was achieved by first taking a background scan of a closed chamber after it had been purged with dry air. Then the chamber was allowed to sit open in the lab for several hours, to allow the chamber to come into equilibrium with the ambient environment. The chamber was then sealed and slowly heated while concentration measurements of the water content were recorded. Chamber temperatures of 29.976°C, 30.036°C, 31.010°C, and 32.031°C were held constant while multiple FTIR measurements over approximately 5 minutes were recorded. The difference between the minimum chamber temperature and the maximum chamber temperature (ΔT) along with the difference between the minimum measured concentration and the maximum measured concentration (Δc) was then averaged for the four temperatures tested. The data was then extrapolated for a ΔT of zero, which corresponded to $\Delta c = 0.025$ ppm. Therefore, the repeatability of the FTIR measurements has a maximum variation of ±0.025 ppm at the same

temperature and pressure. Tabular data from these tests can be found in section A.5.4 Figure 71 and Table 9. Since repeatability data is based on the correlated concentration and not the absorbance the repeatability calculations captured both the error associated with the correlation between absorbance and concentration along with the repeatability of the FTIR in its measurements.

5.3 Pressure Effects

A comparison between an open system (constant pressure) model and a closed system model was done to define the two possible extremes the data could demonstrate. Over the course of experiments internal pressure was seen to play a significant role in the final vapor concentration. In some cases the difference between the two models was as much as 10% in the predicted moles in the vapor space across a pressure change of 1.3 psia (or 0.09 atm). As system pressure is increased the equilibrium vapor concentration decreases. This can be supported by Raoult's Law (Equation 3.8), as the pressure increases the ratio of $\frac{P^{sat}}{P}$ decreases thus decreasing the vapor mole fraction.

5.3.1 Pressure Effects on Experiment Results

In initial experiments the internal chamber pressure was not monitored during the evaporation test. The assumption was that the pressure increase would be insignificant compared to the total pressure, since >99% of the vapor space would contain the non-condensable species.

In addition, the fluid reservoir in the ActivePipette system had to be vented to ambient pressure, so it would not be possible to run the experiments under any significant pressure.

Envision a force balance, if at the reservoir side of the fluid supply there is ambient pressure plus the pressure due to the height of the fluid, and the internal chamber pressure on the nozzle side of the fluid delivery. When the two pressures are equal the fluid will dispense into the chamber, however, if the pressure on the delivery side (chamber pressure) is larger and the surface tension of the fluid is small enough the fluid can be pushed in the opposite direction (back into the reservoir). Fluids with high surface tension, like water, can handle relative pressure ranges of ±100 mm. This allowable relative pressure range is lower for fluids with lower surface tensions, like ethanol.

Experiments began with the testing of pure ethanol droplets. It was observed that in some cases the fluid would pull back into the reservoir bottle at some point during the test, generally after 1-2 hours. However, this phenomenon was not observed for all tests. It was first verified that the delivery line was clean, and that the ActivePipette was not clogged. In order to try and resolve the issue the relative pressure was adjusted both up and down (by moving the absolute height of the reservoir bottle with respect to the nozzle tip). However, once the fluid pulled back into the reservoir it could not be maintained in the fluid delivery line for any length of time, unless the chamber was fully disassembled and restarted. Once testing began with pure water droplets, the phenomenon of fluid pull back did not occur. Finally, when ethanol-water mixture droplets were tested the same pull back phenomenon returned, but again not in all tests.

With the addition of a pressure transducer mounted in the evaporation chamber, it was determined that for experiments where pure ethanol droplets or ethanol-water mixture droplets were being dispensed, the internal chamber pressure would increase 0.02 atm at which point

fluid pull back occurred and the test failed. While in tests with pure water the chamber pressure increased <0.01 atm and leveled off, and the fluid never pulled back. Therefore, coupling the pressure change in the evaporation chamber with the difference in surface tension between the two fluids (0.0728 N/m at 293K for water and 0.0228 N/m at 293K for ethanol) it was determined that the pull back was caused by too much force on the nozzle side of the force balance. Further investigation revealed that for experiments involving pure ethanol or ethanol-water droplets in which the fluid did not pull back, there was a small leak at the top of the evaporation chamber which acted as a relief valve. The variation between experiments that failed, due to fluid pull back, and those that did not fail was attributed to an inconsistency in the tightening of the screws which held the nozzle at the top of the chamber lid. When screws were not fully tightened it allowed the rubber stopper to not fully seal properly into the lid causing a small leak. Since the rubber stopper had a thickness of 0.065 inches and diameter of 0.61 inches it would not require a significant internal pressure to force an edge of the stopper up enough to relieve the excess pressure.

Tests with water droplets were first used, Figure 11. The test began with a droplet rate of 200 drops/second, after 40 minutes the internal pressure had increased 0.65 kPa. Droplets were momentarily stopped, seen as a drop in pressure, before the droplet rate was increased to 1000 drops/second, and further increased to 2000 drops/second. In the 100 minute test the internal pressure increased 1.10 kPa before remaining constant, the leveling of pressure was due to vapor saturation occurring. However, the test never failed due to fluid pull back.

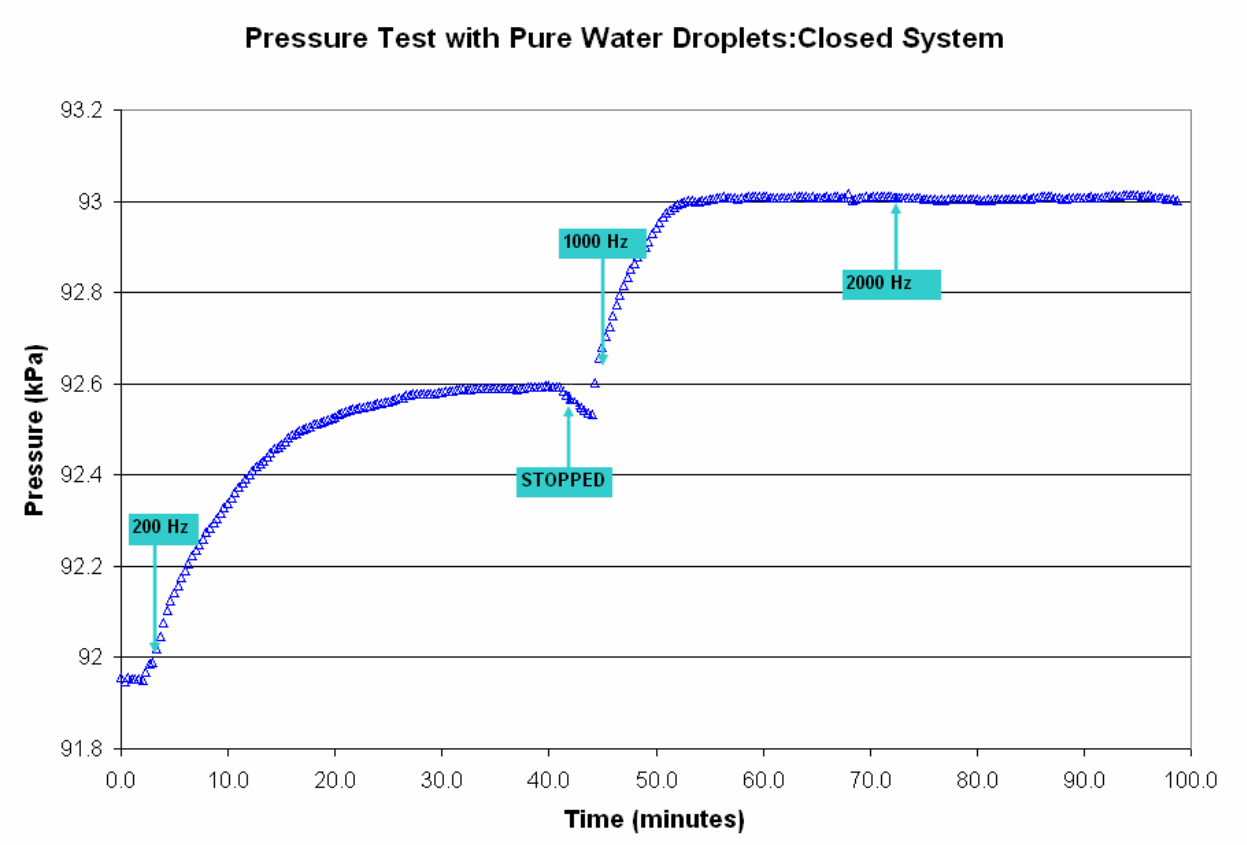

Figure 11: Pressure Test Using Pure Water Droplet in a Closed System

Next, pure ethanol was tested using the same procedure as above. Figure 12 shows the internal pressure measurements during the test. The test began with a droplet rate of 200 drops/second. The internal pressure continued to increase until around 120 minuets the test failed due to fluid pull back. This failure occurred after the internal pressure had increased by nearly 5 kPa to 94 kPa. The fluid line was then re-primed, during which the internal pressure decreased since droplets were no longer being dispensed. After re-priming the test continued until the same pressure of 94 kPa was reached, at which point the test failed again.

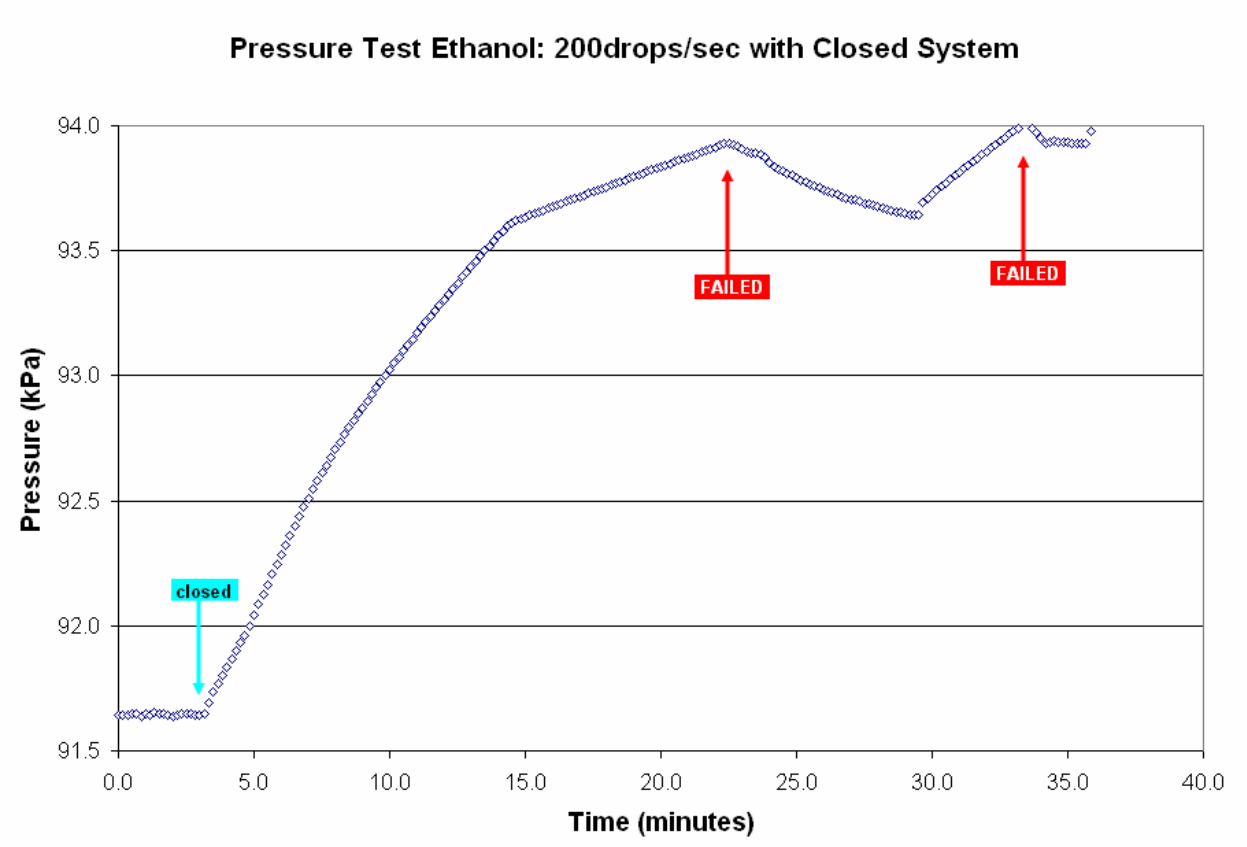

Figure 12: Pressure Test Using Ethanol in a Closed System

Results from a final pressure test with pure ethanol droplets being dispensed at a rate of 200 drops/second are displayed in Figure 13. During this test droplets started with the chamber closed, followed by several minutes of increasing internal pressure. Then manually the edge of the stopper on the lid was lifted up, as can be seen by a decrease of internal pressure back to ambient. Next the stopper was sealed and the pressure resumed increasing. Once again the edge of the stopper was lifted and the pressure returned to ambient, for the next 45 minutes the chamber was left with a small leak, and the pressure remained constant. Finally, the system was closed a final time until the test failed due to fluid pull back when the internal pressure nearly reached 94 kPa, the same pressure that failure occurred in the previous ethanol pressure test.

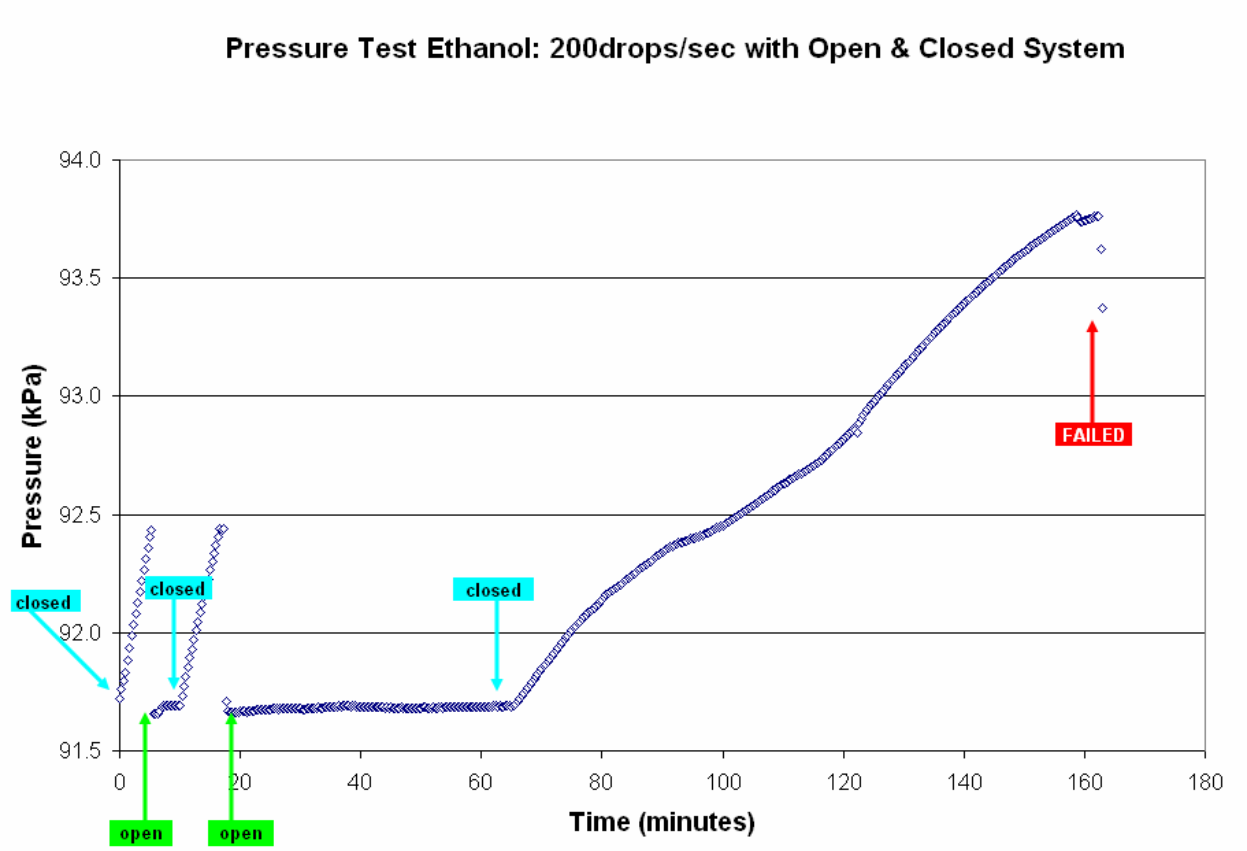

Figure 13: Pressure Test Using Ethanol in an Open and Closed System

By conducting these pressure tests it is possible to see the maximum internal pressure the ActivePipette can handle before fluid pull back occurs. From these tests it was concluded that a pressure increase larger than 5 kPa would cause an experiment to fail. This size of pressure increase occurs in both pure ethanol and ethanol-water mixture tests due to the relatively large vapor generation compared to that in pure water experiments. The tests also confirmed that a very minimal leak was all that was necessary to relieve the excess internal pressure.

In conclusion, experiments would only run to completion if pure water was being dispensed or if the internal pressure was equilibrated, via a leak, when pure ethanol or ethanol-water mixture fluids were being dispensed. Therefore, in order to accurately model the conditions present in the experiments two models were required. Ethanol and ethanol-water

experiments required an open system model which specified a constant pressure be maintained by assuming that the non-condensing species was being vented to the ambient. The assumption that only the non-condensable species was lost out of the chamber is somewhat arguable based on the vapor densities of each species. Ranked in order of lightest to heaviest is $water < ethanol < nitrogen < air$. Since the vapor space was composed of more than 99% non-condensable species (either air or nitrogen), in a well-mixed system only small fraction of the ethanol or water vapor would be lost compared to the larger quantity of non-condensable. In the case of ethanol experiments the average over prediction of vapor concentration by the open system model was 3.4%, and for ethanol-water experiments the average over prediction for the water vapor concentration was 4.4%. In the ethanol-water test the ethanol vapor concentration was under predicted by the model by 3.7%.

5.3.2 Pressure Effects on Model Predictions

In modeling the evaporation of liquid droplets, the two extreme pressure cases can be classified as an open system (or constant pressure) or a closed system (pressure calculated from ideal gas law). While arguments can be given for which model is best suited in demonstrating the observed behavior in each experiment, the data should lie between the two extreme cases. In theory the relative trend of the experimental data towards one extreme or the other will either validate or discredit assumptions made on the behavior of each experiment. In the case that data were to appear split between the two extremes would suggest that there were other neglected effects in the experiment.

The graphs below show the general trend in an open system model based on the ambient pressure in the case of pure ethanol droplets (Figure 14) and for the case of pure water droplets (Figure 15). As the ambient pressure increases from 0.90 atm to 1.00 atm, and then to 1.10 atm, the predicted equilibrium vapor concentration (in terms of ppm (mg of water vapor/L dry air)) decreases for the same temperature. As temperature increases the equilibrium vapor concentration increases linearly.

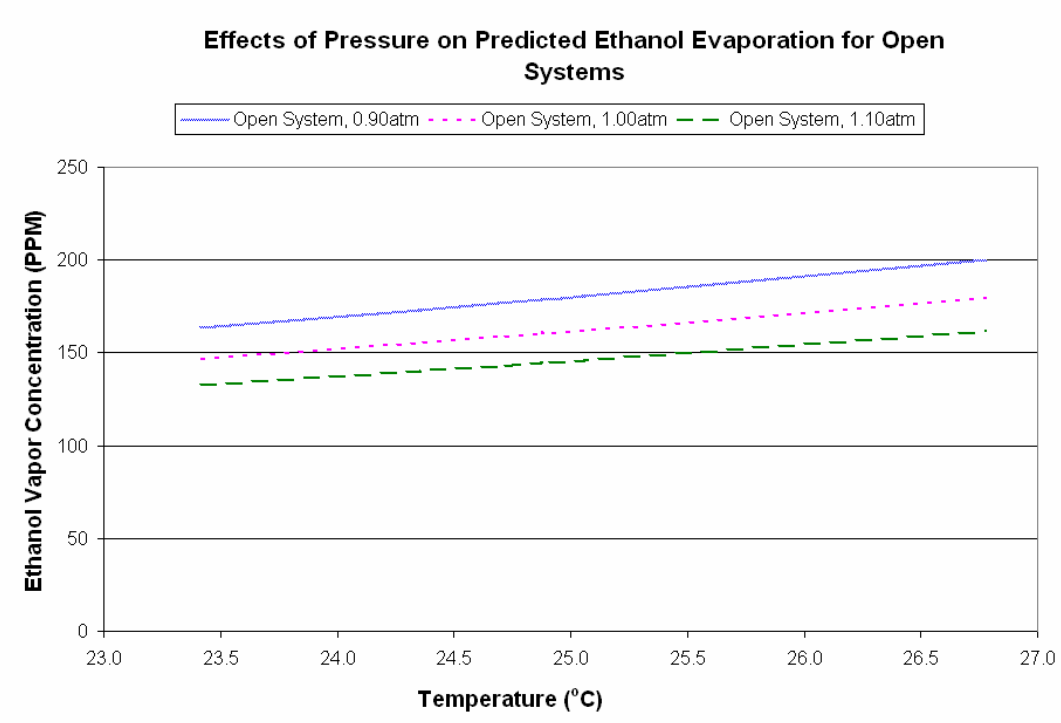

Figure 14: Effect of Pressure on the Predicted Ethanol Concentration in an Open System

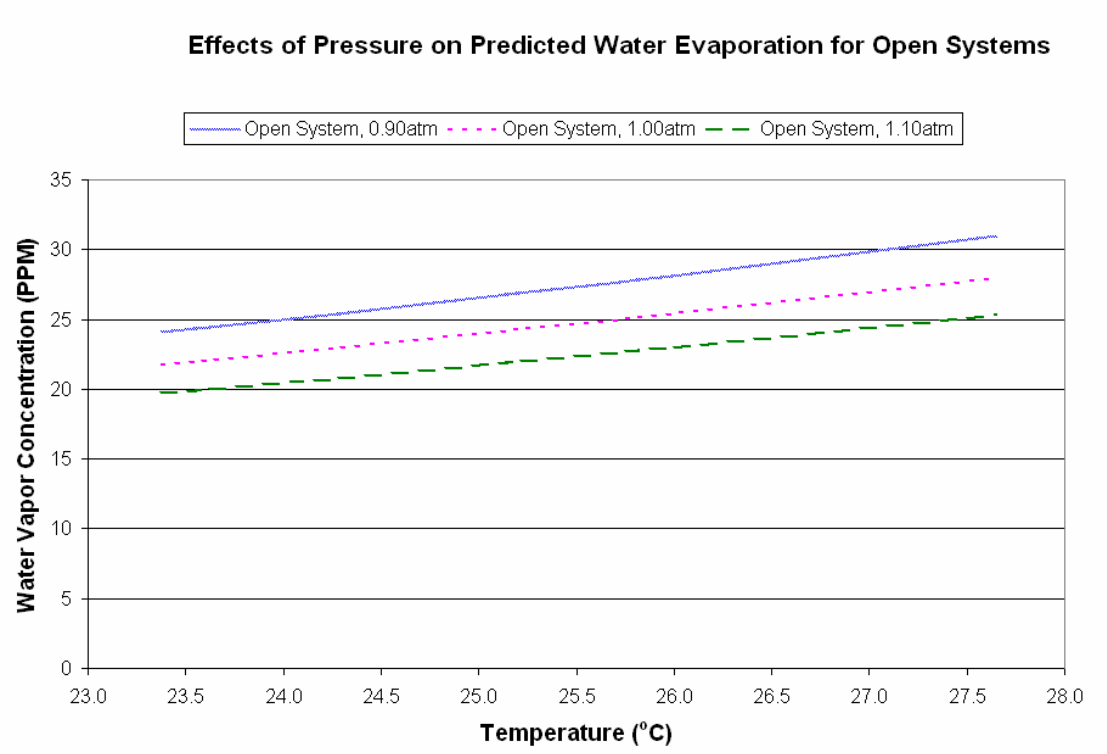

Figure 15: Effect of Pressure on the Predicted Water Concentration in an Open System

This trend can be validated by consulting published psychrometric charts for various elevations (or pressures). Figure 16 validates that as the pressure increases (or elevation decreases) the specific humidity (or concentration) of water vapor in air at 100% RH decreases. This trend is identical for all temperatures. Furthermore, Figure 16 shows that as temperature is increased the concentration increases for the same ambient pressure. Both trends, concentration decrease with pressure increase and concentration increase with temperature increase are observed in the open system models.

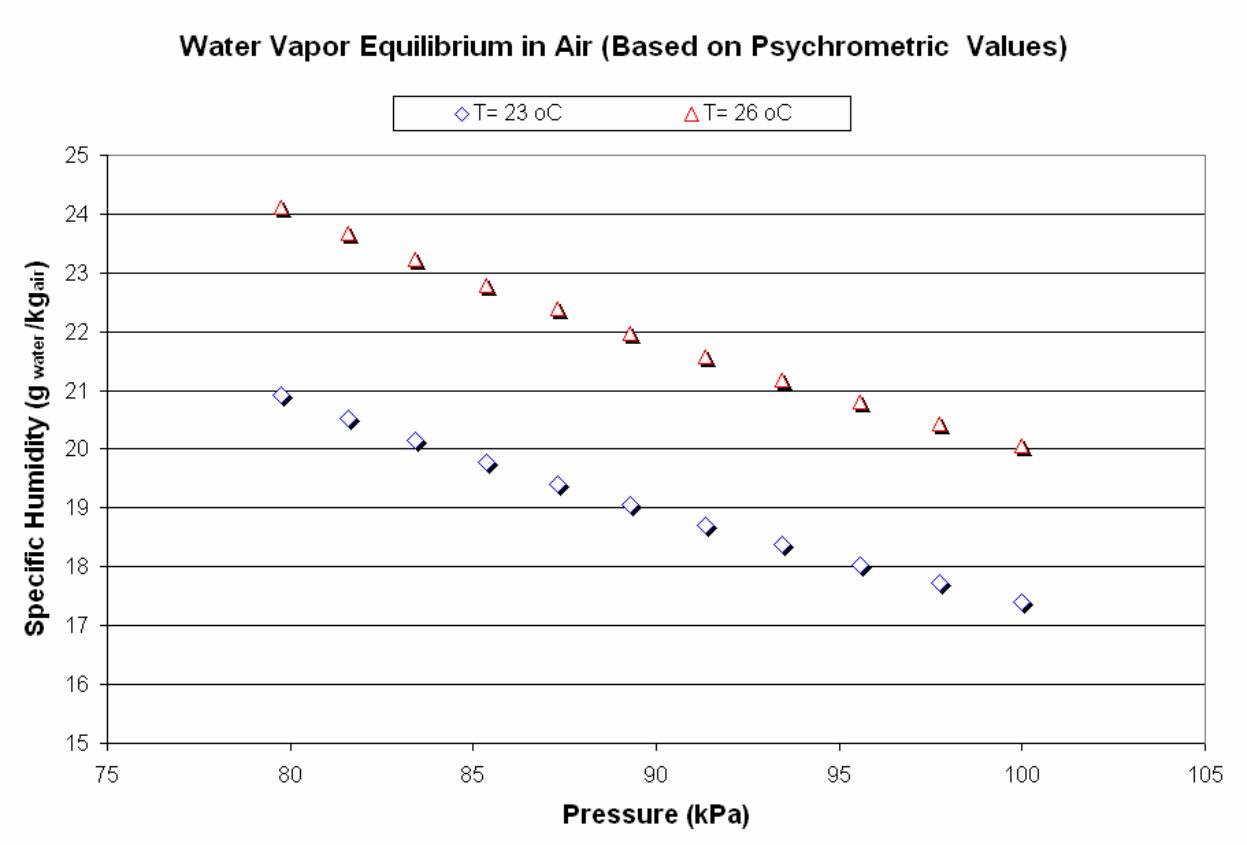

Figure 16: Psychrometric Concentration Trends for Various Temperatures and Pressures

5.4 Ethanol Experiments

As discussed in earlier sections, the uncertainties in measured values come from the accuracy in the FTIR measuring a consistent concentration for the same temperature, and from the accuracy in the calculated relation between absorbance and concentration. This deviation in the experimental data was found to be ±0.025 ppm. Error bars have been placed on each experimental data point, however, since the deviation is so small compared to the total concentration the error bars appear as a single dash near the center of each data point. In the model the deviation was significantly larger at ±4.943 ppm which is a result of the ±0.458^{o}C

error associated with the temperature measurements. All of the data collected during each ethanol experiment is located in section A.3.

Based on the assumption that pure ethanol experiments had to operate with the internal evaporation chamber at the same pressure as the ambient pressure, we would assume that when experiment results were compared to predictions from both an open system model and a closed system model that the data would cluster closer to the open system predictions. Figure 17 confirms that the experimental data indeed falls closer to predictions from the open system model than predictions of the closed system model. In addition, the data also demonstrates the appropriate trend of increasing concentration with increasing temperature.

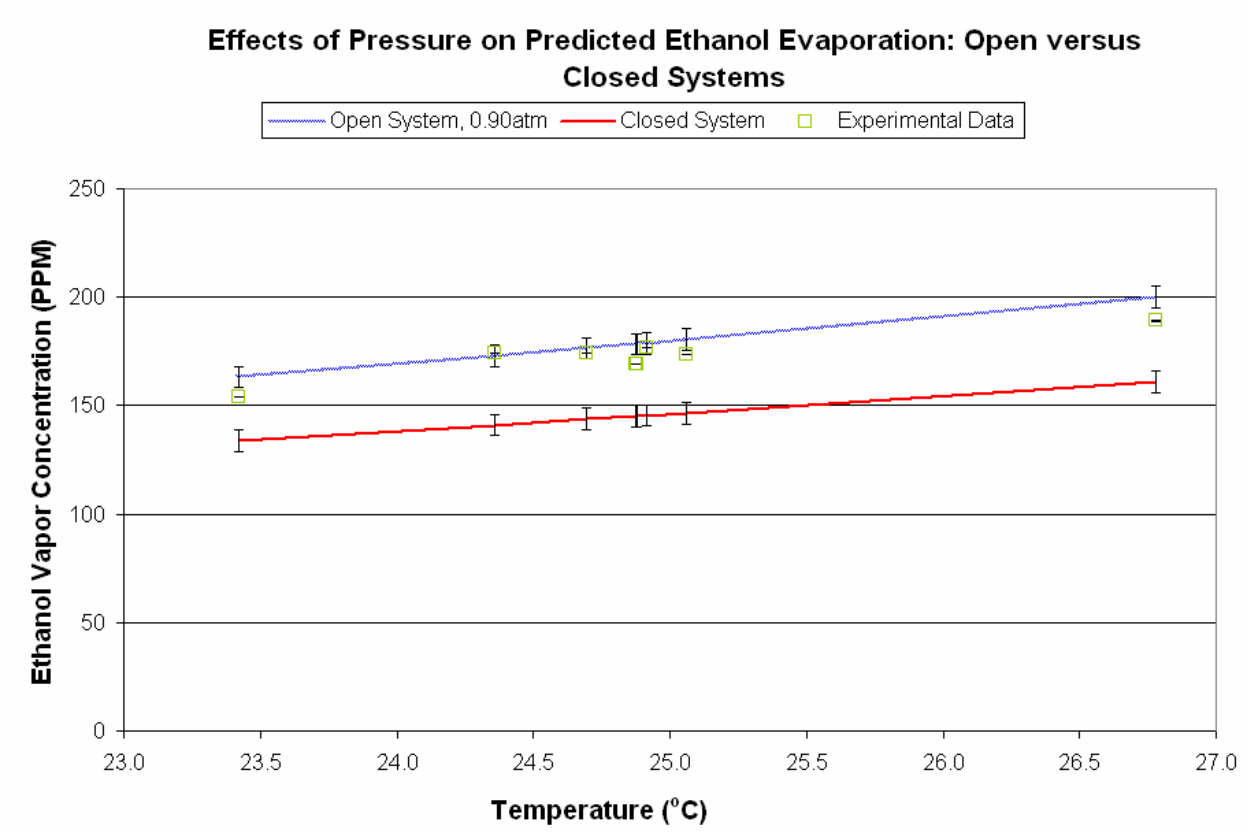

Figure 17: Comparison of Ethanol Data and Predictions from Open and Closed System Model

5.4.1 Reproducibility of Ethanol Experiments

It is important that for all experiments we can conclude that the results are both believable and repeatable. Figure 18 highlights three ethanol tests all conducted with a droplet rate of 100 drops/second, and all with similar final temperatures. The concentration profile results for Test #5, Test #10, and Test #12 all appear to follow the same trend. Each trend progresses with an initial surge of vapor being produced followed by a slow decrease in rate until the concentration levels at equilibrium despite droplets continually being added to the system. Test #10 and Test #12 appear to nearly lie point-for-point on top of each other, while Test #5 shows a slightly slower initial concentration, but eventually equilibrates to the same concentration. However, the difference in Test #5 was that a different nozzle was used, this nozzle generated slightly smaller droplets and therefore it took more droplets to reach the same concentrations seen earlier from the other two tests.

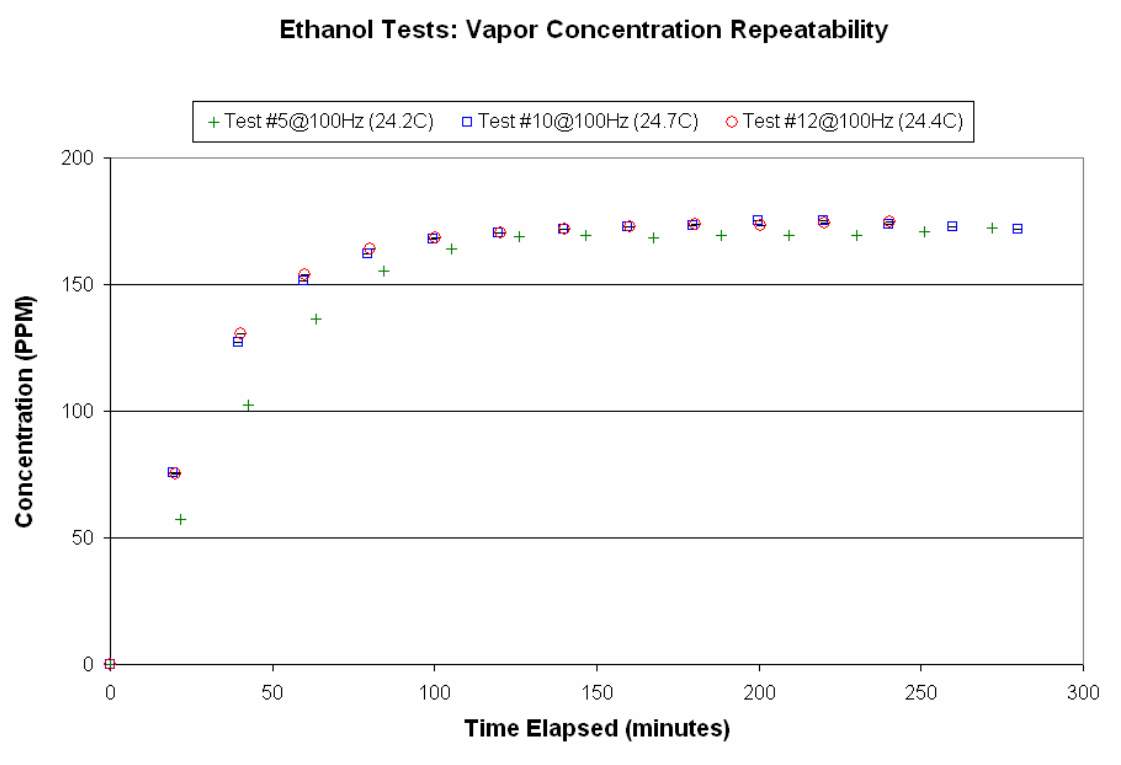

Figure 18: Vapor Concentration Repeatability in Ethanol Experiments

In Figure 19 we see the same three tests (#5, #10, and #12) but instead of changes in vapor concentration, there is the trend in chamber temperature. Similar to what was seen in the concentration trends; all three tests show nearly identical (maximum deviation at any time of <0.5°C) internal chamber temperatures throughout the experiments. However, the chamber temperatures all began at approximately 30°C (due to pre-heating with Kapton heaters) and steadily decreased to the laboratory ambient temperature (approximately 24°C). From the temperature data we can conclude that each test was subjected to similar, initial chamber temperature, laboratory temperature, and heat loss; resulting in final chamber temperatures of 24.2°C, 24.7°C, and 24.2°C for Test #5, #10, and #12 respectively.

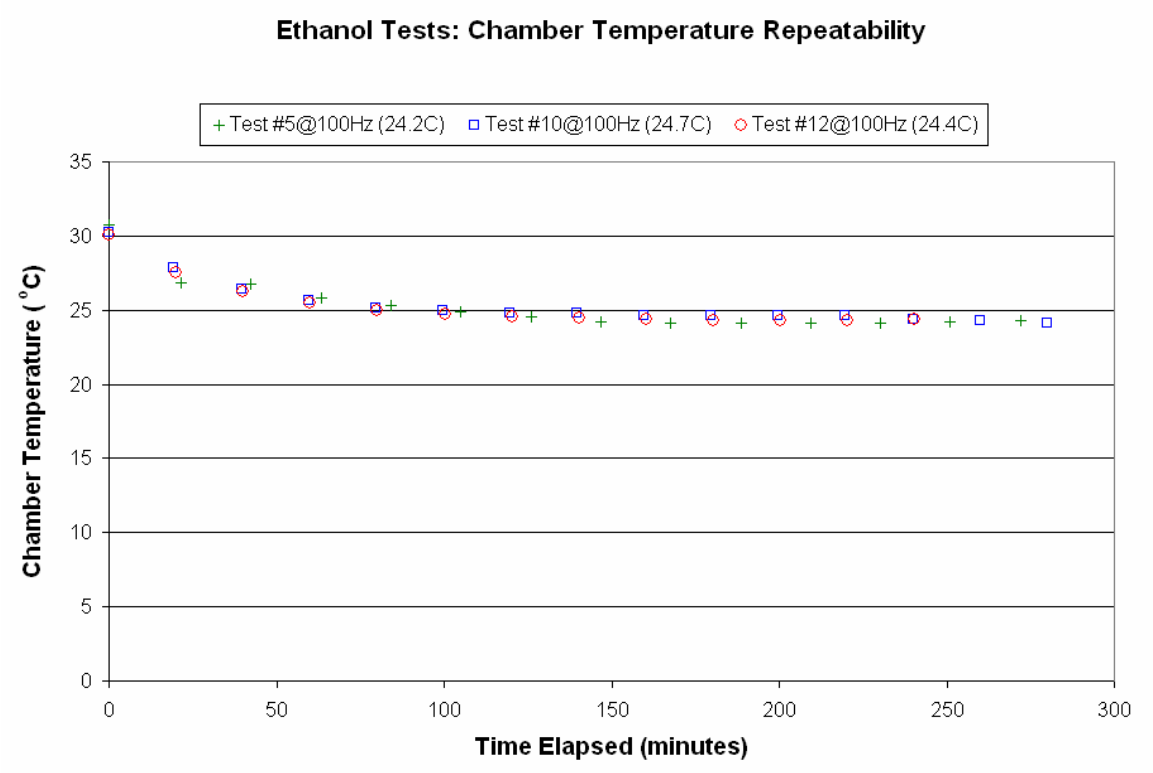

Figure 19: Temperature Repeatability in Ethanol Experiments

Among the three ethanol tests there was a final temperature range of 0.5°C with a corresponding range in final concentration of 5.17 ppm. The highest temperature is associated with the highest concentration, and so forth.

5.4.2 Theoretical and Experimental Comparison

Since Test #5, Test #10, and Test #12 were already compared against each other Figure 20 and Figure 21 show only Test#12 against all the remaining ethanol tests conducted.

The first key observation is to note the variation in droplet rate among the tests. Droplet rates range from 25 drops/second to 200 drops/second. Progressing from the slowest droplet rate

(Test #8) with an elapsed experiment time of nearly 1000 minutes to reach equilibrium, to Test #7 with a droplet rate of 50 drops/second where equilibrium was reached in less than 500 minutes. With each increase in droplet rate the time to equilibrium is shortened and the initial concentration slope becomes steeper.

The second key observation is with Test #11, run at 50 drops/second, which shows an irregular trend compared to all the previous trends. From Figure 21 the chamber temperature in Test #11, unlike all other tests, remained warmer for a longer period of time. This increased temperature caused a large vapor generation, but once the chamber temperature began to decrease to the typical laboratory temperature the internal concentration was already larger that dictated by equilibrium at the cooler temperature. This caused ethanol to condense out of the vapor space, resulting in the over-shoot trend seen in Figure 20.

The final observation is between the concentration profiles of Test #12 at 100 drops/second and Test #37 at 200 drops/second. We would expect to see the test with the larger droplet rate to reach equilibrium first and lie above tests with lower droplet rates. However, Test #12 lies above Test #37 despite the increase in droplet rates. This deviation from the known behavior, while not fully understood, could be attributed to the time scale of the vapor mixing. Since droplets are falling at a rate of 100 drops/second and 200 drops/second it is possible that there is a limit to how quickly the newly evaporated ethanol can disperse out of the path of the next falling droplet. Droplet evaporation is driven by the concentration gradient across the liquid-vapor interface. We could argue that if previously evaporated ethanol did not have time to disperse out of the path of the next droplet, that each succeeding droplet would see an unnatural decreased concentration gradient at the liquid-vapor interface, thus slowing the mass transfer rate. Therefore, if at rates of 25 drops/second, 50 drops/second, and 100 drops/second there was

enough time between droplets for the vapor to remain well mixed, but at a rate of 200 drops/second there was not enough time for diffusion to occur. The result could be seen as a "flip-flop" in the orientation of concentration profiles at the higher droplet rates. Another possible cause is that at the higher droplet rates agglomeration was taking place. While this behavior was not observed it would explain the data trend since agglomeration would decrease the mass transfer area thus decreasing the rate of evaporation.

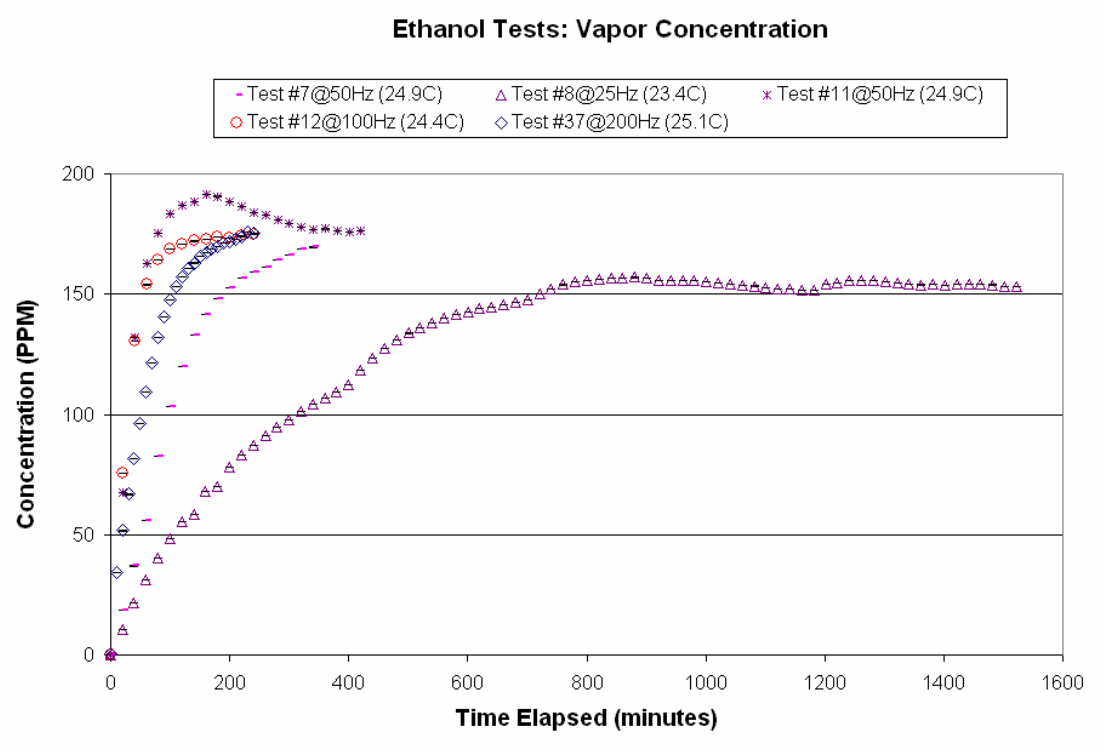

Figure 20: Comparison of Vapor Concentration for All Ethanol Experiments

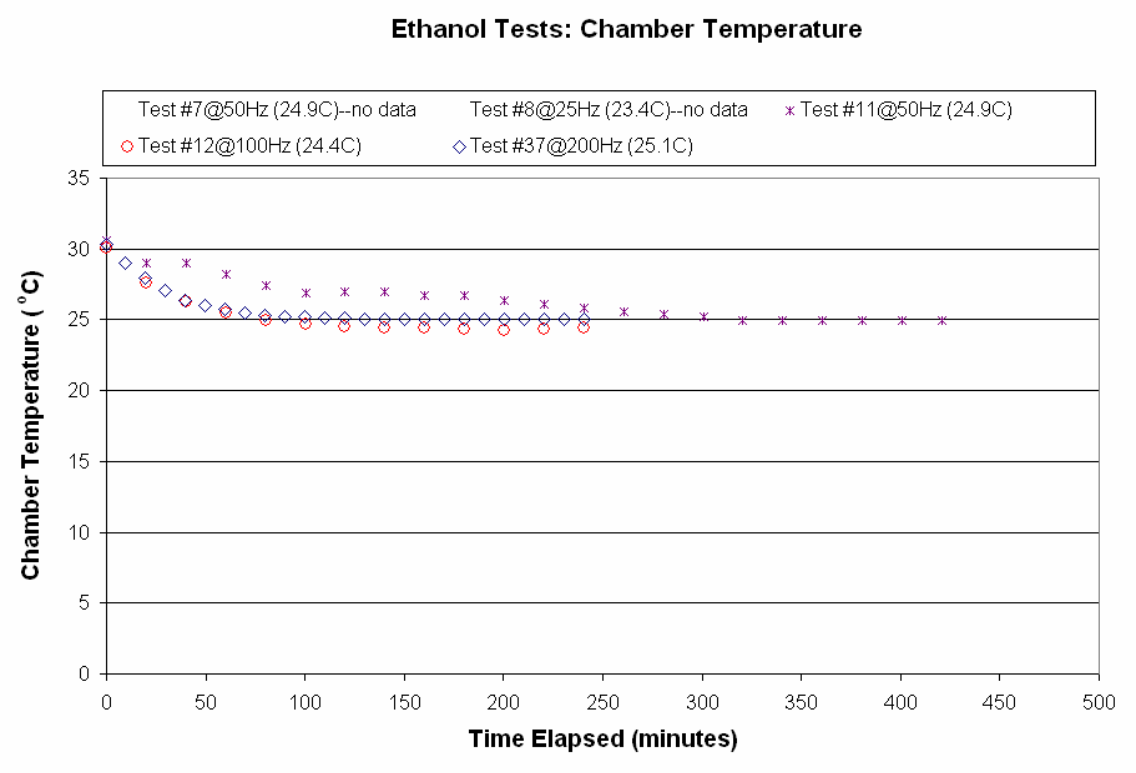

Figure 21: Comparison of Chamber Temperature for All Ethanol Experiments

A significant effort has been made to distinguish between a typical concentration profile and one irregularly affected by chamber temperature or mixing effects. Therefore, it is important to confirm that the theoretical model demonstrated a similar concentration profile. Below in Figure 22 experimental results from Test #12 were placed together with an open system model prediction under the same conditions. It is important to note that in representing the model results no parameter fits were performed. The solid curve represents the open system model prediction of an ethanol droplet evaporating in a nitrogen environment with a final vapor temperature of 24.36^{o}C and a droplet rate of 100 drops/second. From the graph we see that the model shows the typical concentration profile trend. In addition, the experimental and mathematical data are nearly identical (3.4% average deviation in final concentration). This deviation could be a result of errors in properties such as density, viscosity, diffusivity, and

temperature, and therefore adjustments in any of these parameters could decrease the deviation in the predicted results.

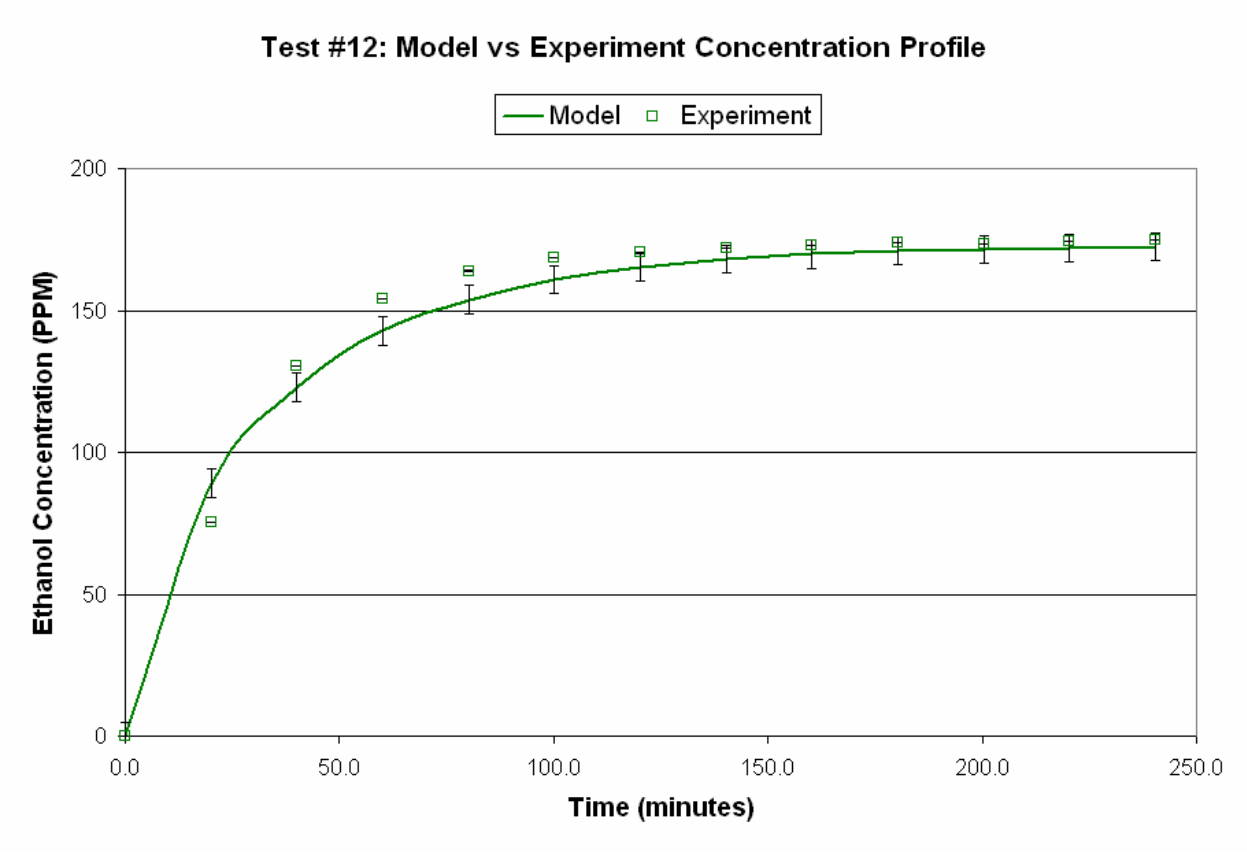

Figure 22: Comparison of Concentration Profile in Test #12 for Open System Model and Experimental Data

A comparison of the final experimental results and open system model results for all the pure ethanol droplet conditions is shown together in Figure 23. The same data is also found in tabular format in Table 2. In addition, there is a numerical measure of the deviation from the experiment results to the predicted model results. From these deviations we can see a maximum deviation of 5.7% in Test #8, and a minimum deviation of -0.7% in Test #12. The average deviation across all experiments was 3.4%. A positive deviation represents a predicted concentration larger than the measured concentration, where a negative deviation represents a

predicted concentration smaller than the measured concentration. Under the majority of cases the deviation is positive, suggesting that the model generally over-predicts the true equilibrium.

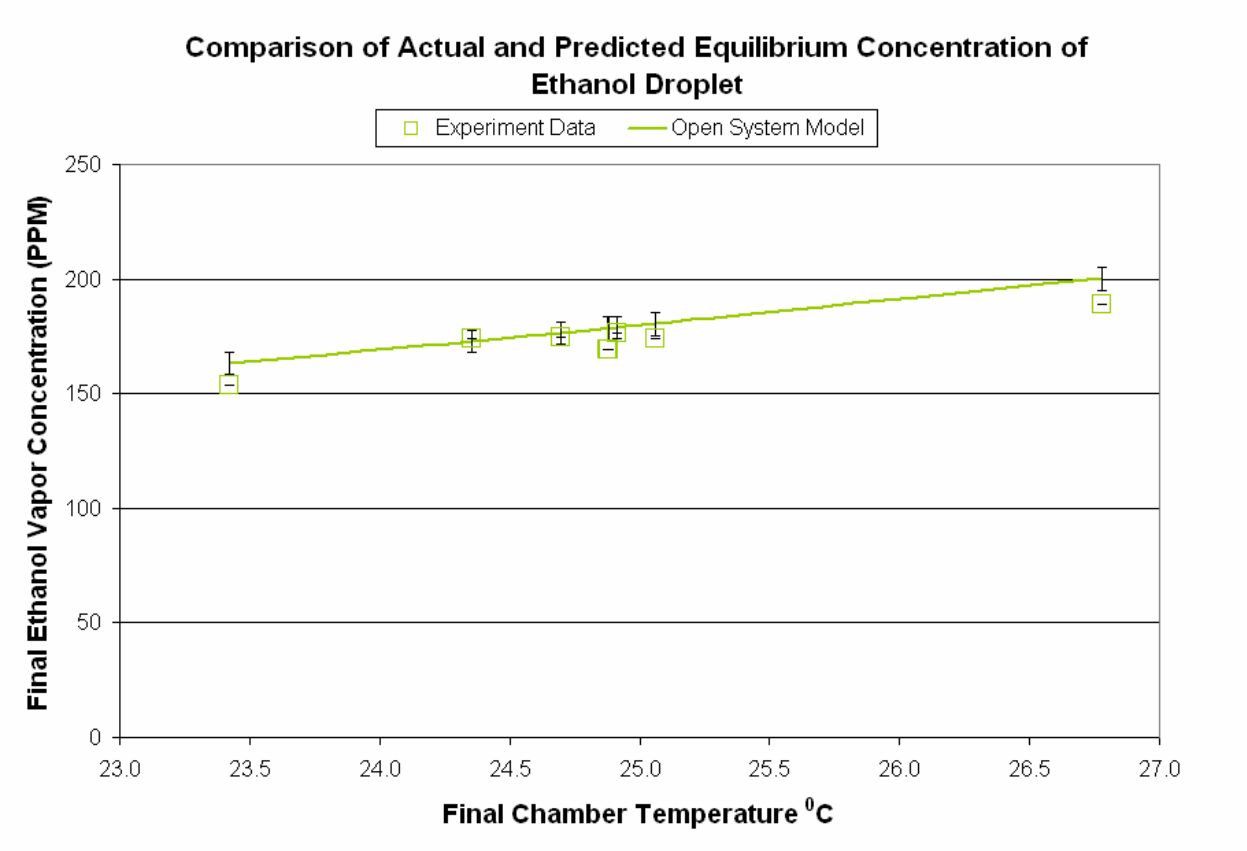

Figure 23: Comparison of Measured and Predicted Equilibrium Concentrations of Ethanol Droplet at Various Temperatures

Test #	Temperature °C	Temperature K	Open System Model (0.90atm) PPM (mg/L)	Test PPM	Deviation (Model-Test)
5	24.9	298.0	178.38	169.24	5.1%
7	24.9	298.0	178.44	169.25	5.1%
8	23.4	296.6	163.29	153.90	5.7%
11	26.8	299.9	200.17	189.09	5.5%
37	25.1	298.2	180.40	173.87	3.6%
10	24.7	297.8	176.50	174.41	1.2%
11b	24.9	298.1	178.77	176.66	1.2%
12	24.4	297.5	172.90	174.06	-0.7%
					3.4%

Table 2: Tabular Results of Ethanol Droplet Experiments

Results from Test 11 and Test 11b occurred during the same evaporation test. Test 11 occurred due to a prolonged period in which the laboratory temperature remained constant at an increased temperature before cooling to a final equilibrium captured by Test 11b results. From the above comparisons and discussion, it can be concluded that the open system model does a very good job at predicting the evaporation of pure ethanol droplets in a nitrogen environment. There is still an average over-prediction of 3.4% which can be attributed to underlying assumptions made in the model that may not be the best assumptions. For example, the effects of vapor diffusion and mixing should be included in the model since it is possible that at higher droplet rates the assumption of a well-mixed vapor may not be true.

5.5 Water Experiments

As discussed in earlier sections, the uncertainties in measured values come from the accuracy in the FTIR measuring a consistent concentration for the same temperature, and from the accuracy in the calculated relation between absorbance and concentration. This deviation was found to be ±0.025 ppm. Error bars have been placed on each experimental data point, however, since the deviation is so small compared to the total concentration the error bars appear as a single hash near the center of each data point. In addition, there is also an uncertainty in the final chamber temperature of ±0.458^{o}C, which results in a model error of ±0.593 ppm (also seen as error bars located along model trend). The full collection of all data collected during each water experiment is located in section A.3.

Pure water droplet experiments had the advantage of true equilibrium data from psychrometric charts. These known concentration-temperature data enabled a better certainty on

the absolute accuracy of both the experimental data and the open system model predicted values.

Based on pressure tests discussed in earlier sections, we would predict that the pure water experiment data would cluster closer to the closed system predictions. Figure 24 confirms our predictions. From earlier discussions we know that in an open system the system pressure is smaller than in a closed system model, and therefore, the open system model should predict larger concentrations than the closed system model at the same temperature. In the figure below we see that the experimental data all lay either on or slightly below the closed system prediction. As in the ethanol comparison, the data also demonstrates the appropriate trend of increasing concentration with increasing temperature.

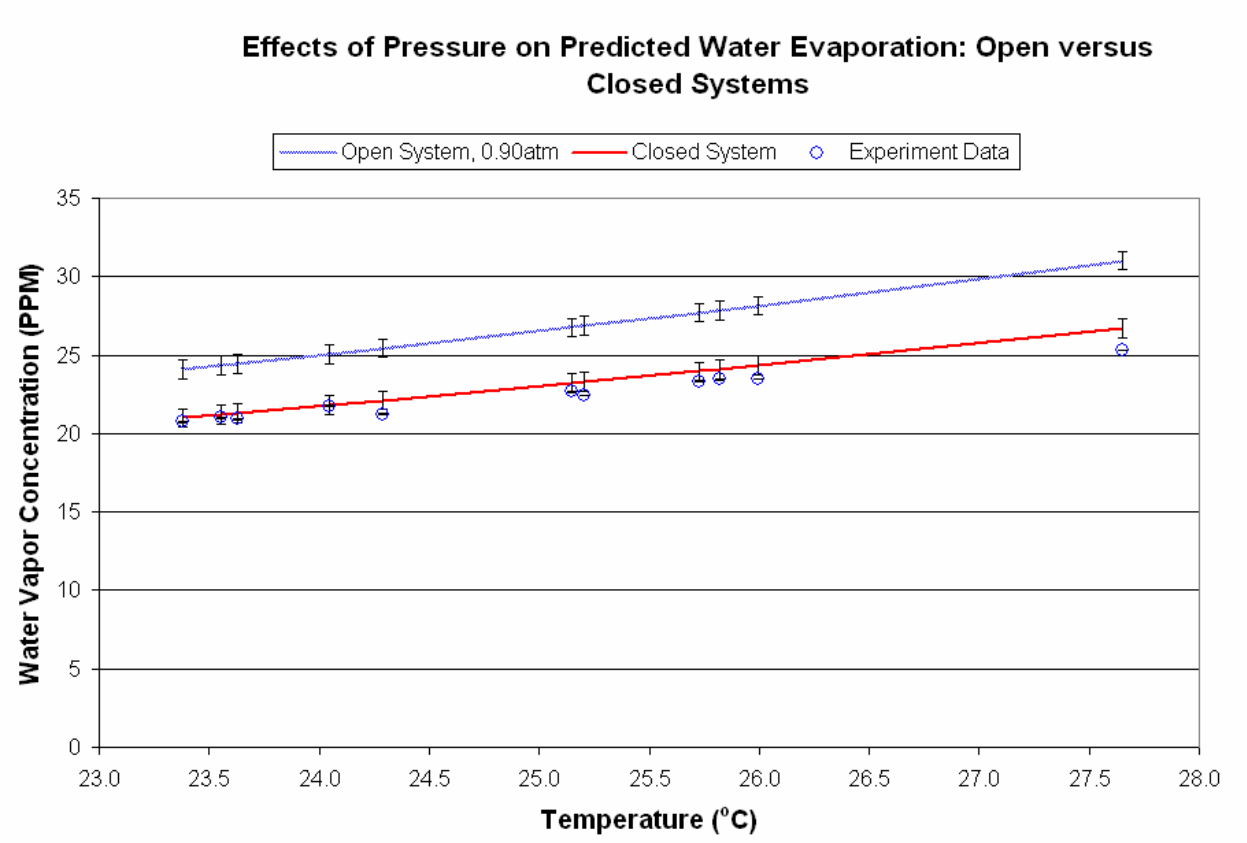

Figure 24: Comparison of Water Concentration Experiments versus an Open System Prediction and a Closed System Prediction

5.5.1 Repeatability of Water Experiments

In Figure 25 the repeatability of pure water experiments is highlighted by three tests all conducted with a continuous droplet rate of 100 drops/second. The concentration profile results for Test #13, Test #14, and Test #18 all appear to follow the same trend as seen in the ethanol experiments. Each trend progresses with an initial surge of vapor being produced followed by a slow decrease in rate until the concentration reaches equilibrium despite droplets continually being added to the system. In these experiments we observed in the first 100 minutes a spread of approximately ±20% as opposed to the ±2% spread seen in the ethanol tests, despite the closeness of the final temperatures. From the data we see an expected data spread based on final vapor temperature, where Test #18 (with a final temperature of 24.3^{o}C) has the highest concentration profile followed by Test #14 and Test #13 (each with a final temperature of 23.6^{o}C). In comparing point-by-point between Test #13 and Test #14 we see that the two sets of data diverge due to their initial water vapor concentration at the start of their experiments but merge to < ±1% in 50 minutes.

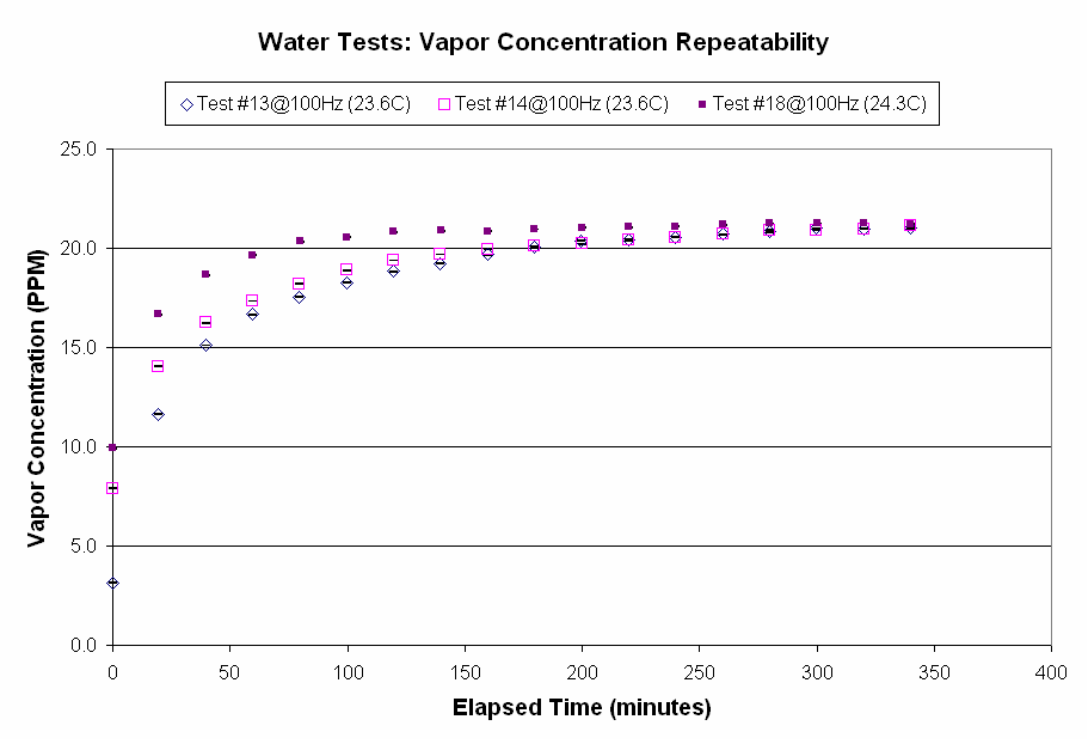

Figure 25: Vapor Concentration Repeatability in Water Experiments

Studying the temperature profiles of Test #13 and Test #14 in Figure 26 we note that the highest temperature (as presumed by the final temperature) was in Test #18, followed by Test #14 with Test #13 running the coolest profile of the three. This arrangement, among the tests, of temperature profiles support the concentration profile arrangement. So while, small differences did occur between the three water tests it can be concluded that they are certainly repeatable.

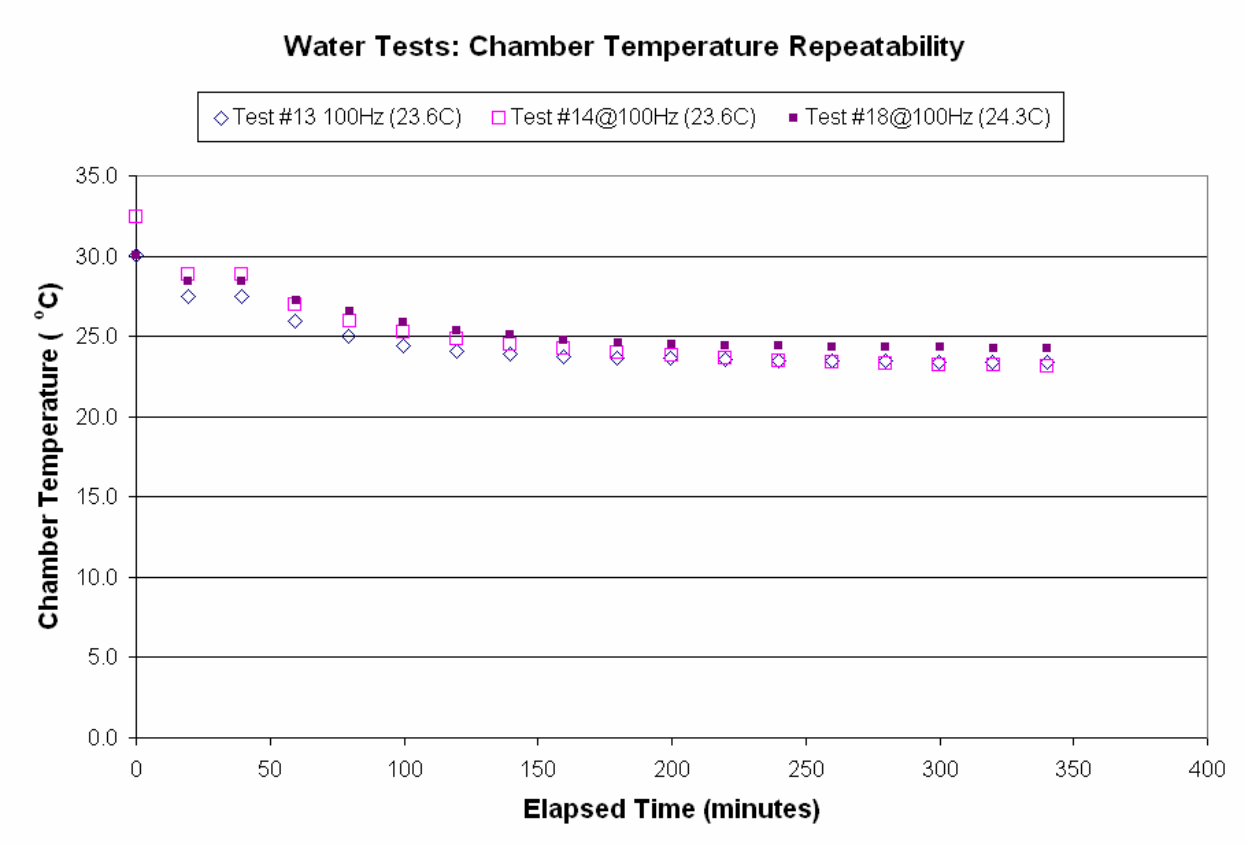

Figure 26: Chamber Temperature Repeatability in Water Experiments

Over a temperature range of 0.7°C, among the three water experiments there was a corresponding concentration range of 0.30 ppm. In the repeatability analysis, the highest temperature was associated with the highest concentration as would be expected.

5.5.2 Theoretical and Experimental Comparison

Since there were eleven pure water experiments, and graphically displaying all the information would become extremely cluttered, the resulting graphical data has been separated into three plots. The first, Figure 27, compares the five experiments run with a droplet rate of

100 drops/second. From this figure, we have already discussed the variations between Test #13, Test #14, and Test #18; leaving Test #19 and Test #29. Test #29 had the highest final temperature amongst the five experiments, and Test #19 had the next highest final temperature. Test #29 appears to have the highest concentration profile initially and at the end, but shows substantial fluctuations in between. Most likely these drifting concentrations will be due to drifting vapor temperatures, but this will be shown later in the section. Test #19, with the second highest final temperature, demonstrates the lowest temperature profile initially and then ramped-up 2 hours into the experiment

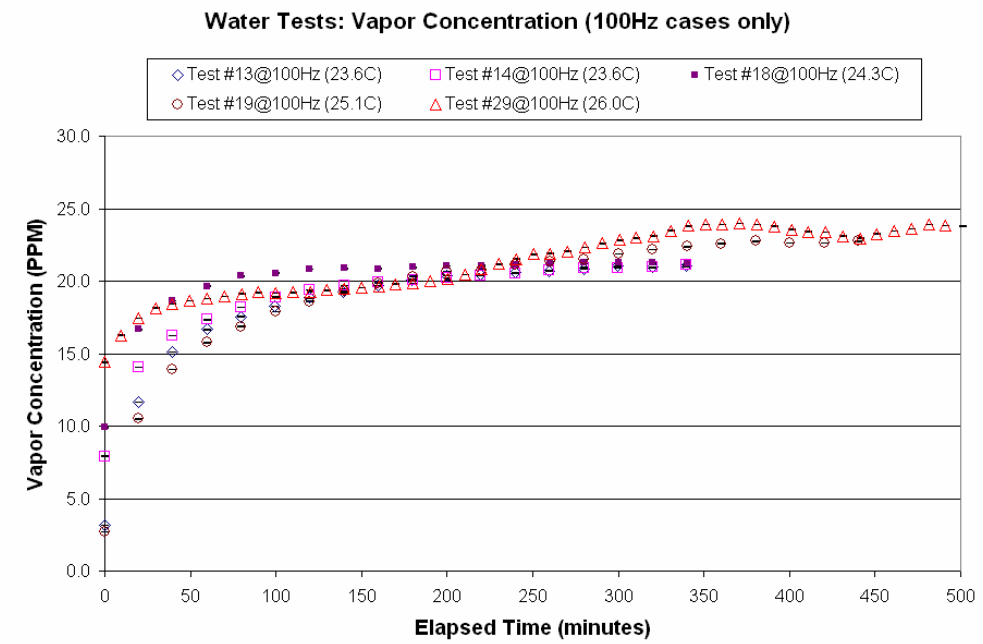

Figure 27: Vapor Concentration Comparison of All 100Hz Water Experiments

Next, in Figure 28 are the concentration profiles for the three pure water experiments which used droplet rates of 300 drops/second. The three tests, Test #27, Test #28, and Test #30, have final temperatures of 25.7°C, 25.8°C, and 27.2°C respectively. Again, the three tests all demonstrate the typical concentration profile. While all three have the same initial slope, Test

#27 and Test #28 equilibrate earlier than Test #30. The profile order corresponds with the final temperatures for each test, with Test #30 (highest final temperature) the highest final concentration, followed by Test #28 and Test #27 which have nearly identical final temperatures and concentrations.

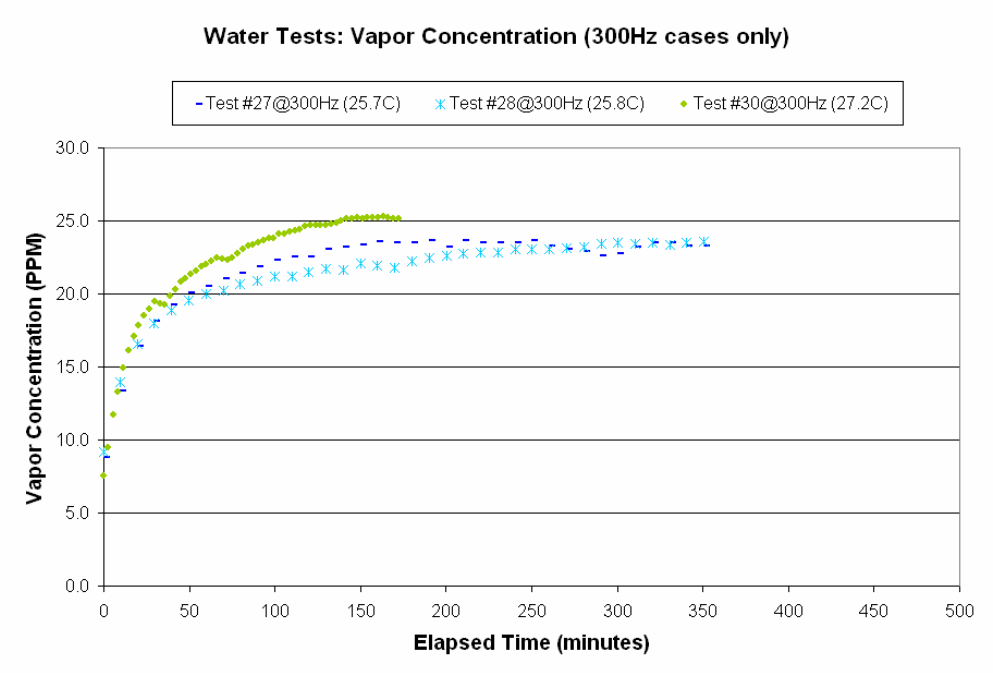

Figure 28: Vapor Concentration Comparison of All 300Hz Water Experiments

Finally, in Figure 29, we compare the remaining pure water concentration profiles (Test #15, Test #16, and Test #26) along with results from Test #13 (100 Hz case) and Test #27 (300 Hz case). Collecting the data in such a way we can clearly compare the trends between tests based on both final chamber temperature and droplet rate. Test #15 has a droplet rate of 50 drops/second and a final temperature of 24.0^{o}C and Test #16 also has a droplet rate of 50 drops/second but a lower final temperature of 23.4^{o}C. From Figure 29 we see that Test #16 has a slightly lower final concentration than Test #15 due to the temperature difference. Their initial concentration trends do not appear to line up, as would be expected; from the first concentration

point we see a 3 ppm difference initial vapor concentrations due to differences in their respective laboratory ambient humidity. This variation in initial concentration causes Test #15 to consistently lie above Test #16 in concentration profiles. Moving upwards in droplet rates, we revisit Test #13 at 100 drops/second and Test #27 at 300 drops/second. As would be expected Test #13 has a steeper slope than either Test #15 or Test #16, and does not have as steep of a slope as Test# 27. Finally, Test #26 with a droplet rate of 1000 drops/second, reaches equilibrium within the first 20 minutes due to the high droplet rate.

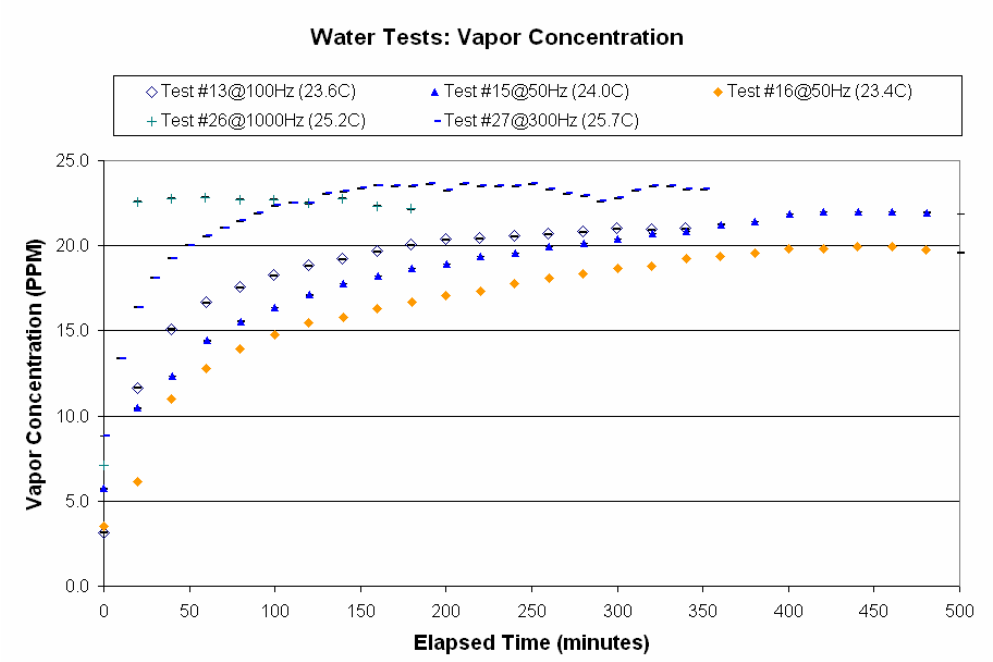

Figure 29: Comparison of Concentration Profiles between Various Water Experiments

Figure 30 shows all the temperature profiles from each of the pure water tests, except Test #30. Data from Test #30 was excluded from the figure because the temperature was manually maintained at the 27.7^{o}C temperature with the film heaters. This test was done to expand the temperature range for the pure water tests since equilibrium concentrations from each test could be numerically verified by comparison with psychrometric data. Laboratory ambient

temperature did not allow for a large range of temperatures, maintained within 2.6°C, so Test #30 expanded the range to 4.3°C. The key observation from Figure 30 is that all the temperature profiles follow very similar trends. Earlier we made a couple assumptions to explain the unusual behavior in Test #29. In this 100 Hz test the concentration profile appeared to follow a drifting trend, in which it had the highest concentration profile initially but then crossed paths with other 100Hz cases before settling at the highest concentration. We assumed this fluctuation in concentration was driven by earlier fluctuations in temperature. Looking in Figure 30 we see the temperature profile for Test #29 starts at 30°C but dropped below 24°C before increasing back up towards 26°C. This rolling trend in chamber temperature directly affected the driving force for mass transfer by changing the equilibrium vapor concentration, which is why we see the temperature change followed closely by a proportional concentration change.

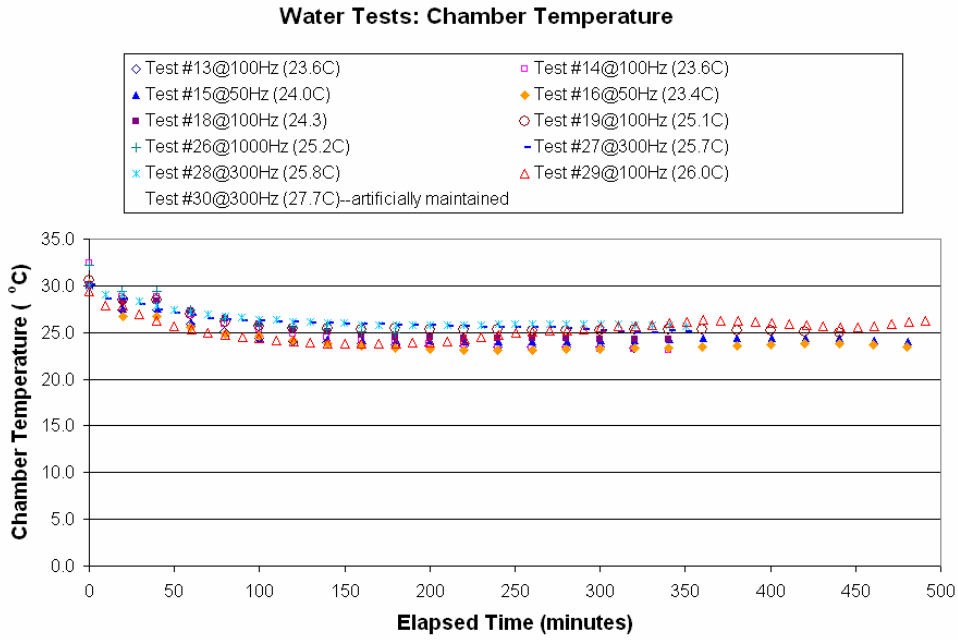

Figure 30: Comparison of Chamber Temperature Profiles between All Water Experiments

It was important to confirm that the theoretical model demonstrated a similar concentration profile. Below in Figure 31 experimental results from Test #13 were placed together with a closed system model data under the same conditions. It is important to note that in representing the model results no parameter fits were performed. The solid curve represents the closed system model prediction of a water droplet evaporating in an ambient air environment with a final vapor temperature of 23.55^{o}C and a droplet rate of 100 drops/second. From the graph we see that the model shows the typical concentration profile trend. However, the predicted and experimental data flip-flop; initially the test data has a steeper slope, but the model has a longer slope, so the two cross after about 60 minutes and the model continues to predict larger concentrations than the test data from that point. This deviation could be a result of errors in properties such as density, viscosity, diffusivity, and temperature, and therefore adjustments in any of these parameters could decrease the deviation in the predicted results.

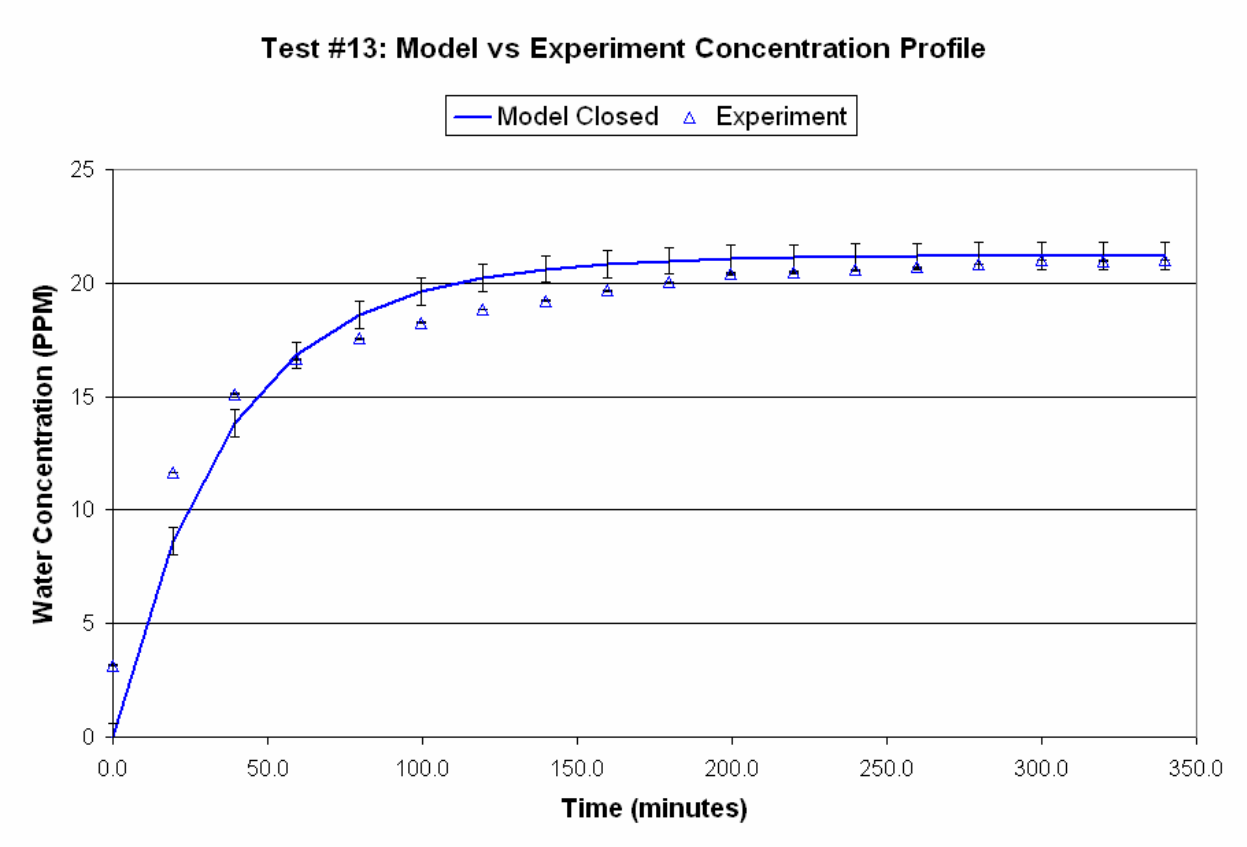

Figure 31: Comparison of Concentration Profile between Closed System Model and Experimental Data for Water Test #13

A comparison of the final experimental results, closed system model results, and psychrometric data for all the pure water droplet conditions is shown together in Figure 32. The same data is also found in tabular format in Table 3. In addition, the table contains a numerical measure of the deviation from the experiment results to the predicted model results, deviation from the experimental data to psychrometric data, and deviation from the model prediction to psychrometric data.

In comparing the experimental data to psychrometric data there's a maximum deviation of 2.71% in Test #15, and a minimum deviation of 0.64% in Test #26 resulting in an average deviation across all tests of 1.40%. A positive deviation represented a measured concentration larger than the psychrometric concentration, where a negative deviation represented a measured

concentration smaller than the psychrometric concentration. Under all but one test condition, Test #18, the experiment showed a larger concentration than from psychrometric data.

Comparing the closed system model predictions to the experimental data there is a maximum deviation of 5.18% in Test #30, a minimum deviation of -0.01% in Test #13, resulting in an average deviation across all tests of 2.57%. A positive deviation represented a predicted concentration larger than the experimental concentration, where a negative deviation represented a predicted concentration smaller than the experimental concentration. Under all but one test condition, Test #15, the model showed a larger concentration than from experimental data. In Test #13 the two sets of data showed nearly identical concentrations (deviation of -0.01%).

Finally, deviations between the model predictions and the psychrometric data will be the summation of the previous comparisons. The resulting maximum deviation was 7.10% in Test #30, the minimum deviation was 0.60% in Test #15, and the average deviation was 3.9%. A positive deviation represented a predicted concentration larger than the psychrometric concentration, where a negative deviation represented a predicted concentration smaller than the psychrometric concentration. Under all test conditions the model over-predicted the true water concentration from psychrometric data.

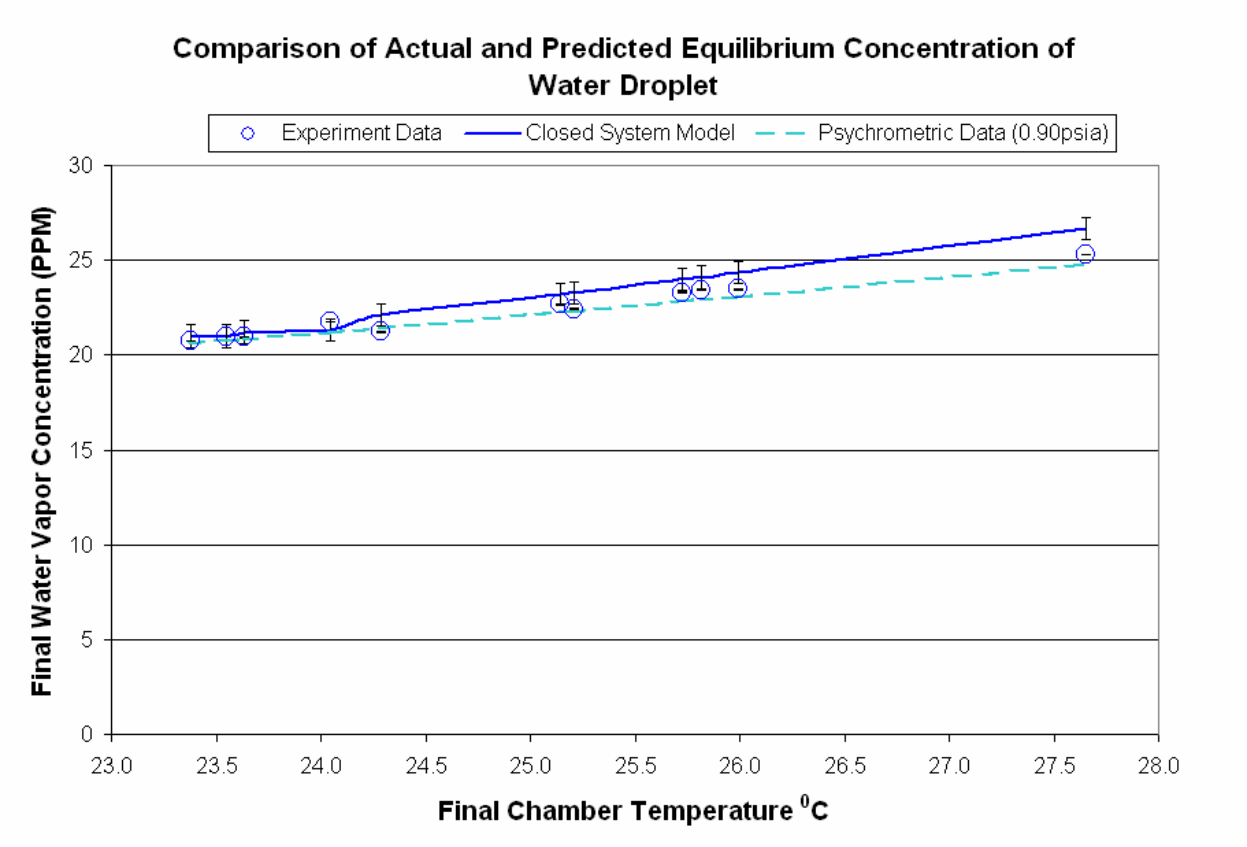

Figure 32: Comparison of Water Equilibrium at Various Temperatures between Psychrometric Data, Experimental Data, and Closed System Model predictions

Test #	Temperature		Model Closed Sys	Test	Psychrometric Chart	Deviation		
	°C	K	PPM (mg/L)	PPM (mg/L)	PPM (mg/L)	Test-Psyc	Model-Test	Model-Psyc
13	23.6	296.7	21.00	21.00	20.74	1.2%	0.0%	1.2%
14	23.6	296.8	21.21	20.93	20.79	0.7%	1.3%	2.0%
15	24.0	297.2	21.30	21.76	21.17	2.7%	-2.1%	0.6%
16	23.4	296.5	21.81	20.74	20.57	0.8%	4.9%	5.7%
18	24.3	297.4	22.12	21.23	21.42	-0.9%	4.0%	3.2%
19	25.1	298.3	23.21	22.70	22.24	2.0%	2.2%	4.2%
26	25.2	298.4	23.29	22.44	22.30	0.6%	3.6%	4.2%
27	25.7	298.9	23.98	23.29	22.82	2.0%	2.9%	4.8%
28	25.8	299.0	24.10	23.45	22.89	2.4%	2.7%	5.0%
29	26.0	299.1	24.34	23.47	23.08	1.7%	3.6%	5.2%
30	27.7	300.8	26.68	25.30	24.80	2.0%	5.2%	7.1%
						1.4%	**2.6%**	**3.9%**

Table 3: Tabular Results of Water Droplet Experiments

In comparing across all the test cases, the overall experimental temperature range was 4.3°C and showed a concentration range of 4.6 ppm, while humidity data showed a concentration range of 4.2 ppm, and the models predicted a concentration range of 5.7 ppm.

From the above comparisons and discussion, it can be concluded that the closed system model does a very good job at predicting the evaporation of pure water droplets in an air environment. There is still an average over-prediction of 4% which can be attributed to underlying assumptions made in the model that may not best describe the system.

5.6 Multicomponent Experiments

As discussed in earlier sections, the uncertainties in measured values come from the accuracy in the FTIR measuring a consistent concentration for the same temperature, and from the accuracy in the calculated relation between absorbance and concentration. This deviation was found to be ±0.025 ppm. Error bars have been placed on each experimental data point, however, since the deviation is so small compared to the total concentration the error bars appear as a single hash near the center of each data point. In addition, there is also an uncertainty in the final chamber temperature of ±0.458°C, resulting in a ±3.04 ppm and ±0.490 ppm error in ethanol and water concentration prediction, respectively. The full collection of all data during each ethanol-water mixture experiment is located in section A.3.

Based on the assumption that all ethanol-water mixture droplet experiments had to operate with the internal evaporation chamber at the same pressure as the ambient pressure, we would assume that when experimental results were compared to predictions from both an open system model and a closed system model that the data would cluster closer to the open system

predictions. First we compare predictions from an open system and a closed system against experimental data for ethanol vapor concentration. In Figure 33 and Figure 34 lines are no longer used to connect the data as seen in Figure 17 and Figure 24 for pure ethanol and pure water experiments, respectively. This is because the data no longer represents the concentration-temperature profile of the same fluid mixture, but rather the concentration of different mixtures at different temperatures. In Figure 33 all experimental data except for the 20.975% ethanol case (Test #25) lie closer to the open system model prediction than the closed system model prediction. In Figure 34 there are three tests in which the measured experimental condition lies closer to the closed system prediction than to the open system prediction, Test #22, Test #25, and Test #35. However, in the majority of cases we can confirm that the experimental data indeed demonstrates the trends of an open system more than that of a closed system. From the two figures we also see a general trend that higher liquid ethanol compositions resulted in higher ethanol vapor concentrations and lower water concentrations. In addition, comparing the two tests which had a 50% liquid mole percent (Test #23 and Test #22), Test #22 which had a higher final temperature also had a higher final vapor concentration of ethanol and water than measured in Test #23 which had a lower final temperature.

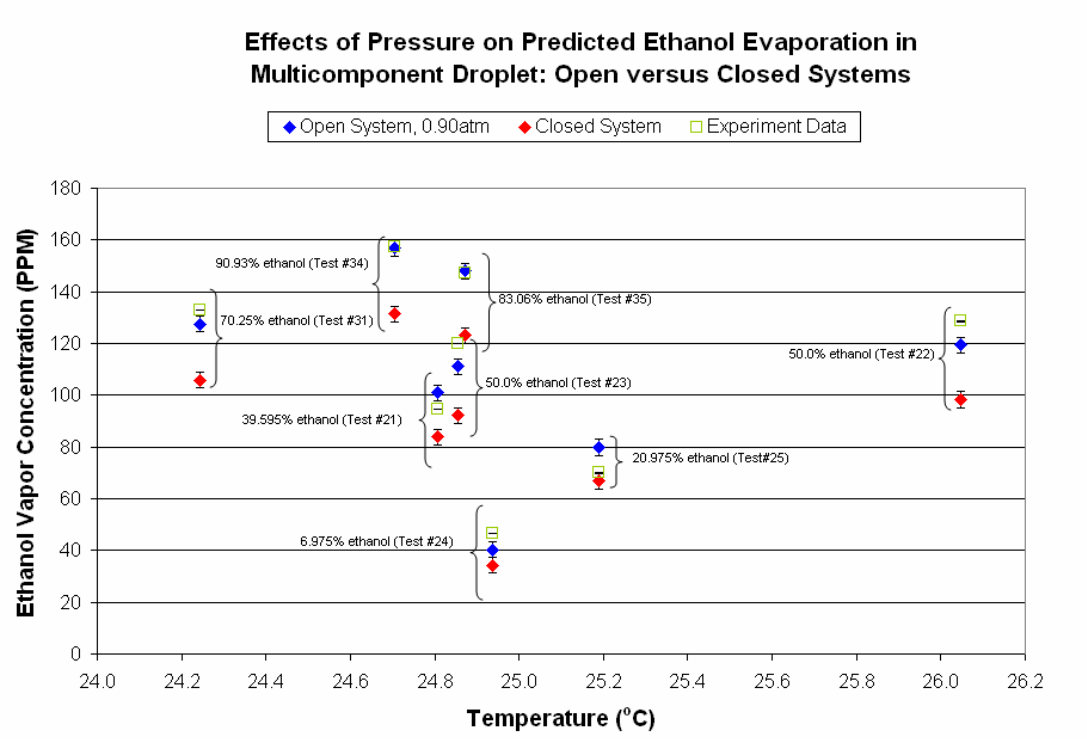

Figure 33: Comparison of Ethanol Vapor Concentration (in Multicomponent Droplet Experiments) Versus Open System Model Prediction and Closed System Model Prediction

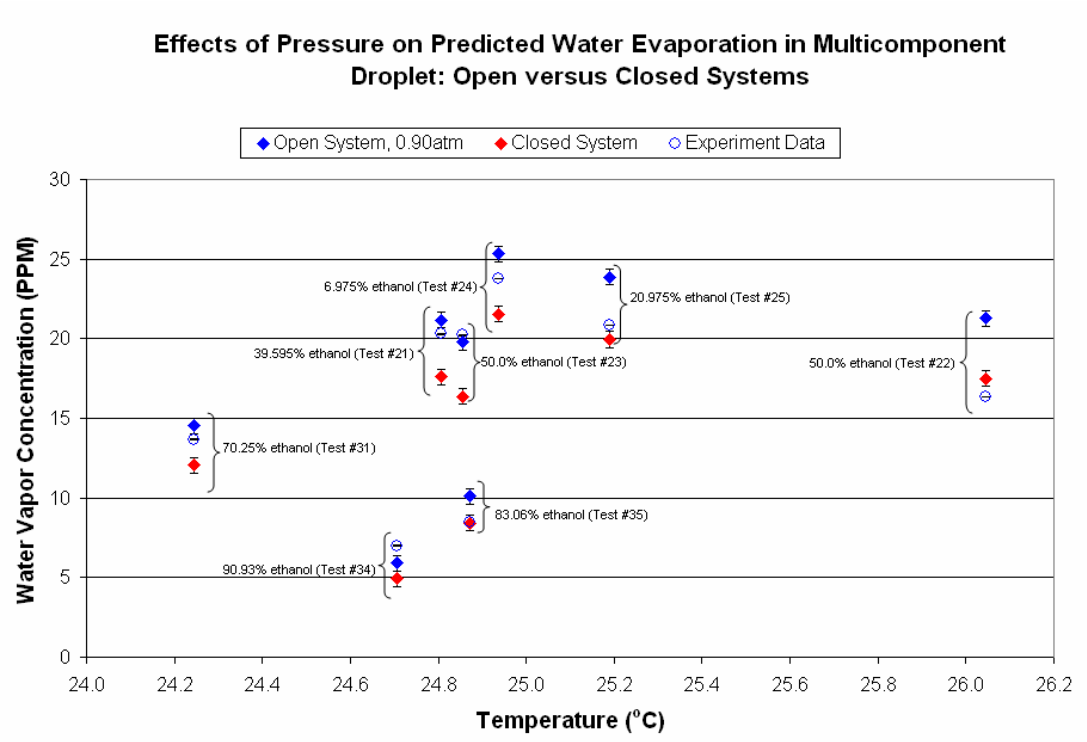

Figure 34: Comparison of Water Vapor Concentration (in Multicomponent Droplet Experiments) Versus Open System Model Prediction and Closed System Model Prediction

5.6.1 Theoretical and Experimental Comparison

To verify that the model could capture similar concentration profiles for a multicomponent fluid as had been captured in the pure fluid case; data from Test #31 was compared with time dependent concentrations from the open system model. Figure 35 shows both the ethanol and water concentration profiles from experimental data and predicted data. It is important to note that in representing the model results no parameter fits were performed. The solid curve represents the open system model prediction of a 70.3 mole% ethanol - 29.7 mole% water droplet evaporating in an ambient air environment with a final vapor temperature of 24.24^{o}C and a droplet rate of 300 drops/second. In Figure 35 we observe that the model slightly over-predicts the water profile, and slightly under predicts the ethanol profile. However, if the total concentrations were compared we would notice that the model is predicting almost the same total concentration as seen from the test data. This deviation could be a result of errors in properties such as density, viscosity, diffusivity, and temperature, and therefore adjustments in any of these parameters could decrease the deviation in the predicted results.

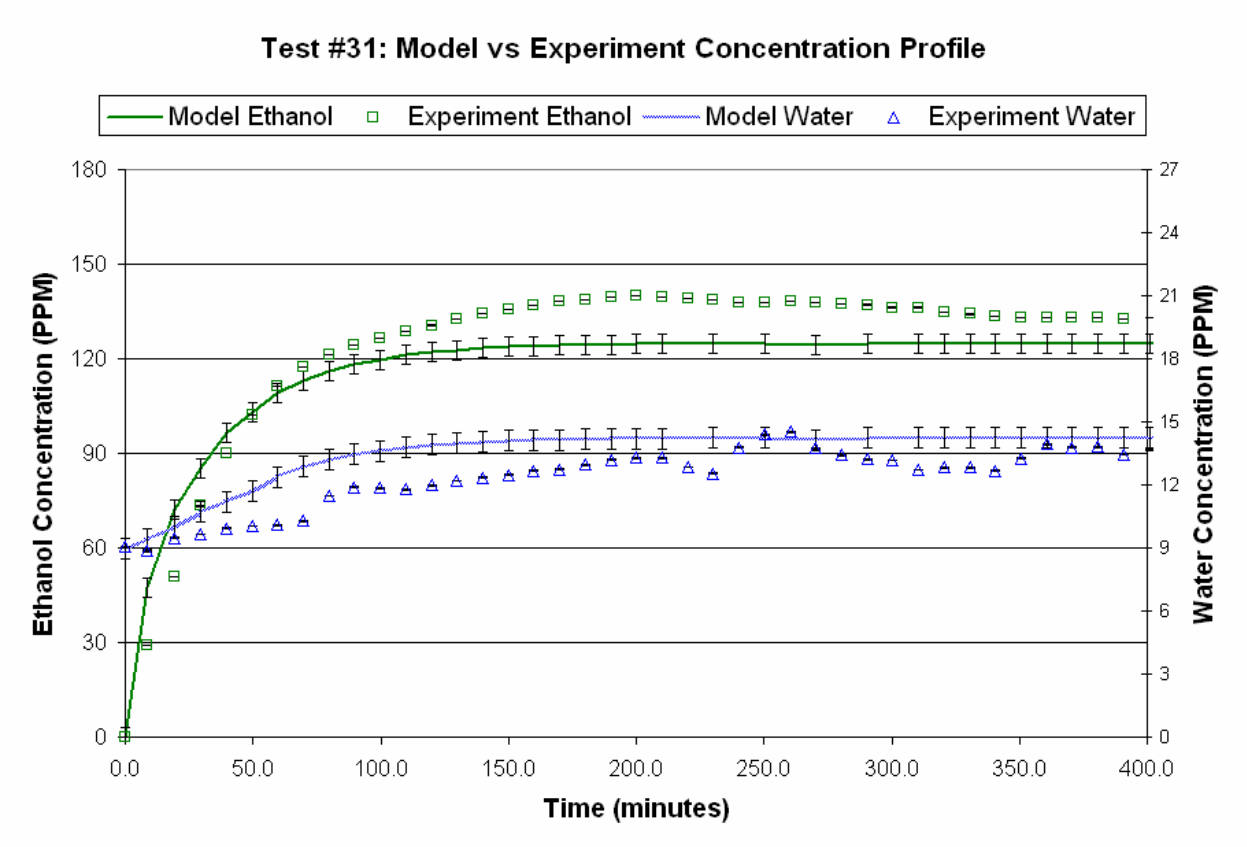

Figure 35: Comparison of Concentration Profile between Open System Model and Experimental Data for Multicomponent Test #31

Figure 36 (below) is a collection of all the final concentrations for all the multicomponent fluid mixture experiments. On the left y-axis is the final ethanol concentration while on the right y-axis is the final water concentration. From the data we see that the predicted data is very close to the measured concentrations for all cases. In most cases the model over-predicted the water concentration, while under-predicting the ethanol concentration; similar to the trend seen in Figure 35. However, overall the model predicted the ethanol vapor composition better than the water vapor composition. The reason for this is unclear, but one possible cause could be that in general water is a difficult fluid to model due to its polarity.

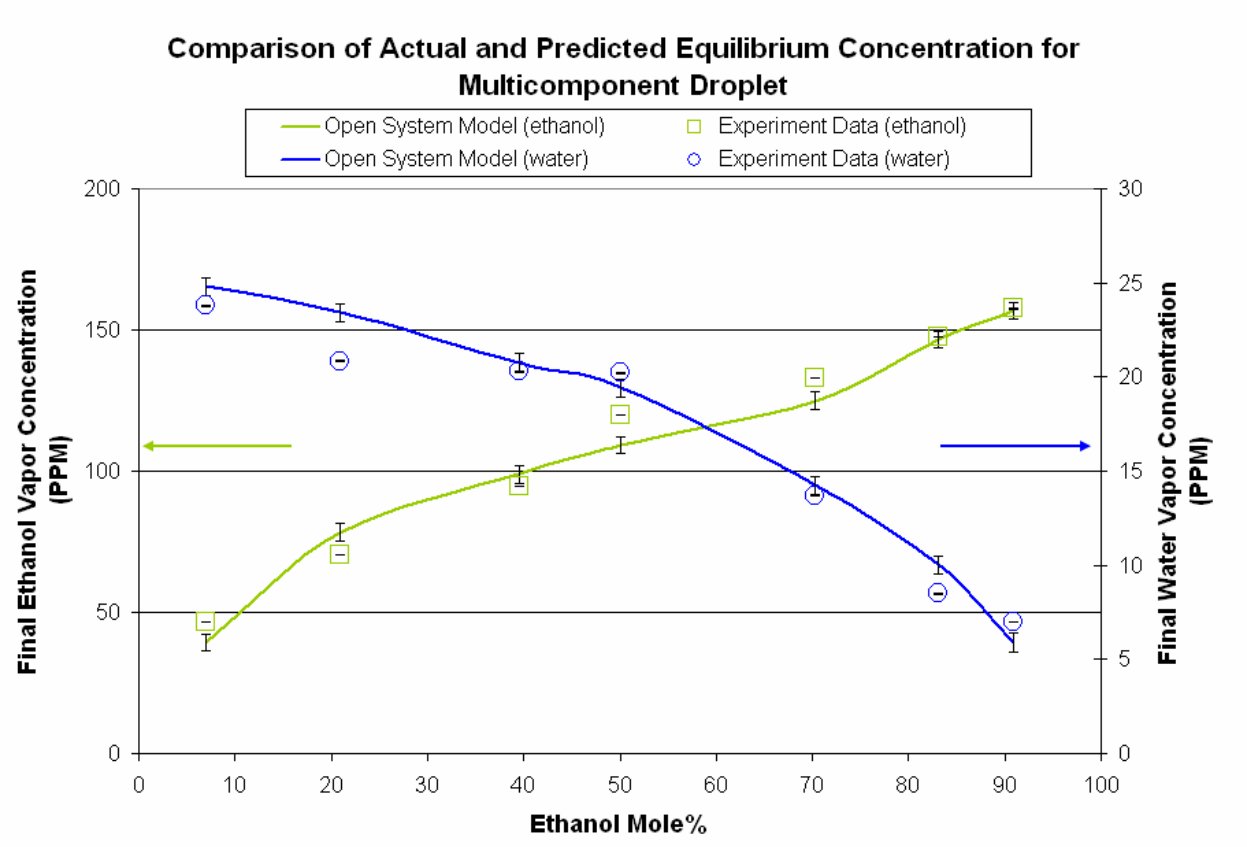

Figure 36: Comparison of Open System Model Predictions and Experimental Data for Multicomponent Droplet Experiment Vapor Concentrations of Ethanol and Water

In addition, Table 4 shows the numerical deviation between the open system model predictions for each test case and the experimentally measured concentrations. A minimum deviation in ethanol concentration data was -0.5% in Test #34 and Test #35, the maximum deviation was -18.0% in Test #24, resulting in an overall deviation between ethanol data of -3.7%. A minimum deviation in the water data was 2.3% in Test #21, and a maximum deviation of 21.7% in Test #22, resulting in an average deviation of 4.4%.

Test #	Temperature		Composition	Model		Test		Deviation Model -Test	
				PPM (mg/L)	PPM (mg/L)	PPM (mg/L)	PPM (mg/L)		
	°C	K	Ethanol Mole %	Ethanol	Water	Ethanol	Water	Ethanol	Water
23	24.9	298.0	50.000	109.19	19.41	119.81	20.22	-9.7%	-4.2%
21	24.8	298.0	39.595	98.87	20.76	94.46	20.29	4.5%	2.3%
22	26.0	299.2	50.000	117.37	20.90	128.54	16.36	-9.5%	21.7%
24	24.9	298.1	6.975	39.42	24.81	46.52	23.78	-18.0%	4.2%
25	25.2	298.3	20.975	78.39	23.41	70.35	20.84	10.3%	11.0%
31	24.2	297.4	70.250	124.99	14.24	132.90	13.68	-6.3%	3.9%
34	24.7	297.9	90.930	156.80	5.90	157.54	7.00	-0.5%	-18.7%
35	24.9	298.0	83.060	146.72	10.01	147.40	8.49	-0.5%	15.2%
								-2.9%	**5.6%**

Table 4: Tabular Results of Ethanol-Water Mixture Droplet Experiments

While the mixed-fluid results showed a larger degree of deviation, overall the average deviation remained below 4.5%. The increased deviation from pure fluid modeling to mixed-fluid modeling was expected since the model algorithm and mass flux is more complicated in the mixed-fluid case than for pure fluids.

CHAPTER 6: CONCLUSION AND RECOMMENDATONS

The research has provided an in depth investigation into binary droplet evaporation behavior while reaching equilibrium concentrations. This chapter summarizes the important conclusions that can be drawn from the experimental results and analysis. Recommendations for future research are also given so that further improvements can be made in the future. There is still work to be done to capture more of the system phenomena, for example the effects of liquid and vapor mixing and interaction between droplets, at which point the models can be used to predict evaporation behavior in sprays.

6.1 Conclusions

The main goal of the research was to provide a fundamental modeling tool for the understanding of multicomponent system evaporation. The research has focused on studying the evaporation of pure ethanol, pure water, and various composition mixtures of ethanol and water.

The research indicated that pure water experiments provided similar results to known psychrometric data (less than 1.4% deviation) and an over-prediction by the closed system model of 4.0%. In addition, the open system model showed an average over-prediction to experimental data of 3.4%. Finally, the open system model used to predict the evaporation of the ethanol-water mixtures showed an average under-prediction for the ethanol portion of -3.7% and an average over-prediction for the water portion of 4.4%. It was shown that pure ethanol and pure water experiments could be repeated with good accuracy. The slope of the concentration profile was also found to be dictated by both the droplet rate used and the heat loss (or change in

temperature) of the evaporation chamber. Experiments with larger droplet rates had steeper slopes and reached equilibrium faster. In the comparison between predicted and experimental results it is import to note two things. The first is that the parameters in the model were never fit to correspond with measured data, but were rather modeled based on the few inputs of temperature, pressure (open or closed), liquid mole fractions, and vapor mole fractions. The second observation is that all predicted results appeared to have a systematic deviation from the experimental data, in which the model was always over predicting or under predicting. This leads to the possibility that an error in one or more properties was the cause. However, there is still a strong argument towards deviations also being caused by the assumption of a well-mixed vapor phase.

6.2 Recommendations

As mentioned, there is still much to be investigated before multicomponent evaporation is fully understood. Future research should focus on a more detailed determination of the data which could only be estimated at this time. Improvements could be made in the experimental design and the experimental scope by including more automated control of temperatures and by broadening the test temperature, pressure and fluid mixture range.

While the current experimental design allowed for all the critical parameters to be monitored there are aspects of the design that if changed, would significantly increase the flexibility of the experiment. Some changes would include a programmable heater for the evaporation chamber. While the current design contained four film heaters, which performed well in heating the chamber, the design required that the power supply to the heaters be manually

adjusted in the case that a constant internal temperature was to be maintained. This was a very tedious and inexact process with inevitable temperature fluctuations, not to mention that experiments which took 6-10 hours to run had to be monitored and adjusted constantly. Had a programmable temperature controller been in place, the testing of a larger temperature range would have been more feasible. The final design change would have been to outfit the reservoir in a programmable temperature bath. That way the reservoir temperature could be monitored and controlled if necessary. Currently, tests were run with room temperature reservoir fluid, and while room temperature fluctuations were assumed to play a minimal role in the temperature of the reservoir fluid, the available control would have been an increased certainty.

6.2.1 Future Work

This, and similar, work is invaluable for the pursuit of more advanced alternative fluids. With the ability to customize a fluid for a specific application, comes a greater potential of improving the efficiency of processes. In addition, this research brings us one step closer to manufacturing custom fluid mixtures for specific needs and regulations. However, to get to this point more testing and analysis is needed.

It would be suggested that future experiments be run over a larger chamber temperature range so that a more complete analysis of equilibrium behavior can be tested against the numerical model. With the use of a temperature controller for the evaporation chamber, the internal vapor temperature could be held constant, thus affecting the final equilibrium concentrations.

To fully understand the droplet evaporation behavior it is proposed that a PDPA be used to study the droplet velocity and diameter. This information could be used to better represent droplet size and velocity distributions. Such analysis would need to be done for all fluid mixtures to determine the dependence composition plays on size and velocity. In addition, the frequency at which the droplet generator is set should be varied to determine if droplet frequency plays a role in the size and velocity of droplets. In addition, by altering the nozzle design the droplet diameter size ranges can be altered to test the effect on transient concentration behavior. In the case that research proceeded with additional fluids, it would be valuable to further relate the fluid surface tension to velocity and size from the droplet generator.

Furthering the study by including other fluids and fluid mixtures would lead to an increased generality in the evaporation model. Therefore, from extending this study to other fluids it would be possible to increase the confidence in the numerical model.

It is believed that once an acceptable level of confidence is achieved in the multicomponent droplet evaporation model, that the model should be adapted for the case of spray evaporation. Such a numerical model would take into consideration population distribution functions of droplet size, concentration and velocity. Additionally, there would be significant interaction effects between droplets, which would dramatically vary the evaporation rate of each component based on its location within the spray cone. Both the theoretical and experimental work would be complex to capture the unsteady evaporation of a multicomponent droplet in a spray environment. Concurrently, research as to the heat transfer capabilities of fluids and fluid mixtures should be pursued. This analysis could be accomplished by studying the CHF curves of fluid mixtures such as ethanol-water. Since heat removal is not the only important aspect to choosing an alternative fluid it would also be necessary to evaluate the

compatibility of alternative fluids with spraycool technology and the electrical equipment spray cooling is used on.

The present research has indicated that there are still many areas which need to be further researched to provide a better understanding of multicomponent evaporation. Multicomponent diffusion and evaporation phenomena are complex even in the simplistic case of single droplet evaporation because both the liquid and vapor effects must be evaluated simultaneously. Therefore, when interacting effects between droplets are also evaluated the numerical complexity increases because unlike in the single droplet case the vapor concentration gradient can be dramatically different for each droplet in the spray, and spatially unique contributions from each droplet can no longer be averaged together as a bulk contribution.

APPENDIX

A.1 Nomenclature

A,	Absorbance
a,	Absorptivity
B,	Inverted binary diffusion coefficient
b,	Path length
c,	Concentration
c_p,	Heat capacity
D,	Binary diffusion coefficients
d,	Diameter
E,	Van Laar binary interaction parameter
$Freq$,	Droplet frequency rate
H,	Enthalpy
J,	Molar diffusion flux relative to molar average velocity
K,	Characteristic constant for the evaporating substance
k,	Mass transfer coefficient
L,	Constant defined as $L \equiv a \cdot b$
MW,	Molecular weight
M,	Mass (gram or kgram basis)
m,	Mass (mole basis)
N,	Molar flux relative to a stationary reference

n, Total number of species

P, Pressure

$\mathcal{P}$, Modal invertible matrix

R, Universal gas constant; $8.314 \frac{Pa \cdot m^3}{mole \cdot K}$

T, Temperature

t, Time

u, Velocity

W, Liquid mass

x, Liquid phase mole fraction

y, Vapor phase mole fraction

z, Direction coordinate

Q, Arbitrary pure component property

q, Arbitrary mass (or mole) fraction or component

Greek Letters

α, Heat transfer coefficient, thermal diffusivity

β, Stefan diffusion bootstrap coefficient

δ, Kronecker delta

ε, Lennard-Jones parameter

Φ, Mass transfer rate factor

Γ, Thermodynamic factor

γ, Activity coefficient

η, Dynamic viscosity

κ, Boltzmann's constant $= 1.38066 \times 10^{-23}\ J/K$

Λ, Determinacy coefficient parameter

λ, Latent heat of vaporization

μ, Thermal conductivity

ν, Kinematic viscosity

π, pi; 3.14

ρ, Density of fluid

σ, Lennard-Jones molecular diameter

ς, Flux Ratio

ϖ, Determinacy coefficient

Ω, Lennard-Jones collision integral

Ξ, High flux correction factor

Ψ', First Antoine constant

Ψ'', Second Antoine constant

Ψ''', Third Antoine constant

Dimensionless Parameters

Nu, Nusselt number, $\frac{hL}{\mu}$

Pr, Prandtl number, $\frac{\eta c_p}{\mu}$

Re,	Reynolds number, $\frac{Lu\rho}{\eta}$

Subscripts

1,	Ethanol property or parameter
2,	Water property or parameter
3,	Air (or Nitrogen) property or parameter
a,	Air property or parameter
b,	Bulk phase property or parameter
e,	Equilibrium state property or parameter
ep,	Exposure property or parameter
i,	Component i property or parameter
j,	Component j property or parameter
k,	Component k property or parameter
l,	Liquid phase property or parameter
$mass$,	Specifies mass units
m,	Molecular property or parameter
n,	Component n property or parameter
p,	Droplet property or component
v,	Vapor phase property or parameter

Superscripts

$\bullet$,	Referring to the finite transfer rates

$calibrated$,	Calibrated measurement
new ,	Current value in a convergence loop
$non-calibrated$,	Non-calibrated measurement
old ,	Previous value in a convergence loop
ref ,	Reference state property or parameter
sat ,	Saturation property or parameter
$total$,	Total property or parameter
vap ,	Vaporization state property or parameter

Miscellaneous

$\bar{}$,	Overall denotes average parameter
$\wedge$,	Eigenvalues of corresponding matrix
Δ ,	State change (final – initial)
$\lvert\ \rvert$,	Denotes absolute value

Matrix Operations and Notation

$(\ )$,	Column matrix
$[\ ]$,	Square matrix
$[\ ]^{-1}$,	Inverse of a square matrix
$\lVert\ \rVert$,	Determinant of a square matrix
I,	Identity matrix

A.2 Mixed Fluid Computer Model: Closed System with Non-Condensable Air

```
    % Courtney Bonuccelli: 3-Component Droplet Model %
    %% CASE: Constant Reservoir Composition
          % Mass and Mole Basis Option
          % Ethanol-Water-Air
          % Linearized theory
          % Closed System                %%
%-----------------------------------------------------------------%
%-----------------------------------------------------------------%
    clc
    clear
    format compact
        global Tgo To hn tflight MW1 MW2 MW3 mv3o X x Y y mv_total mv1 mv2 mv3 Mv_total Mv1 Mv2 Mv3 R vp Volume ti Hz

            disp(' _____________________________________________________ ')
            disp('|          CASE: Constant-Composition Reservoir       |')
            disp('|    Ethanol/Water Droplet Analysis with Non Condensible Air   |')
            disp('|                        Closed System                |')
            disp('|                                                     |')
            disp('|                    Courtney Bonuccelli              |')
            disp('|                                                     |')
            disp('|_____________________ September 2006 _____________________|')
            disp('  ')
            disp('  ')
%-----------------------------------------------------------------%
%-----------------------------------------------------------------%

    %%% VARIABLE DEFINITIONS %%%
    %   A(i)--------------------------- Antoine constant    (-)
    %   alpha-------------------------- Heat transfer coefficient   (W/m2.K)
    %   B------------------------------ Matrix function of inverted binary diffusion coefficients   (s/m2)
    %   B(i)--------------------------- Antoine constant    (-)
    %   B(ij)-------------------------- Inverse of binary diffusion coefficient (s/m2)
    %   Beq(ij)------------------------ Van Laar binary interaction parameter   (-)
    %   beta--------------------------- Stefan diffusion bootstrap matrix   (-)
    %   beta(ij)----------------------- Stefan diffusion bootstrap parameter    (-)
    %   C(i)--------------------------- Antoine constant    (-)
    %   const-------------------------- KT/e for water-ethanol diffusivity  (-)
    %   count-------------------------- Array placement counter (-)
    %   cp_liquid(i)------------------- Heat capacity of the liquid (kJ/kg.K)
    %   cp_vapor(i)-------------------- Heat capacity of the vapor  (kJ/kg.K)
    %   cpliquid_avg------------------- Average heat capacity of the liquid (kJ/kg.K)
    %   cpvapor_avg-------------------- Average heat capacity of the vapor  (kJ/kg.K)
    %   ct----------------------------- Total molar concentration   (mole/m3)
    %   D------------------------------ Diffusivity of ethanol-water    (cm2/s)
    %   D(ij)-------------------------- Diffusivity coefficient (m2/s)
    %   D_hat-------------------------- Eigenvalues of [D]  (m2/s)
    %   denominator-------------------- Number of time steps    (-)
    %   detB--------------------------- Determinate of [B]  (s/m2)
    %   dHref(i)----------------------- dHvap(i)+dH(i)  (kJ/kg)
    %   dHvap(i)----------------------- Heat of vaporization at Tref    (kJ/kg)
    %   Dideal------------------------- Ideal solution matrix function of Ficks diffusion coefficients  (m2/s)
    %   Dideal(ij)--------------------- Ideal solution diffusion coefficient of Ficks   (m2/s)
    %   differ(ij)--------------------- Differential equation for calculation of [r]    (-)
    %   dp----------------------------- Diameter of droplet (m)
    %   dp_micron---------------------- Diameter of droplet in microns  (micon)
    %   E_hat(i)----------------------- Eigenvalues of [E] high flux correction factors (-)
    %   gamma(i)----------------------- Activity coefficient    (-)
    %   H1(i)-------------------------- Enthalpy at Tvap    (kJ/kg)
    %   H2(i)-------------------------- Enthalpy at Tref    (kJ/kg)
    %   hn----------------------------- Axial distance from nozzle (top-bottom) (m)
    %   i------------------------------ Number of droplets  (-)
    %   J------------------------------ Matrix of molar diffusion flux relative to molar average velocity   (mole/m2.s)
    %   Je----------------------------- Guess matrix of molar diffusion flux relative to molar average velocity     (mole/m2.s)
```

```
64      %   k------------------------------ Matrix of mass transfer MC coefficients (m/s)
65      %   k_hat(i)------------------------ Eigenvalues of [k]  (m/s)
66      %   kdot---------------------------- Matrix of finite MC mass transfer coefficients  (m/s)
67      %   kdot_hat(i)--------------------- Eigenvalues of [kdot]   (m/s)
68      %   Latent_heat(i)------------------ Latent heat term in energy balance  (kJ/m2.s)
69      %   m(i)---------------------------- Moles of component in liquid    (mole)
70      %   M(i)---------------------------- Mass of component liquid    (kg)
71      %   M_total------------------------- Total mass in liquid    (kg)
72      %   M_total------------------------- Total mole in liquid    (mole)
73      %   Mv(i)--------------------------- Mass of component vapor (kg)
74      %   Mv(i)--------------------------- Moles of component in vapor (mole)
75      %   mv_total------------------------ Total mole in vapor (mole)
76      %   mv_total------------------------ Total mass in vapor (kg)
77      %   MW(i)--------------------------- Molecular weight of component   (g/mole)
78      %   N------------------------------- Matrix molar flux relative to stationary reference  (mole/m2.s)
79      %   Ne------------------------------ Guess matrix molar flux relative to stationary reference    (mole/m2.s
80      %   Nmass(i)------------------------ Mass Flux   (kg/m2.s)
81      %   NN1----------------------------- Same as (Ne)    (mole/m2.s)
82      %   NN2----------------------------- Same as (N) (mole/m2.s)
83      %   Nt------------------------------ Total molar flux relative to stationary reference   (mole/m2.s)
84      %   Nu------------------------------ Nusselt number  (-)
85      %   omega(ij)----------------------- Collision integral  (-)
86      %   P------------------------------- System pressure (Pa)
87      %   Pc(i)--------------------------- Component critical pressure (Pa)
88      %   phi_hat(i)---------------------- Eigenvalue of mass transfer parameter   (-)
89      %   Pr------------------------------ Prandtl number  (-)
90      %   Psat(i)------------------------- Component saturation pressure   (Pa)
91      %   R------------------------------- Universal gas constant  (J/mole.K)
92      %   R------------------------------- Matrix of thermodynamic factors (-)
93      %   r(ij)--------------------------- Thermodynamic factor    (-)
94      %   Re------------------------------ Reynolds number (-)
95      %   rholiquid(i)-------------------- Component liquid density    (kg/m3)
96      %   rholiquid_avg------------------- Average liquid density  (kg/m3)
97      %   rholiquid_avg_mole-------------- Molar average liquid density    (mole/m3)
98      %   rholiquid_mole(i)--------------- Molar liquid component density  (mole/m3)
99      %   rhovapor(i)--------------------- Component vapor density (kg/m3)
100     %   rhovapor_avg-------------------- Average vapor density   (kg/m3)
101     %   rhovapor_mole(i)---------------- Molar average vapor density (mole/m3)
102     %   rhovaporavg_mole---------------- Molar average vapor density (mole/m3)
103     %   sigma(i)------------------------ Collision diameter  (A)
104     %   sigma(ij)----------------------- Average collision diameter  (A)
105     %   T------------------------------- Liquid temperature  (K)
106     %   Tc(i)--------------------------- Critical componet temperature   (K)
107     %   tflight------------------------- Total time of droplet flight    (s)
108     %   Tg------------------------------ Vapor tempertaure   (K)
109     %   Tg_start------------------------ Initial vapor temperature after first droplet   (K)
110     %   thermcond(i)-------------------- Thermal conductivity    (W/m.K)
111     %   thermcond_avg------------------- Average thermal conductivity    (W/m.K)
112     %   ti------------------------------ Incrimental model time  (s)
113     %   tmodel-------------------------- Duration of model = tflight (s)
114     %   Tref---------------------------- Arbitrary reference temperature     (K)
115     %   tt------------------------------ Full model time array   (s)
116     %   Tvap---------------------------- Temperature of dHstandard   (K)
117     %   unit---------------------------- Mass/Mole fraction index    (-)
118     %   Vdroplet------------------------ Volume of one droplet   (m3)
119     %   viscliquid(i)------------------- Component liquid viscosity  (kg/m.s)
120     %   viscliquid_avg------------------ Average liquid viscosity    (kg/m.s)
121     %   viscvapor(i)-------------------- Vapor viscosity (W/m.K)
122     %   viscvapor_avg------------------- Average vapor viscosity (W/m.K)
123     %   Volume-------------------------- Total chamber volume    (m3)
124     %   volume_drop--------------------- Post-evaporated droplet volume  (m3)
125     %   vp------------------------------ Average droplet velocity    (m/s)
126     %   W------------------------------  Width of spray cell (end-end)   (m)
```

```
%   X(i)--------------------------- Bulk liquid mass fraction   (-)
%   X(i)--------------------------- Bulk liquid mole fraction   (-)
%   y(i)--------------------------- Vapor mole fraction (-)
%   y(i)--------------------------- Vapor mass fraction (-)
%   ye(i)-------------------------- Equilibrium mole fraction   (-)
%   Z------------------------------ Differential equation based on total moles/mass in vapor/liquid (-)
%   ZZ----------------------------- Incrimental model Z (-)

%-----------------------------------------------------------------%
%-----------------------------------------------------------------%
    %%% NOTES %%%
    % Upper case letters = mass units (kg)
    % Lower case letters = mole units (mole)
    % subscript 'o' = initial
    % subscript 'e' = equilibrium
    % no subscript = final
%-----------------------------------------------------------------%
%-----------------------------------------------------------------%
    Hz=120000000000;

    %%% INPUT PARAMETERS %%%
        disp('  ')
        i = 0;          % counter for number of droplets
        Repeat = 1;     % initial setting, can be changed after first droplet

        %dpo = input('  Droplet Diameter (m) =');
        dp_microns = 60;
        dpo = dp_microns/1000000
        %To = input('  Initial droplet temperature (K) =');
        To = 297.39
        Tgo = To;
        %Tgo = input('  Bulk air temperature (K) =');
        %Tgo = 298.35
        %vp = input('  Velocity of droplet (m/s) =');
        vp = 2;                     % m/s
        hn_inch = 2.407;            % inch
        hn = hn_inch*0.0254;        % m
        tmodel = hn/vp              % s
        % Incrimental Time
        denominator = 10;
        ti = tmodel/denominator;

            disp('  ')
            disp('  Choose Mass or Mole Unit Convention')
            disp('   1) Mass')
            disp('   2) Mole')
            unit = input('  Desired Units:');

            disp('  ')

        if unit == 1     % GIVEN MASS Fraction
            disp('  NOTE: Xi < 0.999')
            disp('  ')

    % Bulk Liquid MASS fractions
            Xol = input('  Initial Liquid Mass Fraction of Ethanol = ');
            Xo2 = 1 - Xol;
            Xo3 = 0;
    % Bulk Vapor MASS fractions
            Yol = input('  Initial Vapor Mass Fraction of Ethanol = ');
            Yo2 = input('  Initial Vapor Mass Fraction of Water = ');
            Yo3 = 1 - (Yol + Yo2);
        end
```

```
190
191         if unit == 2     % GIVEN MOLE Fraction
192             disp('  NOTE: xi < 0.999')
193             disp('  ')
194
195     % Bulk Liquid MOLE fractions
196             xol = input('  Initial Liquid Mole Fraction of Ethanol = ');
197             xo2 = 1 - xol;
198             xo3 = 0;
199     % Bulk Vapor MOLE fractions
200             yol = input('  Initial Vapor Mole Fraction of Ethanol = ');
201             yo2 = input('  Initial Vapor Mole Fraction of Water = ');
202             yo3 = 1 - (yol + yo2);
203         end
204 %-----------------------------------------------------------------%
205 %-----------------------------------------------------------------%
206
207     % CONSTANTS
208     Volume = 4.0903912409e-4;               % m3
209         tflight = tmodel;                   % s
210         Vdroplet = 4/3*pi*dpo^3;            % m3
211         R = 8.314;                          % J/mole.K = Pa.m3/mole.K
212
213    % Molecular Weight
214         MW1 = 46.070;                       % g/mole
215         MW2 = 18.016;                       % g/mole
216         MW3 = 29.000;                       % g/mole
217
218     % Liquid Density
219         rholiquid_1o = -0.00206303*To^2 + 0.39218376*To + 872.28248265;      % kg/m3
220         rholiquid_2o = -0.00260*To^2 + 1.22410*To + 859.98;                  % kg/m3
221         rholiquid_mole1o = (rholiquid_1o*1000)/MW1;                          % mole/m3
222         rholiquid_mole2o = (rholiquid_2o*1000)/MW2;                          % mole/m3
223
224     % Vapor Density
225         rhovapor_1o = 8.61e-33*Tgo^12.645;                                   % kg/m3
226         rhovapor_2o = 8.9045470000e-42*Tgo^15.919690000;                     % kg/m3
227         rhovapor_3o = 0.000002459*Tgo^2 - 0.00432027*Tgo + 2.263469056;      % kg/m3
228         rhovapor_mole1o = (rhovapor_1o*1000)/MW1;                            % mole/m3
229         rhovapor_mole2o = (rhovapor_2o*1000)/MW2;                            % mole/m3
230         rhovapor_mole3o = (rhovapor_3o*1000)/MW3;                            % mole/m3
231
232     % Liquid Viscocity
233         viscliquid_1o = 0.0000000173*Tgo^2-0.0000124791*Tgo+0.0022941277;                          % Pa.s = kg/m.s
234         viscliquid_2o = -3.18277543e-9*Tgo^3+3.24799267e-6*Tgo^2-1.11019267e-3*Tgo+1.27527670e-1;  % Pa.s = kg/m.s
235 %-----------------------------------------------------------------%
236 %-----------------------------------------------------------------%
237     while i < 300 %Repeat == 1;
238         i = i+1;                    % counts number of droplets used
239         count = ((denominator+1)*i) - denominator;        % array placement counter
240
241     %%% CALCULATIONS %%%
242         if unit == 1     % GIVEN MASS FRACTION
243     % Average Mass Density
244             if i > 1
245                 Yol = Y(1,1);
246                 Yo2 = Y(2,1);
247                 Yo3 = 1 - (Yol + Yo2);
248             end
249             %%% For all droplets %%%
250             rholiquido_avg = rholiquid_1o*Xol+rholiquid_2o*Xo2;               % kg/m3
251             rhovaporo_avg = rhovapor_1o*Yol+rhovapor_2o*Yo2+rhovapor_3o*Yo3;  % kg/m3
252
```

```
253      % Average Liquid Mass Viscosity
254              viscliquido_avg = viscliquid_1o*Xo1+viscliquid_2o*Xo2;            % kg/m.s
255
256      % Mass Liquid (1-drop)
257              %%% For all droplets %%%
258              M_totalo = rholiquido_avg*Vdroplet;  % kg
259              M1o = M_totalo*Xo1;                  % kg
260              M2o = M_totalo*Xo2;                  % kg
261              M3o = M_totalo*Xo3;                  % kg
262
263      % Mass Vapor
264              %%% For first droplet %%%
265              Mv_totalo = rhovaporo_avg*Volume;    % kg
266              Mv1o = Mv_totalo*Yo1;                % kg
267              Mv2o = Mv_totalo*Yo2;                % kg
268              Mv3o = Mv_totalo*Yo3;                % kg
269
270              %%% For all other droplets %%%
271              if i > 1
272                  Mv_totalo = Mv_total;           % kg
273                  Mv1o = Mv1;                     % kg
274                  Mv2o = Mv2;                     % kg
275                  Mv3o = Mv3;                     % kg
276              end
277
278      % Mole Liquid (1-drop)
279              %%% For all droplets %%%
280              m1o = M1o*1000/MW1;                 % mole
281              m2o = M2o*1000/MW2;                 % mole
282              m3o = M3o*1000/MW3;                 % mole
283              m_totalo = m1o + m2o + m3o;         % mole
284
285      % Mole Vapor
286              %%% For first droplet %%%
287              mv1o = Mv1o*1000/MW1;               % mole
288              mv2o = Mv2o*1000/MW2;               % mole
289              mv3o = Mv3o*1000/MW3;               % mole
290              mv_totalo = mv1o + mv2o + mv3o;     % mole
291
292              %%% For all other droplets %%%
293              if i > 1
294                  mv_totalo = mv_total;           % mole
295                  mv1o = mv1;                     % mole
296                  mv2o = mv2;                     % mole
297                  mv3o = mv3;                     % mole
298              end
299
300       % Mole Fraction of Liquid
301              %%% For all droplets %%%
302              xo1 = m1o/m_totalo;                  % []
303              xo2 = m2o/m_totalo;                  % []
304              xo3 = m3o/m_totalo;                  % []
305
306      % Mole Fraction of Vapor
307              %%% For all droplets %%%
308              yo1 = mv1o/mv_totalo;                % []
309              yo2 = mv2o/mv_totalo;                % []
310              yo3 = mv3o/mv_totalo;                % []
311
312      % Average Mole Density
313              %%% For all droplets %%%
314              rholiquido_avg_mole = rholiquid_molelo*xo1+rholiquid_mole2o*xo2;                    % mole/m3
315              rhovaporo_avg_mole = rhovapor_molelo*yo1+rhovapor_mole2o*yo2+rhovapor_mole3o*yo3;   % mole/m3
```

```
316
317             disp('  ')
318             disp(' _____INITIAL RESULTS_____ ')
319             disp('  Initial Liquid Mass | Mole Fraction:')
320             [Xol xol;Xo2 xo2]
321             disp('  Initial Vapor Mass | Mole Fraction:')
322             [Yol yol;Yo2 yo2]
323         end
324
325         if unit == 2     % GIVE MOLE FRACTION
326     % Average Mole Density
327             %%% For first droplet %%%
328             if i > 1
329                 yol = y(1,1);                   % []
330                 yo2 = y(2,1);                   % []
331                 yo3 = 1 - (yol + yo2);          % []
332             end
333             %%% For all droplets %%%
334             rholiquido_avg_mole = rholiquid_molelo*xol+rholiquid_mole2o*xo2;                    % mole/m3
335             rhovaporo_avg_mole = rhovapor_molelo*yol+rhovapor_mole2o*yo2+rhovapor_mole3o*yo3;   % mole/m3
336
337     % Mole Liquid (1-drop)
338             %%% For all droplets %%%
339             m_totalo = rholiquido_avg_mole*Vdroplet;     % mole
340             mlo = m_totalo*xol;                          % mole
341             m2o = m_totalo*xo2;                          % mole
342             m3o = m_totalo*xo3;                          % mole
343
344     % Mole Vapor
345             %%% For first droplet %%%
346             mv_totalo = rhovaporo_avg_mole*Volume;       % mole
347             mvlo = mv_totalo*yol;                        % mole
348             mv2o = mv_totalo*yo2;                        % mole
349             mv3o = mv_totalo*yo3;                        % mole
350
351             %%% For all other droplets %%%
352             if i > 1
353                 mv_totalo = mv_total;                  % mole
354                 mvlo = mvl;                            % mole
355                 mv2o = mv2;                            % mole
356                 mv3o = mv3;                            % mole
357             end
358
359     % Mass Liquid (1-drop)
360             %%% For all droplets %%%
361             Mlo = mlo*MWl/1000;                        % kg
362             M2o = m2o*MW2/1000;                        % kg
363             M3o = m3o*MW3/1000;                        % kg
364             M_totalo = Mlo+M2o+M3o;                    % kg
365
366     % Mass Vapor
367             %%% For first droplet %%%
368             Mvlo = mvlo*MWl/1000;                      % kg
369             Mv2o = mv2o*MW2/1000;                      % kg
370             Mv3o = mv3o*MW3/1000;                      % kg
371             Mv_totalo = Mvlo+Mv2o+Mv3o;                % kg
372
373             %%% For all other droplets %%%
374             if i > 1
375                 Mv_totalo = Mv_total;                  % kg
376                 Mvlo = Mvl;                            % kg
377                 Mv2o = Mv2;                            % kg
378                 Mv3o = Mv3;                            % kg
```

```
            end

    % Mass Fraction of Liquid
            %%% For all droplets %%%
            Xol = Mlo/M_totalo;                         % []
            Xo2 = M2o/M_totalo;                         % []
            Xo3 = M3o/M_totalo;                         % []

    % Mass Fraction of Vapor
            %%% For all droplets %%%
            Yol = Mvlo/Mv_totalo;                       % []
            Yo2 = Mv2o/Mv_totalo;                       % []
            Yo3 = Mv3o/Mv_totalo;                       % []

    % Average Mass Density
            %%% For all droplets %%%
            rholiquido_avg = rholiquid_1o*Xol+rholiquid_2o*Xo2;                 % kg/m3
            rhovaporo_avg = rhovapor_1o*Yol+rhovapor_2o*Yo2+rhovapor_3o*Yo3;    % kg/m3

    % Average Mass Liquid Viscocity
            %%% For all droplets %%%
            viscliquido_avg = viscliquid_1o*Xol+viscliquid_2o*Xo2;              % mole/m.s

            disp('  ')
            disp(' _____________________INITIAL RESULTS_____________________ ')
            disp('  Initial Liquid Mole | Mass Fraction:')
            [xol Xol;xo2 Xo2]
            disp('  Initial Vapor Mole | Mass Fraction:')
            [yol Yol;yo2 Yo2]
        end
%-------------------------------------------------------------%
%-------------------------------------------------------------%

    %%% Differential Expressions and Initial Values %%%
        % Initial Vapor Temperature for first drop
        i
        if i == 1
                Tg_start = Tgo;
            end

        [t,Z] = ode15s('round_air_closed',[0:ti:tmodel],[mlo*Hz; m2o*Hz; mvlo; mv2o; To; Tg_start]);  % [seconds, mole or K]

        % Initial Vapor Temperature after first drop
            Tg_start = Z(denominator,6);

            % Display Variables
            ZZ(count:(count+denominator),1)=Z(1:(denominator+1),3); % Displays moles ethanol in vapor
            ZZ(count:(count+denominator),2)=Z(1:(denominator+1),4); % Displays moles water in vapor
            ZZ(count:(count+denominator),3)=Z(1:(denominator+1),5); % Displays liquid temperature
            ZZ(count:(count+denominator),4)=Z(1:(denominator+1),6); % Displays vapor temperature
            if i>1                                                  % Displays time
                tt(count:(count+denominator),1)=t(1:(denominator+1),1)+((tmodel+(0.011))*(i-1));
            else
                tt(count:(count+denominator),1)=t(1:(denominator+1),1);
            end
%-------------------------------------------------------------%
    %%% PRINT RESULTS %%%
        if unit ==1     % GIVEN MASS Fraction
            disp('  ')
            disp(' _____________________FINAL RESULTS_____________________ ')
            disp('  Liquid Impingement Mass | Mole Fraction:')
            [X x]
            disp('  Final Vapor Mass | Mole Fraction')
```

```
            [Y y]
        end

        if unit ==2     % GIVEN MOLE Fraction
            disp('  ')
            disp(' ____________________________FINAL RESULTS_____________________________ ')
            disp('  Liquid Impingement Mole | Mass Fraction:')
            [x X]
            disp('  Final Vapor Mole | Mass Fraction')
            [y Y]
            disp('  ')
        end

            disp('  ')
            disp(' ____________________________________________________________________________________________ ')
            disp(' ____________________________________________________________________________________________ ')
%-------------------------------------------------------------%
            %disp(' Additional Droplet:')
            %disp(       '0 = no')
            %disp(       'l = yes')
            %Repeat = input (' Would you like to run model with another droplet?')
        end

%-------------------------------------------------------------%
%-------------------------------------------------------------%
            disp('  ')
            disp(' ____________________________________________________________________________________________ ')
            disp(' ____________________________________________________________________________________________ ')

    % Displays all varaibles
            who

            subplot(2,2,1)
            plot(tt,ZZ(:,1))
            xlabel('Time (s)')
            ylabel('Mole of Ethanol in Air')

            subplot(2,2,2)
            plot(tt,ZZ(:,2))
            xlabel('Time (s)')
            ylabel('Mole of Water in Air')

            subplot(2,2,3)
            plot(tt,ZZ(:,3))
            xlabel('Time (s)')
            ylabel('Droplet Temperature')

            subplot(2,2,4)
            plot(tt,ZZ(:,4))
            xlabel('Time (s)')
            ylabel('Vapor Temperature')
%---------------------------END-----------------------------%
```

```
    % Courtney Bonuccelli: 3-Component Droplet Model %
    %% CASE: Constant Reservoir Composition
           % Mass and Mole Basis Option
           % Ethanol-Water-Air
           % Linearized theory
           % Closed System                  %%

        function dZ = round_air_closed(t,Z)
        global Tgo To hn tflight MW1 MW2 MW3 mv3o X x Y y mv_total mv1 mv2 mv3 Mv_total Mv1 Mv2 Mv3 R vp Volume ti Hz

        dZ = zeros(6,1);
%-------------------------------------------------------------%
%-------------------------------------------------------------%
    % CALCULATE NEW Values

    % Mole in Liquid (1-drop)
        m1 = Z(1)/Hz;                    % mole
        m2 = Z(2)/Hz;                    % mole
        m_total = m1 + m2;            % mole

    % Mass in Liquid (1-drop)
        M1 = m1*MW1/1000;             % kg
        M2 = m2*MW2/1000;             % kg
        M_total = M1+M2;              % kg

    % Mole Fraction in Liquid
        x1 = m1/m_total;              % []
        x2 = m2/m_total;              % []
        x = [x1;x2];                  % []

    % Mass Fraction in Liquid
        X1 = M1/M_total;              % []
        X2 = M2/M_total;              % []
        X = [X1;X2];                  % []

    % NEW Moles in Vapor
        mv1 = Z(3);                   % mole
        mv2 = Z(4);                   % mole
        mv3 = mv3o;                   % mole
        mv_total = mv1+mv2+mv3;       % mole

    % NEW Mass in Vapor
        Mv1 = mv1*MW1/1000;           % kg
        Mv2 = mv2*MW2/1000;           % kg
        Mv3 = mv3*MW3/1000;           % kg
        Mv_total = Mv1+Mv2+Mv3;       % kg

    % NEW Mole Fraction in Vapor
        y1 = mv1/mv_total;            % []
        y2 = mv2/mv_total;            % []
        y3 = mv3/mv_total;            % []
        y = [y1;y2];                  % []

    % NEW Mass Fraction in Vapor
        Y1 = Mv1/Mv_total;            % []
        Y2 = Mv2/Mv_total;            % []
        Y3 = Mv3/Mv_total;            % []
        Y = [Y1;Y2];                  % []

    %%% COMPONENT PROPERTIES %%%
    % Density-Liquid
        rholiquid_1 = -0.00206303*Z(6)^2 + 0.39218376*Z(6) + 872.28248265;      % kg/m^3
        rholiquid_2 = -0.00260*Z(6)^2 + 1.22410*Z(6) + 859.98;                  % kg/m3
```

```
64          rholiquid_molel = (rholiquid_1*1000)/MW1;                                   % mole/m^3
65          rholiquid_mole2 = (rholiquid_2*1000)/MW2;                                   % mole/m^3
66      % Density-Vapor
67          rhovapor_1 = 8.61e-33*Z(5)^12.645;                                          % kg/m^3
68          rhovapor_2 = 8.9045470000e-42*Z(5)^15.919690000;                            % kg/m3
69          rhovapor_3 = 0.000002459*Z(5)^2 - 0.00432027*Z(5) + 2.263469056;            % kg/m^3
70          rhovapor_molel = (rhovapor_1*1000)/MW1;                                     % mole/m^3
71          rhovapor_mole2 = (rhovapor_2*1000)/MW2;                                     % mole/m^3
72          rhovapor_mole3 = (rhovapor_3*1000)/MW3;                                     % mole/m^3
73
74      % Heat Capacity-Liquid
75          cpliquid_1 = 0.00004995594*Z(6)^2-0.02150489431*Z(6)+4.39444181686;                                 % kJ/kg.K
76          cpliquid_2 = 3.0648E-09*Z(6)^4-4.0826E-06*Z(6)^3+0.0020438*Z(6)^2-0.45523*Z(6)+42.214;              % kJ/kg.K
77      % Heat Capacity-Vapor
78          cpvapor_1 = 0.00326190*Z(5) + 0.45405137;                           % NIST                          % kJ/kg.K
79          cpvapor_2 = 3.9375E-10*Z(5)^4-3.8879E-07*Z(5)^3+0.00014337*Z(5)^2-0.022353*Z(5)+3.0243;             % kJ/kg.K
80          cpvapor_3 = 0.0000104*Z(5)^4-0.0002038*Z(5)^3+0.0016174*Z(5)^2-0.0045910*Z(5)+1.0090565;            % kJ/kg.K
81
82      % Viscosity-Liquid
83          viscliquid_1 = 0.0000000173*Z(6)^2-0.0000124791*Z(6)+0.0022941277;                                  % Pa.s = kg/m.s
84          viscliquid_2 = -3.18277543e-9*Z(6)^3+3.24799267e-6*Z(6)^2-1.11019267e-3*Z(6)+1.27527670e-1;         % Pa.s = kg/m.s
85      % Viscocity-Vapor
86          viscvapor_1 = 0.00002974839*Z(5)-0.00023331278;             % penoncello                            % Pa.s
87          viscvapor_2 = 3.087E-08*Z(5)+6.8243E-07;                                                            % Pa.s
88          viscvapor_3 = 1.1599E-09*Z(5)^4-2.6019E-08*Z(5)^3+2.4277E-07*Z(5)^2+5.1405E-09*Z(5)+1.5788E-05;     % Pa.s
89
90      % Thermal Conductivity-Vapor
91          thermcond_1 = 0.00000013*Z(5)^2+0.0000191*Z(5)-0.00071496;    % penoncello                            % W/m.K
92          thermcond_2 = 0.0000799*Z(5)-0.0052281;                                                             % W/m.K
93          thermcond_3 = -2.33499E-08*Z(5)^2 + 8.91233E-05*Z(5) + 1.60834E-03;
94
95      %%% AVERAGE PROPERTIES %%%
96      % Density-Liquid
97          rholiquid_avg = rholiquid_1*X1 + rholiquid_2*X2;                                        % kg/m^3
98          rholiquid_avg_mole = rholiquid_molel*x1 + rholiquid_mole2*x2;                           % mole/m^3
99      % Density-Vapor
100         rhovapor_avg = rhovapor_1*Y1 + rhovapor_2*Y2 + rhovapor_3*Y3;                           % kg/m^3
101         rhovapor_avg_mole = rhovapor_molel*y1 + rhovapor_mole2*y2 + rhovapor_mole3*y3;          % mole/m^3
102
103     % Heat Capacity-Liquid
104         cpliquid_avg = cpliquid_1*X1 + cpliquid_2*X2;                       % kJ/kg.K
105     % Heat Capacity-Vapor
106         cpvapor_avg = cpvapor_1*Y1 + cpvapor_2*Y2+ cpvapor_3*Y3;            % kJ/kg.K
107
108     % Viscosity-Liquid
109         viscliquid_avg = viscliquid_1*X1 + viscliquid_2*X2;                 % kg/m.s = Pa.s
110     % Viscocity-Vapor
111         viscvapor_avg = viscvapor_1*Y1 + viscvapor_2*Y2 + viscvapor_3*Y3;   % kg/m.s = Pa.s
112
113     % Thermal Conductivity-Vapor
114         thermcond_avg = thermcond_1*Y1 + thermcond_2*Y2 + thermcond_3*Y3;   % W/m.K
115
116     % Concentration and Pressure
117         ct_1 = mv1/Volume;              % mole/m^3
118         ct_2 = mv2/Volume;              % mole/m^3
119         ct_3 = mv3/Volume;              % mole/m^3
120         ct=ct_1+ct_2+ct_3;              % mole/m^3
121
122         P_1= ct_1*R*Z(5);               % Pa
123         P_2= ct_2*R*Z(5);               % Pa
124         P_3= ct_3*R*Z(5);               % Pa
125         P=P_1+P_2+P_3;                  % Pa
126
```

```
    % New Droplet Diameter
        volume_drop = (M1/rholiquid_1)+(M2/rholiquid_2);            % m^3
        dp = ((3*volume_drop)/(pi*4))^(1/3);                        % m

    % Energy Balance relations
        Pr = 1000*cpvapor_avg*viscvapor_avg/thermcond_avg;      % []
        Re = rhovapor_avg*dp*vp/viscvapor_avg;                  % []
        Nu = 2 + 0.6*(Re)^0.5*(Pr)^0.33;                % Nu = (alpha*dp)/kair
        alpha = Nu*thermcond_avg/dp;                    % W/m^2 K

%-----------------------------------------------------------------%
%-----------------------------------------------------------------%
    % Latent Heat of Liquid
            Tvap1 = 351.65;
            Tvap2 = 373.15;
            Tref = Z(5);
            dHvap1 = 836.336;
            dHvap2 = 2253.55;
    % ethanol
            H1_1 = (6.99*Tvap1 + (39.74le-3*Tvap1^2)/2 - (11.926e-6*Tvap1^3)/3)/11.0036;                                % kJ/kg
            H2_1 = (6.99*Tref + (39.74le-3*Tref^2)/2 - (11.926e-6*Tref^3)/3)/11.0036;                                    % kJ/kg
            dH1 = H1_1 - H2_1;          % kJ/kg
            dHref_1 = dHvap1 + dH1;     % kJ/kg
    % water
            H1_2=(3.9375E-10*Tvap2^5)/5-(3.8879E-07*Tvap2^4)/4+(0.00014337*Tvap2^3)/3-(0.022353*Tvap2^2)/2+3.0243*Tvap2;   % kJ/kg
            H2_2=(3.9375E-10*Tref^5)/5-(3.8879E-07*Tref^4)/4+(0.00014337*Tref^3)/3-(0.022353*Tref^2)/2+3.0243*Tref;        % kJ/kg
            dH2 = H1_2 - H2_2;          % kJ/kg
            dHref_2 = dHvap2 + dH2;     % kJ/kg

    % Critical Properties
        Tc_1 = 513.9;           % K
        Tc_2 = 647.1;           % K
        Tc_3 = 132.2;           % K

        Pc_1 = 63*101325;       % Pa
        Pc_2 = 218.3*101325;    % Pa
        Pc_3 = 37*101325;       % Pa

    % Diffusivity coefficients
    % water-ethanol - Chapman-Enskog theory (low density gases)
        sigma_1 = 4.455;                        % Angstrom
        sigma_2 = 2.649;                        % Angstrom
        sigma_12 = 0.5*(sigma_1+sigma_2);       % Angstrom
        e_k_1 = 391;                            % K
        e_k_2 = 356;                            % K
        e_k_12 = (e_k_1*e_k_2)^(1/2);           % K
        val = 1/e_k_12;                         % 1/K
        const = val*Z(5);                       % []
        omega_12 = 1.0004*(const)^2 - 2.6724*(const) + 3.1105;
        D_12 = (0.0018583*((Z(5)^3*(1/MW1 + 1/MW2))^0.5)*1/((P/101325)*sigma_12^2*omega_12))/10000;    % m^2/s
        D_21 = D_12;

    % ethanol-air
        D_13 = 1.337/P;      % m^2/s (Welty, Wicks, Wilson, Rorrer)
        D_31 = D_13;

    % water-air
        D_23 = 2.634/P;      % m^2/s (Welty, Wicks, Wilson, Rorrer)
        D_32 = D_23;
%-----------------------------------------------------------------%
%-----------------------------------------------------------------%

    %%% Equilibrium Calculations --> determine interface y
```

```
% antoine calculations
% log Psat = A-B/(T+C) where T[=]oC and Psat[=]mmHg
    A_1 = 8.1122;
    B_1 = 1592.864;
    C_1 = 226.184;
    Psat_1 = (10^(A_1 - B_1/((Z(5) - 273.15) + C_1)))*133.32236;     % Pa

    A_2 = 8.10765;
    B_2 = 1750.286;
    C_2 = 235;
    Psat_2 = (10^(A_2 - B_2/((Z(5) - 273.15) + C_2)))*133.32236;     % Pa

% gamma calculations
    Beq_12 = 1.5054;     % Twu,Coon,Bluck
    Beq_21 = .9994;      % Twu,Coon,Bluck
    gamma_1 = exp(Beq_12/(1+(Beq_12*x1/(Beq_21*(1-x1)))))^2);
    gamma_2 = exp(Beq_21/(1+(Beq_21*(1-x1)/(Beq_12*x1)))^2);

% equilibrium mole fraction
    ye1 = x1*gamma_1*Psat_1/P;
    ye2 = x2*gamma_2*Psat_2/P;
    ye3 = 1-(ye1+ye2);
    ye = [ye1;ye2];
% COMPUTE [k]
% matrix [B]
    B_11 = ye1/D_13 + ye2/D_12 + ye3/D_13;          % m^2/s
    B_22 = ye2/D_23 + ye1/D_21 + ye3/D_23;          % m^2/s
    B_12 = -ye1*(1/D_12 - 1/D_13);                  % m^2/s
    B_21 = -ye2*(1/D_21 - 1/D_23);                  % m^2/s
    B = [B_11 B_12; B_21 B_22];                     % m^2/s

% matrix [D]
    detB = (B_11*B_22)-(B_12*B_21);
    Dideal_11 = (1/detB)*B_22;                                      % m^2/s
    Dideal_22 = (1/detB)*B_11;                                      % m^2/s
    Dideal_12 = -(1/detB)*B_12;                                     % m^2/s
    Dideal_21 = -(1/detB)*B_21;                                     % m^2/s

    D = [Dideal_11 Dideal_12; Dideal_21 Dideal_22];                 % m^2/s

% eigenvalues of [D]
    D_hat = eig(D);                                 % m^2/s

% eigenvalues of [k] equation 9.3.37
    k_hat1 = 2*(D_hat(1,1)/(pi*tflight))^(1/2);     % m/s^0.5
    k_hat2 = 2*(D_hat(2,1)/(pi*tflight))^(1/2);     % m/s^0.5

% matrix [k] equation 8.4.32
    k = (k_hat1*(D-D_hat(2,1)*eye(2)))/(D_hat(1,1)-D_hat(2,1))+(k_hat2*(D-D_hat(1,1)*eye(2)))/(D_hat(2,1)-D_hat(1,1));

% ESTIMATE FLUX Ne
%matrix [beta]
    beta_11 = 1 + ye1/ye3;                      % []
    beta_22 = 1 + ye2/ye3;                      % []
    beta_12 = ye1/ye3;                          % []
    beta_21 = ye2/ye3;                          % []
    beta = [beta_11 beta_12; beta_21 beta_22];  % []

% Je
    Je = ct*k*(ye-y);           % mole/m^2.s
% Ne
    Ne = (beta)*(Je);           % mole/m^2.s
% total flux
```

```
253         Nt = Ne(1,1) + Ne(2,1);     % mole/m^2.s
254
255     % CALCULATE FLUX N
256     % matrix [phi] equation 9.3.38
257         phi_hat1 = Nt/(ct*k_hat1);
258         phi_hat2 = Nt/(ct*k_hat2);
259
260     %matrix [E] equation 9.3.39
261         E_hat1 = (exp((-phi_hat1^2)/pi))/(1+erf(phi_hat1/(pi^.5)));
262         E_hat2 = (exp((-phi_hat2^2)/pi))/(1+erf(phi_hat2/(pi^.5)));
263
264     % matrix [kdot] equation 8.4.25 and 8.4.32
265         kdot_hat1 = k_hat1*E_hat1;
266         kdot_hat2 = k_hat2*E_hat2;
267
268         kdot = (kdot_hat1*(D-D_hat(2,1)*eye(2)))/(D_hat(1,1)-D_hat(2,1))+(kdot_hat2*(D-D_hat(1,1)*eye(2)))/(D_hat(2,1)-D_hat(1,1));
269
270     %J
271         J = ct*kdot*(ye-y);
272     %N
273         N = beta*J;                 % mole/m^2.s
274         Nmass_1 = 1000*N(1,1)*MW1;  % kgethanol/m^2.s
275         Nmass_2 = 1000*N(1,1)*MW2;  % kgwater/m^2.s
276
277     % CHECK CONVERGENCE
278     % Define origninal flux = NN1
279     % Define recalculated flux = NN2
280         NN1 = Ne;                   % mole/m^2.s
281         NN2 = N;                    % mole/m^2.s
282
283         while abs(NN1(1,1)-NN2(1,1))>0 , abs(NN1(2,1)-NN2(2,1))>0;
284
285             % CALCULATE FLUX NN1
286             % matrix [phi]
287                 NN1 = N;                    % mole/m^2.s
288                 nt = NN1(1,1) + NN1(2,1);   % mole/m^2.s
289                 phi_hat1 = Nt/(ct*k_hat1);
290                 phi_hat2 = Nt/(ct*k_hat2);
291             % matrix [E] equation 9.3.39
292                 E_hat1 = (exp((-phi_hat1^2)/pi))/(1+erf(phi_hat1/(pi^.5)));
293                 E_hat2 = (exp((-phi_hat2^2)/pi))/(1+erf(phi_hat2/(pi^.5)));
294             % matrix [kdot] equation 8.4.25 and 8.4.32
295                 kdot_hat1 = k_hat1*E_hat1;
296                 kdot_hat2 = k_hat2*E_hat2;
297                 kdot = (kdot_hat1*(D-D_hat(2,1)*eye(2)))/(D_hat(1,1)-D_hat(2,1))+(kdot_hat2*(D-D_hat(1,1)*eye(2)))/(D_hat(2,1)-D_hat(1,1)
298             % J
299                 J = ct*kdot*(ye-y);         % mole/m^2.s
300
301             %N
302                 NN2 = beta*J;               % mole/m^2.s
303                 N = NN2;                    % mole/m^2.s
304
305                 Nmass_1 = 1000*N(1,1)*MW1;  % kgethanol/m^2.s
306                 Nmass_2 = 1000*N(1,1)*MW2;  % kgwater/m^2.s
307             end
308
309 %-----------------------------------------------------------------%
310 %-----------------------------------------------------------------%
311
312     %%% CONSERVATION OF MASS %%%
313     % DROPLET
314     % dW(loss)  [mole/s]
315         dZ(1) = -pi*dp^2*N(1,1)*Hz;
```

```
316          dZ(2) = -pi*dp^2*N(2,1)*Hz;
317
318      % AIR
319      % dW(gain)  [mole/s]
320          dZ(3) = pi*dp^2*N(1,1)*Hz;
321          dZ(4) = pi*dp^2*N(2,1)*Hz;
322
323      % CONSERVATION OF ENERGY on SYSTEM   --> dTg/dt = -DEdrop(# of drops)/(rhoair*Cpair*Volume)  [K/s]
324      Latent_heat_1 =((dHref_1+cpvapor_1*(Z(6)-Tref))*Nmass_1); % kJ/m^2.s
325      Latent_heat_2 =((dHref_2+cpvapor_2*(Z(6)-Tref))*Nmass_2); % kJ/m^2.s
326
327      % Droplet Temperature dZ = sensible heat - latent heat
328      dZ(5) = (alpha*0.001*(Z(6)-Z(5))-(Latent_heat_1+Latent_heat_2))*((pi*dp^2)/((M1+M2)*cpliquid_avg)); % [K/s]
329
330      % Gas Temperature dZ =-[dZ(5)*((dZ(3)+dZ(4))*ti*cpliquid_avg)]/(Mv_total*cpvapor_avg)
331      dZ(6) = -dZ(5)*((M1+M2)*cpliquid_avg)/(Mv_total*cpvapor_avg);  % [K/s]
332
333  %-----------------------------END-------------------------------%
```

A.3 Experimental Results: Graphical and Tabular

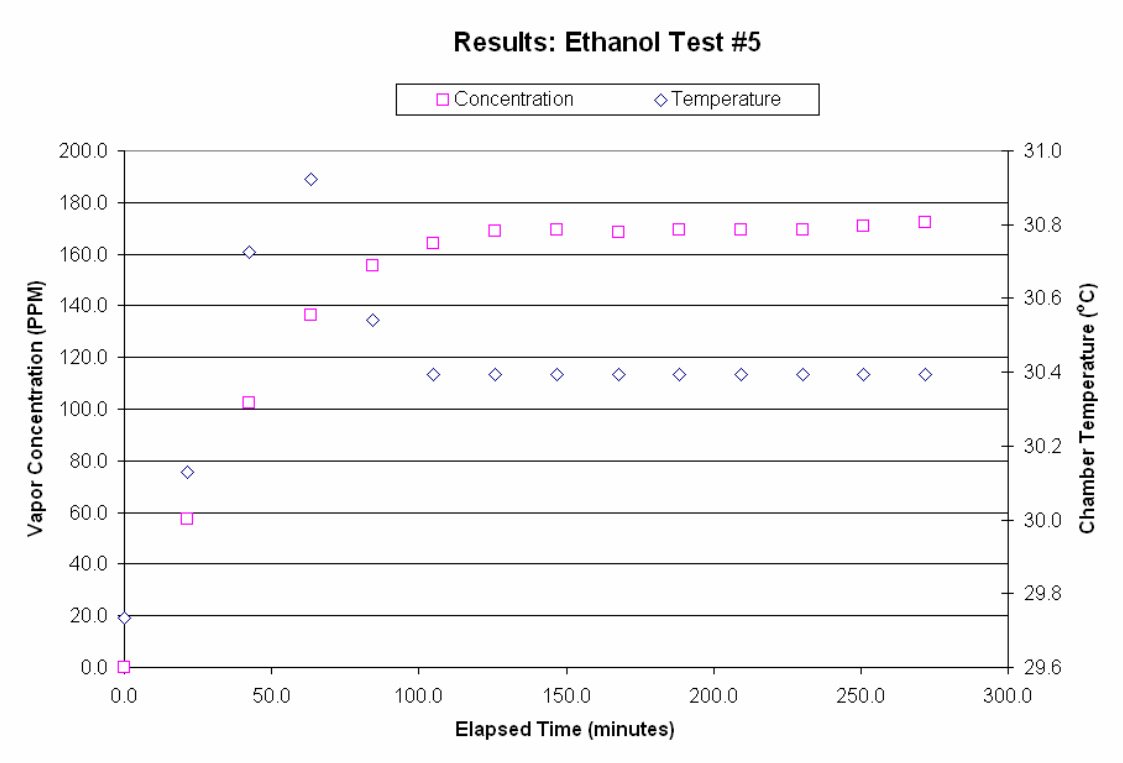

Figure 37: Concentration and Temperature Profile Data of Ethanol Test #5

TEST5: 03-21-06

Ethanol, de-gassed
run continuous
100drop/sec

Time	Absorbance		Concentration			Temperature
Elapsed (min)	*2987.4*	*2900.6*	*2987.4*	*2900.6*	*average*	°C
0.0	0.0000	0.0000	0.000	0.000	0.000	29.733
21.6	0.5370	0.4520	57.207	57.313	57.260	30.129
42.4	0.9610	0.8050	102.375	102.073	102.224	30.726
63.3	1.2850	1.0720	136.891	135.929	136.410	30.922
84.2	1.4650	1.2200	156.066	154.695	155.381	30.542
105.1	1.5470	1.2890	164.802	163.444	164.123	30.394
125.9	1.5970	1.3230	170.128	167.755	168.942	30.394
146.8	1.6080	1.3220	171.300	167.628	169.464	30.394
167.6	1.5980	1.3170	170.235	166.994	168.615	30.394
188.5	1.6090	1.3210	171.407	167.501	169.454	30.394
209.4	1.6110	1.3210	171.620	167.501	169.561	30.394
230.2	1.6010	1.3260	170.555	168.135	169.345	30.394
251.1	1.6140	1.3420	171.939	170.164	171.052	30.394
272.0	1.6280	1.3510	173.431	171.305	172.368	30.394

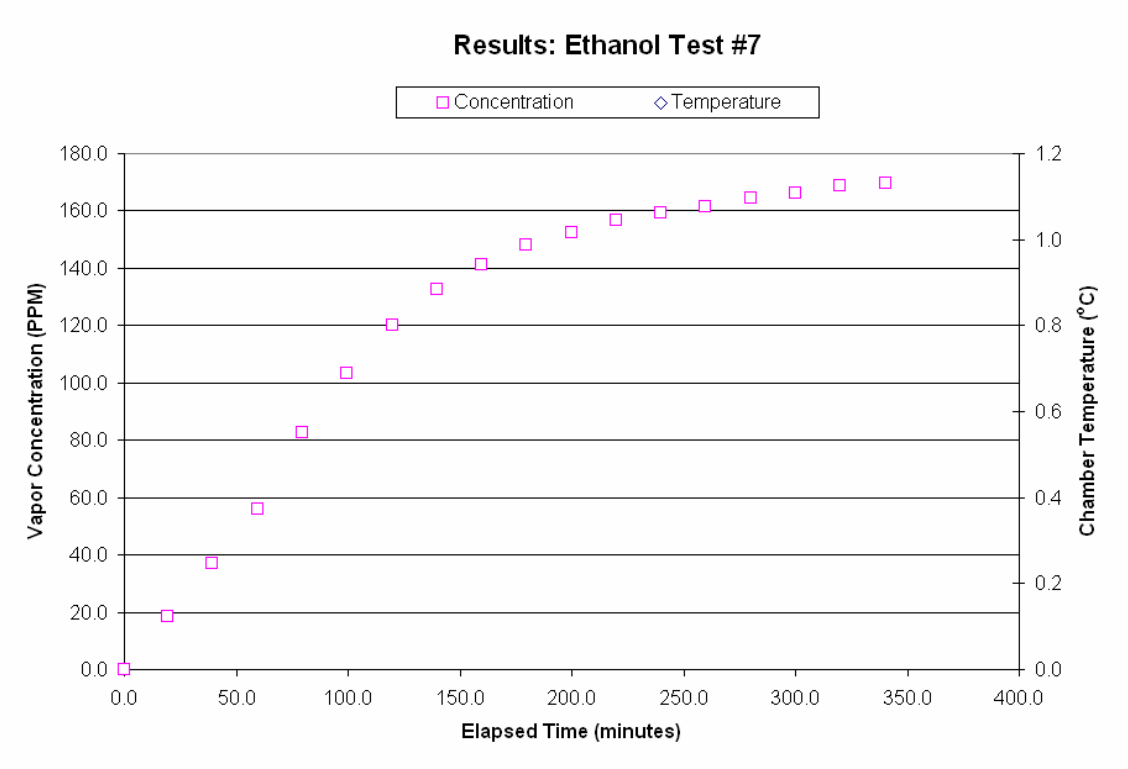

Figure 38: Concentration and Temperature Profile Data of Ethanol Test #7

TEST7: 03-28-06

Ethanol, de-gassed
run continuous
50drop/sec

Time	Absorbance		Concentration			Temperature
Elapsed (min)	*2987.4*	*2900.6*	*2987.4*	*2900.6*	*average*	°C
0.0	0.0000	0.0000	0.000	0.000	0.000	
19.5	0.1730	0.1460	18.430	18.513	18.471	
39.5	0.3480	0.2920	37.072	37.025	37.049	
59.5	0.5240	0.4400	55.822	55.792	55.807	
79.6	0.7770	0.6500	82.774	82.419	82.597	
99.6	0.9750	0.8130	103.867	103.088	103.477	
119.7	1.1310	0.9430	120.485	119.571	120.028	
139.7	1.2520	1.0430	133.376	132.251	132.813	
159.7	1.3370	1.1060	142.431	140.240	141.335	
179.8	1.4040	1.1570	149.568	146.706	148.137	
199.8	1.4520	1.1850	154.682	150.257	152.469	
219.8	1.4830	1.2240	157.984	155.202	156.593	
239.9	1.5070	1.2470	160.541	158.118	159.330	
259.9	1.5190	1.2690	161.819	160.908	161.364	
280.0	1.5560	1.2840	165.761	162.810	164.285	
300.0	1.5750	1.3010	167.785	164.965	166.375	
320.1	1.5990	1.3220	170.341	167.628	168.985	
340.1	1.5960	1.3330	170.022	169.023	169.522	

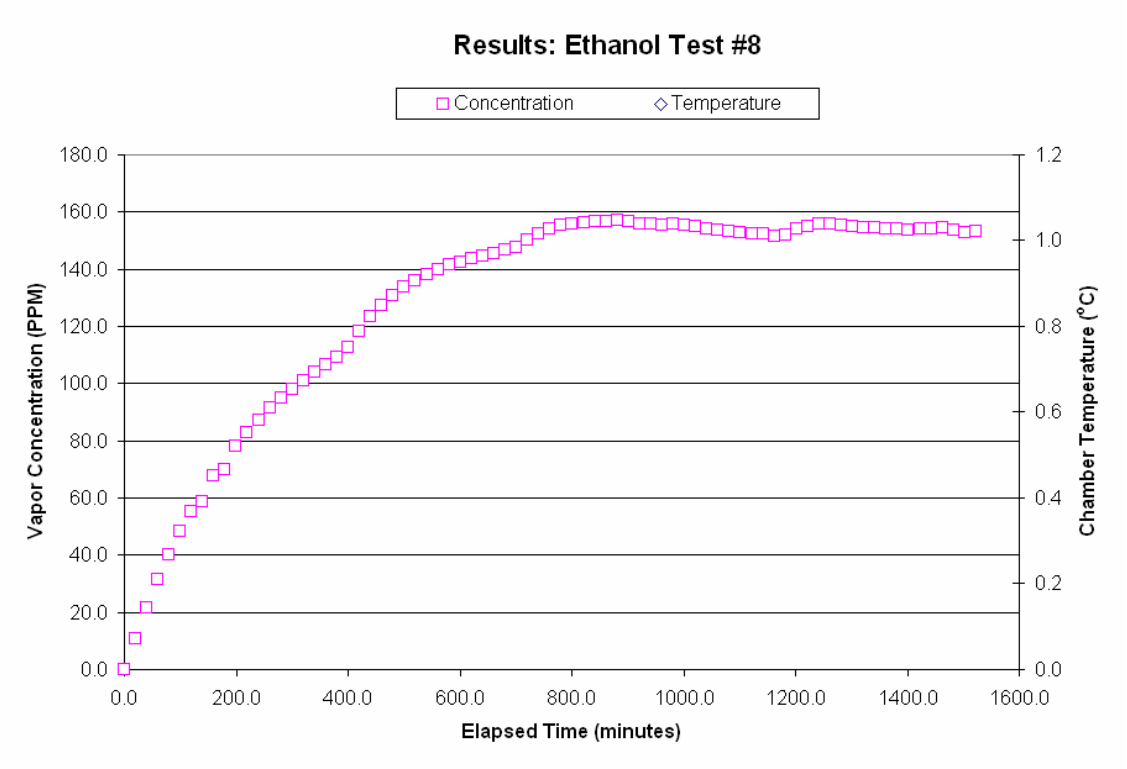

Figure 39: Concentration and Temperature Profile Data of Ethanol Test #8

TEST8: 03-29-06

Ethanol, de-gassed
run continuous
25drop/sec

Time	Absorbance		Concentration			Temperature
Elapsed (min)	*2987.4*	*2900.6*	*2987.4*	*2900.6*	*average*	°C
0.0	0.0000	0.0000	0.0000	0.0000	0.0000	
19.5	0.1000	0.0840	10.6530	10.6511	10.6521	
39.5	0.2030	0.1710	21.6256	21.6826	21.6541	
59.5	0.2940	0.2480	31.3198	31.4462	31.3830	
79.6	0.3770	0.3180	40.1618	40.3221	40.2419	
99.6	0.4520	0.3810	48.1516	48.3104	48.2310	
119.7	0.5200	0.4380	55.3956	55.5380	55.4668	
139.7	0.5180	0.4890	55.1825	62.0047	58.5936	
159.7	0.6380	0.5360	67.9661	67.9643	67.9652	
179.8	0.6890	0.5240	73.3992	66.4427	69.9209	
199.8	0.7340	0.6180	78.1930	78.3618	78.2774	
219.8	0.7800	0.6540	83.0934	82.9265	83.0100	
239.9	0.8180	0.6890	87.1415	87.3645	87.2530	
259.9	0.8590	0.7190	91.5093	91.1685	91.3389	
279.9	0.8900	0.7470	94.8117	94.7189	94.7653	
300.0	0.9190	0.7720	97.9011	97.8888	97.8949	
320.0	0.9520	0.7950	101.4166	100.8052	101.1109	
340.0	0.9800	0.8190	104.3994	103.8484	104.1239	
360.1	1.0040	0.8410	106.9561	106.6380	106.7970	
380.1	1.0270	0.8600	109.4063	109.0471	109.2267	
400.1	1.0600	0.8840	112.9218	112.0903	112.5061	
420.2	1.1150	0.9300	118.7810	117.9231	118.3520	
440.3	1.1610	0.9690	123.6813	122.8682	123.2748	
460.3	1.1980	1.0010	127.6229	126.9258	127.2744	
480.3	1.2340	1.0280	131.4580	130.3494	130.9037	
500.4	1.2590	1.0520	134.1213	133.3925	133.7569	
520.4	1.2770	1.0720	136.0388	135.9285	135.9837	
540.5	1.2990	1.0880	138.3825	137.9573	138.1699	
560.5	1.3180	1.1010	140.4065	139.6057	140.0061	
580.6	1.3330	1.1150	142.0045	141.3809	141.6927	
600.6	1.3400	1.1240	142.7502	142.5221	142.6361	
620.6	1.3560	1.1310	144.4547	143.4097	143.9322	
640.7	1.3610	1.1380	144.9873	144.2973	144.6423	
660.7	1.3660	1.1480	145.5200	145.5653	145.5426	
680.8	1.3820	1.1520	147.2245	146.0724	146.6485	
700.8	1.3900	1.1630	148.0767	147.4672	147.7720	
720.8	1.4130	1.1820	150.5269	149.8764	150.2017	
740.9	1.4360	1.1940	152.9771	151.3980	152.1875	
760.9	1.4530	1.2070	154.7881	153.0464	153.9172	
781.0	1.4680	1.2160	156.3860	154.1876	155.2868	
801.0	1.4660	1.2230	156.1730	155.0752	155.6241	
821.0	1.4720	1.2270	156.8122	155.5824	156.1973	
841.1	1.4750	1.2310	157.1318	156.0896	156.6107	
861.1	1.4750	1.2290	157.1318	155.8360	156.4839	
881.2	1.4810	1.2310	157.7709	156.0896	156.9302	
901.2	1.4770	1.2320	157.3448	156.2164	156.7806	
921.2	1.4680	1.2240	156.3860	155.2020	155.7940	
941.3	1.4660	1.2230	156.1730	155.0752	155.6241	
961.3	1.4650	1.2210	156.0665	154.8216	155.4440	
981.3	1.4700	1.2200	156.5991	154.6948	155.6469	
1001.3	1.4650	1.2180	156.0665	154.4412	155.2538	
1021.4	1.4600	1.2150	155.5338	154.0608	154.7973	
1041.4	1.4500	1.2100	154.4685	153.4268	153.9476	
1061.5	1.4480	1.2050	154.2554	152.7928	153.5241	
1081.5	1.4480	1.2030	154.2554	152.5392	153.3973	
1101.5	1.4380	1.2000	153.1901	152.1588	152.6745	
1121.6	1.4350	1.1970	152.8706	151.7784	152.3245	
1141.6	1.4340	1.1970	152.7640	151.7784	152.2712	
1161.7	1.4240	1.1940	151.6987	151.3980	151.5484	
1181.7	1.4250	1.1960	151.8053	151.6516	151.7284	
1201.8	1.4490	1.2110	154.3620	153.5536	153.9578	
1221.8	1.4600	1.2160	155.5338	154.1876	154.8607	
1241.8	1.4660	1.2260	156.1730	155.4556	155.8143	
1261.8	1.4680	1.2240	156.3860	155.2020	155.7940	
1281.9	1.4700	1.2180	156.5991	154.4412	155.5201	
1301.9	1.4610	1.2170	155.6403	154.3144	154.9774	
1322.0	1.4580	1.2130	155.3207	153.8072	154.5640	
1342.0	1.4540	1.2130	154.8946	153.8072	154.3509	
1362.0	1.4490	1.2100	154.3620	153.4268	153.8944	
1382.1	1.4530	1.2090	154.7881	153.3000	154.0440	
1402.1	1.4500	1.2080	154.4685	153.1732	153.8208	
1422.1	1.4560	1.2100	155.1077	153.4268	154.2672	
1442.2	1.4510	1.2100	154.5750	153.4268	154.0009	
1462.2	1.4550	1.2120	155.0012	153.6804	154.3408	
1482.2	1.4500	1.2090	154.4685	153.3000	153.8842	
1502.3	1.4410	1.2020	153.5097	152.4124	152.9611	
1522.3	1.4400	1.2040	153.4032	152.6660	153.0346	

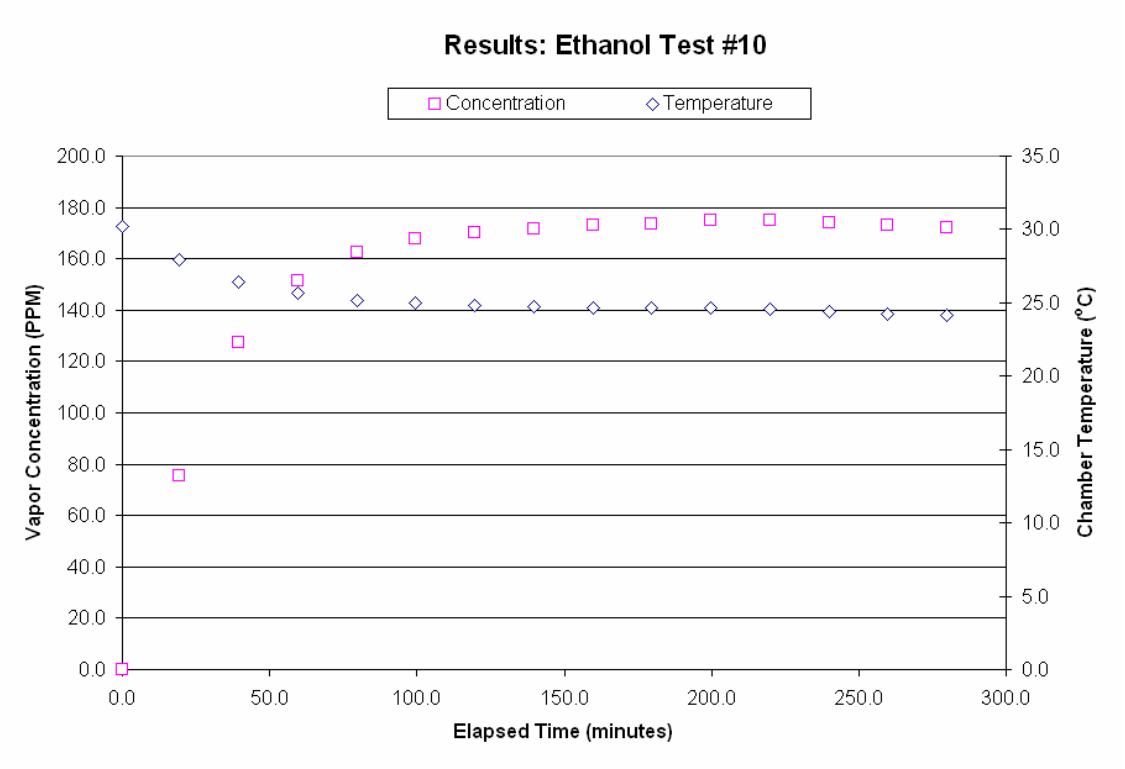

Figure 40: Concentration and Temperature Profile Data of Ethanol Test #10

TEST10: 03-31-06

Ethanol, de-gassed
run continuous
100drop/sec

Time	Absorbance		Concentration			Temperature
Elapsed (min)	*2987.4*	*2900.6*	*2987.4*	*2900.6*	*average*	°C
0.0	0.0000	0.0000	0.000	0.000	0.000	30.242
19.4	0.7090	0.5960	75.530	75.572	75.551	27.900
39.5	1.2000	1.0010	127.836	126.926	127.381	26.428
59.5	1.4270	1.1890	152.018	150.764	151.391	25.650
79.5	1.5330	1.2720	163.310	161.288	162.299	25.176
99.6	1.5890	1.3130	169.276	166.487	167.882	24.952
119.6	1.6100	1.3330	171.513	169.023	170.268	24.842
139.6	1.6240	1.3450	173.005	170.545	171.775	24.773
159.7	1.6410	1.3500	174.816	171.179	172.997	24.650
179.7	1.6390	1.3590	174.603	172.320	173.461	24.627
199.8	1.6590	1.3690	176.733	173.588	175.161	24.662
219.8	1.6560	1.3720	176.414	173.968	175.191	24.600
239.8	1.6400	1.3640	174.709	172.954	173.832	24.419
259.9	1.6360	1.3520	174.283	171.432	172.858	24.265
279.9	1.6240	1.3480	173.005	170.925	171.965	24.142

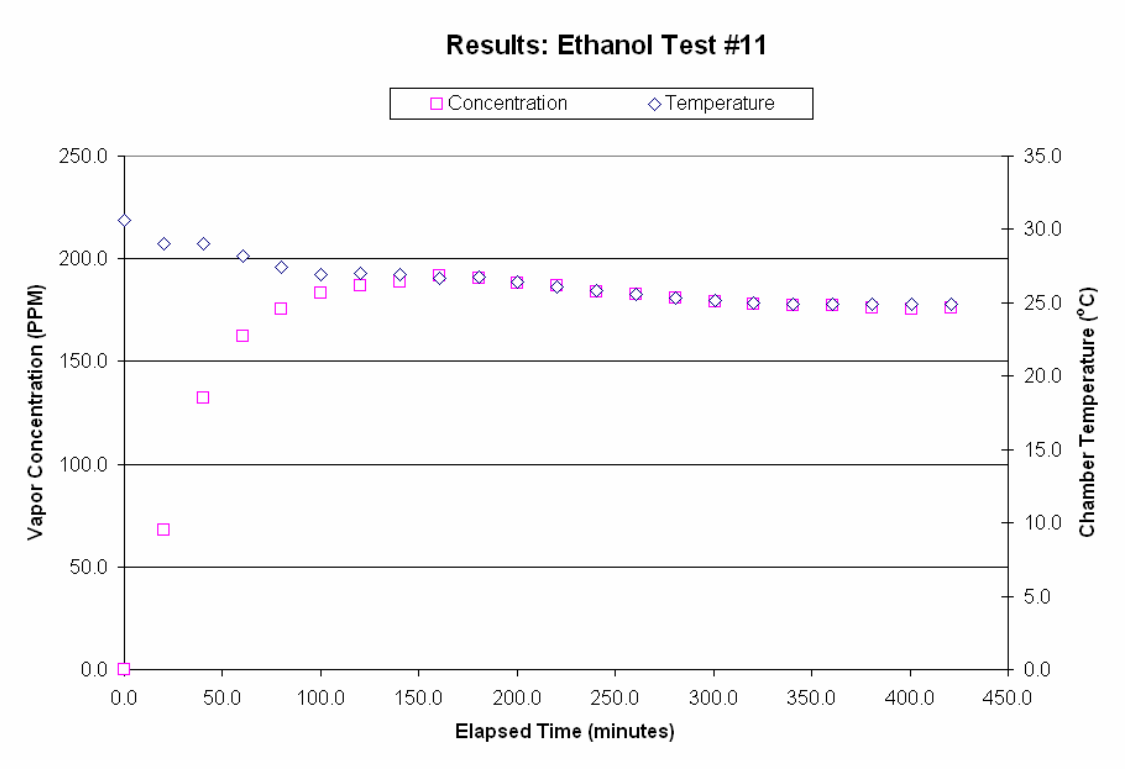

Figure 41: Concentration and Temperature Profile Data of Ethanol Test #11

TEST11: 04-06-06

Ethanol, de-gassed
run continuous
50drop/sec

Time	Absorbance		Concentration			Temperature
Elapsed (min)	*2987.4*	*2900.6*	*2987.4*	*2900.6*	*average*	°C
0.0	0.0000	0.0000	0.000	0.000	0.000	30.606
20.1	0.5870	0.5740	62.533	72.783	67.658	29.045
40.1	1.2380	1.0410	131.884	131.998	131.941	29.045
60.2	1.5270	1.2810	162.671	162.430	162.550	28.195
80.2	1.6480	1.3840	175.561	175.490	175.526	27.462
100.2	1.7270	1.4390	183.977	182.464	183.221	26.920
120.3	1.7570	1.4720	187.173	186.648	186.911	26.985
140.3	1.7820	1.4750	189.836	187.029	188.432	26.938
160.4	1.8130	1.4980	193.139	189.945	191.542	26.676
180.4	1.8000	1.4950	191.754	189.565	190.659	26.729
200.4	1.7700	1.4820	188.558	187.916	188.237	26.400
220.4	1.7560	1.4680	187.067	186.141	186.604	26.102
240.5	1.7230	1.4510	183.551	183.985	183.768	25.811
260.5	1.7160	1.4420	182.805	182.844	182.825	25.555
280.5	1.6930	1.4310	180.355	181.449	180.902	25.347
300.6	1.6770	1.4180	178.651	179.801	179.226	25.188
320.6	1.6630	1.4090	177.159	178.660	177.910	24.985
340.6	1.6570	1.4000	176.520	177.519	177.019	24.918
360.7	1.6570	1.4010	176.520	177.645	177.083	24.918
380.7	1.6490	1.3930	175.668	176.631	176.149	24.911
400.7	1.6450	1.3890	175.242	176.124	175.683	24.910
420.8	1.6460	1.3950	175.348	176.885	176.116	24.907

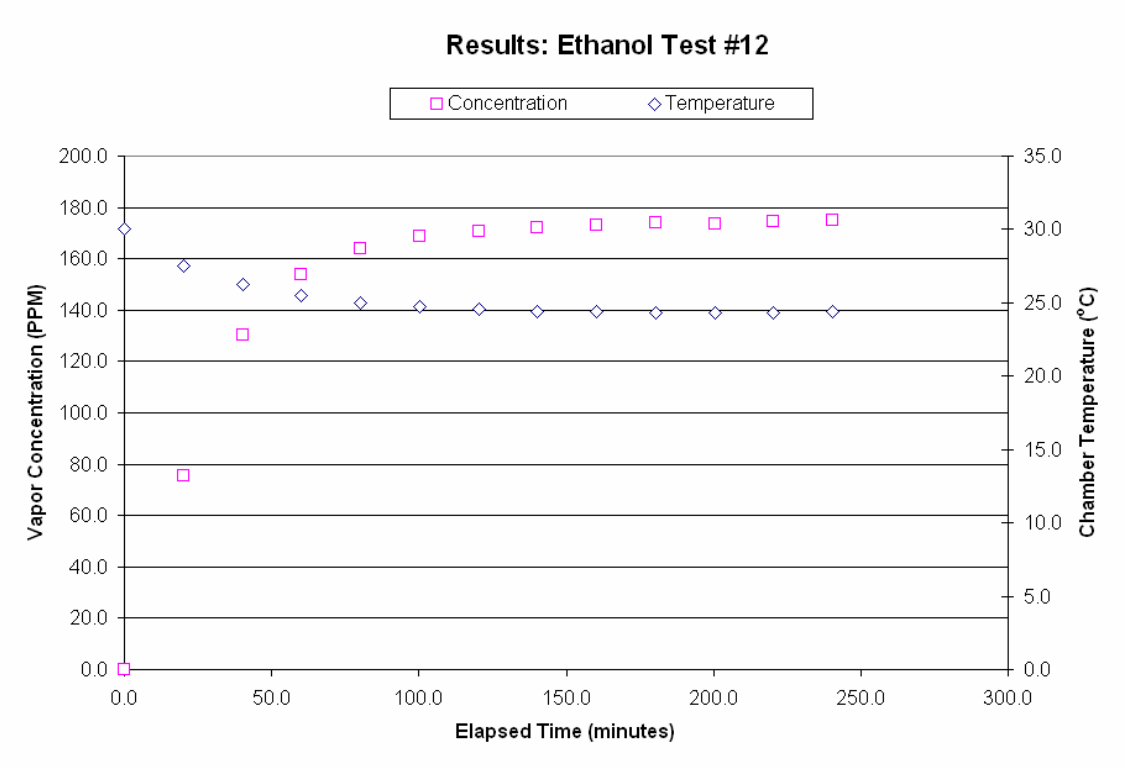

Figure 42: Concentration and Temperature Profile Data of Ethanol Test #12

TEST12: 04-09-06

Ethanol, de-gassed
run continuous
100drop/sec

Time	Absorbance		Concentration			Temperature
Elapsed (min)	*2987.4*	*2900.6*	*2987.4*	*2900.6*	*average*	°C
0.0	0.0000	0.0000	0.000	0.000	0.000	30.078
20.1	0.6530	0.6420	69.564	81.405	75.485	27.551
40.1	1.2280	1.0260	130.819	130.096	130.457	26.236
60.2	1.4530	1.2070	154.788	153.046	153.917	25.453
80.2	1.5520	1.2830	165.335	162.683	164.009	24.983
100.2	1.5990	1.3150	170.341	166.741	168.541	24.701
120.2	1.6220	1.3280	172.792	168.389	170.590	24.539
140.3	1.6400	1.3360	174.709	169.403	172.056	24.435
160.3	1.6430	1.3460	175.029	170.671	172.850	24.403
180.4	1.6540	1.3520	176.201	171.432	173.816	24.331
200.4	1.6430	1.3540	175.029	171.686	173.357	24.276
220.4	1.6520	1.3610	175.988	172.573	174.280	24.336
240.5	1.6540	1.3670	176.201	173.334	174.767	24.407

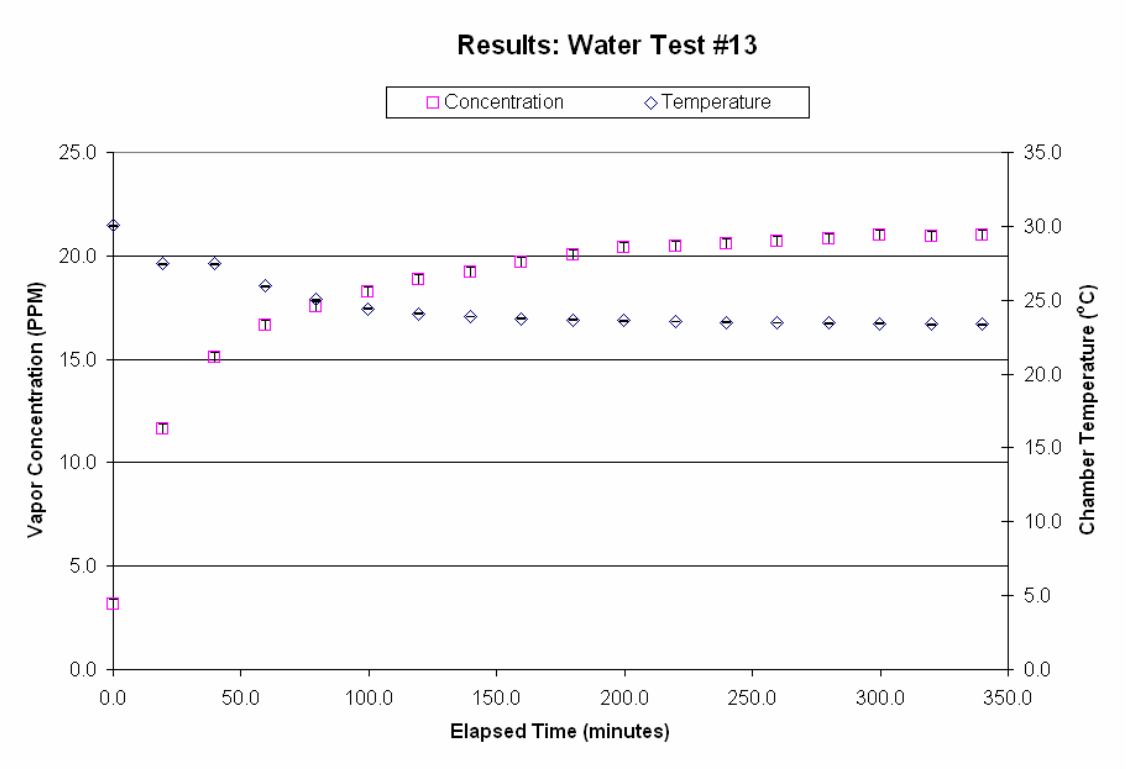

Figure 43: Concentration and Temperature Profile Data of Water Test #13

TEST13: 04-14-06

Water, de-gassed
run continuous
100drop/sec

AMBIENT PPM
g/kg = 2.20
kg/m^3 = 1.08
PPM = 2.38

Time	Absorbance		Concentration		Temperature	Concentration		
Elapsed (min)	*1558.2*	*1652.7*	*1558.2*	*1652.7*	°C	*1558.2*	*1652.7*	*average*
0.0	0.0070	0.0050	0.797	0.731	30.041	3.180	3.114	3.147
19.4	0.0780	0.0660	8.883	9.655	27.459	11.266	12.038	11.652
39.5	0.1080	0.0900	12.300	13.166	27.459	14.682	15.549	15.116
59.5	0.1210	0.1010	13.780	14.776	25.946	16.163	17.158	16.661
79.5	0.1290	0.1070	14.691	15.653	25.030	17.074	18.036	17.555
99.6	0.1350	0.1120	15.375	16.385	24.425	17.757	18.767	18.262
119.6	0.1400	0.1160	15.944	16.970	24.090	18.327	19.353	18.840
139.6	0.1430	0.1190	16.286	17.409	23.895	18.668	19.791	19.230
159.7	0.1470	0.1220	16.741	17.848	23.763	19.124	20.230	19.677
179.7	0.1510	0.1240	17.197	18.140	23.666	19.579	20.523	20.051
199.7	0.1530	0.1270	17.425	18.579	23.608	19.807	20.962	20.385
219.8	0.1540	0.1270	17.538	18.579	23.550	19.921	20.962	20.441
239.8	0.1550	0.1280	17.652	18.725	23.492	20.035	21.108	20.572
259.8	0.1560	0.1290	17.766	18.872	23.468	20.149	21.254	20.702
279.9	0.1570	0.1300	17.880	19.018	23.453	20.263	21.401	20.832
299.9	0.1590	0.1310	18.108	19.164	23.410	20.491	21.547	21.019
319.9	0.1580	0.1310	17.994	19.164	23.380	20.377	21.547	20.962
340.0	0.1590	0.1310	18.108	19.164	23.379	20.491	21.547	21.019

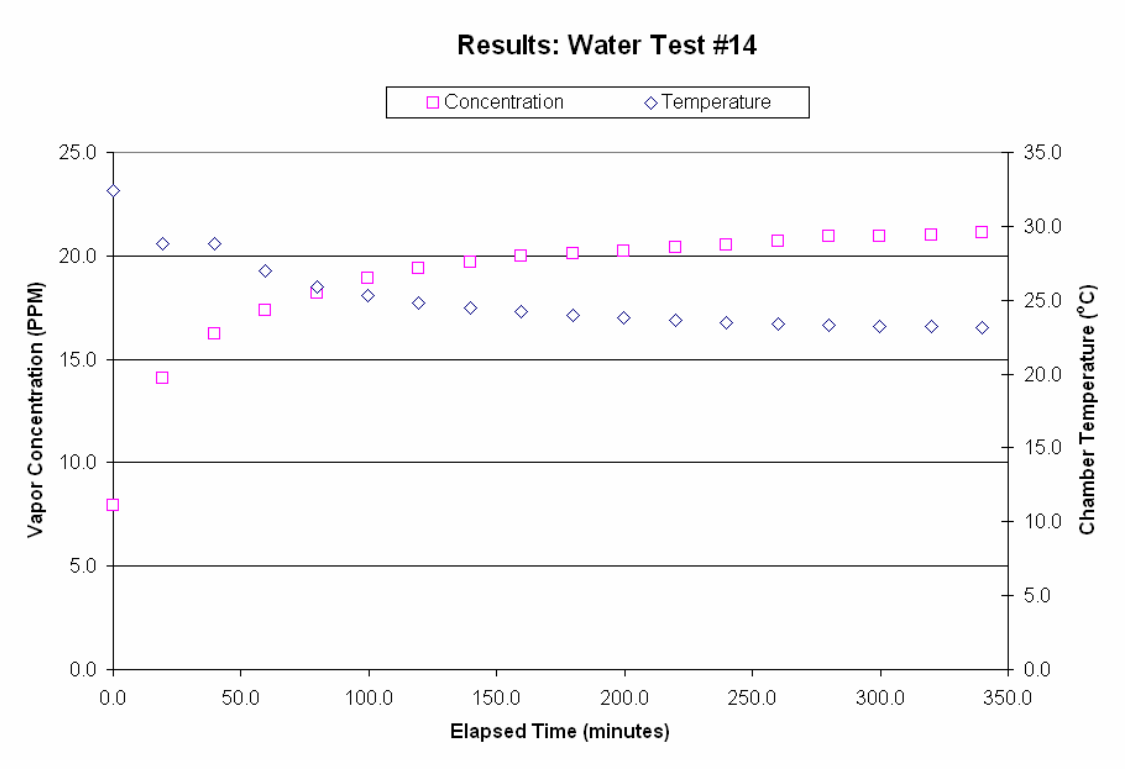

Figure 44: Concentration and Temperature Profile Data of Water Test #14

TEST14: 04-20-06

Water, de-gassed
run continuous
100drop/sec

AMBIENT PPM
g/kg = 7.19
kg/m^3 = 1.08
PPM = 7.748

Time	Absorbance		Concentration		Temperature	Concentration		
Elapsed (min)	*1558.2*	*1652.7*	*1558.2*	*1652.7*	°C	*1558.2*	*1652.7*	*average*
0.0	0.0013	0.0012	0.150	0.170	32.436	7.899	7.918	7.908
19.5	0.0537	0.0445	6.116	6.510	28.845	13.864	14.258	14.061
39.5	0.0724	0.0598	8.245	8.748	28.845	15.994	16.497	16.245
59.5	0.0818	0.0676	9.316	9.889	26.950	17.064	17.638	17.351
79.6	0.0891	0.0736	10.147	10.767	25.910	17.896	18.516	18.206
99.6	0.0950	0.0785	10.819	11.484	25.301	18.568	19.232	18.900
119.6	0.0992	0.0821	11.297	12.011	24.833	19.046	19.759	19.402
139.7	0.1020	0.0840	11.616	12.289	24.510	19.365	20.037	19.701
159.7	0.1040	0.0860	11.844	12.581	24.257	19.593	20.330	19.961
179.7	0.1050	0.0870	11.958	12.727	24.011	19.706	20.476	20.091
199.8	0.1060	0.0880	12.072	12.874	23.776	19.820	20.622	20.221
219.8	0.1080	0.0890	12.300	13.020	23.647	20.048	20.768	20.408
239.8	0.1090	0.0900	12.414	13.166	23.507	20.162	20.915	20.538
259.9	0.1110	0.0910	12.641	13.313	23.385	20.390	21.061	20.725
279.9	0.1120	0.0930	12.755	13.605	23.293	20.504	21.354	20.929
299.9	0.1120	0.0930	12.755	13.605	23.236	20.504	21.354	20.929
320.0	0.1130	0.0930	12.869	13.605	23.199	20.618	21.354	20.986
340.0	0.1140	0.0940	12.983	13.752	23.121	20.731	21.500	21.116

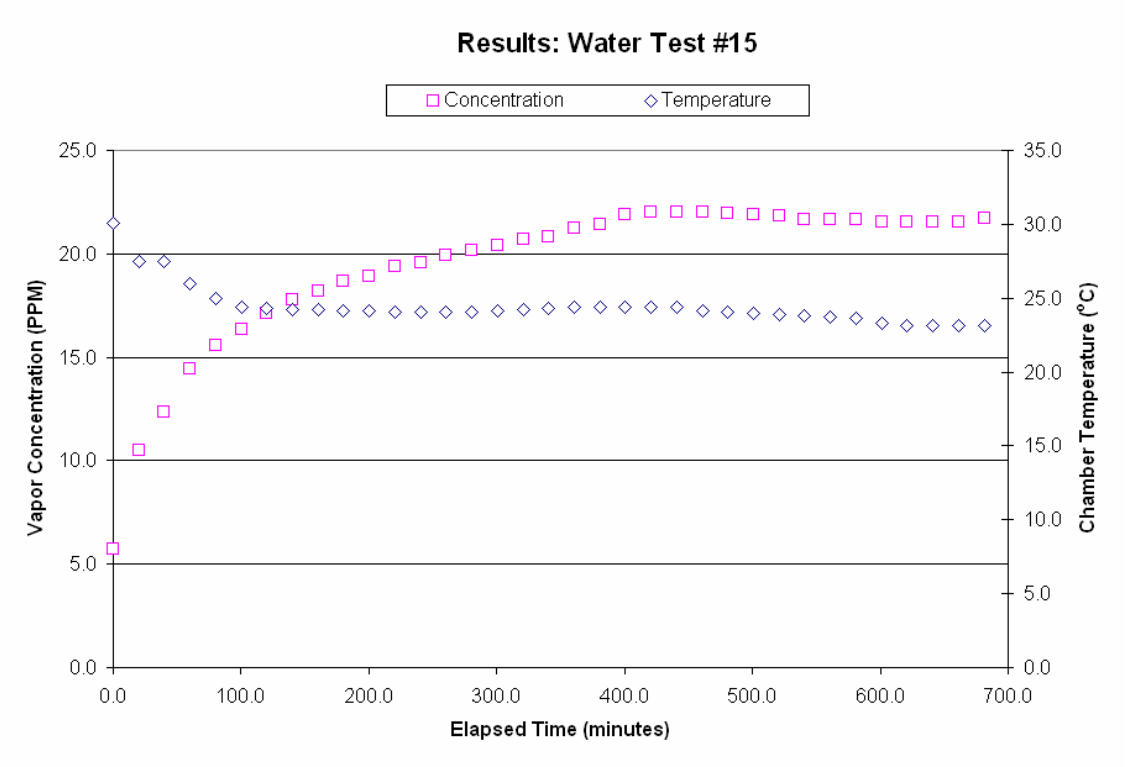

Figure 45: Concentration and Temperature Profile Data of Water Test #15

TEST15: 04-27-06

Water, de-gassed
run continuous
50drop/sec

AMBIENT PPM
g/kg = 4.90
kg/m^3 = 1.08
PPM = 5.300

Time Elapsed (min)	Absorbance 1558.2	Absorbance 1652.7	Concentration 1558.2	Concentration 1652.7	Temperature °C	Concentration 1558.2	Concentration 1652.7	Concentration average
0.0	0.0037	0.0032	0.421	0.468	30.054	5.721	5.768	5.744
20.0	0.0439	0.0366	5.000	5.354	27.485	10.299	10.654	10.477
40.1	0.0545	0.0539	6.207	7.885	27.485	11.506	13.185	12.346
60.1	0.0777	0.0645	8.849	9.436	26.019	14.149	14.735	14.442
80.1	0.0872	0.0723	9.931	10.577	24.988	15.230	15.877	15.553
100.2	0.0942	0.0780	10.728	11.411	24.360	16.028	16.710	16.369
120.2	0.1010	0.0830	11.502	12.142	24.300	16.802	17.442	17.122
140.3	0.1060	0.0880	12.072	12.874	24.250	17.371	18.173	17.772
160.3	0.1100	0.0910	12.527	13.313	24.200	17.827	18.612	18.220
180.3	0.1140	0.0940	12.983	13.752	24.150	18.283	19.051	18.667
200.3	0.1160	0.0960	13.211	14.044	24.100	18.510	19.344	18.927
220.4	0.1200	0.0990	13.666	14.483	24.020	18.966	19.783	19.374
240.4	0.1220	0.1000	13.894	14.629	24.020	19.194	19.929	19.561
260.5	0.1250	0.1030	14.236	15.068	24.020	19.535	20.368	19.952
280.5	0.1270	0.1040	14.464	15.214	24.020	19.763	20.514	20.139
300.5	0.1290	0.1060	14.691	15.507	24.100	19.991	20.807	20.399
320.6	0.1320	0.1080	15.033	15.800	24.200	20.333	21.099	20.716
340.6	0.1330	0.1090	15.147	15.946	24.300	20.446	21.245	20.846
360.7	0.1360	0.1120	15.488	16.385	24.400	20.788	21.684	21.236
380.7	0.1380	0.1130	15.716	16.531	24.410	21.016	21.831	21.423
400.7	0.1420	0.1160	16.172	16.970	24.430	21.471	22.270	21.870
420.7	0.1430	0.1170	16.286	17.116	24.410	21.585	22.416	22.001
440.8	0.1430	0.1170	16.286	17.116	24.390	21.585	22.416	22.001
460.8	0.1430	0.1170	16.286	17.116	24.170	21.585	22.416	22.001
480.8	0.1420	0.1170	16.172	17.116	24.060	21.471	22.416	21.944
500.9	0.1420	0.1160	16.172	16.970	23.980	21.471	22.270	21.870
520.9	0.1410	0.1160	16.058	16.970	23.880	21.357	22.270	21.814
540.9	0.1400	0.1150	15.944	16.824	23.810	21.244	22.123	21.683
561.0	0.1400	0.1150	15.944	16.824	23.740	21.244	22.123	21.683
581.0	0.1400	0.1150	15.944	16.824	23.600	21.244	22.123	21.683
601.1	0.1390	0.1140	15.830	16.677	23.300	21.130	21.977	21.553
621.1	0.1390	0.1140	15.830	16.677	23.150	21.130	21.977	21.553
641.1	0.1390	0.1140	15.830	16.677	23.120	21.130	21.977	21.553
661.2	0.1390	0.1140	15.830	16.677	23.110	21.130	21.977	21.553
681.2	0.1410	0.1150	16.058	16.824	23.100	21.357	22.123	21.740

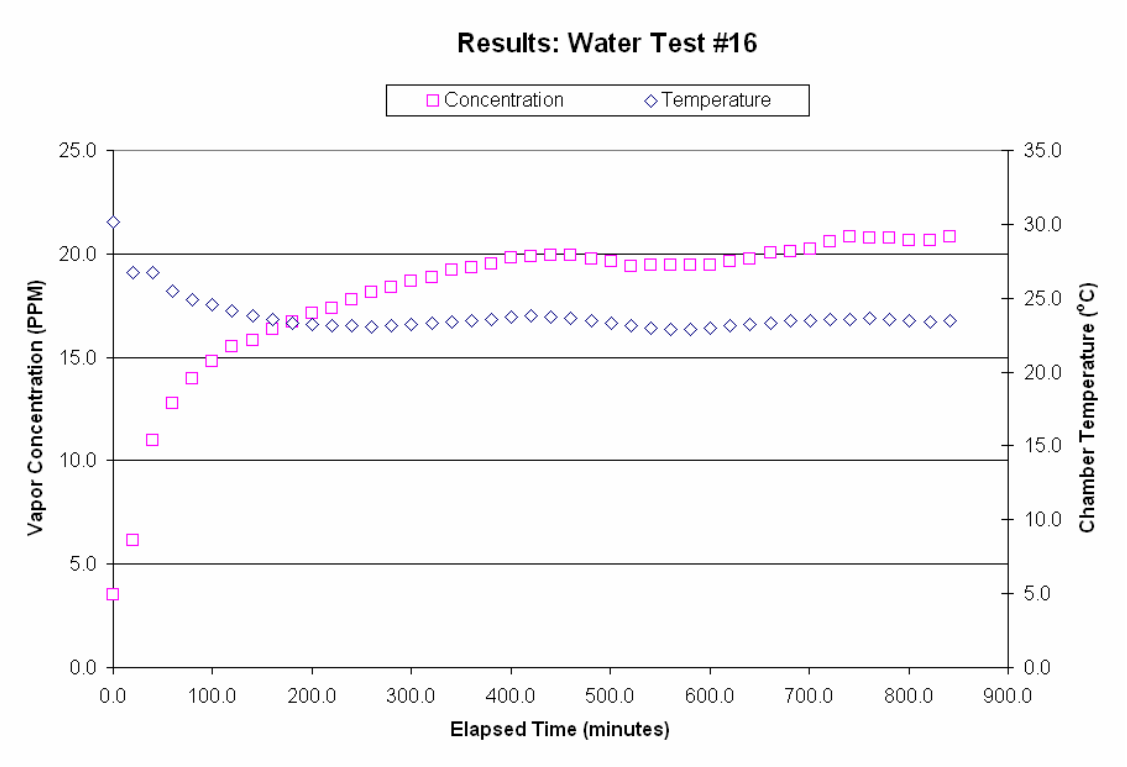

Figure 46: Concentration and Temperature Profile Data of Water Test #16

TEST16: 05-03-06

Water, de-gassed
run continuous
50drop/sec

AMBIENT PPM
g/kg = 2.97
kg/m^3 = 1.08
PPM = 3.207

Time	Absorbance		Concentration		Temperature	Concentration		
Elapsed (min)	1558.2	1652.7	1558.2	1652.7	°C	1558.2	1652.7	average
0.0	0.0027	0.0023	0.307	0.336	30.183	3.515	3.544	3.529
19.7	0.0043	0.0370	0.490	5.413	26.742	3.697	8.620	6.158
39.7	0.0660	0.0560	7.516	8.046	26.742	10.724	11.253	10.988
59.8	0.0810	0.0680	9.225	9.948	25.506	12.432	13.155	12.793
79.8	0.0910	0.0760	10.364	11.118	24.863	13.571	14.325	13.948
99.8	0.0980	0.0820	11.161	11.996	24.559	14.368	15.203	14.786
119.9	0.1040	0.0870	11.844	12.727	24.122	15.051	15.935	15.493
139.9	0.1070	0.0890	12.186	13.020	23.788	15.393	16.227	15.810
159.9	0.1110	0.0930	12.641	13.605	23.519	15.848	16.812	16.330
180.0	0.1150	0.0950	13.097	13.898	23.337	16.304	17.105	16.704
200.0	0.1180	0.0980	13.439	14.337	23.197	16.646	17.544	17.095
220.1	0.1200	0.1000	13.666	14.629	23.151	16.873	17.836	17.355
240.1	0.1240	0.1030	14.122	15.068	23.110	17.329	18.275	17.802
260.1	0.1270	0.1060	14.464	15.361	23.096	17.671	18.568	18.119
280.1	0.1290	0.1070	14.691	15.653	23.173	17.898	18.860	18.379
300.2	0.1320	0.1090	15.033	15.946	23.243	18.240	19.153	18.697
320.2	0.1330	0.1100	15.147	16.092	23.301	18.354	19.299	18.827
340.2	0.1360	0.1130	15.488	16.531	23.378	18.696	19.738	19.217
360.3	0.1370	0.1140	15.602	16.677	23.479	18.810	19.884	19.347
380.3	0.1390	0.1150	15.830	16.824	23.594	19.037	20.031	19.534
400.3	0.1410	0.1170	16.058	17.116	23.684	19.265	20.323	19.794
420.4	0.1420	0.1170	16.172	17.116	23.765	19.379	20.323	19.851
440.4	0.1420	0.1180	16.172	17.263	23.764	19.379	20.470	19.924
460.5	0.1420	0.1180	16.172	17.263	23.653	19.379	20.470	19.924
480.5	0.1400	0.1170	15.944	17.116	23.499	19.151	20.323	19.737
500.5	0.1390	0.1160	15.830	16.970	23.310	19.037	20.177	19.607
520.6	0.1380	0.1140	15.716	16.677	23.130	18.923	19.884	19.404
540.6	0.1380	0.1150	15.716	16.824	22.970	18.923	20.031	19.477
560.7	0.1380	0.1150	15.716	16.824	22.898	18.923	20.031	19.477
580.7	0.1380	0.1150	15.716	16.824	22.875	18.923	20.031	19.477
600.7	0.1380	0.1150	15.716	16.824	22.988	18.923	20.031	19.477
620.8	0.1390	0.1160	15.830	16.970	23.108	19.037	20.177	19.607
640.8	0.1400	0.1170	15.944	17.116	23.225	19.151	20.323	19.737
660.8	0.1430	0.1190	16.286	17.409	23.337	19.493	20.616	20.054
680.9	0.1440	0.1190	16.400	17.409	23.438	19.607	20.616	20.111
700.9	0.1450	0.1200	16.513	17.555	23.486	19.721	20.762	20.241
721.0	0.1480	0.1220	16.855	17.848	23.519	20.062	21.055	20.559
741.0	0.1500	0.1240	17.083	18.140	23.544	20.290	21.347	20.819
761.1	0.1490	0.1240	16.969	18.140	23.600	20.176	21.347	20.762
781.1	0.1490	0.1240	16.969	18.140	23.593	20.176	21.347	20.762
801.1	0.1480	0.1230	16.855	17.994	23.500	20.062	21.201	20.632
821.2	0.1480	0.1230	16.855	17.994	23.417	20.062	21.201	20.632
841.2	0.1500	0.1240	17.083	18.140	23.464	20.290	21.347	20.819

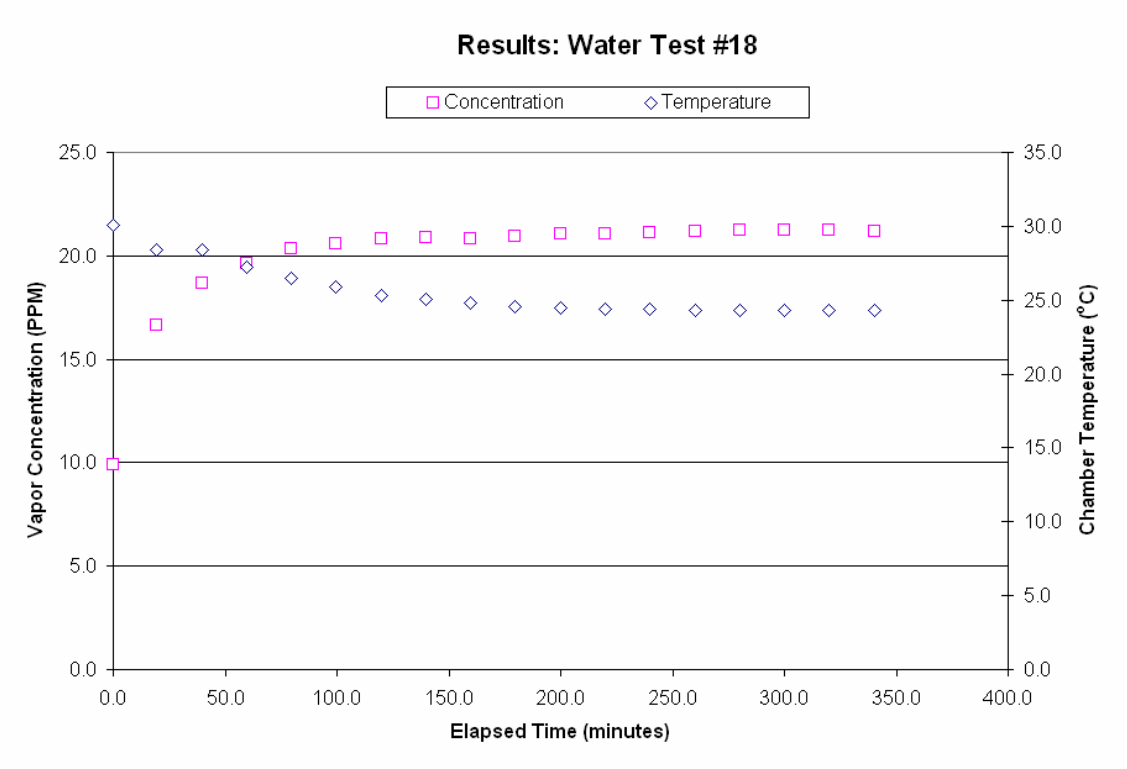

Figure 47: Concentration and Temperature Profile Data of Water Test #18

TEST18: 05-08-06

Water, de-gassed
run continuous
100drop/sec

AMBIENT PPM
g/kg = 8.58
kg/m^3 = 1.07
PPM = 9.213

Time	Absorbance		Concentration		Temperature	Concentration		
Elapsed (min)	*1558.2*	*1652.7*	*1558.2*	*1652.7*	°C	*1558.2*	*1652.7*	*average*
0.0	0.0007	0.0004	0.080	0.059	30.082	9.922	9.901	9.912
19.6	0.0586	0.0478	6.674	6.993	28.399	16.516	16.835	16.676
39.6	0.0756	0.0615	8.610	8.997	28.399	18.452	18.840	18.646
59.6	0.0826	0.0699	9.407	10.226	27.257	19.250	20.069	19.659
79.7	0.0902	0.0733	10.273	10.723	26.507	20.115	20.566	20.341
99.7	0.0921	0.0748	10.489	10.943	25.899	20.332	20.785	20.558
119.8	0.0943	0.0766	10.739	11.206	25.351	20.582	21.049	20.815
139.8	0.0949	0.0771	10.808	11.279	25.055	20.650	21.122	20.886
159.8	0.0947	0.0768	10.785	11.235	24.773	20.628	21.078	20.853
179.8	0.0956	0.0776	10.888	11.352	24.552	20.730	21.195	20.963
199.9	0.0963	0.0783	10.967	11.455	24.490	20.810	21.297	21.054
219.9	0.0966	0.0784	11.001	11.469	24.401	20.844	21.312	21.078
239.9	0.0969	0.0785	11.036	11.484	24.375	20.878	21.327	21.102
260.0	0.0977	0.0791	11.127	11.572	24.348	20.969	21.414	21.192
280.0	0.0983	0.0795	11.195	11.630	24.338	21.038	21.473	21.255
300.1	0.0981	0.0796	11.172	11.645	24.301	21.015	21.488	21.251
320.1	0.0983	0.0796	11.195	11.645	24.278	21.038	21.488	21.263
340.1	0.0979	0.0792	11.149	11.586	24.278	20.992	21.429	21.211

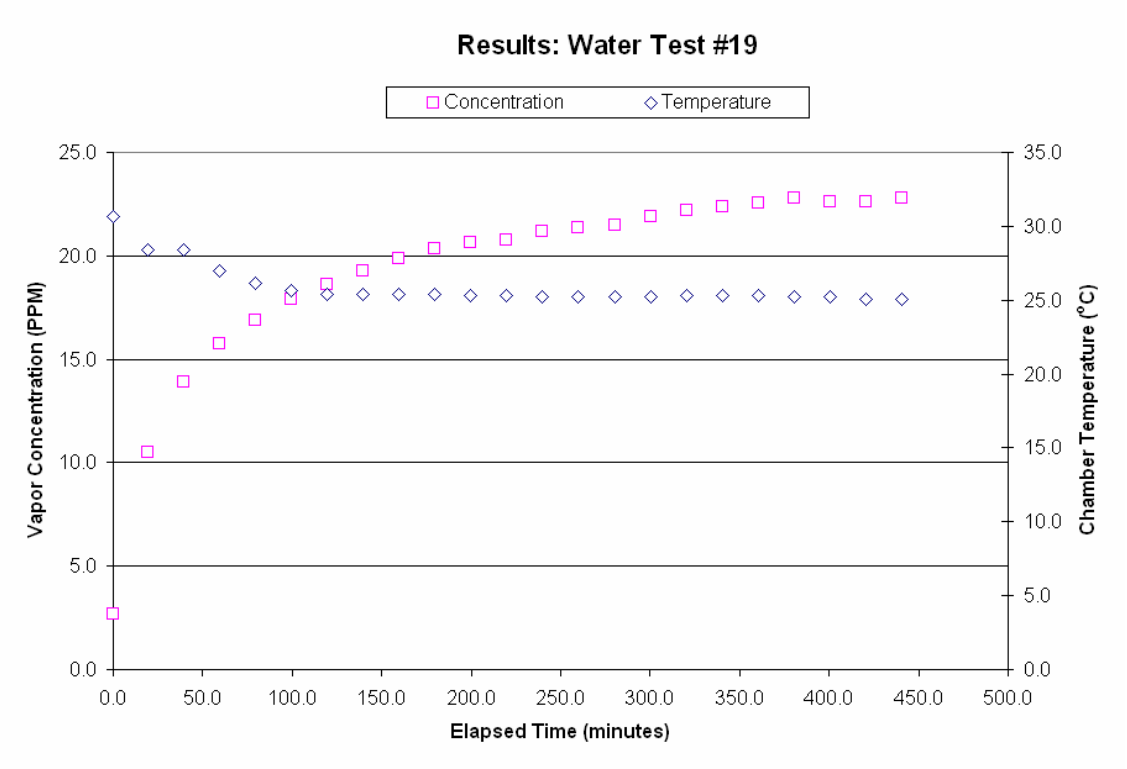

Figure 48: Concentration and Temperature Profile Data of Water Test #19

TEST19: 05-09-06

Water, de-gassed
run continuous
100drop/sec

AMBIENT PPM
g/kg = 1.74
kg/m^3 = 1.08
PPM = 1.874

Time	Absorbance		Concentration		Temperature	Concentration		
Elapsed (min)	*1558.2*	*1652.7*	*1558.2*	*1652.7*	°C	*1558.2*	*1652.7*	*average*
0.0	0.0070	0.0060	0.797	0.878	30.615	2.672	2.752	2.712
19.6	0.0730	0.0610	8.314	8.924	28.422	10.188	10.798	10.493
39.6	0.1020	0.0850	11.616	12.435	28.422	13.491	14.309	13.900
59.7	0.1180	0.0980	13.439	14.337	26.998	15.313	16.211	15.762
79.7	0.1270	0.1060	14.464	15.507	26.110	16.338	17.381	16.860
99.7	0.1360	0.1130	15.488	16.531	25.620	17.363	18.405	17.884
119.8	0.1420	0.1180	16.172	17.263	25.430	18.046	19.137	18.592
139.8	0.1480	0.1230	16.855	17.994	25.431	18.730	19.868	19.299
159.8	0.1530	0.1270	17.425	18.579	25.370	19.299	20.454	19.876
179.9	0.1570	0.1300	17.880	19.018	25.375	19.754	20.892	20.323
199.9	0.1600	0.1320	18.222	19.311	25.324	20.096	21.185	20.641
219.9	0.1610	0.1330	18.336	19.457	25.298	20.210	21.331	20.771
240.0	0.1640	0.1360	18.677	19.896	25.268	20.552	21.770	21.161
260.0	0.1660	0.1370	18.905	20.042	25.226	20.779	21.916	21.348
280.1	0.1670	0.1380	19.019	20.188	25.211	20.893	22.063	21.478
300.1	0.1700	0.1410	19.361	20.627	25.207	21.235	22.502	21.868
320.1	0.1730	0.1430	19.702	20.920	25.273	21.577	22.794	22.185
340.2	0.1750	0.1440	19.930	21.066	25.322	21.804	22.941	22.372
360.2	0.1760	0.1460	20.044	21.359	25.299	21.918	23.233	22.576
380.2	0.1780	0.1470	20.272	21.505	25.245	22.146	23.379	22.763
400.3	0.1770	0.1460	20.158	21.359	25.248	22.032	23.233	22.633
420.3	0.1770	0.1460	20.158	21.359	25.072	22.032	23.233	22.633
440.3	0.1780	0.1470	20.272	21.505	25.018	22.146	23.379	22.763

Figure 49: Concentration and Temperature Profile Data of Mixture Test #20

TEST20: 05-10-06

Mix, de-gassed
run continuous
100drop/sec

AMBIENT PPM
g/kg = 6.28
kg/m^3 = 1.07
PPM = 6.737

Time	Water Absorbance		Water Concentration		Water Concentration			Ethanol Absorbance		Ethanol Concentration			Temperature
Elapsed (min)	*1558.2*	*1652.7*	*1558.2*	*1652.7*	*1558.2*	*1652.7*	*average*	*2900.6*	*2987.4*	*2900.6*	*2987.4*	*average*	°C
0.0	0.0083	0.0069	0.945	1.009	7.683	7.747	7.715	0.0004	0.0005	0.049	0.050	0.050	30.450
19.6	0.0131	0.0112	1.492	1.638	8.229	8.376	8.303	0.0064	0.0077	0.812	0.820	0.816	28.034
39.7	0.0184	0.0156	2.096	2.282	8.833	9.020	8.926	0.0068	0.0081	0.862	0.863	0.863	28.034
59.7	0.0202	0.0171	2.300	2.502	9.038	9.239	9.138	0.0067	0.0081	0.850	0.863	0.856	26.720
79.7	0.0218	0.0185	2.483	2.706	9.220	9.444	9.332	0.0071	0.0084	0.903	0.899	0.901	25.992
99.8	0.0232	0.0196	2.642	2.867	9.380	9.605	9.492	0.0070	0.0083	0.881	0.888	0.885	25.551
119.8	0.0510	0.0430	5.808	6.291	12.546	13.028	12.787	0.1210	0.1440	15.343	15.340	15.341	25.383
139.8	0.0600	0.0500	6.833	7.315	13.571	14.052	13.811	0.1590	0.1890	20.161	20.134	20.148	25.324
159.9	0.0522	0.0438	5.945	6.408	12.682	13.145	12.914	0.1570	0.1870	19.907	19.921	19.914	25.298
179.9	0.0494	0.0416	5.626	6.086	12.363	12.823	12.593	0.1550	0.1850	19.654	19.708	19.681	25.349
200.0	0.0486	0.0409	5.535	5.983	12.272	12.721	12.497	0.1540	0.1840	19.527	19.602	19.564	25.424
220.0	0.0492	0.0415	5.603	6.071	12.341	12.809	12.575	0.1530	0.1820	19.400	19.388	19.394	25.432
240.0	0.0493	0.0416	5.615	6.086	12.352	12.823	12.588	0.1520	0.1810	19.273	19.282	19.278	25.506
260.0	0.0506	0.0424	5.763	6.203	12.500	12.940	12.720	0.1510	0.1800	19.147	19.175	19.161	25.637
280.1	0.0500	0.0420	5.694	6.144	12.432	12.882	12.657	0.1500	0.1790	19.020	19.069	19.044	25.711
300.1	0.0510	0.0420	5.808	6.144	12.546	12.882	12.714	0.1490	0.1780	18.893	18.962	18.928	25.734

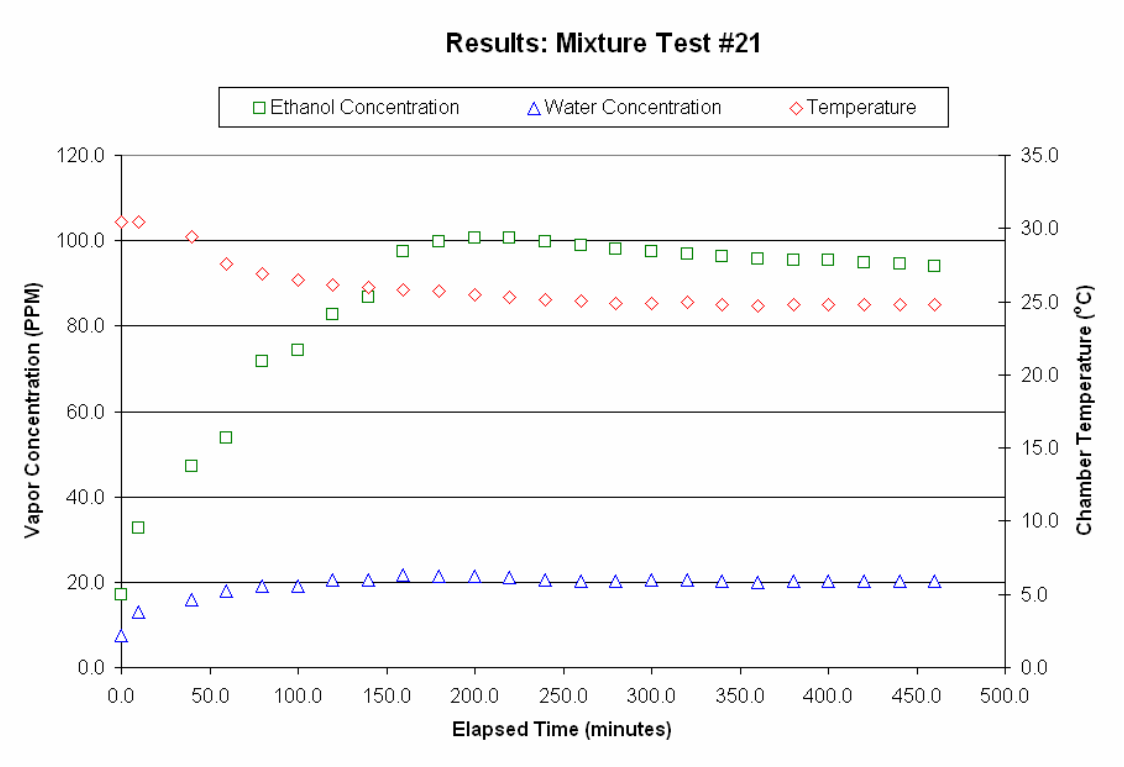

Figure 50: Concentration and Temperature Profile Data of Mixture Test #21

TEST21: 05-11-06

Mix, de-gassed
run continuous
100drop/sec

AMBIENT PPM
g/kg = 6.91
kg/m^3 = 1.07
PPM = 7.412

Time	Water				Water			Ethanol					Temperature
	Absorbance		Concentration		Concentration			Absorbance		Concentration			
Elapsed (min)	1558.2	1652.7	1558.2	1652.7	1558.2	1652.7	average	2900.6	2987.4	2900.6	2987.4	average	°C
0.0	0.0019	0.0016	0.215	0.236	7.627	7.648	7.638	0.0002	0.0000	17.022	17.000	17.011	30.430
9.5	0.0473	0.0396	5.387	5.793	12.799	13.205	13.002	0.1230	0.1470	32.596	32.660	32.628	30.430
39.5	0.0723	0.0604	8.234	8.836	15.646	16.248	15.947	0.2380	0.2830	47.178	47.148	47.163	29.398
59.6	0.0885	0.0740	10.079	10.826	17.491	18.238	17.865	0.2400	0.4050	47.432	60.145	53.788	27.567
79.6	0.0985	0.0823	11.218	12.040	18.630	19.452	19.041	0.4300	0.5130	71.524	71.650	71.587	26.941
99.7	0.0990	0.0830	11.275	12.142	18.687	19.555	19.121	0.4510	0.5380	74.186	74.313	74.250	26.484
119.7	0.1110	0.0930	12.641	13.605	20.054	21.017	20.536	0.5180	0.6190	82.682	82.942	82.812	26.168
139.7	0.1110	0.0930	12.641	13.605	20.054	21.017	20.536	0.5490	0.6550	86.613	86.777	86.695	25.971
159.8	0.1210	0.1010	13.780	14.776	21.192	22.188	21.690	0.6340	0.7570	97.391	97.643	97.517	25.790
179.8	0.1190	0.0990	13.552	14.483	20.965	21.895	21.430	0.6520	0.7800	99.673	100.093	99.883	25.691
199.8	0.1190	0.0990	13.552	14.483	20.965	21.895	21.430	0.6580	0.7880	100.434	100.946	100.690	25.447
219.9	0.1150	0.0960	13.097	14.044	20.509	21.456	20.983	0.6580	0.7880	100.434	100.946	100.690	25.301
239.9	0.1110	0.0920	12.641	13.459	20.054	20.871	20.462	0.6510	0.7790	99.546	99.987	99.767	25.141
259.9	0.1090	0.0900	12.414	13.166	19.826	20.579	20.202	0.6440	0.7700	98.659	99.028	98.843	25.085
280.0	0.1090	0.0900	12.414	13.166	19.826	20.579	20.202	0.6380	0.7640	97.898	98.389	98.143	24.890
300.0	0.1100	0.0920	12.527	13.459	19.940	20.871	20.405	0.6330	0.7580	97.264	97.750	97.507	24.920
320.0	0.111	0.092	12.641	13.459	20.054	20.871	20.462	0.6290	0.7520	96.757	97.111	96.934	24.966
340.1	0.11	0.091	12.527	13.313	19.940	20.725	20.332	0.6250	0.7470	96.249	96.578	96.414	24.820
360.1	0.107	0.089	12.186	13.020	19.598	20.432	20.015	0.6200	0.7410	95.615	95.939	95.777	24.691
380.1	0.108	0.09	12.300	13.166	19.712	20.579	20.145	0.6170	0.7390	95.235	95.726	95.480	24.789
400.2	0.109	0.091	12.414	13.313	19.826	20.725	20.275	0.6160	0.7380	95.108	95.619	95.364	24.808
420.2	0.109	0.091	12.414	13.313	19.826	20.725	20.275	0.6130	0.7330	94.728	95.086	94.907	24.807
440.3	0.109	0.091	12.414	13.313	19.826	20.725	20.275	0.6100	0.7280	94.347	94.554	94.451	24.805
460.3	0.11	0.091	12.527	13.313	19.940	20.725	20.332	0.6060	0.7250	93.840	94.234	94.037	24.811

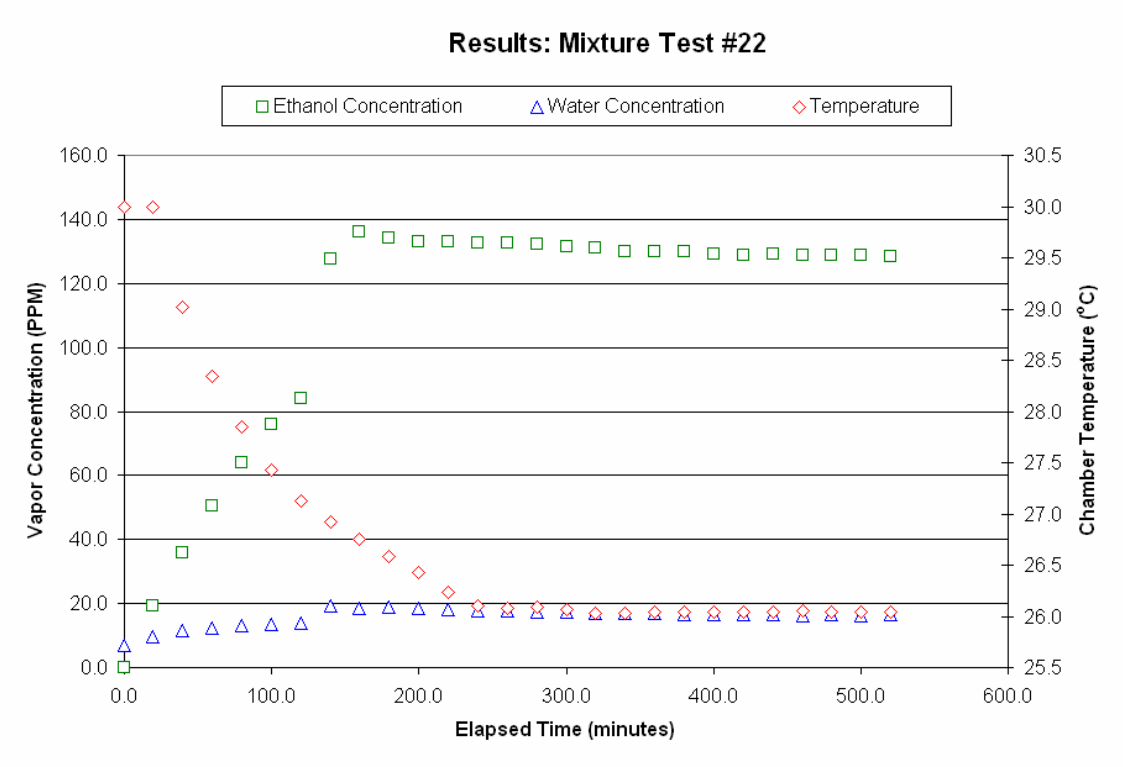

Figure 51: Concentration and Temperature Profile Data of Mixture Test #22

TEST22: 05-12-06

Mix, de-gassed
run continuous
100drop/sec

AMBIENT PPM
g/kg = 6.28
kg/m^3 = 1.07
PPM = 6.737

Time	Water Absorbance		Water Concentration		Water Concentration			Ethanol Absorbance		Ethanol Concentration			Temperature
Elapsed (min)	1558.2	1652.7	1558.2	1652.7	1558.2	1652.7	average	2900.6	2987.4	2900.6	2987.4	average	°C
0.0	0.0031	0.0025	0.348	0.372	7.086	7.109	7.097	0.0007	0.0008	0.084	0.083	0.083	29.994
19.5	0.0261	0.0214	2.972	3.131	9.710	9.868	9.789	0.1510	0.1800	19.147	19.175	19.161	29.994
39.6	0.0403	0.0329	4.590	4.813	11.327	11.550	11.439	0.2810	0.3360	35.631	35.794	35.712	29.017
59.6	0.0487	0.0398	5.546	5.822	12.284	12.560	12.422	0.3970	0.4750	50.339	50.602	50.470	28.344
79.7	0.0532	0.0434	6.059	6.349	12.796	13.087	12.941	0.5030	0.6020	63.780	64.131	63.955	27.846
99.7	0.0594	0.0484	6.765	7.081	13.502	13.818	13.660	0.5970	0.7140	75.699	76.062	75.881	27.422
119.7	0.0625	0.0509	7.118	7.446	13.855	14.184	14.020	0.6590	0.7920	83.561	84.372	83.966	27.131
139.8	0.1070	0.0870	12.186	12.727	18.923	19.465	19.194	0.9950	1.2080	126.165	128.688	127.427	26.925
159.8	0.1010	0.0830	11.502	12.142	18.240	18.880	18.560	1.0620	1.2900	134.661	137.424	136.042	26.754
179.8	0.1040	0.0850	11.844	12.435	18.582	19.172	18.877	1.0470	1.2700	132.759	135.293	134.026	26.580
199.9	0.1020	0.0830	11.616	12.142	18.354	18.880	18.617	1.0360	1.2620	131.364	134.441	132.902	26.425
219.9	0.0970	0.0800	11.047	11.703	17.784	18.441	18.113	1.0370	1.2630	131.491	134.547	133.019	26.229
239.9	0.0950	0.0770	10.819	11.265	17.557	18.002	17.779	1.0350	1.2580	131.237	134.015	132.626	26.104
260.0	0.0940	0.0770	10.705	11.265	17.443	18.002	17.722	1.0370	1.2570	131.491	133.908	132.699	26.077
280.0	0.0910	0.0750	10.364	10.972	17.101	17.709	17.405	1.0360	1.2520	131.364	133.376	132.370	26.093
300.0	0.0900	0.0740	10.250	10.826	16.987	17.563	17.275	1.0280	1.2470	130.349	132.843	131.596	26.062
320.1	0.089	0.073	10.136	10.679	16.873	17.417	17.145	1.0220	1.2460	129.589	132.736	131.162	26.034
340.1	0.0873	0.0715	9.942	10.460	16.680	17.197	16.939	1.0150	1.2340	128.701	131.458	130.080	26.029
360.2	0.086	0.071	9.794	10.387	16.532	17.124	16.828	1.0120	1.2320	128.321	131.245	129.783	26.042
380.2	0.0857	0.0704	9.760	10.299	16.497	17.036	16.767	1.0130	1.2310	128.447	131.138	129.793	26.038
400.2	0.0839	0.0688	9.555	10.065	16.292	16.802	16.547	1.0110	1.2230	128.194	130.286	129.240	26.047
420.3	0.085	0.069	9.680	10.094	16.418	16.832	16.625	1.0090	1.2190	127.940	129.860	128.900	26.046
440.3	0.0829	0.0682	9.441	9.977	16.179	16.715	16.447	1.0100	1.2200	128.067	129.967	129.017	26.045
460.3	0.0816	0.0673	9.293	9.845	16.031	16.583	16.307	1.0080	1.2190	127.813	129.860	128.837	26.054
480.4	0.0824	0.0679	9.384	9.933	16.122	16.671	16.396	1.007	1.217	127.687	129.647	128.667	26.046
500.4	0.0816	0.0672	9.293	9.831	16.031	16.568	16.299	1.006	1.217	127.560	129.647	128.603	26.042
520.4	0.0824	0.0678	9.384	9.919	16.122	16.656	16.389	1.003	1.216	127.179	129.540	128.360	26.042

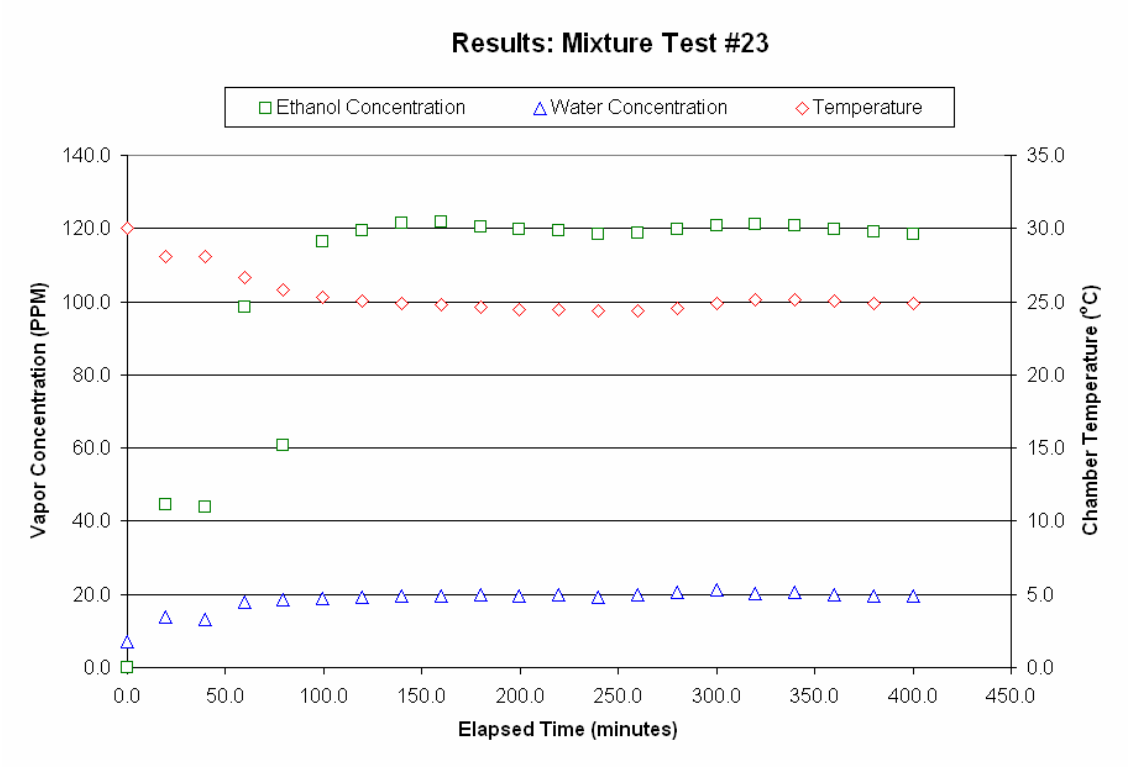

Figure 52: Concentration and Temperature Profile Data of Mixture Test #23

TEST23: 05-17-06

Mix, de-gassed
run continuous
300drop/sec

AMBIENT PPM
g/kg = 6.28
kg/m^3 = 1.07
PPM = 6.737

Time	Water				Water			Ethanol					Temperature
	Absorbance		Concentration		Concentration			Absorbance		Concentration			
Elapsed (min)	*1558.2*	*1652.7*	*1558.2*	*1652.7*	*1558.2*	*1652.7*	*average*	*2900.6*	*2987.4*	*2900.6*	*2987.4*	*average*	°C
0.0	0.0029	0.0023	0.328	0.341	7.065	7.078	7.072	0.0000	0.0000	0.000	0.000	0.000	29.986
19.5	0.0594	0.0487	6.765	7.124	13.502	13.862	13.682	0.3530	0.4190	44.760	44.636	44.698	28.056
39.5	0.0550	0.0452	6.264	6.612	13.001	13.350	13.175	0.3460	0.4110	43.872	43.784	43.828	28.056
59.6	0.0939	0.0772	10.694	11.294	17.431	18.031	17.731	0.7760	0.9270	98.396	98.753	98.575	26.624
79.6	0.1000	0.0820	11.389	11.996	18.126	18.733	18.430	0.8710	0.1046	110.442	11.143	60.792	25.799
99.6	0.1030	0.0850	11.730	12.435	18.468	19.172	18.820	0.9110	1.0980	115.514	116.970	116.242	25.311
119.7	0.1070	0.0880	12.186	12.874	18.923	19.611	19.267	0.9350	1.1290	118.557	120.272	119.415	25.009
139.7	0.1100	0.0910	12.527	13.313	19.265	20.050	19.657	0.9510	1.1490	120.586	122.403	121.494	24.881
159.8	0.1090	0.0890	12.414	13.020	19.151	19.757	19.454	0.9530	1.1510	120.839	122.616	121.728	24.762
179.8	0.1130	0.0920	12.869	13.459	19.607	20.196	19.901	0.9450	1.1390	119.825	121.338	120.581	24.613
199.8	0.1110	0.0910	12.641	13.313	19.379	20.050	19.714	0.9400	1.1300	119.191	120.379	119.785	24.447
219.9	0.1120	0.0920	12.755	13.459	19.493	20.196	19.844	0.9340	1.1280	118.430	120.166	119.298	24.438
239.9	0.1070	0.0870	12.186	12.727	18.923	19.465	19.194	0.9280	1.1170	117.669	118.994	118.332	24.400
259.9	0.1140	0.0930	12.983	13.605	19.720	20.343	20.032	0.9310	1.1230	118.050	119.633	118.842	24.370
280.0	0.1180	0.0970	13.439	14.190	20.176	20.928	20.552	0.9380	1.1310	118.937	120.485	119.711	24.518
300.0	0.1260	0.1020	14.350	14.922	21.087	21.659	21.373	0.9470	1.1410	120.079	121.551	120.815	24.839
320.0	0.117	0.095	13.325	13.898	20.062	20.635	20.349	0.9490	1.1440	120.332	121.870	121.101	25.151
340.1	0.117	0.096	13.325	14.044	20.062	20.782	20.422	0.9450	1.1430	119.825	121.764	120.794	25.160
360.1	0.114	0.093	12.983	13.605	19.720	20.343	20.032	0.9400	1.1310	119.191	120.485	119.838	25.013
380.1	0.11	0.09	12.527	13.166	19.265	19.904	19.584	0.9330	1.1230	118.303	119.633	118.968	24.853
400.2	0.109	0.089	12.414	13.020	19.151	19.757	19.454	0.9280	1.1180	117.669	119.101	118.385	24.856

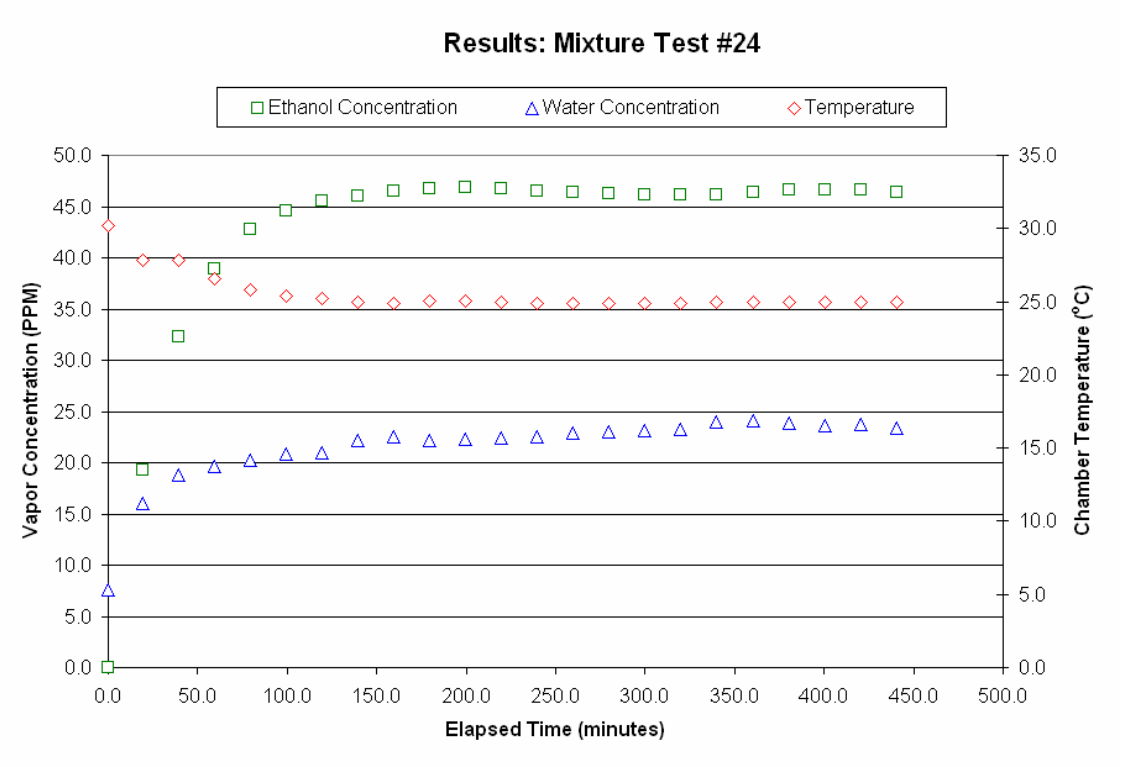

Figure 53: Concentration and Temperature Profile Data of Mixture Test #24

TEST24: 05-18-06

Mix, de-gassed
run continuous
500drop/sec

AMBIENT PPM
g/kg = 6.28
kg/m^3 = 1.07
PPM = 6.737

Time	Water		Water		Water			Ethanol					Temperature
	Absorbance		Concentration		Concentration			Absorbance		Concentration			
Elapsed (min)	1558.2	1652.7	1558.2	1652.7	1558.2	1652.7	average	2900.6	2987.4	2900.6	2987.4	average	°C
0.0	0.0073	0.0059	0.827	0.857	7.564	7.595	7.579	0.0000	0.0000	0.000	0.000	0.000	30.156
19.5	0.0805	0.0651	9.168	9.524	15.905	16.261	16.083	0.1520	0.1810	19.273	19.282	19.278	27.803
39.6	0.1040	0.0840	11.844	12.289	18.582	19.026	18.804	0.2540	0.3030	32.207	32.279	32.243	27.803
59.7	0.1120	0.0900	12.755	13.166	19.493	19.904	19.698	0.3070	0.3660	38.927	38.990	38.959	26.568
79.7	0.1170	0.0940	13.325	13.752	20.062	20.489	20.276	0.3370	0.4020	42.731	42.825	42.778	25.837
99.7	0.1210	0.0980	13.780	14.337	20.518	21.074	20.796	0.3520	0.4190	44.633	44.636	44.635	25.413
119.7	0.1230	0.0990	14.008	14.483	20.745	21.220	20.983	0.3590	0.4280	45.521	45.595	45.558	25.180
139.8	0.1330	0.1070	15.147	15.653	21.884	22.391	22.137	0.3630	0.4330	46.028	46.127	46.078	25.005
159.8	0.1360	0.1100	15.488	16.092	22.226	22.830	22.528	0.3660	0.4370	46.408	46.554	46.481	24.906
179.8	0.1330	0.1080	15.147	15.800	21.884	22.537	22.211	0.3680	0.4390	46.662	46.767	46.714	25.012
199.9	0.1340	0.1080	15.261	15.800	21.998	22.537	22.268	0.3680	0.4410	46.662	46.980	46.821	25.022
219.9	0.1350	0.1090	15.375	15.946	22.112	22.683	22.398	0.3680	0.4400	46.662	46.873	46.768	24.960
240.0	0.1360	0.1100	15.488	16.092	22.226	22.830	22.528	0.3660	0.4380	46.408	46.660	46.534	24.905
260.0	0.1390	0.1120	15.830	16.385	22.568	23.122	22.845	0.3650	0.4360	46.282	46.447	46.364	24.865
280.0	0.1400	0.1130	15.944	16.531	22.681	23.268	22.975	0.3640	0.4350	46.155	46.341	46.248	24.864
300.1	0.1410	0.1140	16.058	16.677	22.795	23.415	23.105	0.3640	0.4340	46.155	46.234	46.194	24.893
320.1	0.142	0.115	16.172	16.824	22.909	23.561	23.235	0.3630	0.4340	46.028	46.234	46.131	24.901
340.1	0.149	0.12	16.969	17.555	23.706	24.293	23.999	0.3630	0.4340	46.028	46.234	46.131	24.929
360.2	0.15	0.121	17.083	17.701	23.820	24.439	24.130	0.3650	0.4360	46.282	46.447	46.364	24.947
380.2	0.147	0.119	16.741	17.409	23.479	24.146	23.812	0.3670	0.4380	46.535	46.660	46.598	24.947
400.2	0.146	0.117	16.627	17.116	23.365	23.854	23.609	0.3670	0.4380	46.535	46.660	46.598	24.951
420.3	0.146	0.118	16.627	17.263	23.365	24.000	23.682	0.367	0.438	46.535	46.660	46.598	24.941
440.3	0.144	0.116	16.400	16.970	23.137	23.707	23.422	0.365	0.437	46.282	46.554	46.418	24.950

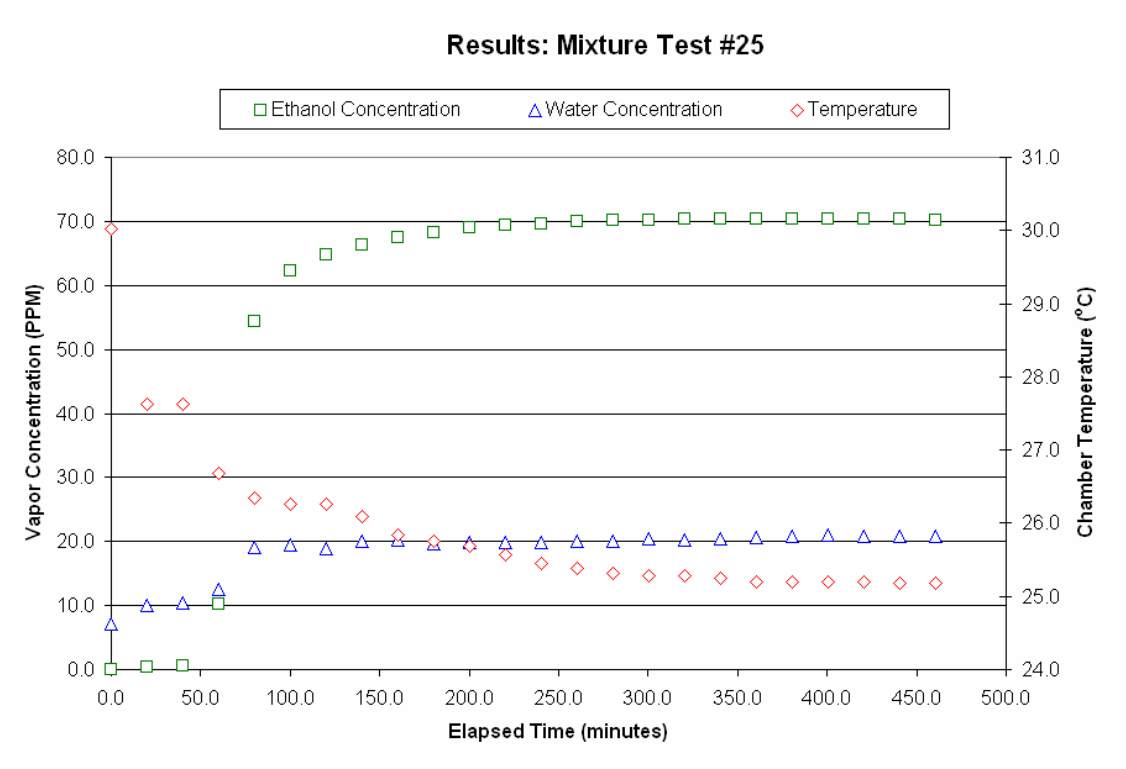

Figure 54: Concentration and Temperature Profile Data of Mixture Test #25

TEST25: 05-19-06

Mix, de-gassed
run continuous
500drop/sec

AMBIENT PPM
g/kg = 5.88
kg/m^3 = 1.07
PPM = 6.312

Time	Water				Water			Ethanol					Temperature
	Absorbance		Concentration		Concentration			Absorbance		Concentration			
Elapsed (min)	1558.2	1652.7	1558.2	1652.7	1558.2	1652.7	average	2900.6	2987.4	2900.6	2987.4	average	°C
0.0	0.0062	0.0051	0.702	0.748	7.013	7.059	7.036	0.0004	0.0000	0.055	0.000	0.027	30.018
20.1	0.0323	0.0260	3.679	3.804	9.990	10.115	10.053	0.0034	0.0042	0.431	0.443	0.437	27.634
40.1	0.0345	0.0279	3.929	4.082	10.241	10.393	10.317	0.0042	0.0051	0.526	0.540	0.533	27.634
60.1	0.0539	0.0435	6.138	6.364	12.450	12.676	12.563	0.0807	0.0964	10.233	10.269	10.251	26.690
80.2	0.1100	0.0890	12.527	13.020	18.839	19.332	19.086	0.4280	0.5100	54.270	54.330	54.300	26.342
100.2	0.1130	0.0920	12.869	13.459	19.181	19.771	19.476	0.4900	0.5850	62.132	62.320	62.226	26.258
120.5	0.1080	0.0870	12.300	12.727	18.611	19.039	18.825	0.5100	0.6090	64.667	64.877	64.772	26.266
140.5	0.1190	0.0960	13.552	14.044	19.864	20.356	20.110	0.5220	0.6240	66.189	66.475	66.332	26.090
160.3	0.1210	0.0970	13.780	14.190	20.092	20.502	20.297	0.5310	0.6350	67.330	67.647	67.488	25.837
180.3	0.1160	0.0930	13.211	13.605	19.523	19.917	19.720	0.5370	0.6430	68.091	68.499	68.295	25.759
200.4	0.1160	0.0940	13.211	13.752	19.523	20.063	19.793	0.5420	0.6490	68.725	69.138	68.932	25.691
220.4	0.1160	0.0940	13.211	13.752	19.523	20.063	19.793	0.5460	0.6530	69.232	69.564	69.398	25.561
240.5	0.1160	0.0940	13.211	13.752	19.523	20.063	19.793	0.5490	0.6540	69.613	69.671	69.642	25.445
260.5	0.1180	0.0950	13.439	13.898	19.750	20.210	19.980	0.5510	0.6570	69.866	69.990	69.928	25.382
280.5	0.1180	0.0960	13.439	14.044	19.750	20.356	20.053	0.5520	0.6590	69.993	70.203	70.098	25.315
300.6	0.1210	0.0980	13.780	14.337	20.092	20.648	20.370	0.5530	0.6600	70.120	70.310	70.215	25.279
320.6	0.12	0.097	13.666	14.190	19.978	20.502	20.240	0.5540	0.6610	70.247	70.416	70.331	25.278
340.7	0.121	0.098	13.780	14.337	20.092	20.648	20.370	0.5550	0.6620	70.373	70.523	70.448	25.245
360.7	0.123	0.1	14.008	14.629	20.320	20.941	20.630	0.5540	0.6620	70.247	70.523	70.385	25.189
380.8	0.125	0.101	14.236	14.776	20.548	21.087	20.817	0.5550	0.6620	70.373	70.523	70.448	25.198
400.8	0.126	0.102	14.350	14.922	20.661	21.234	20.948	0.5550	0.6610	70.373	70.416	70.395	25.195
420.8	0.125	0.101	14.236	14.776	20.548	21.087	20.817	0.555	0.66	70.373	70.310	70.342	25.190
440.9	0.125	0.101	14.236	14.776	20.548	21.087	20.817	0.554	0.66	70.247	70.310	70.278	25.185
460.9	0.125	0.101	14.236	14.776	20.548	21.087	20.817	0.553	0.659	70.120	70.203	70.162	25.185

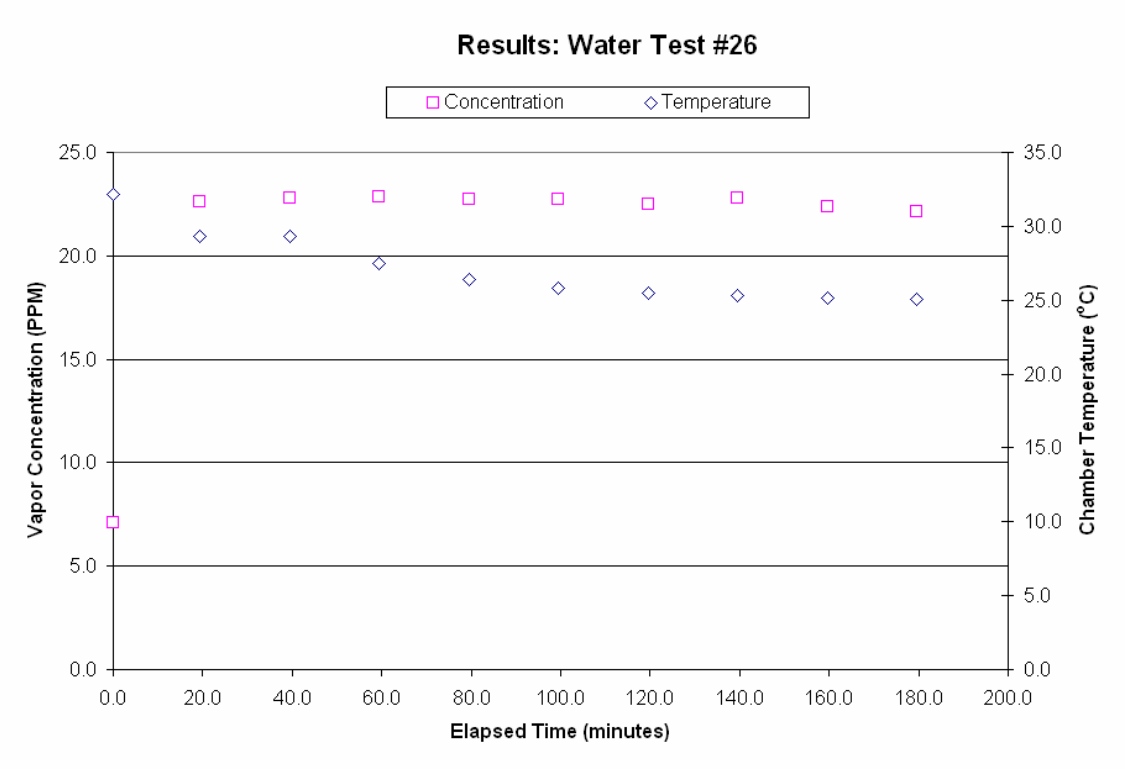

Figure 55: Concentration and Temperature Profile Data of Water Test #26

TEST26: 05-23-06

Water, de-gassed
run continuous
1000drop/sec

AMBIENT PPM
g/kg = 6.43
kg/m^3 = 1.08
PPM = 6.946

Time	Absorbance		Concentration		Temperature	Concentration		
Elapsed (min)	*1558.2*	*1652.7*	*1558.2*	*1652.7*	°C	*1558.2*	*1652.7*	*average*
0.0	0.0014	0.0010	0.161	0.149	32.170	7.106	7.095	7.101
19.4	0.1360	0.1080	15.488	15.800	29.359	22.434	22.745	22.590
39.4	0.1380	0.1090	15.716	15.946	29.359	22.662	22.892	22.777
59.5	0.1380	0.1100	15.716	16.092	27.452	22.662	23.038	22.850
79.5	0.1370	0.1090	15.602	15.946	26.432	22.548	22.892	22.720
99.5	0.1370	0.1090	15.602	15.946	25.836	22.548	22.892	22.720
119.6	0.1340	0.1080	15.261	15.800	25.494	22.206	22.745	22.476
139.6	0.1370	0.1100	15.602	16.092	25.294	22.548	23.038	22.793
159.6	0.1330	0.1070	15.147	15.653	25.119	22.093	22.599	22.346
179.7	0.1310	0.1060	14.919	15.507	25.024	21.865	22.453	22.159

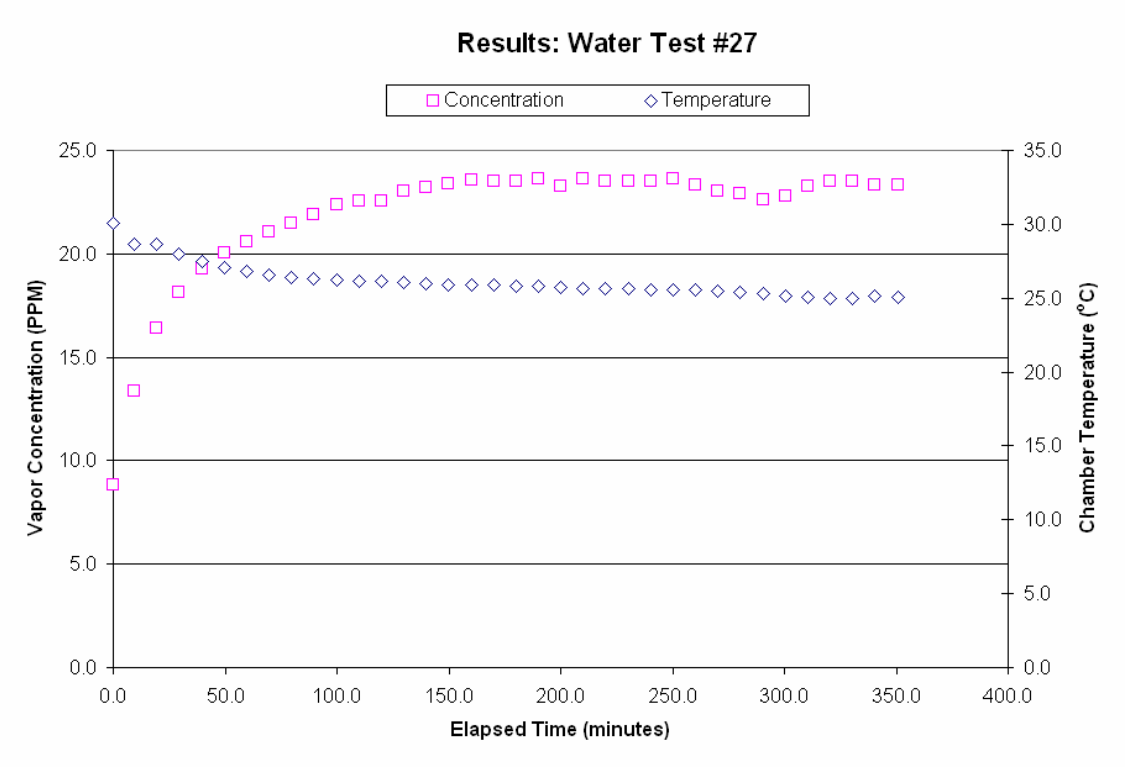

Figure 56: Concentration and Temperature Profile Data of Water Test #27

TEST27: 05-24-06

Water, de-gassed
run continuous
300drop/sec

AMBIENT PPM
g/kg = 8.19
kg/m^3 = 1.08
PPM = 8.827

Time	Absorbance		Concentration		Temperature	Concentration		
Elapsed (min)	1558.2	1652.7	1558.2	1652.7	°C	1558.2	1652.7	average
0.0	0.0000	0.0000	0.000	0.000	30.093	8.827	8.827	8.827
9.5	0.0394	0.0316	4.487	4.623	28.637	13.314	13.449	13.382
19.5	0.0660	0.0520	7.516	7.607	28.637	16.343	16.434	16.388
29.5	0.0810	0.0640	9.225	9.363	27.970	18.051	18.189	18.120
39.6	0.0910	0.0720	10.364	10.533	27.455	19.190	19.360	19.275
49.6	0.0980	0.0770	11.161	11.265	27.078	19.987	20.091	20.039
59.6	0.1020	0.0810	11.616	11.850	26.780	20.443	20.676	20.560
69.7	0.1070	0.0840	12.186	12.289	26.535	21.012	21.115	21.064
79.7	0.1100	0.0870	12.527	12.727	26.396	21.354	21.554	21.454
89.7	0.1140	0.0900	12.983	13.166	26.274	21.810	21.993	21.901
99.8	0.1180	0.0930	13.439	13.605	26.212	22.265	22.432	22.348
109.8	0.1200	0.0940	13.666	13.752	26.186	22.493	22.578	22.536
119.8	0.1200	0.0940	13.666	13.752	26.115	22.493	22.578	22.536
129.9	0.1240	0.0980	14.122	14.337	26.036	22.948	23.163	23.056
139.9	0.1250	0.0990	14.236	14.483	25.991	23.062	23.310	23.186
149.9	0.1270	0.1000	14.464	14.629	25.934	23.290	23.456	23.373
160.0	0.1290	0.1010	14.691	14.776	25.909	23.518	23.602	23.560
170.0	0.1280	0.1010	14.577	14.776	25.860	23.404	23.602	23.503
180.0	0.1280	0.1010	14.577	14.776	25.810	23.404	23.602	23.503
190.1	0.1290	0.1020	14.691	14.922	25.790	23.518	23.748	23.633
200.1	0.1260	0.0990	14.350	14.483	25.755	23.176	23.310	23.243
210.1	0.1290	0.1020	14.691	14.922	25.678	23.518	23.748	23.633
220.2	0.1280	0.1010	14.577	14.776	25.636	23.404	23.602	23.503
230.2	0.1280	0.1010	14.577	14.776	25.607	23.404	23.602	23.503
240.2	0.1280	0.1010	14.577	14.776	25.596	23.404	23.602	23.503
250.3	0.1290	0.1020	14.691	14.922	25.575	23.518	23.748	23.633
260.3	0.1260	0.1000	14.350	14.629	25.562	23.176	23.456	23.316
270.3	0.1240	0.0980	14.122	14.337	25.514	22.948	23.163	23.056
280.4	0.1230	0.0970	14.008	14.190	25.408	22.835	23.017	22.926
290.4	0.1200	0.0950	13.666	13.898	25.286	22.493	22.724	22.609
300.4	0.1220	0.0960	13.894	14.044	25.158	22.721	22.871	22.796
310.5	0.1260	0.0990	14.350	14.483	25.059	23.176	23.310	23.243
320.5	0.1280	0.1010	14.577	14.776	24.983	23.404	23.602	23.503
330.5	0.1280	0.1010	14.577	14.776	24.952	23.404	23.602	23.503
340.6	0.1260	0.1000	14.350	14.629	25.144	23.176	23.456	23.316
350.6	0.1260	0.1000	14.350	14.629	25.044	23.176	23.456	23.316

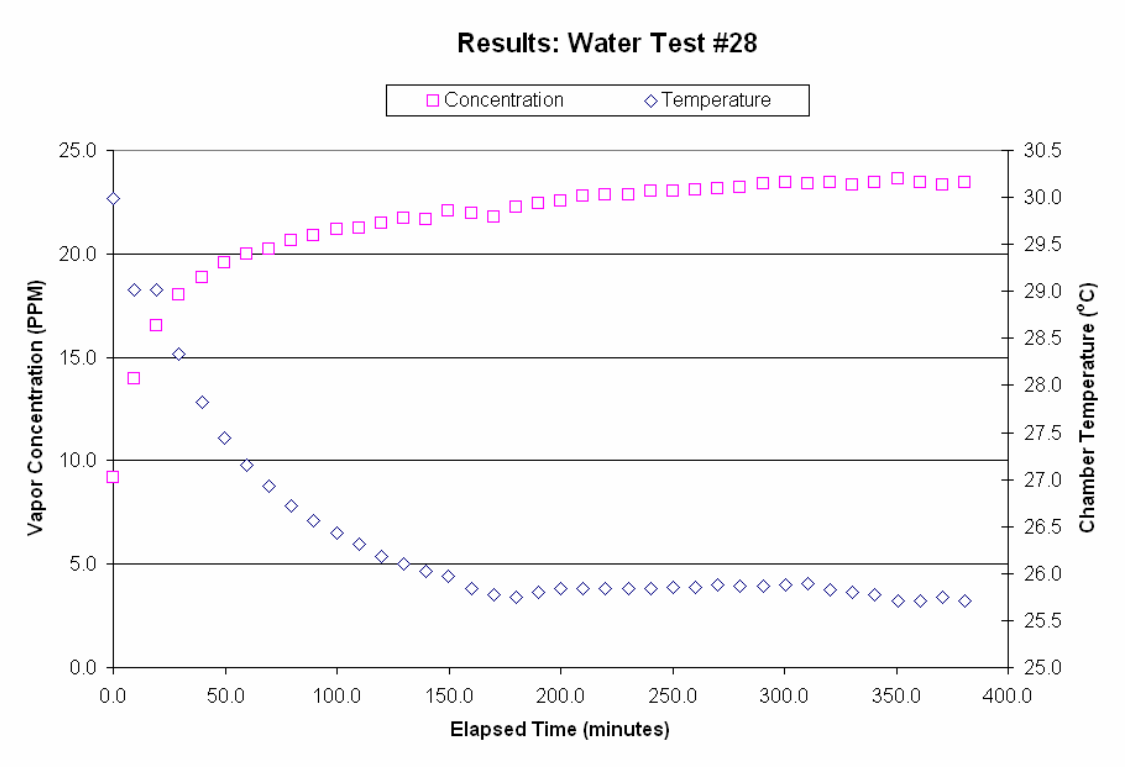

Figure 57: Concentration and Temperature Profile Data of Water Test #28

TEST28: 05-25-06

Water, de-gassed
run continuous
300drop/sec

AMBIENT PPM
g/kg = 8.37
kg/m^3 = 1.07
PPM = 8.988

Time	Absorbance		Concentration		Temperature	Concentration		
Elapsed (min)	1658.2	1652.7	1658.2	1652.7	°C	1658.2	1652.7	average
0.0	0.0017	0.0014	0.191	0.208	29.991	9.179	9.195	9.187
9.5	0.0432	0.0343	4.920	5.018	29.018	13.907	14.005	13.956
19.5	0.0660	0.0520	7.516	7.607	29.018	16.504	16.595	16.549
29.5	0.0790	0.0620	8.997	9.070	28.336	17.985	18.058	18.021
39.5	0.0860	0.0680	9.794	9.948	27.828	18.782	18.935	18.859
49.6	0.0920	0.0730	10.478	10.679	27.439	19.465	19.667	19.566
59.6	0.0960	0.0760	10.933	11.118	27.154	19.921	20.106	20.013
69.7	0.0980	0.0770	11.161	11.265	26.933	20.148	20.252	20.200
79.7	0.1020	0.0800	11.616	11.703	26.720	20.604	20.691	20.647
89.7	0.1040	0.0820	11.844	11.996	26.562	20.832	20.984	20.908
99.8	0.1060	0.0840	12.072	12.289	26.425	21.059	21.276	21.168
109.8	0.1070	0.0840	12.186	12.289	26.309	21.173	21.276	21.225
119.8	0.1090	0.0860	12.414	12.581	26.188	21.401	21.569	21.485
129.9	0.1110	0.0880	12.641	12.874	26.098	21.629	21.861	21.745
139.9	0.1110	0.0870	12.641	12.727	26.028	21.629	21.715	21.672
149.9	0.1140	0.0900	12.983	13.166	25.967	21.971	22.154	22.062
160.0	0.1130	0.0890	12.869	13.020	25.840	21.857	22.008	21.932
170.0	0.1120	0.0880	12.755	12.874	25.777	21.743	21.861	21.802
180.0	0.1160	0.0910	13.211	13.313	25.749	22.198	22.300	22.249
190.1	0.1170	0.0930	13.325	13.605	25.805	22.312	22.593	22.452
200.1	0.1180	0.0940	13.439	13.752	25.840	22.426	22.739	22.583
210.1	0.1200	0.0950	13.666	13.898	25.837	22.654	22.885	22.770
220.2	0.1210	0.0950	13.780	13.898	25.840	22.768	22.885	22.827
230.2	0.1210	0.0950	13.780	13.898	25.841	22.768	22.885	22.827
240.2	0.1220	0.0970	13.894	14.190	25.844	22.882	23.178	23.030
250.3	0.1220	0.0970	13.894	14.190	25.858	22.882	23.178	23.030
260.3	0.1230	0.0970	14.008	14.190	25.860	22.996	23.178	23.087
270.3	0.1230	0.0980	14.008	14.337	25.877	22.996	23.324	23.160
280.4	0.1240	0.0980	14.122	14.337	25.872	23.109	23.324	23.217
290.4	0.1260	0.0990	14.350	14.483	25.864	23.337	23.471	23.404
300.4	0.1260	0.1000	14.350	14.629	25.885	23.337	23.617	23.477
310.5	0.1260	0.0990	14.350	14.483	25.888	23.337	23.471	23.404
320.5	0.1260	0.1000	14.350	14.629	25.821	23.337	23.617	23.477
330.5	0.1250	0.0990	14.236	14.483	25.806	23.223	23.471	23.347
340.6	0.1260	0.1000	14.350	14.629	25.773	23.337	23.617	23.477
350.6	0.1270	0.1010	14.464	14.776	25.715	23.451	23.763	23.607
360.6	0.1260	0.1000	14.350	14.629	25.709	23.337	23.617	23.477
370.7	0.1250	0.0990	14.236	14.483	25.752	23.223	23.471	23.347
380.7	0.1260	0.1000	14.350	14.629	25.714	23.337	23.617	23.477

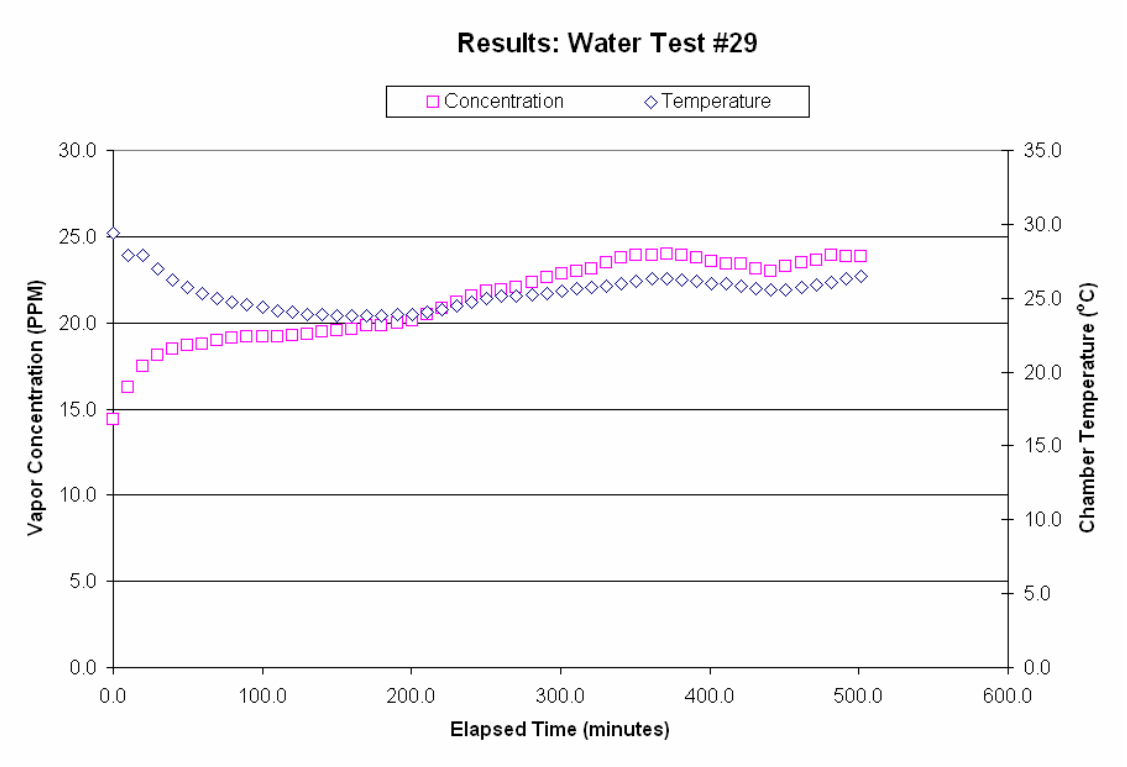

Figure 58: Concentration and Temperature Profile Data of Water Test #29

TEST29: 05-25-06

Water, de-gassed
run continuous
100drop/sec

AMBIENT PPM
g/kg = 6.88
kg/m^3 = 1.08
PPM = 7.449

Time	Absorbance		Concentration		Temperature	Concentration		
Elapsed (min)	1558.2	1652.7	1558.2	1652.7	°C	1558.2	1652.7	average
0.0	0.0009	0.0007	0.099	0.101	29.438	14.398	14.400	14.399
9.6	0.0172	0.0135	1.959	1.975	27.874	16.258	16.274	16.266
19.7	0.0274	0.0216	3.120	3.160	27.874	17.420	17.459	17.439
29.7	0.0335	0.0264	3.815	3.862	26.944	18.114	18.161	18.138
39.7	0.0362	0.0286	4.123	4.184	26.259	18.422	18.483	18.453
49.7	0.0379	0.0300	4.316	4.389	25.714	18.616	18.688	18.652
59.8	0.0390	0.0310	4.442	4.535	25.311	18.741	18.834	18.788
69.8	0.0405	0.0321	4.612	4.696	24.989	18.912	18.995	18.953
79.9	0.0418	0.0334	4.760	4.886	24.732	19.060	19.185	19.123
89.9	0.0427	0.0340	4.863	4.974	24.532	19.162	19.273	19.218
99.9	0.0425	0.0338	4.840	4.945	24.350	19.139	19.244	19.192
109.9	0.0426	0.0341	4.852	4.989	24.181	19.151	19.288	19.219
120.0	0.0431	0.0343	4.908	5.018	24.024	19.208	19.317	19.262
130.0	0.0440	0.0350	5.011	5.120	23.923	19.310	19.420	19.365
140.1	0.0448	0.0354	5.102	5.179	23.855	19.401	19.478	19.440
150.1	0.0456	0.0362	5.193	5.296	23.828	19.492	19.595	19.544
160.1	0.0464	0.0368	5.284	5.384	23.804	19.584	19.683	19.633
170.2	0.0479	0.0379	5.455	5.544	23.799	19.754	19.844	19.799
180.2	0.0483	0.0383	5.501	5.603	23.837	19.800	19.902	19.851
190.2	0.0495	0.0393	5.637	5.749	23.876	19.937	20.049	19.993
200.3	0.0507	0.0402	5.774	5.881	23.916	20.073	20.180	20.127
210.3	0.0537	0.0424	6.116	6.203	24.030	20.415	20.502	20.459
220.3	0.0567	0.0449	6.457	6.569	24.222	20.757	20.868	20.812
230.4	0.0599	0.0474	6.822	6.934	24.461	21.121	21.234	21.177
240.4	0.0629	0.0498	7.163	7.285	24.705	21.463	21.585	21.524
250.4	0.0657	0.0520	7.482	7.607	24.956	21.782	21.906	21.844
260.5	0.0662	0.0524	7.539	7.666	25.104	21.839	21.965	21.902
270.5	0.0676	0.0534	7.699	7.812	25.168	21.998	22.111	22.055
280.6	0.0700	0.0552	7.972	8.075	25.199	22.271	22.375	22.323
290.6	0.0724	0.0573	8.245	8.383	25.342	22.545	22.682	22.613
300.7	0.0743	0.0587	8.462	8.587	25.509	22.761	22.887	22.824
310.7	0.0757	0.0598	8.621	8.748	25.670	22.920	23.048	22.984
320.8	0.0768	0.0607	8.746	8.880	25.723	23.046	23.179	23.112
330.8	0.0801	0.0632	9.122	9.246	25.798	23.422	23.545	23.483
340.8	0.0830	0.0653	9.453	9.553	25.969	23.752	23.852	23.802
350.9	0.0839	0.0662	9.555	9.685	26.168	23.854	23.984	23.919
360.9	0.0838	0.0662	9.544	9.685	26.313	23.843	23.984	23.913
371.0	0.0844	0.0666	9.612	9.743	26.293	23.911	24.042	23.977
381.0	0.0838	0.0663	9.544	9.699	26.215	23.843	23.998	23.921
391.0	0.0825	0.0654	9.396	9.568	26.147	23.695	23.867	23.781
401.1	0.0806	0.0637	9.179	9.319	26.009	23.478	23.618	23.548
411.1	0.0791	0.0630	9.008	9.216	25.947	23.308	23.516	23.412
421.2	0.0791	0.0627	9.008	9.173	25.807	23.308	23.472	23.390
431.2	0.0767	0.0606	8.735	8.865	25.635	23.034	23.165	23.099
441.2	0.0755	0.0596	8.598	8.719	25.565	22.898	23.018	22.958
451.2	0.0777	0.0619	8.849	9.056	25.557	23.148	23.355	23.251
461.3	0.0797	0.0633	9.077	9.260	25.703	23.376	23.560	23.468
471.3	0.0807	0.0643	9.191	9.407	25.881	23.490	23.706	23.598
481.3	0.0835	0.0664	9.509	9.714	26.089	23.809	24.013	23.911
491.4	0.0832	0.0656	9.475	9.597	26.283	23.775	23.896	23.835
501.4	0.0828	0.0656	9.430	9.597	26.478	23.729	23.896	23.813

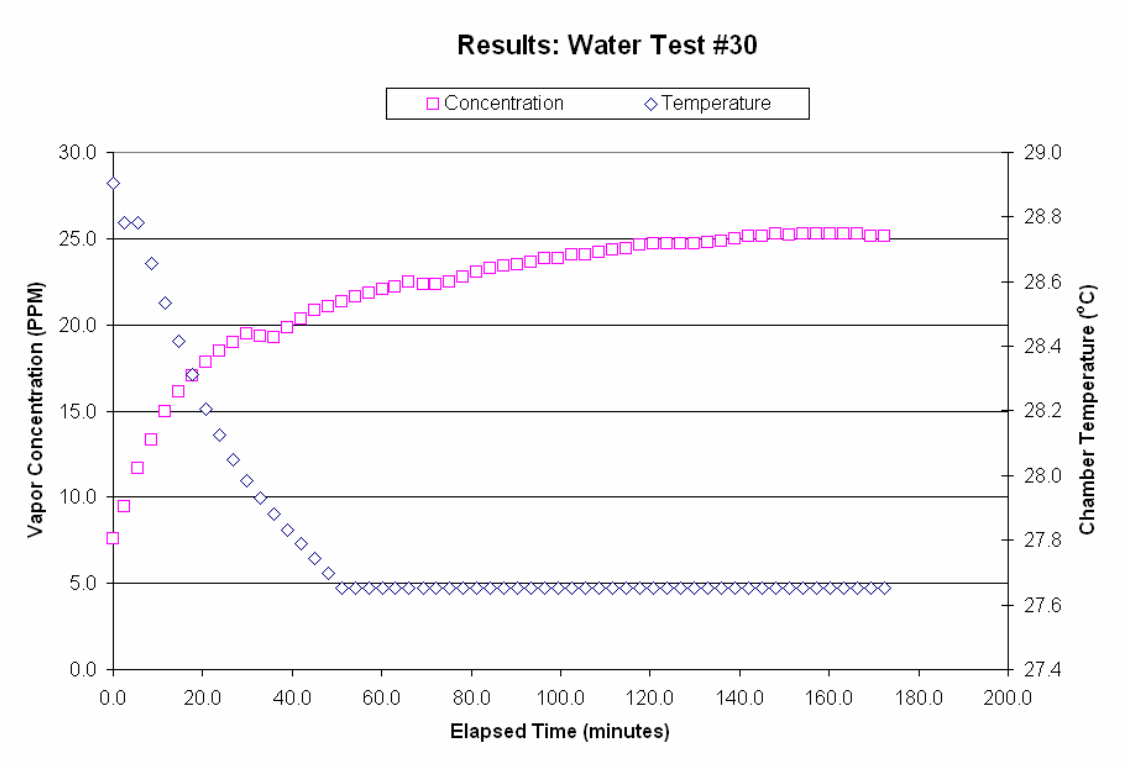

Figure 59: Concentration and Temperature Profile Data of Water Test #30

TEST30: 05-26-06

Water, de-gassed
run continuous
300drop/sec

AMBIENT PPM
g/kg = 6.87
kg/m^3 = 1.06
PPM = 7.310

Time	Absorbance		Concentration		Temperature	Concentration		
Elapsed (min)	*1558.2*	*1652.7*	*1558.2*	*1652.7*	°C	*1558.2*	*1652.7*	*average*
0.0	0.0022	0.0018	0.251	0.263	28.906	7.560	7.573	7.567
2.4	0.0187	0.0147	2.130	2.151	28.781	9.439	9.460	9.450
5.5	0.0383	0.0302	4.362	4.418	28.781	11.672	11.728	11.700
8.5	0.0523	0.0413	5.956	6.042	28.657	13.266	13.352	13.309
11.6	0.0666	0.0525	7.585	7.680	28.536	14.895	14.990	14.942
14.6	0.0768	0.0606	8.746	8.865	28.415	16.056	16.175	16.116
17.6	0.0851	0.0670	9.692	9.802	28.313	17.001	17.111	17.056
20.7	0.0920	0.0724	10.478	10.592	28.204	17.787	17.901	17.844
23.7	0.0975	0.0768	11.104	11.235	28.125	18.414	18.545	18.479
26.7	0.1020	0.0800	11.616	11.703	28.051	18.926	19.013	18.970
29.8	0.1060	0.0840	12.072	12.289	27.984	19.382	19.598	19.490
32.8	0.1050	0.0830	11.958	12.142	27.932	19.268	19.452	19.360
35.8	0.1040	0.0820	11.844	11.996	27.880	19.154	19.306	19.230
38.8	0.1100	0.0860	12.527	12.581	27.831	19.837	19.891	19.864
41.9	0.1140	0.0890	12.983	13.020	27.791	20.293	20.330	20.311
44.9	0.1180	0.0930	13.439	13.605	27.745	20.748	20.915	20.832
48.0	0.1200	0.0940	13.666	13.752	27.696	20.976	21.061	21.019
51.0	0.1230	0.0960	14.008	14.044	27.654	21.318	21.354	21.336
54.0	0.1250	0.0980	14.236	14.337	27.654	21.545	21.646	21.596
57.1	0.1270	0.1000	14.464	14.629	27.654	21.773	21.939	21.856
60.1	0.1290	0.1010	14.691	14.776	27.654	22.001	22.085	22.043
63.1	0.1310	0.1020	14.919	14.922	27.654	22.229	22.232	22.230
66.1	0.1330	0.1040	15.147	15.214	27.654	22.457	22.524	22.490
69.2	0.1320	0.1030	15.033	15.068	27.654	22.343	22.378	22.360
72.2	0.1310	0.1030	14.919	15.068	27.654	22.229	22.378	22.303
75.3	0.1330	0.1040	15.147	15.214	27.654	22.457	22.524	22.490
78.3	0.1350	0.1060	15.375	15.507	27.654	22.684	22.817	22.751
81.3	0.1380	0.1080	15.716	15.800	27.654	23.026	23.109	23.068
84.4	0.1400	0.1090	15.944	15.946	27.654	23.254	23.256	23.255
87.4	0.1410	0.1100	16.058	16.092	27.654	23.368	23.402	23.385
90.4	0.1420	0.1110	16.172	16.238	27.654	23.482	23.548	23.515
93.5	0.1430	0.1120	16.286	16.385	27.654	23.595	23.694	23.645
96.5	0.1450	0.1130	16.513	16.531	27.654	23.823	23.841	23.832
99.6	0.1450	0.1130	16.513	16.531	27.654	23.823	23.841	23.832
102.6	0.1470	0.1150	16.741	16.824	27.654	24.051	24.133	24.092
105.6	0.1470	0.1150	16.741	16.824	27.654	24.051	24.133	24.092
108.7	0.1480	0.1160	16.855	16.970	27.654	24.165	24.280	24.222
111.7	0.1490	0.1170	16.969	17.116	27.654	24.279	24.426	24.352
114.7	0.1500	0.1170	17.083	17.116	27.654	24.393	24.426	24.409
117.7	0.1510	0.1190	17.197	17.409	27.654	24.506	24.719	24.613
120.8	0.1520	0.1190	17.311	17.409	27.654	24.620	24.719	24.669
123.8	0.1520	0.1190	17.311	17.409	27.654	24.620	24.719	24.669
126.9	0.1520	0.1190	17.311	17.409	27.654	24.620	24.719	24.669
129.9	0.1520	0.1190	17.311	17.409	27.654	24.620	24.719	24.669
132.9	0.1530	0.1200	17.425	17.555	27.654	24.734	24.865	24.800
135.9	0.1540	0.1200	17.538	17.555	27.654	24.848	24.865	24.856
139.0	0.1550	0.1210	17.652	17.701	27.654	24.962	25.011	24.987
142.0	0.1560	0.1220	17.766	17.848	27.654	25.076	25.157	25.117
145.1	0.1560	0.1220	17.766	17.848	27.654	25.076	25.157	25.117
148.1	0.1570	0.1230	17.880	17.994	27.654	25.190	25.304	25.247
151.1	0.1570	0.1220	17.880	17.848	27.654	25.190	25.157	25.174
154.1	0.1570	0.1230	17.880	17.994	27.654	25.190	25.304	25.247
157.2	0.1570	0.1230	17.880	17.994	27.654	25.190	25.304	25.247
160.2	0.1570	0.1230	17.880	17.994	27.654	25.190	25.304	25.247
163.3	0.1580	0.1230	17.994	17.994	27.654	25.304	25.304	25.304
166.3	0.1570	0.1230	17.880	17.994	27.654	25.190	25.304	25.247
169.3	0.1560	0.1220	17.766	17.848	27.654	25.076	25.157	25.117
172.4	0.1560	0.1220	17.766	17.848	27.654	25.076	25.157	25.117

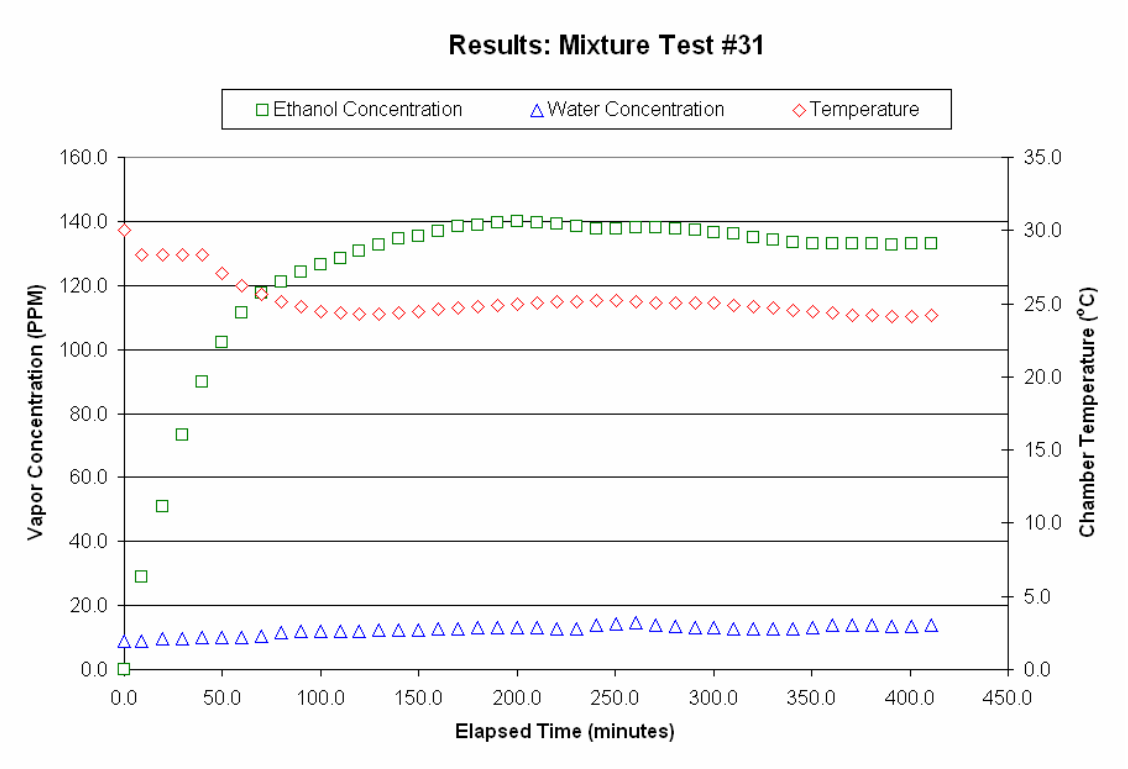

Figure 60: Concentration and Temperature Profile Data of Mixture Test #31

TEST31: 06-02-06

Mix, de-gassed
run continuous
300drop/sec

AMBIENT PPM
g/kg = 8.00
kg/m³ = 1.08
PPM = 8.649

Time	Water				Water			Ethanol					Temperature
	Absorbance		Concentration		Concentration			Absorbance		Concentration			
Elapsed (min)	1568.2	1652.7	1568.2	1652.7	1568.2	1652.7	average	2900.6	2987.4	2900.6	2987.4	average	°C
0.0	0.0034	0.0027	0.387	0.394	9.036	9.042	9.039	0.0000	0.0000	0.000	0.000	0.000	30.006
8.7	0.0017	0.0016	0.198	0.226	8.847	8.877	8.862	0.2290	0.2720	29.037	28.976	29.007	28.349
19.6	0.0067	0.0068	0.768	0.844	9.416	9.493	9.455	0.4020	0.4790	50.973	51.028	51.001	28.349
29.6	0.0085	0.0072	0.968	1.053	9.617	9.702	9.659	0.5770	0.6890	73.163	73.399	73.281	28.349
39.6	0.0107	0.0094	1.219	1.375	9.867	10.024	9.946	0.7080	0.8460	89.774	90.124	89.949	28.349
49.7	0.0116	0.0100	1.321	1.463	9.970	10.112	10.041	0.8040	0.9620	101.946	102.482	102.214	27.036
59.7	0.0118	0.0104	1.344	1.521	9.993	10.170	10.081	0.8750	1.0470	110.949	111.537	111.243	26.255
69.7	0.0134	0.0118	1.526	1.726	10.175	10.375	10.275	0.9230	1.1080	117.035	118.035	117.535	25.616
79.8	0.0240	0.0199	2.733	2.911	11.382	11.560	11.471	0.9550	1.1380	121.093	121.231	121.162	25.146
89.8	0.0275	0.0228	3.132	3.335	11.781	11.984	11.882	0.9790	1.1670	124.136	124.321	124.228	24.771
99.8	0.0272	0.0225	3.098	3.292	11.746	11.940	11.843	0.9970	1.1880	126.419	126.558	126.488	24.487
109.9	0.0267	0.0222	3.041	3.248	11.689	11.896	11.793	1.0120	1.2080	128.321	128.688	128.504	24.335
119.9	0.0283	0.0234	3.223	3.423	11.872	12.072	11.972	1.0280	1.2290	130.349	130.925	130.637	24.299
129.9	0.0302	0.0250	3.439	3.657	12.088	12.306	12.197	1.0450	1.2490	132.505	133.056	132.780	24.323
140.0	0.0315	0.0260	3.587	3.804	12.236	12.452	12.344	1.0580	1.2660	134.153	134.867	134.510	24.385
150.0	0.0326	0.0270	3.713	3.950	12.361	12.599	12.480	1.0670	1.2740	135.295	135.719	135.507	24.482
160.0	0.0343	0.0283	3.906	4.140	12.555	12.789	12.672	1.0760	1.2870	136.436	137.104	136.770	24.608
170.1	0.035	0.0286	3.986	4.184	12.635	12.833	12.734	1.0870	1.3020	137.831	138.702	138.266	24.699
180.1	0.0368	0.0301	4.191	4.403	12.840	13.052	12.946	1.0920	1.3030	138.465	138.809	138.637	24.783
190.1	0.0388	0.0319	4.419	4.667	13.067	13.315	13.191	1.0990	1.3100	139.352	139.554	139.453	24.881
200.2	0.0397	0.0326	4.521	4.769	13.170	13.418	13.294	1.1020	1.3180	139.732	140.407	140.070	24.945
210.2	0.0396	0.0324	4.510	4.740	13.159	13.389	13.274	1.098	1.312	139.225	139.767	139.496	25.017
220.2	0.0357	0.0296	4.066	4.330	12.714	12.979	12.847	1.095	1.311	138.845	139.661	139.253	25.123
230.3	0.0333	0.0274	3.792	4.008	12.441	12.657	12.549	1.091	1.302	138.338	138.702	138.520	25.171
240.3	0.0474	0.0334	5.398	4.886	14.047	13.535	13.791	1.086	1.293	137.704	137.743	137.724	25.218
250.3	0.0507	0.0392	5.774	5.735	14.423	14.383	14.403	1.083	1.298	137.323	138.276	137.800	25.205
260.4	0.0508	0.0409	5.785	5.983	14.434	14.632	14.533	1.085	1.301	137.577	138.596	138.086	25.102
270.4	0.0438	0.0356	4.988	5.208	13.637	13.857	13.747	1.084	1.298	137.450	138.276	137.863	25.060
280.4	0.0408	0.0335	4.647	4.901	13.295	13.550	13.422	1.082	1.294	137.197	137.850	137.523	25.064
290.5	0.0392	0.0319	4.464	4.667	13.113	13.315	13.214	1.078	1.292	136.689	137.637	137.163	25.049
300.5	0.0387	0.0317	4.407	4.637	13.056	13.286	13.171	1.072	1.283	135.929	136.678	136.303	25.012
310.6	0.0337	0.0294	3.838	4.301	12.487	12.950	12.718	1.07	1.285	135.675	136.891	136.283	24.919
320.6	0.0358	0.0293	4.077	4.286	12.726	12.935	12.830	1.061	1.271	134.534	135.400	134.967	24.814
330.6	0.0357	0.0292	4.066	4.272	12.714	12.920	12.817	1.054	1.264	133.646	134.654	134.150	24.704
340.7	0.0343	0.0284	3.906	4.155	12.555	12.803	12.679	1.049	1.257	133.012	133.908	133.460	24.582
350.7	0.0395	0.0322	4.498	4.711	13.147	13.359	13.253	1.044	1.252	132.378	133.376	132.877	24.474
360.8	0.0453	0.0371	5.159	5.427	13.808	14.076	13.942	1.044	1.253	132.378	133.482	132.930	24.352
370.8	0.0439	0.036	5.000	5.267	13.648	13.915	13.782	1.043	1.253	132.251	133.482	132.867	24.223
380.8	0.0444	0.0363	5.057	5.310	13.705	13.959	13.832	1.044	1.255	132.378	133.695	133.037	24.176
390.9	0.0411	0.0338	4.681	4.945	13.329	13.593	13.461	1.041	1.252	131.998	133.376	132.687	24.148
400.9	0.0428	0.0352	4.874	5.149	13.523	13.798	13.661	1.043	1.256	132.251	133.802	133.027	24.160
410.9	0.0432	0.0354	4.920	5.179	13.569	13.827	13.698	1.042	1.255	132.125	133.695	132.910	24.177

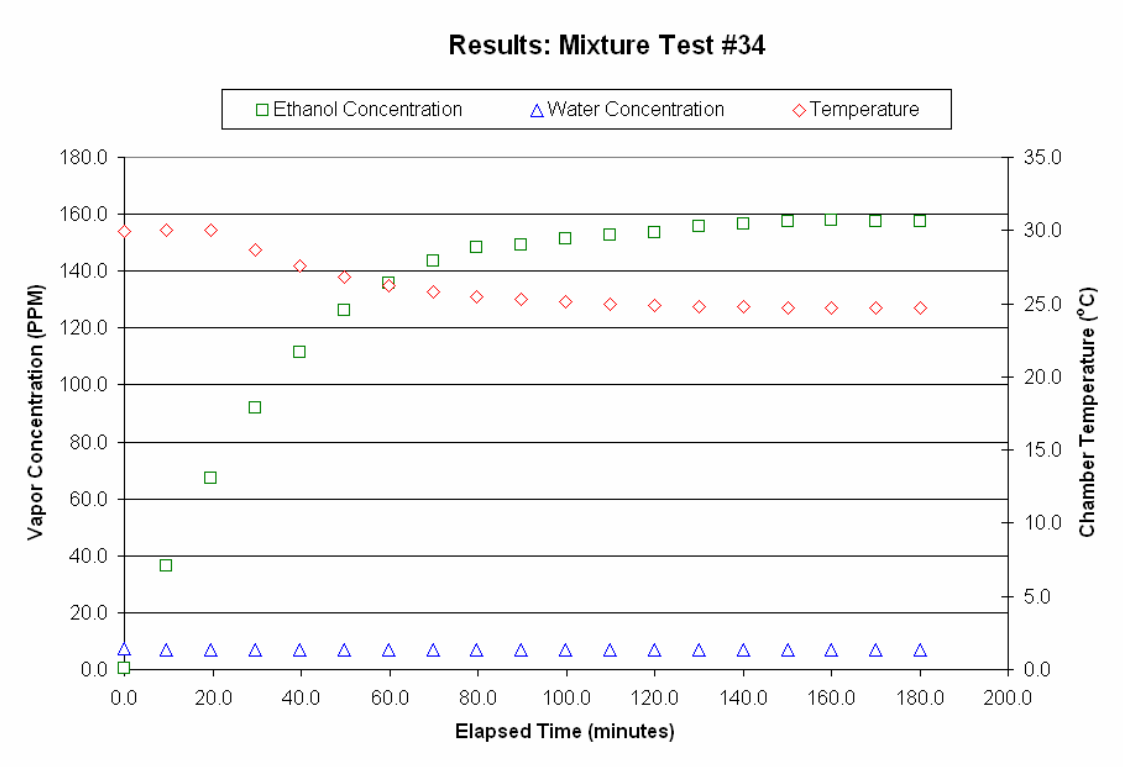

Figure 61: Concentration and Temperature Profile Data of Mixture Test #34

TEST34: 06-15-06

Mix, de-gassed
run continuous
300drop/sec

AMBIENT PPM
g/kg = 6.47
kg/m^3 = 1.08
PPM = 6.999

Time	Water Absorbance		Water Concentration		Water Concentration			Ethanol Absorbance		Ethanol Concentration			Temperature
Elapsed (min)	1558.2	1652.7	1558.2	1652.7	1558.2	1652.7	average	2900.6	2987.4	2900.6	2987.4	average	°C
0.0	0.0023	0.0018	0.261	0.256	7.260	7.255	7.257	0.0024	0.0029	0.308	0.310	0.309	29.969
9.5	0.0000	0.0000	0.000	0.000	6.999	6.999	6.999	0.2870	0.3400	36.391	36.220	36.306	30.029
19.6	0.0000	0.0000	0.000	0.000	6.999	6.999	6.999	0.5310	0.6310	67.330	67.220	67.275	30.029
29.7	0.0000	0.0000	0.000	0.000	6.999	6.999	6.999	0.7250	0.8600	91.929	91.616	91.773	28.634
39.7	0.0000	0.0000	0.000	0.000	6.999	6.999	6.999	0.8800	1.0480	111.583	111.643	111.613	27.575
49.7	0.0000	0.0000	0.000	0.000	6.999	6.999	6.999	0.9940	1.1880	126.038	126.558	126.298	26.817
59.8	0.0000	0.0000	0.000	0.000	6.999	6.999	6.999	1.0710	1.2770	135.802	136.039	135.920	26.225
69.8	0.0000	0.0000	0.000	0.000	6.999	6.999	6.999	1.1290	1.3540	143.156	144.242	143.699	25.795
79.8	0.0000	0.0000	0.000	0.000	6.999	6.999	6.999	1.1660	1.3930	147.848	148.396	148.122	25.478
89.9	0.0000	0.0000	0.000	0.000	6.999	6.999	6.999	1.1770	1.4030	149.242	149.462	149.352	25.274
99.9	0.0000	0.0000	0.000	0.000	6.999	6.999	6.999	1.1930	1.4250	151.271	151.805	151.538	25.104
109.9	0.0000	0.0000	0.000	0.000	6.999	6.999	6.999	1.2020	1.4350	152.412	152.871	152.641	24.981
120.0	0.0000	0.0000	0.000	0.000	6.999	6.999	6.999	1.2160	1.4370	154.188	153.084	153.636	24.881
130.0	0.0000	0.0000	0.000	0.000	6.999	6.999	6.999	1.2220	1.4690	154.948	156.493	155.720	24.827
140.1	0.0000	0.0000	0.000	0.000	6.999	6.999	6.999	1.2290	1.4740	155.836	157.025	156.431	24.776
150.1	0.0000	0.0000	0.000	0.000	6.999	6.999	6.999	1.2370	1.4820	156.850	157.877	157.364	24.751
160.1	0.0000	0.0000	0.000	0.000	6.999	6.999	6.999	1.2360	1.4900	156.724	158.730	157.727	24.726
170.2	0.0000	0.0000	0.000	0.000	6.999	6.999	6.999	1.2360	1.4880	156.724	158.517	157.620	24.707
180.2	0.0000	0.0000	0.000	0.000	6.999	6.999	6.999	1.2360	1.4850	156.724	158.197	157.460	24.705

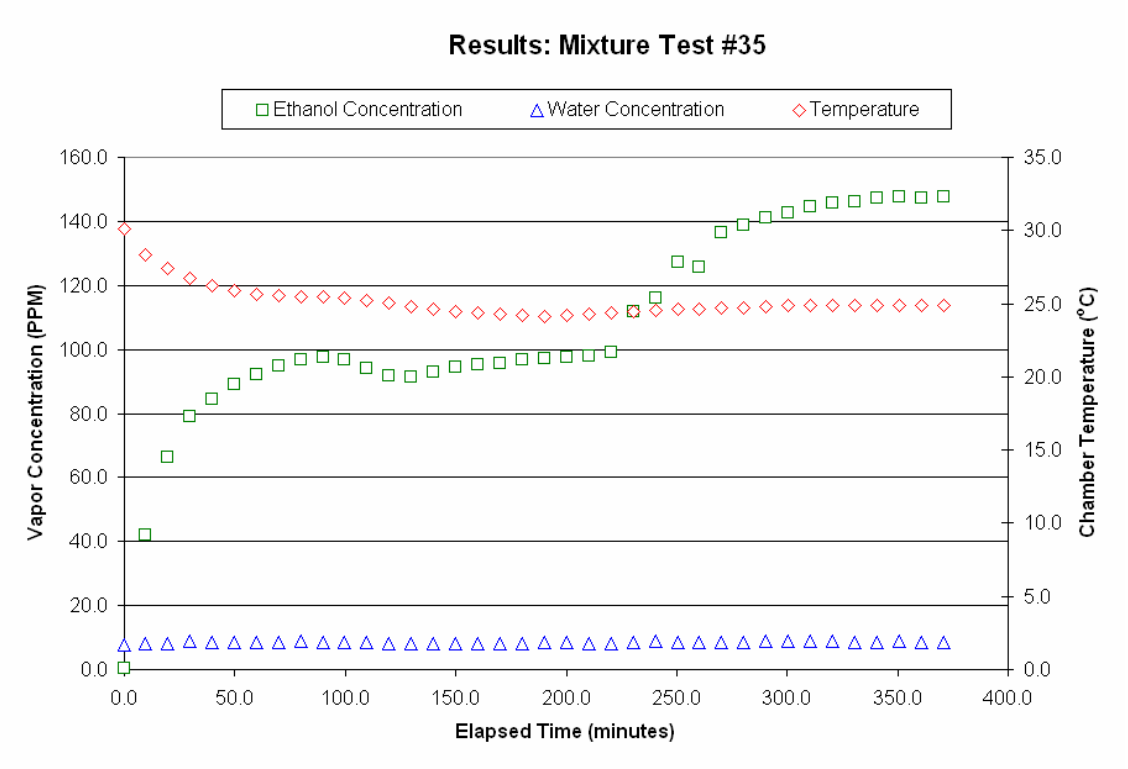

Figure 62: Concentration and Temperature Profile Data of Mixture Test #35

TEST35: 06-15-06

Mix, de-gassed
run continuous
300drop/sec

AMBIENT PPM
g/kg = 6.85
kg/m^3 = 1.08
PPM = 7.411

Time	Water				Water			Ethanol					Temperature
	Absorbance		Concentration		Concentration			Absorbance		Concentration			
Elapsed (min)	1558.2	1652.7	1558.2	1652.7	1558.2	1652.7	average	2900.6	2987.4	2900.6	2987.4	average	°C
0.0	0.0025	0.0019	0.287	0.278	7.698	7.689	7.694	0.0020	0.0023	0.249	0.247	0.248	30.135
9.5	0.0053	0.0044	0.605	0.647	8.016	8.058	8.037	0.3300	0.3930	41.844	41.866	41.855	28.354
19.6	0.0068	0.0058	0.773	0.850	8.185	8.261	8.223	0.5230	0.6250	66.316	66.581	66.449	27.380
29.6	0.0111	0.0091	1.264	1.331	8.675	8.742	8.709	0.6230	0.7450	78.996	79.365	79.180	26.699
39.7	0.0100	0.0084	1.139	1.229	8.550	8.640	8.595	0.6660	0.7950	84.448	84.691	84.570	26.233
49.7	0.0099	0.0086	1.127	1.258	8.539	8.669	8.604	0.7010	0.8380	88.886	89.272	89.079	25.873
59.7	0.0101	0.0088	1.150	1.287	8.561	8.699	8.630	0.7260	0.8690	92.056	92.575	92.315	25.654
69.8	0.0105	0.0090	1.198	1.312	8.609	8.723	8.666	0.7470	0.8920	94.719	95.025	94.872	25.519
79.8	0.0107	0.0092	1.214	1.349	8.625	8.760	8.693	0.7630	0.9120	96.748	97.155	96.951	25.468
89.8	0.0104	0.0088	1.186	1.289	8.597	8.700	8.648	0.7680	0.9180	97.382	97.795	97.588	25.444
99.8	0.0072	0.0073	0.814	1.062	8.226	8.473	8.349	0.7620	0.9100	96.621	96.942	96.782	25.382
109.9	0.0069	0.0068	0.790	0.989	8.202	8.400	8.301	0.7420	0.8860	94.085	94.386	94.235	25.245
119.9	0.0057	0.0054	0.650	0.786	8.062	8.197	8.129	0.7220	0.8630	91.549	91.935	91.742	25.041
130.0	0.0050	0.0062	0.573	0.904	7.984	8.315	8.150	0.7190	0.8620	91.168	91.829	91.499	24.834
140.0	0.0051	0.0060	0.576	0.882	7.987	8.293	8.140	0.7330	0.8730	92.944	93.001	92.972	24.627
150.0	0.0053	0.0063	0.598	0.926	8.009	8.337	8.173	0.7420	0.8870	94.085	94.492	94.288	24.474
160.1	0.0061	0.0054	0.694	0.793	8.105	8.204	8.154	0.7490	0.8970	94.972	95.557	95.265	24.388
170.1	0.0055	0.0060	0.629	0.879	8.040	8.290	8.165	0.7540	0.9010	95.606	95.984	95.795	24.295
180.2	0.0059	0.0054	0.672	0.787	8.083	8.198	8.141	0.7600	0.9090	96.367	96.836	96.602	24.219
190.2	0.0101	0.0087	1.147	1.265	8.558	8.677	8.617	0.7630	0.9160	96.748	97.581	97.165	24.159
200.2	0.0086	0.0074	0.975	1.081	8.386	8.492	8.439	0.7650	0.9210	97.001	98.114	97.558	24.206
210.3	0.0066	0.0061	0.752	0.885	8.163	8.296	8.230	0.7680	0.9230	97.382	98.327	97.854	24.284
220.3	0.0058	0.0059	0.656	0.857	8.067	8.269	8.168	0.7800	0.9330	98.903	99.392	99.148	24.361
230.3	0.0073	0.0066	0.830	0.970	8.241	8.381	8.311	0.8790	1.0540	111.456	112.283	111.869	24.456
240.4	0.0123	0.0107	1.401	1.559	8.812	8.971	8.891	0.9120	1.0960	115.641	116.757	116.199	24.532
250.4	0.0089	0.0087	1.012	1.265	8.424	8.677	8.550	0.9950	1.2020	126.165	128.049	127.107	24.595
260.4	0.0103	0.0091	1.168	1.325	8.580	8.737	8.658	1.0390	1.1260	131.744	119.953	125.848	24.654
270.5	0.0103	0.0091	1.174	1.328	8.585	8.740	8.662	1.0680	1.2880	135.421	137.211	136.316	24.714
280.5	0.0098	0.0088	1.119	1.286	8.531	8.697	8.614	1.0880	1.3120	137.957	139.767	138.862	24.745
290.5	0.0105	0.0093	1.196	1.365	8.607	8.776	8.692	1.1040	1.3360	139.986	142.324	141.155	24.803
300.6	0.0114	0.0103	1.295	1.502	8.706	8.914	8.810	1.1118	1.3580	140.975	144.668	142.821	24.846
310.6	0.0112	0.0099	1.280	1.451	8.691	8.862	8.777	1.1260	1.3760	142.776	146.585	144.680	24.880
320.6	0.0106	0.0095	1.204	1.382	8.615	8.794	8.704	1.1380	1.3810	144.297	147.118	145.708	24.894
330.7	0.0097	0.0088	1.099	1.289	8.510	8.700	8.605	1.1430	1.3840	144.931	147.438	146.184	24.868
340.7	0.0094	0.0085	1.073	1.238	8.484	8.649	8.566	1.1490	1.3960	145.692	148.716	147.204	24.865
350.7	0.0103	0.0093	1.174	1.362	8.585	8.773	8.679	1.1510	1.4010	145.946	149.249	147.597	24.871
360.8	0.0089	0.0081	1.012	1.191	8.424	8.602	8.513	1.1510	1.3970	145.946	148.822	147.384	24.873
370.8	0.0085	0.0080	0.966	1.163	8.377	8.574	8.476	1.1550	1.3960	146.453	148.716	147.584	24.857

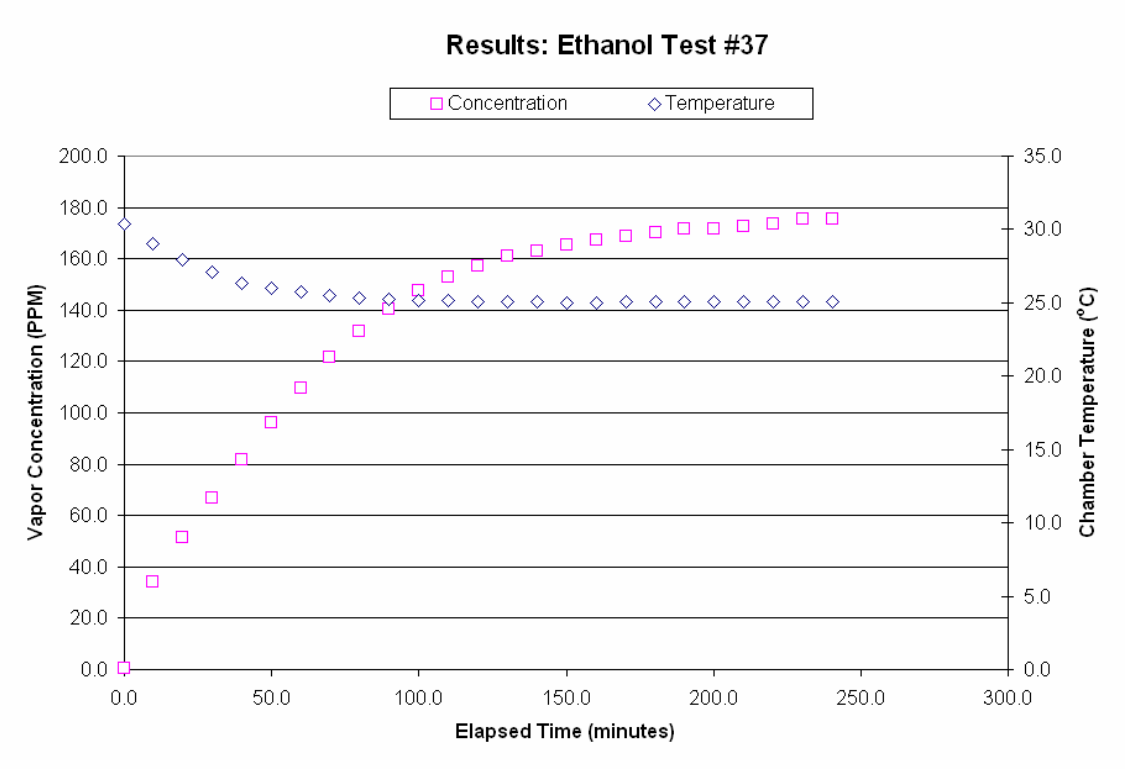

Figure 63: Concentration and Temperature Profile Data of Ethanol Test #37

TEST37: 08-11-06

Ethanol, de-gassed
run continuous
200drop/sec

Time	Absorbance		Concentration			Temperature
Elapsed (min)	*2987.4*	*2900.6*	*2987.4*	*2900.6*	*average*	°C
0.0	0.0036	0.0030	0.381	0.382	0.382	30.359
9.6	0.3190	0.2690	33.983	34.109	34.046	29.004
19.6	0.4020	0.4770	42.825	60.483	51.654	27.919
29.7	0.6260	0.5270	66.688	66.823	66.755	27.070
39.7	0.7660	0.6450	81.602	81.785	81.694	26.364
49.8	0.9020	0.7570	96.090	95.987	96.038	25.965
59.8	1.0280	0.8620	109.513	109.301	109.407	25.708
69.9	1.1440	0.9550	121.870	121.093	121.482	25.493
79.9	1.2420	1.0360	132.310	131.364	131.837	25.345
89.9	1.3260	1.1030	141.259	139.859	140.559	25.251
100.0	1.3900	1.1600	148.077	147.087	147.582	25.180
110.0	1.4410	1.2030	153.510	152.539	153.024	25.123
120.0	1.4810	1.2340	157.771	156.470	157.120	25.089
130.0	1.5160	1.2640	161.499	160.274	160.887	25.046
140.1	1.5360	1.2800	163.630	162.303	162.966	25.034
150.1	1.5620	1.3000	166.400	164.839	165.619	25.016
160.2	1.5780	1.3120	168.104	166.360	167.232	25.020
170.2	1.5930	1.3210	169.702	167.501	168.602	25.044
180.2	1.6030	1.3340	170.768	169.150	169.959	25.049
190.2	1.6190	1.3440	172.472	170.418	171.445	25.036
200.3	1.6210	1.3480	172.685	170.925	171.805	25.071
210.3	1.6280	1.3550	173.431	171.813	172.622	25.046
220.4	1.6400	1.3630	174.709	172.827	173.768	25.064
230.4	1.6630	1.3740	177.159	174.222	175.691	25.076
240.4	1.6590	1.3740	176.733	174.222	175.478	25.081

A.4 Property Equations

A.4.1 Diffusivity

$$D_{water-air} = 2.634P^{-1} \ \frac{m^2}{s} \quad [1]$$

$$D_{ethanol-air} = 1.337P^{-1} \ \frac{m^2}{s} \quad [1]$$

$$\Omega_{ethanol-water} = 1.0004 \cdot \left(\frac{kT}{\varepsilon_{ethanol-water}} \right)^2 - 2.6724 \cdot \left(\frac{kT}{\varepsilon_{ethanol-water}} \right) + 3.1105 \quad [2]$$

$$D_{water-ethanol} = \frac{1.8583 \times 10^{-6}}{P \cdot \sigma_{ethanol-water} \cdot \Omega_{ethanol-water}} \left[T^3 \left(\frac{1}{MW_{ethanol}} + \frac{1}{MW_{water}} \right) \right]^{1/2} \ \frac{m^2}{s} \quad [2]$$

A.4.2 Equilibrium (Van Laar Equation)

$$A_{12} = 1.5054 \quad [3]$$

$$A_{21} = 0.9994 \quad [3]$$

$$\ln \gamma_1 = A_{12} \left[1 + \frac{A_{12} x_1}{A_{21} x_2} \right]^{-2}$$

$$\ln \gamma_2 = A_{21} \left[1 + \frac{A_{21} x_2}{A_{12} x_1} \right]^{-2}$$

[1] Welty, Wicks, Wilson, and Rorrer, Fundamental of Momentum, Heat, and Mass Transfer. New York: John Wiley & Sons (2001).

[2] Bird, Stewart, and Lightfoot, Transport Phenomena. New York: John Wiley & Sons (2002).

[3] Smith, VanNess, and Abbott, Chemical Engineering Thermodynamics. Boston: McGraw Hill (2001).

A.4.3 Ethanol Properties

$MW = 46.07 \frac{\text{g}}{\text{mole}}$

$\rho_L = -2.06\times10^{-3}T^2 + 3.92\times10^{-1}T + 872.28 \frac{\text{kg}}{\text{m}^3}$ 250 - 420K [4]

$\rho_V = 8.61\times10^{-33}T^{12.65} \frac{\text{kg}}{\text{m}^3}$ 250 - 420K [4]

$\mu_L = 1.73\times10^{-8}T^2 - 1.25\times10^{-5}T + 2.29\times10^{-3} \frac{kg}{\text{m}\cdot\text{s}}$ 270 - 360K [4]

$\mu_V = 2.97\times10^{-5}T - 2.33\times10^{-4} \frac{kg}{\text{m}\cdot\text{s}}$ 250 - 420K [4]

$Cp_L = 5.00\times10^{-5}T^2 - 2.15\times10^{-2}T + 4.39 \frac{\text{kJ}}{\text{kg}\cdot\text{K}}$ 250 - 420K [4]

$Cp_V = -1.08\times10^{-6}T^2 + 3.61\times10^{-3}T + 6.35\times10^{-1} \frac{\text{kJ}}{\text{kg}\cdot\text{K}}$ 200 - 400K [4]

$k_V = 1.3\times10^{-7}T^2 + 1.91\times10^{-5}T - 7.15\times10^{-4} \frac{W}{m\cdot K}$ 250 - 400K [5]

$dH_{vap} = 836.336 \frac{\text{kJ}}{\text{kg}}$

$T_{vap} = 351.65 \frac{\text{K}}{1}$

$H(T) = -3.61\times10^{-7}T^3 - 1.81\times10^{-3}T^2 + 6.35\times10^{-1}T \frac{\text{kJ}}{\text{kg}}$

$\Delta H_{ref} = H(T_{vap}) - H(T_{ref}) + dH_{vap} \frac{\text{kJ}}{\text{kg}}$

$T_{critical} = 516.3 \frac{\text{K}}{1}$ [3]

$P_{critical} = 6383475 \frac{\text{Pa}}{1}$ [3]

$\sigma = 4.445\times10^{-10} \frac{\text{m}}{1}$ [3]

$$\text{Antoine Parameters}: \log(P_{sat}) = \Omega' - \frac{\Omega''}{T + \Omega'''}, \quad \text{P}_{\text{sat}}[=]\text{mmHg}, \quad T[=]^{\text{o}}C$$ [3]

$\Omega' = 8.1122$

$\Omega'' = 1592.864$

$\Omega''' = 226.184$

$$\text{Antoine Parameters}: \ln(P_{sat}) = \Omega' - \frac{\Omega''}{T + \Omega'''}, \quad \text{P}_{\text{sat}}[=]\text{kPa}, \quad T[=]^{\text{o}}C$$ [3]

$\Omega' = 16.6758$

$\Omega'' = 3674.4900$

$\Omega''' = 226.450$

[3] Smith, VanNess, and Abbott, Chemical Engineering Thermodynamics. Boston: McGraw Hill (2001).

[4] Linstrom, P.J. and Mallard, W.G. NIST Chemistry Webbook (July 2001 Release); http://webbook.nist.gov/chemistry/ (2001).

[5] Penoncello, S. ISRProps, Isothermal System Research Fluid Property Calculator. (2006)

A.4.4 Water Properties

$MW = 18.06 \frac{\text{g}}{\text{mole}}$

$\rho_L = -3.52\times10^{-3}T^2 + 1.85T + 758.95 \frac{\text{kg}}{\text{m}^3}$ 280 - 370K [4]

$\rho_V = 2.64\times10^{-40}T^{1.53\times10^{1}} \frac{\text{kg}}{\text{m}^3}$ 273 - 360K [4]

$\mu_L = -3.18\times10^{-9}T^3 + 3.25\times10^{-6}T^2 - 1.11\times10^{-3}T + 1.28\times10^{-1} \frac{kg}{\text{m}\cdot\text{s}}$ 273 - 360K [4]

$\mu_V = 3.09\times10^{-8}T + 6.82\times10^{-7} \frac{kg}{\text{m}\cdot\text{s}}$ 273 - 360K [4]

$Cp_L = 3.06\times10^{-9}T^4 - 4.08\times10^{-6}T^3 + 2.04\times10^{-3}T^2 - 4.55\times10^{-1}T + 42.21 \frac{\text{kJ}}{\text{kg}\cdot\text{K}}$ 273 - 370K [4]

$Cp_V = 3.94\times10^{-10}T^4 - 3.89\times10^{-7}T^3 + 1.43\times10^{-3}T^2 - 2.23\times10^{-2}T + 3.02 \frac{\text{kJ}}{\text{kg}\cdot\text{K}}$ 273 - 370K [4]

$k_V = 8.00\times10^{-5}T - 5.23\times10^{-3} \frac{W}{m\cdot K}$ 273 - 373K [4]

$dH_{vap} = 2253.55 \frac{\text{kJ}}{\text{kg}}$

$T_{vap} = 373.15 \frac{\text{K}}{1}$

$H(T) = 7.88\times10^{-11}T^5 - 9.72\times10^{-8}T^4 + 4.78\times10^{-4}T^3 - 1.11\times10^{-2}T^2 + 3.02T \frac{\text{kJ}}{\text{kg}}$

$\Delta H_{ref} = H(T_{vap}) - H(T_{ref}) + dH_{vap} \frac{\text{kJ}}{\text{kg}}$

$T_{critical} = 647.4 \frac{\text{K}}{1}$ [3]

$P_{critical} = 22119247.5 \frac{\text{Pa}}{1}$ [3]

$\sigma = 2.649\times10^{-10} \frac{\text{m}}{1}$ [3]

$$\text{Antoine Parameters}: \log(P_{sat}) = \Omega' - \frac{\Omega''}{T + \Omega'''}, \quad \text{P}_{\text{sat}}[=]\text{mmHg}, \quad T[=]^{\text{o}}C$$ [3]

$\Omega' = 8.108$

$\Omega'' = 1750.286$

$\Omega''' = 235.000$

$$\text{Antoine Parameters}: \ln(P_{sat}) = \Omega' - \frac{\Omega''}{T + \Omega'''}, \quad \text{P}_{\text{sat}}[=]\text{kPa}, \quad T[=]^{\text{o}}C$$ [3]

$\Omega' = 16.262$

$\Omega'' = 3799.890$

$\Omega''' = 226.350$

[3] Smith, VanNess, and Abbott, Chemical Engineering Thermodynamics. Boston: McGraw Hill (2001).

[4] Linstrom, P.J. and Mallard, W.G. NIST Chemistry Webbook (July 2001 Release); http://webbook.nist.gov/chemistry/ (2001).

A.4.5 Air Properties

$MW = 29.00 \frac{\text{g}}{\text{mole}}$

$\rho_V = 2.45\times10^{-6}T^2 - 4.32\times10^{-3}\text{T} + 2.26 \frac{\text{kg}}{\text{m}^3}$ 250 - 1000K [1]

$\mu_V = 1.16\times10^{-9}T^4 - 2.60\times10^{-8}T^3 + 2.43\times10^{-7}\text{T}^2 + 5.14\times10^{-9}\text{T} + 1.58\times10^{-5} \frac{kg}{\text{m}\cdot\text{s}}$ 250 - 1000K [1]

$Cp_V = -3.67\times10^{-10}T^3 + 8.09\times10^{-7}T^2 - 3.48\times10^{-4}T + 1.05 \frac{\text{kJ}}{\text{kg}\cdot\text{K}}$ 250 - 1000K [1]

$k_V = 2.21\times10^{-6}T^4 - 4.95\times10^{-5}T^3 + 4.62\times10^{-4}T^2 - 2.34\times10^{-4}T + 2.21\times10^{-2} \frac{W}{\text{m}\cdot\text{K}}$ 250 - 1000K [1]

$T_{critical} = 132.2 \frac{\text{K}}{1}$ [3]

$P_{critical} = 3749025 \frac{\text{Pa}}{1}$ [6]

A.4.6 Nitrogen Properties

$MW = 28.02 \frac{\text{g}}{\text{mole}}$

$\rho_V = -4.0\times10^{-9}T^3 + 1.00\times10^{-5}\text{T}^2 - 8.40\times10^{-3}\text{T} + 2.88 \frac{\text{kg}}{\text{m}^3}$ 250 - 1000K [1]

$\mu_V = -1.50\times10^{-11}T^2 + 5.10\times10^{-8}T + 3.91\times10^{-6} \frac{kg}{\text{m}\cdot\text{s}}$ 250 - 1000K [1]

$Cp_V = -3.56\times10^{-10}T^3 + 8.38\times10^{-7}T^2 - 4.14\times10^{-4}T + 1.10 \frac{\text{kJ}}{\text{kg}\cdot\text{K}}$ 250 - 1000K [1]

$k_V = -2.57\times10^{-8}T^2 + 8.81\times10^{-5}T + 1.96\times10^{-3} \frac{W}{\text{m}\cdot\text{K}}$ 250 - 1000K [1]

$T_{critical} = 126.2 \frac{\text{K}}{1}$ [6]

$P_{critical} = 3394388 \frac{\text{Pa}}{1}$ [6]

[1] Welty, Wicks, Wilson, and Rorrer, Fundamental of Momentum, Heat, and Mass Transfer. New York: John Wiley & Sons (2001).
[3] Smith, VanNess, and Abbott, Chemical Engineering Thermodynamics. Boston: McGraw Hill (2001).
[6] Felder and Rousseau, Elementary Principles of Chemical Processes. New York: John Wiley & Sons (2000).

A.5 Experiment Design

A.5.1 ActivePipette System and Signal Driver Interface (dimensions, specs, and screen shots)

Parameter	Min.	Typical	Max.	Units
Length		19	27	mm
Width (w/out serial number)		4.4	4.4	mm
Width (w/ serial number)			6.35	mm
Nozzle Diameter	38.5	40	41.5	μm
Drop Volume	35	100	270	pL
Drop Volume: Variation		1		%CV
Drop Diameter	40	60	80	μL
Dispense Rate drops per second (drop-on-demand)	1		1000	Hz
Dispense Rate drops per second (continuous)	20000	22000	65000	Hz
Flow Rate (drop-on-demand)			0.3	μL/sec
Flow Rate (continuous)		2.2		μL/sec
Drop Trajectory: Deviation Angle	0		2	deg.
Drop Trajectory: Deviation Angle Reproducibility	-0.3		0.3	deg.
Viscosity	0.5	1	6	cP
Temperature	5	20	120	°C
Relative Pressure (dispensing H_2O)	-100	-50	100	mm H_2O
Voltage	-87		87	V

Table 5: ActivePipette System Design Specifications

A.5.2 Data Acquisition

ExceLINX KEITHLEY A Greater Measure of Confidence

Task: Configure Scanning DMM Channels		
Task	Name	Droplet Evaporation Configuration
	Description	
	Created By	cbonuccelli
	Company	ISR
	Date Created	2/15/2006
	Date Modified	9/20/2006
	Status/Cmds	Task stopped successfully
Instrument	Device	KE2700_COM1*
	Password	
	Slot 1 Module	M7700*
	Slot 2 Module	Empty*
	Slot 3 Module	
	Slot 4 Module	
	Slot 5 Module	
	Front Panel Lockout	On
Setup	Line Sync	Off
	Autozero	On
	Display Digits	6½
	DCV Input Divider	Off
	Open TC Detection	Off
	Temp Scale	°C
Limits	Digital Outputs	Off
	Pulse Output	Off
	Polarity	High
	Duration	0.02 sec
	Master Latch	Off

Channel Scan List

Channel			Measurement		Scaling					Alarm Limits						Rep Filter	Sampling		Options			
Enb	List	Tag	Function	Range	Rel	Math	m/ref	b	U	En1	Hi1	Lo1	En2	Hi2	Lo2	Enb	Count	Rate	AC BW	Opt 1	Opt 2	Opt 3	Opt 4
On	101	Temp_1	TEMP	T	Off	None				Off			Off			Off		SLOW		INT			
On	102	Temp_2	TEMP	T	Off	None				Off			Off			Off		SLOW		INT			
On	103	Temp_3	TEMP	T	Off	None				Off			Off			Off		SLOW		INT			
On	104	Temp_4	TEMP	T	Off	None				Off			Off			Off		SLOW		INT			
On	105	Pressure	DCV	100 mV	Off	MXB	300	0	X	Off			Off			Off		SLOW		Volts			

Figure 64: ExceLINX Configuration Page

ExceLINX KEITHLEY A Greater Measure of Confidence

Task: Scan DMM Channels		
Task	19.914629	DMM Scan
	Description	
	Created By	cbonuccelli
	Company	ISR
	Date Created	2/15/2006
	Date Modified	9/20/2006
	Status/Cmds	Task stopped successfully
Configuration	Worksheet	DMM Config
Trigger	Model	Scan
	Source	Timer
	Delay	Auto sec
	Reading Count	INF
	Timer	20 sec
	Monitor	None
	Monitor Limits	None
Data Location	Worksheet	Template
	Starting Col	B
	Starting Row	4
	Organize By	Rows
	Autoincrement	Use one table
	Auto Wrap	On
	Log File	
	Format	Delimited text (comma)
Data Display	Add Channel Tags	No
	Add Channels	No
	Add Units	No
	Scroll Display	No
	Limits	None
	Timestamp	None
	Update Interval	100 msec

Figure 65: ExceLINX Channel Scan Page

A.5.3 Thermocouple Calibration

Water Bath: 35.90°C					
Time (seconds)	Calibrated (°C)	Thermocouple_1 (°C)	Thermocouple_2 (°C)	Thermocouple_3 (°C)	Thermocouple_4 (°C)
0	35.90	36.98	36.42	36.36	36.61
6	35.90	37.00	36.42	36.37	36.61
12	35.90	36.99	36.42	36.36	36.61
18	35.90	37.00	36.42	36.37	36.60
24	35.90	36.99	36.42	36.36	36.60
30	35.90	36.99	36.42	36.36	36.61
36	35.90	36.99	36.41	36.36	36.62
42	35.90	36.99	36.41	36.35	36.60
48	35.90	36.96	36.42	36.36	36.59
54	35.90	36.99	36.42	36.37	36.61
60	35.90	36.98	36.41	36.36	36.61
66	35.90	36.98	36.40	36.36	36.60
72	35.90	36.99	36.40	36.35	36.60
78	35.90	36.99	36.40	36.34	36.61
84	35.90	36.98	36.40	36.34	36.58
90	35.90	36.99	36.41	36.33	36.60
96	35.90	36.99	36.41	36.36	36.61
102	35.90	36.96	36.40	36.34	36.61
108	35.90	36.97	36.41	36.33	36.58
114	35.90	36.97	36.40	36.33	36.59
120	35.90	36.98	36.40	36.35	36.59

Water Bath: 29.80°C					
Time (seconds)	Calibrated (°C)	Thermocouple_1 (°C)	Thermocouple_2 (°C)	Thermocouple_3 (°C)	Thermocouple_4 (°C)
0	29.80	30.37	30.02	30.00	30.17
12	29.80	30.37	30.03	30.00	30.18
24	29.80	30.36	30.01	30.01	30.17
36	29.80	30.36	30.02	30.00	30.18
48	29.80	30.35	30.03	30.01	30.17
60	29.80	30.35	30.03	30.01	30.16
72	29.80	30.35	30.02	30.02	30.18
84	29.80	30.35	30.03	30.01	30.18
96	29.80	30.35	30.03	30.02	30.17
108	29.80	30.35	30.04	30.03	30.18
120	29.80	30.35	30.04	30.04	30.18
132	29.80	30.34	30.05	30.05	30.19
144	29.80	30.34	30.03	30.01	30.15

Water Bath: 21.60°C					
Time (seconds)	Calibrated (°C)	Thermocouple_1 (°C)	Thermocouple_2 (°C)	Thermocouple_3 (°C)	Thermocouple_4 (°C)
0	21.60	21.46	21.49	21.50	21.50
30	21.60	21.45	21.49	21.50	21.51
60	21.60	21.46	21.49	21.49	21.51
90	21.60	21.45	21.48	21.49	21.50
120	21.60	21.46	21.52	21.52	21.54

Table 6: Thermocouple Calibration Data at Three Different Bath Temperatures

Deviation Associated with Calibration

	Average Temperature (°C)					Average Deviation (°C)
	Water Bath: 35.90°C	Water Bath: 29.80°C	Water Bath: 21.60°C	Slope	Intercept	(Predicted-Calibrated)
Calibrated	35.90	29.80	21.60	-	-	-
Thermocouple_1	36.98	30.35	21.46	0.921	1.841	0.458
Thermocouple_2	36.41	30.03	21.49	0.959	0.996	0.203
Thermocouple_3	36.35	30.02	21.50	0.963	0.900	0.183
Thermocouple_4	36.60	30.17	21.51	0.948	1.209	0.313

Deviation Accociated with Repeatability

	Measurement Variation (°C)			Average Deviation (°C)
	Water Bath: 35.90°C	Water Bath: 29.80°C	Water Bath: 21.60°C	
Calibrated	0.000	0.000	0.000	0.000
Thermocouple_1	0.041	0.036	0.011	0.029
Thermocouple_2	0.028	0.034	0.039	0.034
Thermocouple_3	0.040	0.055	0.028	0.041
Thermocouple_4	0.035	0.037	0.037	0.036

Table 7: Thermocouple Calibration Calculations at Three Different Bath Temperatures

	-200°C to 0°C (-5,603µV to 0µV)	0°C to 400°C (0µV to 20,872µV)
c_0 =	0.0	0.0
c_1 =	$2.594\,919\,2 \times 10^{-2}$	$2.592\,800 \times 10^{-2}$
c_2 =	$-2.131\,696\,7 \times 10^{-7}$	$-7.602\,961 \times 10^{-7}$
c_3 =	$7.901\,869\,2 \times 10^{-10}$	$4.637\,791 \times 10^{-11}$
c_4 =	$4.252\,777\,7 \times 10^{-13}$	$-2.165\,394 \times 10^{-15}$
c_5 =	$1.330\,447\,3 \times 10^{-16}$	$6.048\,144 \times 10^{-20}$
c_6 =	$2.024\,144\,6 \times 10^{-20}$	$-7.293\,422 \times 10^{-25}$
c_7 =	$1.266\,817\,1 \times 10^{-24}$	
Error:	0.04°C to -0.02°C	0.03°C to -0.03°C

$t_{90} = c_0 + c_1E + c_2E^2 + c_3E^3 \ldots c_iE^i$
where: t_{90} is the calculated temperature in °C.
E is the measured voltage in microvolts.

Table 8: Type T Thermocouple Inverse Function Polynomial

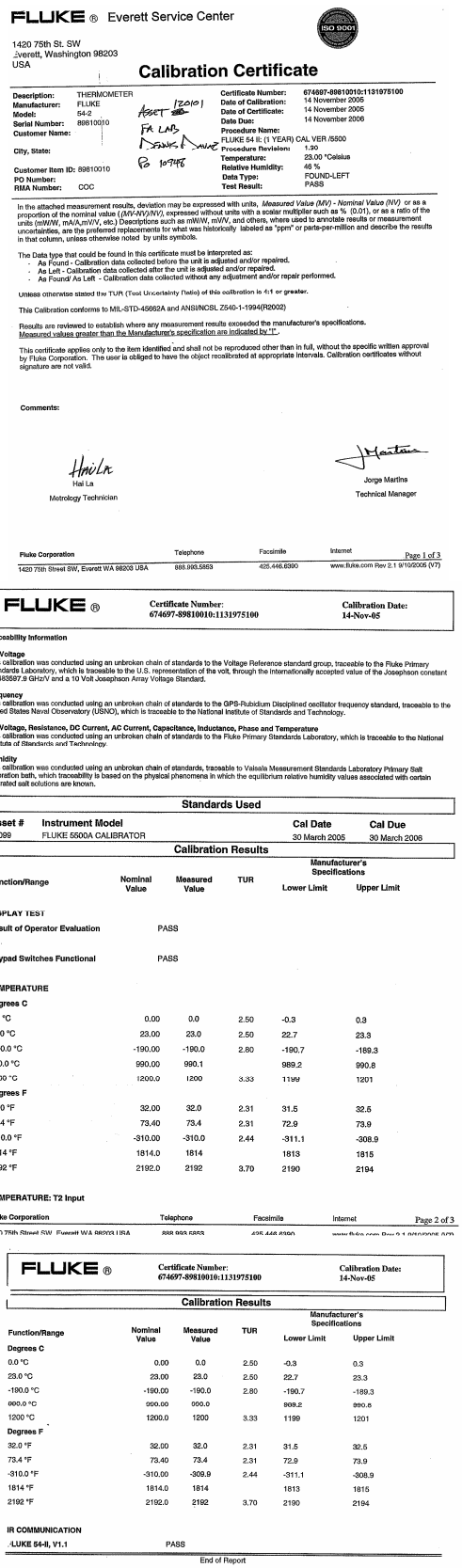

FLUKE ® Everett Service Center

1420 75th St. SW
Everett, Washington 98203
USA

Calibration Certificate

Description:	THERMOMETER	**Certificate Number:**	674697-89810010:1131975100
Manufacturer:	FLUKE	**Date of Calibration:**	14 November 2005
Model:	54-2	**Date of Certificate:**	14 November 2005
Serial Number:	89810010	**Date Due:**	14 November 2006
Customer Name:		**Procedure Name:**	FLUKE 54 II: (1 YEAR) CAL VER /5500
City, State:		**Procedure Revision:**	1.90
		Temperature:	23.00 *Celsius
Customer Item ID:	89810010	**Relative Humidity:**	46 %
PO Number:		**Data Type:**	FOUND-LEFT
RMA Number:	COC	**Test Result:**	PASS

ASSET 12010
FA LAB

In the attached measurement results, deviation may be expressed with units, *Measured Value (MV) - Nominal Value (NV)* or as a proportion of the nominal value (*(MV-NV)/NV*), expressed without units with a scalar multiplier such as % (0.01), or as a ratio of the units (mW/W, mA/A,mV/V, etc.) Descriptions such as mW/W, mV/V, and others, where used to annotate results or measurement uncertainties, are the preferred replacements for what was historically labeled as "ppm" or parts-per-million and describe the results in that column, unless otherwise noted by units symbols.

The Data type that could be found in this certificate must be interpreted as:
- As Found - Calibration data collected before the unit is adjusted and/or repaired.
- As Left - Calibration data collected after the unit is adjusted and/or repaired.
- As Found/ As Left - Calibration data collected without any adjustment and/or repair performed.

Unless otherwise stated the TUR (Test Uncertainty Ratio) of this calibration is 4:1 or greater.

This Calibration conforms to MIL-STD-45662A and ANSI/NCSL Z540-1-1994(R2002)

Results are reviewed to establish where any measurement results exceeded the manufacturer's specifications.
Measured values greater than the Manufacturer's specification are indicated by "f".

This certificate applies only to the item identified and shall not be reproduced other than in full, without the specific written approval by Fluke Corporation. The user is obliged to have the object recalibrated at appropriate intervals. Calibration certificates without signature are not valid.

Comments:

Hai La
Metrology Technician

Jorge Martins
Technical Manager

Fluke Corporation	Telephone	Facsimile	Internet	Page 1 of 3
1420 75th Street SW, Everett WA 98203 USA	888.993.5853	425.446.6390	www.fluke.com Rev 2.1 9/10/2005 (V7)	

FLUKE ®

Certificate Number: 674697-89810010:1131975100

Calibration Date: 14-Nov-05

raceability Information

DC Voltage
This calibration was conducted using an unbroken chain of standards to the Voltage Reference standard group, traceable to the Fluke Primary Standards Laboratory, which is traceable to the U.S. representation of the volt, through the internationally accepted value of the Josephson constant Kj=483597.9 GHz/V and a 10 Volt Josephson Array Voltage Standard.

Frequency
This calibration was conducted using an unbroken chain of standards to the GPS-Rubidium Disciplined oscillator frequency standard, traceable to the United States Naval Observatory (USNO), which is traceable to the National Institute of Standards and Technology.

AC Voltage, Resistance, DC Current, AC Current, Capacitance, Inductance, Phase and Temperature
This calibration was conducted using an unbroken chain of standards to the Fluke Primary Standards Laboratory, which is traceable to the National Institute of Standards and Technology.

Humidity
This calibration was conducted using an unbroken chain of standards, traceable to Vaisala Measurement Standards Laboratory Primary Salt calibration bath, which traceability is based on the physical phenomena in which the equilibrium relative humidity values associated with certain saturated salt solutions are known.

Standards Used

Asset #	Instrument Model	Cal Date	Cal Due
10099	FLUKE 5500A CALIBRATOR	30 March 2005	30 March 2006

Calibration Results

Function/Range	Nominal Value	Measured Value	TUR	Manufacturer's Specifications Lower Limit	Upper Limit
DISPLAY TEST					
Result of Operator Evaluation		PASS			
Keypad Switches Functional		PASS			
TEMPERATURE					
Degrees C					
0.0 °C	0.00	0.0	2.50	-0.3	0.3
23.0 °C	23.00	23.0	2.50	22.7	23.3
-190.0 °C	-190.00	-190.0	2.80	-190.7	-189.3
990.0 °C	990.00	990.1		989.2	990.8
1200 °C	1200.0	1200	3.33	1199	1201
Degrees F					
32.0 °F	32.00	32.0	2.31	31.5	32.5
73.4 °F	73.40	73.4	2.31	72.9	73.9
-310.0 °F	-310.00	-310.0	2.44	-311.1	-308.9
1814 °F	1814.0	1814		1813	1815
2192 °F	2192.0	2192	3.70	2190	2194
TEMPERATURE: T2 Input					

Fluke Corporation	Telephone	Facsimile	Internet	Page 2 of 3
1420 75th Street SW, Everett WA 98203 USA	888.993.5853	425.446.6390	www.fluke.com Rev 2.1 9/10/2005 (V7)	

FLUKE ®

Certificate Number: 674697-89810010:1131975100

Calibration Date: 14-Nov-05

Calibration Results

Function/Range	Nominal Value	Measured Value	TUR	Manufacturer's Specifications Lower Limit	Upper Limit
Degrees C					
0.0 °C	0.00	0.0	2.50	-0.3	0.3
23.0 °C	23.00	23.0	2.50	22.7	23.3
-190.0 °C	-190.00	-190.0	2.80	-190.7	-189.3
990.0 °C	990.00	990.0		989.2	990.8
1200 °C	1200.0	1200	3.33	1199	1201
Degrees F					
32.0 °F	32.00	32.0	2.31	31.5	32.5
73.4 °F	73.40	73.4	2.31	72.9	73.9
-310.0 °F	-310.00	-309.9	2.44	-311.1	-308.9
1814 °F	1814.0	1814		1813	1815
2192 °F	2192.0	2192	3.70	2190	2194
IR COMMUNICATION					
FLUKE 54-II, V1.1		PASS			

End of Report

Figure 66: FLUKE Thermometer Calibration Certificate

A.5.4 FTIR Calibration

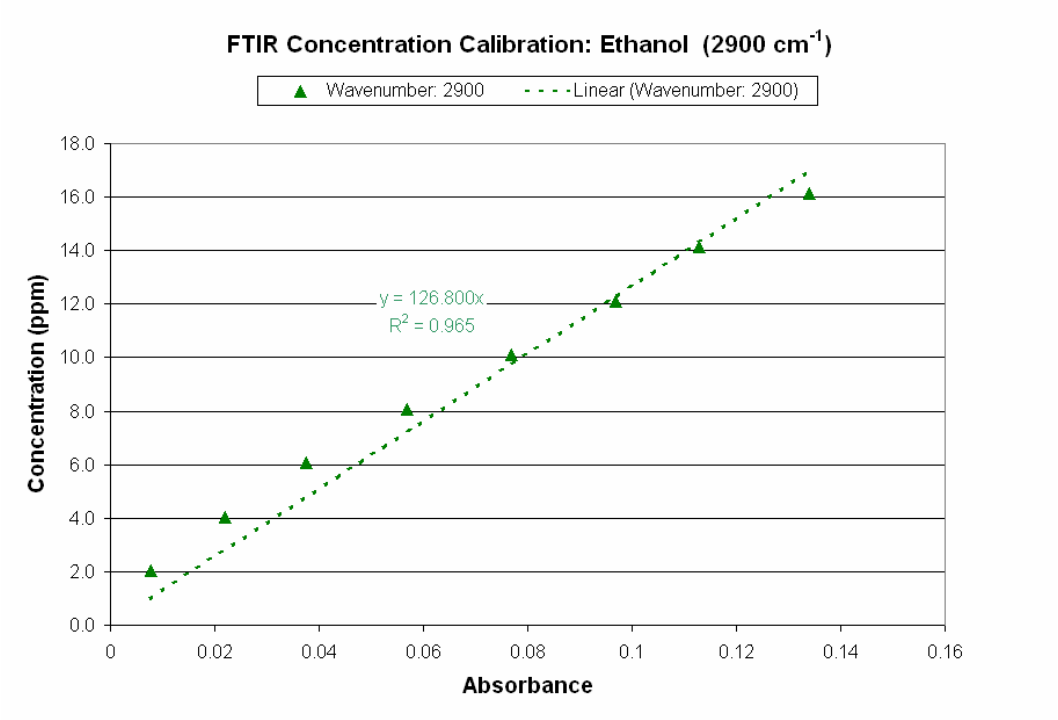

Figure 67: FTIR Concentration Calibration of Ethanol Peak 2900cm^{-1}

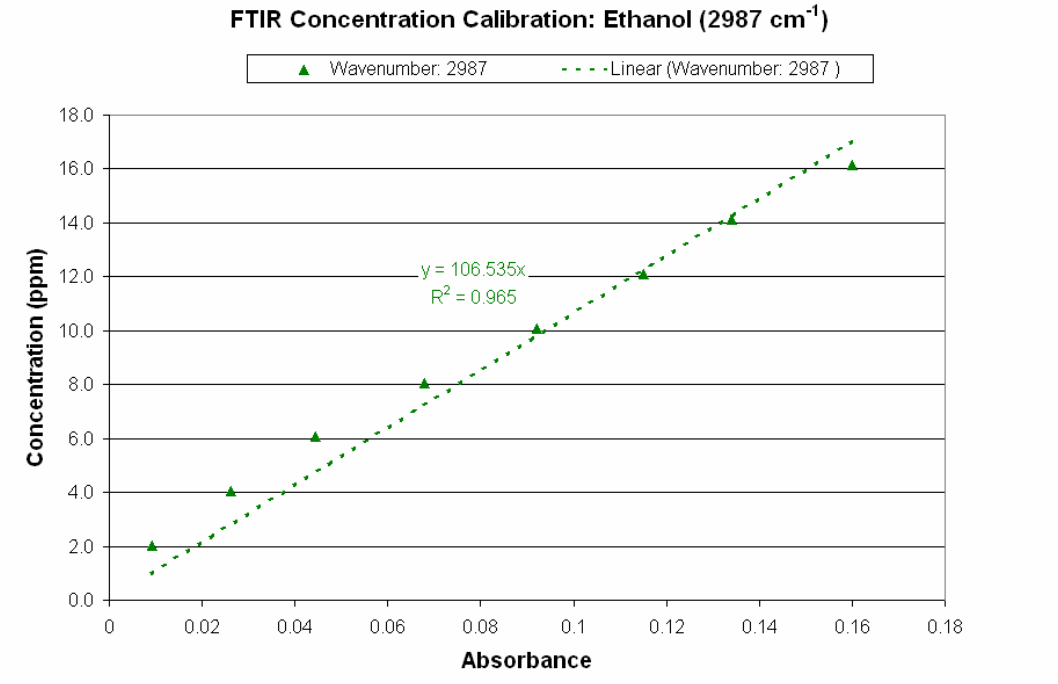

Figure 68: FTIR Concentration Calibration for Ethanol Peak 2987cm^{-1}

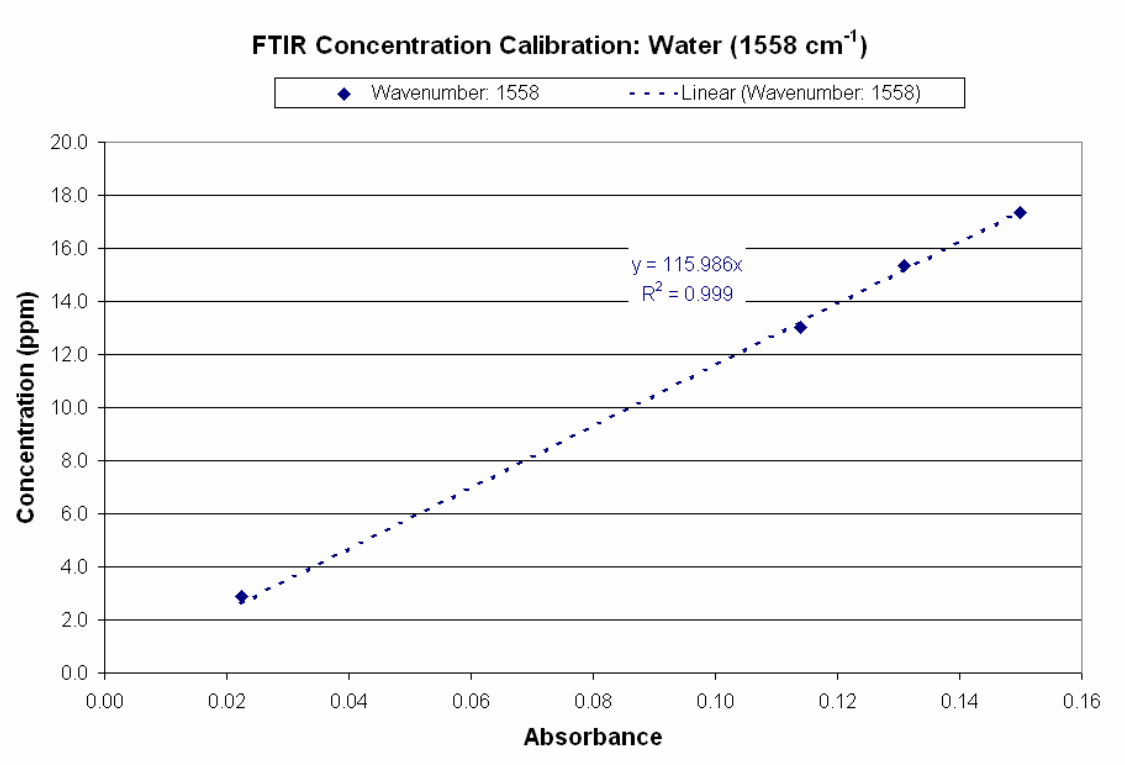

Figure 69: FTIR Concentration Calibration for Water Peak 1558cm^{-1}

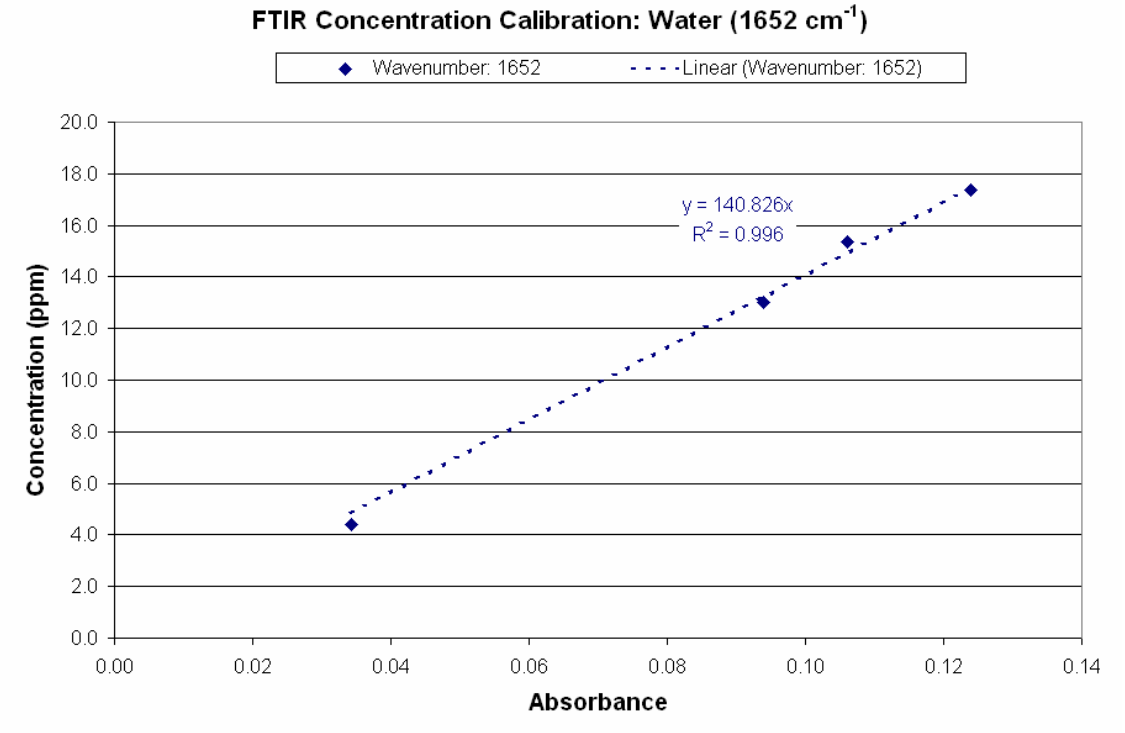

Figure 70: FTIR Concentration Calibration for Water Peak 1652cm^{-1}

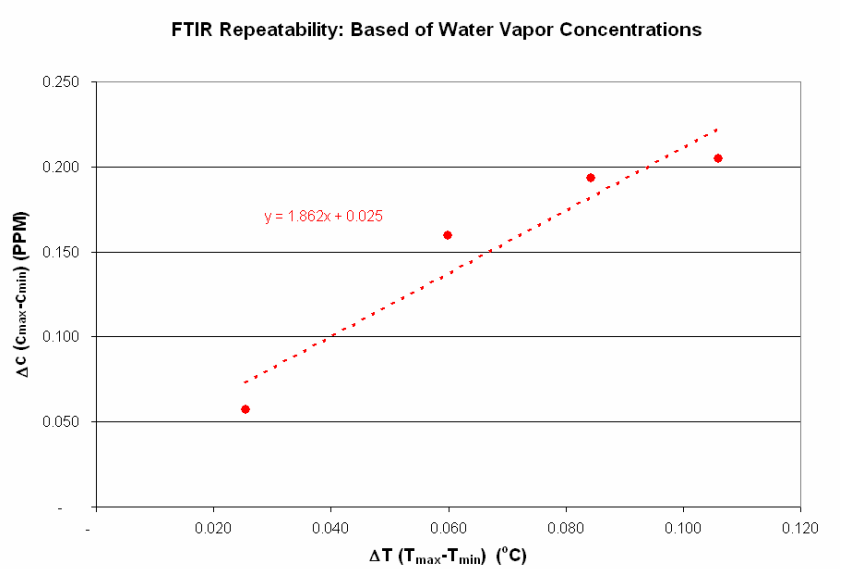

Figure 71: FTIR Measurement Repeatability Experiments Based on Water Vapor Concentration

Time Elapsed (min)	Absorbance	Temperature °C	Concentration PPM
84.2	0.0345	30.025	9.635
85.4	0.0361	30.090	9.817
86.7	0.0344	30.028	9.624
88.0	0.0347	29.984	9.658
89.3	0.0343	30.052	9.612
ΔT = 0.106			
Δc = 0.205			

Time Elapsed (min)	Absorbance	Temperature °C	Concentration PPM
105.7	0.0236	32.043	9.010
106.9	0.0234	32.044	8.988
108.2	0.0233	32.031	8.976
109.5	0.0228	32.043	8.919
110.8	0.0234	32.068	8.988
112.0	0.0230	32.030	8.942
113.5	0.0228	32.023	8.919
114.6	0.0234	31.983	8.988
115.8	0.0244	32.018	9.102
117.1	0.0233	32.022	8.976
118.4	0.0245	32.032	9.113
ΔT = 0.084			
Δc = 0.194			

Time Elapsed (min)	Absorbance	Temperature °C	Concentration PPM
72.6	0.0196	30.977	8.555
73.8	0.0191	30.978	8.498
75.1	0.0194	31.008	8.532
76.4	0.0204	30.997	8.646
77.7	0.0201	31.013	8.612
78.9	0.0197	31.021	8.566
80.2	0.0201	31.022	8.612
81.4	0.0205	31.013	8.657
82.7	0.0203	31.037	8.635
84.0	0.0197	31.022	8.566
85.3	0.0199	31.019	8.589
86.6	0.0201	31.008	8.612
ΔT = 0.060			
Δc = 0.159			

Time Elapsed (min)	Absorbance	Temperature °C	Concentration PPM
94.2	0.0203	29.976	8.635
95.4	0.0207	29.982	8.680
96.7	0.0207	29.969	8.680
98.0	0.0202	29.965	8.623
99.3	0.0206	29.990	8.669
ΔT = 0.026			
Δc = 0.057			

Table 9: Tabular Data of FTIR Reliability Experiments

A.5.6 FTIR Interface

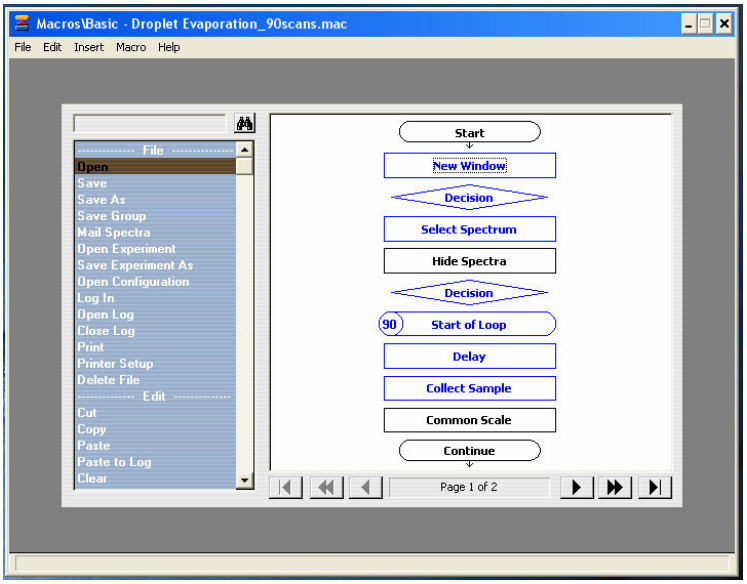

Figure 72: Macros Basic Program for FTIR Scan Loop

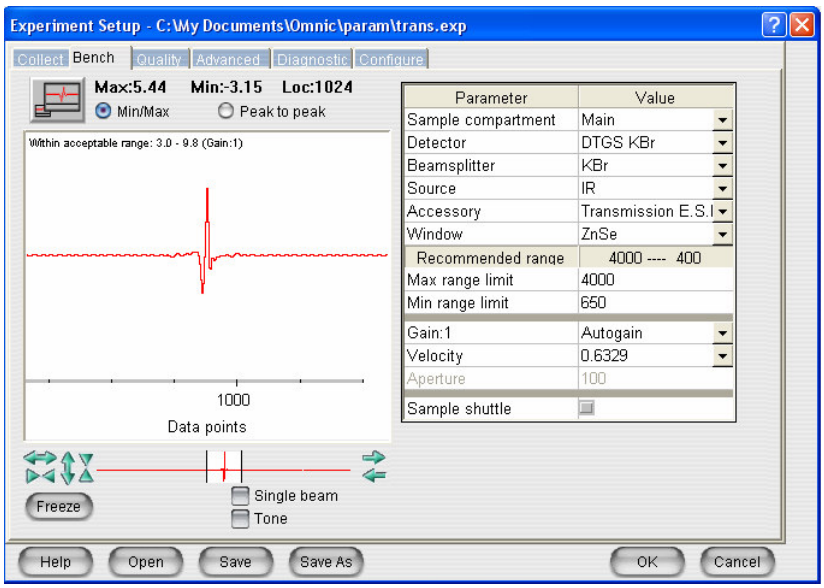

Figure 73: OMNIC Bench Beam Focusing Interface

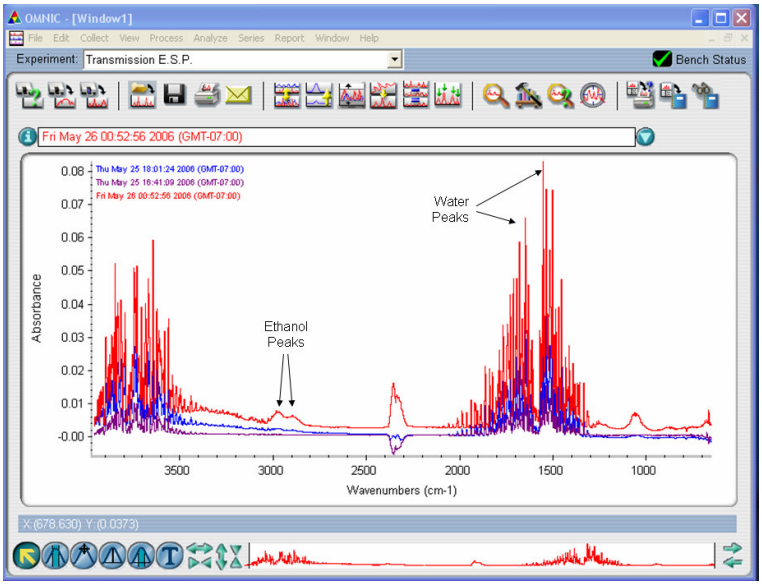

Figure 74: OMNIC Example Absorbance Output for Mixture Droplet Experiment

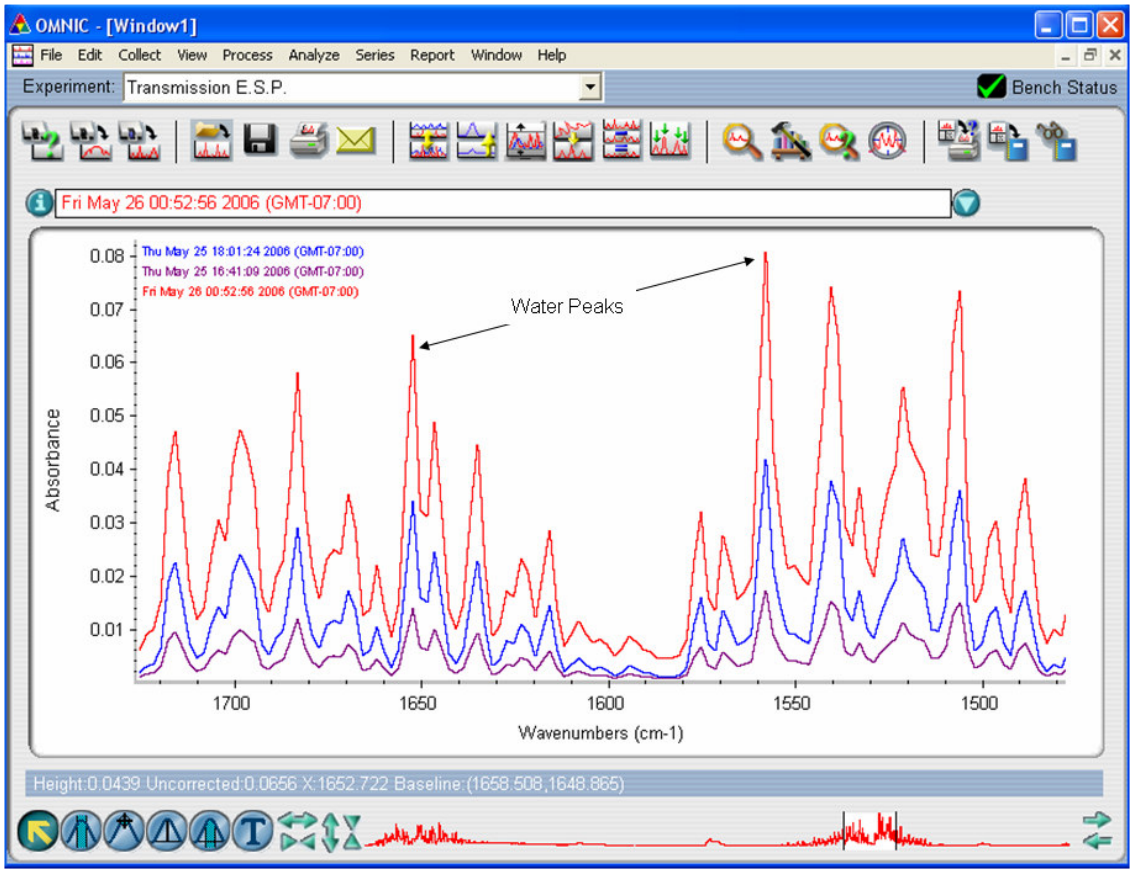

Figure 75: OMNIC Absorbance Output for Mixture Droplet Experiment (Focused on Two Calibrated Water Peaks)

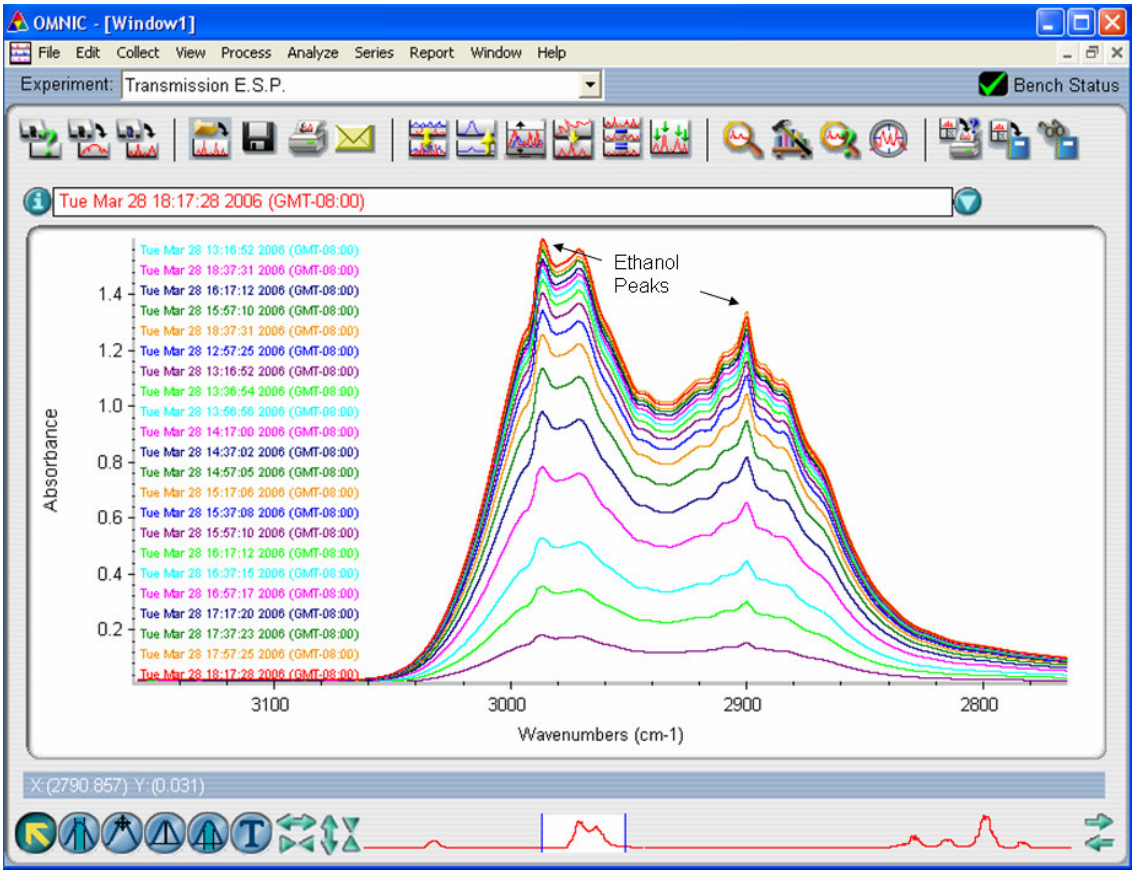

Figure 76: OMNIC Absorbance Output for Mixture Droplet Experiment (Focused on Two Calibrated Ethanol Peaks)

REFERENCES

Abdel-Qader, Z. and Hallett, W., "*The Role of Liquid Mixing in Evaporation of Complex Multicomponent Mixtures: Modeling Using Continuous Thermodynamics – II*," Chem. Eng. Sci. **60**, 1629-1640 (2005).

Aggarwal, S. K. and Chen, G., "*Vaporization Behavior of Fuel Droplets in a Hot Air Stream*," Int. J. Heat Mass Transfer **34-10**, 2669-2673 (1991).

Alopaeus, V. and Norden, H.V., "*A Calculation Method for Multicomponent Mass Transfer Coefficient Correlations*," Computers and Chem. Eng. **23-9**, 1177-1182 (1999).

Alopaeus, V., Aittamaa, J., and Norden, H.V., "*Approximate High Flux Correlations for Multicomponent Mass Transfer Models and Some Explicit Methods*," Chem. Eng. Sci. **54**, 4267-4271 (1999).

Bird, R., Stewart, W., and Lightfoot, E., Transport Phenomena. New York: John Wiley & Sons, 2002.

Charlesworth, D.H. and Marshall Jr., W.R., "*Evaporation from Drops Containing Dissolved Solids*," AIChE J **6**, 9-23 (1960).

Chen, G., Aggarwal, S.K., Jackson,T.A., and Switzer, G.L., "*Experimental Study of Pure and Multicomponent Fuel Droplet Evaporation in a Heated Air Flow*," Atom. Sprays **7**, 317-337 (1997).

Chen, Xiao Dong and Lin, Sean Xu Qi, "*Air Drying of Milk Under Constant and Time Dependent Conditions*," AIChE J **51-6**, 1790-1799 (2005).

Crespo, A. and Linan, L., "*Unsteady Effects of Droplet Evaporation and Combustion*," Combust. Sci. Technol. **11**, 9-18 (1975).

Crowe, C.T., Sharma, M.P., and Stock, D.E., "*The Particle-Source-In-Cell (PSI-CELL) Model for Gas-Droplet Flow*," J. Fluid Eng. **9**, 3289-3302 (1977).

Deng, Z. T., Litchford, R.J., Jeng, S.M. *"Two-dimensional simulation of droplet evaporation at high pressure,"* AIAA Paper 29-3122 (1992).

PsycFunc, (2006). http://www.denysschen.com/catalogue/density.asp

Elerin, T. and Krasovitov, B., "*Evaporation of Liquid Droplets Containing Small Solid Particles*," Int. J. Heat Mass Transfer, **38-12**, 2259-2267 (1995).

Estes,K.E. and Mudawar, I., "*Comparison of Two-Phase Electronic Cooling Using Free Jets and Sprays*," EEP, **10-2**, 975-987 (1995).

Faeth, G.M., "*Current Status of Droplet and Liquid Combustion*," Progress in Engineering and Combustion Science **3-4**, 191-224 (1977).

Faeth, G.M., "*Evaporation and Combustion of Sprays*," Prog. Energy Combust. Sci. **9**, 1-76 (1983).

Frössling, N, "*Evaporation of Falling Drops*," Gerlands Beitr. Geophys. **52**, 170-216 (1938).

Godsave, E. *"The Combustion of Drops in a Fuel Spray,"* Nationl Gas Turbine Establishment (England) Memorandum No. M.95 (1950).

Goldsmith, M. and Penner, S.S., "*On The Burning of Single Drops of Fuel in an Oxidizing Atmosphere*," Jet Propulsion **24**, 245-251 (1954).

Harrje, D.T. and Reardon, F.H. (ed), *"Liquid propellant Rocket Combustion Instability,"* NASA SP-194, 37-102 (1972).

Higbie, R., "*The Rate of Absorption of a Pure Gas into a Still Liquid During Short Periods of Exposure*," Trans. Am. Inst. Chem. Engrs. **31**, 365-383 (1935).

Hoffman, T.W. and Ross, L.L., "*A Theoretical Investigation of the Effects of Mass Transfer on Heat Transfer to an Evaporating Droplet*," Int. J. Heat Mass Transfer **15**, 599-617 (1972).

Hubbard,G.L., Denny, V.E., and Mills, A.F., "*Droplet Evaporation: Effects of Transients and Variable Properties*," Int. J. Heat Mass Transfer **18**, 1003-1008 (1975).

ISR, Isothermal Systems Research Inc. Internal Document. (2005).

Kerstein, A.R., "*Prediction of the Concentration PDF for Evaporating Sprays*," Int. J. Heat Mass Transfer **27**, 1291-1309 (1984).

Kotake, S. and Okuzaki, T., "*Evaporation and Combustion of Fuel Droplet*," Int. J. Heat Mass Transfer **1**, 595-609 (1969).

Krishna, R, "*An Alternative Linearized Theory of Multicomponent Mass Transfer*," Chemical Engineering Sciences **36**, 219-222 (1981).

Krishna, R. and Standart, G.L., "*A Multicomponent Film Model Incorporating a General Matrix Method of Solution to the Maxwell-Stefan Equations*," AIChE J. **22**, 383-389 (1976).

Labowsky, M., "*A Formalism for Calculating the Evaporation Rates of Rapidly Evaporating Interacting Particles*," Combust. Sci. Technol. **18**, 148-151 (1978).

Landis, R. B. and Mills, A. F., "*Effect of Internal Diffusion Resistance on the Evaporation of Binary Droplets*," Fifth Int. Heat Transfer Conf., Tokyo, Japan, Paper B7-9, 345-349 (1974).

Law, C.K., .Xiong, T.Y, and Wang, C.H., "*Alcohol Droplet Vaporization in Humid Air*," Int. J. Heat Mass Transfer **30-7**, 1435-1443 (1987).

Lehtinen, K. E. J., Kulmala, M., Vesala, T., and Jokiniemi, J., "*Analytical Methods to Calculate Condensation Rates of a Multicomponent Droplet*," J. Aerosol Sci. **29-9**, 1035-1044 (1998).

Marchese, A.J. and Dryer, F.L., "*The Effect of Liquid Mass Transport on the Combustion and Extinction of Bi Component Liquid Droplets of Methanol and Water*," Combust. Flame **105**, 104-122 (1996).

Mashayek, F, "*Dynamics of Evaporating Drops. Part I: Formulation and Evaporation Model*," Int. J. Heat Mass Transfer **44**, 1517-1526, (2001).

Masliyah, J. H. and Epstein, N., "*Numerical Solution of Heat and Mass Transfer from Spheroids in Steady Axisymmetric Flow*," Prog. Heat Mass Transfer **6**, 613-632 (1972).

Miller, R. S., Harstad, K., and Bellan, J., "*Evaluation of Equilibrium and Non-Equilibrium Evaporation Models for Many-Droplet Gas-Liquid Flow Simulators*," Int. J. Multiphase Flow **24**, 1025-1055 (1998).

Mudawar, I., "*Assessment of High Heat Flux Thermal Management Schemes*," Keynote Address in Thermal Management ITHERM2000. International Conference on Thermal Mechanics and Thermomechanical Phenomena in Electronic Systems. Las Vegas, Nevada (2000).

Negiz, A., Lagergren, E., and Cinar, A., "*Mathematical Models of Cocurrent Spray Drying*," Ind. Eng. Chem. Res. **34**, 3289-3302 (1995).

Newbold, F.R. and Amundson, N.R., "*A Model for Evaporation of a Multicomponent Droplet*," AIChE Journal **19-1**, 22-30 (1973).

Papadakis, S.E. and King, J.C. "*Air Temperature and Humidity Profile in Spray Drying: 2. Experimental Measurements*," Ind. Eng. Chem. Res. **27**, 2116-2123 (1988).

Prober, R.P., *"The Influence of Spray Particle Size and Distribution in the Combustion of Oil Droplets,"* Philosophical Magazine **37**, 94-105 (1946).

Ranz, W.E. and Marshall, W.R., "*Evaporation from Drops: Part I*," Chem. Eng. Prog. **48**, 141-146 (1952).

Ranz, W.E. and Marshall, W.R., "*Evaporation from Drops: Part II*," Chem. Eng. Prog. **49**, 173-181 (1953).

Sacks, W. *"The Rate of Evaporation of a Kerosene Spray,"* Mechanical Engineering Report (National Research Council of Canada), Note 7 (National Aeronautical Establishment of Canada), Report: MF-2816 (1951).

Santangelo, P., Flowers, D., and Kennedy, I., "*Demonstration of Droplet Size and Vaporization Rate Measurements in the Near Field of a Two-Phase Jet with Lasing Spectroscopy*," Applied Optics **37-24**, 5573-5578 (1998).

Sezen, Y., "*Unsteady Mass Transfer Analysis of Evaporation of a Single Multicomponent Droplet with Diffusion and Constant Rate Processes*," Int. Comm. Heat Mass Transfer **27-4**, 559-568 (2000).

Spalding, D. B. *"The Combustion of Liquid Fuel in a Gas Stream: Part 1,"* Fuel **xxix**, 2-7 (1950); *"The Combustion of Liquid Fuel in a Gas Stream: Part 2,"* Fuel **xxix**, 25-32 (1950).

Stewart, W.E. and Prober, R., "*Matrix Calculations of Multicomponent Mass Transfer in Isothermal Systems*," Ind. Eng. Chem. Fundam. **3**, 224-235 (1964).

Tamim, J. and Hallett, W.L.H., "*A Continuous Thermodynamics Model for Multicomponent Droplet Vaporization*," Chem. Eng. Sci. **50-18**, 2933-2942 (1995).

Taylor, R. and Krishna, R., Multicomponent Mass Transfer. New York: John Wiley & Sons 1993.

Toor, H.L, "*Diffusion in Three Component Gas Mixtures*," AIChE J. **3**, 198-207 (1957).

Toor, H.L., "Solution of the Linearized Equations of Multicomponent Mass Transfer," AIChE J. **10**, 448-455, 460-465 (1964).

Torres, D.J., O'Rourke, P.J., and Amsden, A.A., "*A Discrete Multicomponent Fuel Model*," Atomization and Sprays **13**, 131-172 (2003).

Yuen, M. C. and Chow, L. W., "Heat-Transfer Measurements of Evaporating Liquid Droplets," Int. J. Heat Mass Transfer, Vol. 21, 537-542 (1978).

Zhu, Guang-Sheng and Reitz, R.D., "A Model for High-Pressure Vaporization of Droplets of Complex Liquid Mixtures Using Continuous Thermodynamics," Int. J. Heat Mass Transfer, Vol. 45, 495-507 (2002).